

3D

Print Turkey  
Org

International  
Journal of 3D Printing  
Technologies and Digital Industry

IJ3DPTDI



Uluslararası 3B Yazıcı Teknolojileri  
ve Dijital Endüstri  
Dergisi

Volume:9 Issue:1  
Oct-Apr. 2025

Cilt: 9 Sayı:1  
Ocak-Nisan 2025

DergiPark  
AKADEMİK

TRIZIN



<https://3dprintturkey.org/>



Dergimize 4 dilde (Türkçe Tr, İngilizce En, Rusça Ru ve Ukraynaca Ua) yazı kabul etmekteyiz. Türkçe, Rusça ve Ukraynaca yazılarda İngilizce özet yazılması zorunludur.

## ULUSLARARASI 3B YAZICI TEKNOLOJİLERİ VE DİJİTAL ENDÜSTRİ dergisi,

IJ3DPTDI, Endüstri 4.0 – dijital endüstri teknolojileri, 3B yazıcı teknolojileri, katmanlı-eklemeli imalat teknolojileri ve uygulamaları yani mühendislik, bilim, teknoloji gibi tüm disiplinlerle ilgili araştırmaların sonuçlarını yaymak için açık, hakemli, disiplinlerarası, uluslararası, bilimsel, akademik, online bir dergidir. IJ3DPTDI, Mühendislik, Teknoloji ve Bilimin Endüstri 4.0 daki uygulamaları, tüm araştırmaları, gözden geçirme makalelerini, kısa bilgi paylaşımlarını ve önemli ilerlemeleri sunan teknik notları online yayınlamak için yazarları davet eder.

Endüstri 4.0, Dijital Endüstri, 3B Yazıcılar üzerine tüm bilimsel mühendislik araştırma ve teknoloji alanı konuları;

**3B baskı için tıbbi uygulamalar;** dokuların ve organların biyografik baskıları, 3B vaskülarize organların oluşturulmasında karşılaşılan zorluklar, özelleştirilmiş implantlar ve protezler, düşük maliyetli protez parçaları, cerrahi hazırlık için anatomik modeller, sentetik cilt, kafatası değişimi, tıbbi donatımı, kemik, özel üretilen sensörler, kişiselleştirilmiş ilaç dozu, benzersiz dozaj şekilleri, kompleks ilaç salınım profilleri v.d.

**3B yazıcı uygulama alanları;** tıbbi ve diş hekimliği uygulamaları, diş hekimliği uygulamaları ve materyalleri, yumuşak robotik sistemleri, robot tutucu sistemler, bina uygulamaları, kalıp / kalıp uygulamaları, mimarlık uygulamaları, model uygulamaları, hızlı prototip uygulamaları, görsel sanat uygulamaları, tekstil uygulamaları, dijital fabrikalar, mimari model uygulamaları ve malzemeleri, endüstriyel uygulamalar ve malzemeler, gıda uygulamaları ve malzemeleri, sanatsal uygulamalar ve malzemeler, tarama yöntemleri ve modelleme v.d.

**Endüstri 4.0 ve dijital sanayi;** büyük veri, yapay zeka, dijital yaşam döngüsü, sensör motorları, artırılmış gerçeklik, görselleştirme, sistem simülasyonu, kablosuz iletişim, BİT güvenlik, dijital iş, blok zinciri, veri Güvenliği, özerk robotlar, sistem entegrasyonu, nesnelerin interneti (IoTs), siber güvenlik, bulut bilişim, dijital fabrika v.d.

**3B yazıcı tasarım, modelleme ve analiz;** 3D yazıcı tasarımı, ekstruder tasarımı, 3B baskı için ürün geliştirme, seramik sistemleri tasarımı, gıda sistemleri tasarımı, elektronik bileşenleri, mekanik parçalar, standart bileşenler v.d.

**3B yazıcı malzeme ve mekanik özellikleri;** polimer malzemeler, esnek malzemeler, biyo malzemeler, metalik malzemeler, toz malzeme üretim yöntemleri, ağaç malzemeler, kompozit malzemeler v.d.

**3B yazıcı program kontrol teknolojileri;** kontrol programları, tasarım programları, 3D tarama teknolojileri, DMLS teknolojileri, SLA teknolojileri, SLS teknolojileri, FDM teknolojileri, dijital üretim teknolojileri, diğer 3B yazıcı teknolojileri v.d.

IJ3DPTDI, online yayınlanan bir dergidir ve yılda 3 defa yayınlanır.

- 1.peryot Ocak-Nisan
- 2.peryot Mayıs-Ağustos
- 3.peryot Eylül-Aralık

ISSN 2602-3350

web-site : <http://dergipark.gov.tr/ij3dptdi>

e-mail : [korayozsoy32@gmail.com](mailto:korayozsoy32@gmail.com)



**Dear author,**

Our Journal accepts articles in 4 languages (Turkish Tr, English En, Russian Ru and Ukrainian Ua). Articles in Turkish, Russian and Ukrainian must have an abstract in English.

**International Journal of 3D Printing Technologies and Digital Industry**

IJ3DPTDI, is an open access peer-reviewed, interdisciplinary international platform for disseminating results of relevant research related to all the disciplines of engineering, science, technology etc on Industry 4.0 - digital industry technologies, 3D printer technologies, additive manufacturing technologies and applications . IJ3DPTDI, invites all research, review articles, short communications & technical notes that describe significant advances research in the areas of Engineering, Technology, Science on Industry 4.0, Digital Industry, 3D Printers, additive manufacturing;

**All scientific engineering research & technology area** on Industry 4.0, Digital Industry and 3D printers;

**Medical applications for 3D printing;** bioprinting tissues and organs, challenges in building 3D vascularized organs, customized implants and prostheses, low-cost prosthetic parts, anatomical models for surgical preparation, synthetic skin, cranium replacement, medical equipment, bone, tailor-made sensors, personalized drug dosing, unique dosage forms, complex drug-release profiles ect.

**Application fields;** medical and dental applications, dental practices and materials, soft robotics systems, robot gripper systems, building applications, die/mold applications, architecture applications, models applications, rapid prototype applications, visual arts applications, textile applications, digital factories, architectural-model applications and materials, industrial applications and materials, food applications and materials, artistic practices and materials, scanning methods and modeling ect.

**Digital industry;** big data, artificial intelligence, digital life cycles, sensors actuators, augmented reality, visualization, system simulation, wireless communication, ICT security, digital business, block chain, data safety, autonomous robots, system integration, internet of things (IT's), cyber security, cloud computing, digital factory ect.

**Design, modelling and analysis;** 3D printer design, extruder design, product development, ceramic systems design, food systems design, table system design, electronics components, mechanic components, standard components ect.

**Mechanical properties of filaments;** polymer materials, flexible materials, bio materials, metallic materials, wood materials, composite materials ect.

**Program** – control technologies; control programs, design programs, 3D scanning technologies, DMLS technologies, SLA technologies, SLS technologies, FDM technologies, Digital production technologies, other 3D printer technologies ect.

IJ3DPTDI, Its publication frequency is 3 issues per year.

- 1.Period January-April
- 2.period May-August
- 3.period September-December

**ISSN** 2602-3350

**Web-site:** <http://dergipark.gov.tr/ij3dptdi>

**E-mail:** [korayozsoy32@gmail.com](mailto:korayozsoy32@gmail.com)



### **Уважаемый автор,**

наш журнал принимает статьи на 4-х языках (турецком, английском, русском и украинском). Статьи на турецком, русском и украинском языках должны сопровождаться аннотацией на английском языке.

### **Международный журнал технологий 3D-печати и цифровой индустрии**

**IJ3DPTDI** – это рецензируемое издание с открытым доступом, междисциплинарная международная платформа для обмена результатами исследований по инженерно-конструкторским разработкам, теоретическим исследованиям, усовершенствованию технологий Индустрии 4.0, в том числе – технологий цифровой промышленности, 3D-печати, аддитивного производства и разработки приложений. IJ3DPTDI принимает исследовательские статьи, обзорные статьи, краткие сообщения и технические заметки, которые описывают значимые результаты исследований в области машиностроения, технологии, теоретической основы индустрии 4.0, цифровой промышленности, 3D печати, производства многокомпонентных материалов.

**Тематика журнала включает все научно-технические исследования и обзор технологий Индустрии 4.0, цифровой промышленности и 3D печати. Медицинские технологии 3D-печати:** биопринтинг – воспроизведение объемных моделей тканей и органов, создание трехмерных васкуляризированных органов, индивидуализированных имплантатов и протезов, синтетической кожи, костей, замены частей черепа; удешевление технологии протезирования, разработка анатомических моделей для подготовки хирургов, тестовых хирургических операций, медицинского оборудования; изготовление датчиков с заданным набором характеристик, создание уникальных лекарственных препаратов с индивидуальными дозировками, сложных многокомпонентных лекарственных средств.

**Области применения:** материалы и оборудование для медицины и стоматологии, роботизированные системы на основе биологических прототипов, роботизированные захватные устройства, строительные материалы, пресс-формы, модели и прототипы в архитектуре, моделирование реальных объектов, прототипирование, сфера визуального искусства, текстильная промышленность, цифровые заводы, приложения и материалы для архитектурного моделирования, промышленные образцы и материалы, создание пищевых продуктов, технологии художественной обработки материалов, методы моделирования и сканирования и т.п.

**Цифровая индустрия:** большие данные, искусственный интеллект, жизненный цикл цифровых технологий, приводные механизмы датчиков, расширенная реальность, визуализация, моделирование систем, беспроводная связь, ИТ-безопасность, электронная коммерция, блокчейн технологии, безопасность данных, автономные роботы, системная интеграция, интернет вещей, кибербезопасность, облачные вычисления, цифровое производство.

**Дизайн, моделирование и анализ:** моделирование для 3D печати, экструдера; разработка разнообразных продуктов, проектирование систем керамического производства, усовершенствование технологии производства пищевых продуктов, проектирование предметов мебели, электронных компонентов, механических деталей, стандартных компонентов и т.п.

**Механические свойства нитей:** полимерные материалы, гибкие материалы, биоматериалы, изделия из металла и древесины, композиционные материалы.

**Технологии управления приложениями:** контрольные программы, проектные программы, технологии 3D-сканирования, технологии DMLS, SLA, SLS, FDM, цифровые технологии производства, другие технологии 3D-печати и т.п. Периодичность выхода журнала – 3 раза в год:

1-й выпуск – январь-апрель;

2-й выпуск – май-август;

3-й выпуск – сентябрь-декабрь.

ISSN 2602-3350

Сайт журнала: <http://dergipark.gov.tr/ij3dptdi>

Электронная почта: [korayozsoy32@gmail.com](mailto:korayozsoy32@gmail.com)



## Шановний авторе,

наш журнал приймає статті на 4-х мовах (турецькою, англійською, російською та українською). Статті турецькою, російською та українською мовою повинні супроводжуватися анотацією англійською мовою.

### Міжнародний журнал технологій 3D-друку і цифрової індустрії

**IJ3DPTDI** – це рецензоване видання з відкритим доступом, міждисциплінарна міжнародна платформа для обміну результатами досліджень з інженерно-конструкторських розробок, теоретичних досліджень, удосконалення технологій Індустрії 4.0, в тому числі – технологій цифрової промисловості, 3D-друку, адитивного виробництва і розробки додатків. IJ3DPTDI приймає дослідні статті, оглядові статті, короткі повідомлення і технічні записки, які містять значущі результати досліджень в галузі машинобудування, технології, теоретичній основі індустрії 4.0, цифровій промисловості, 3D друку, виробництва багатокomпонентних матеріалів.

### Тематика журналу охоплює всі науково-технічні дослідження та огляд технологій Індустрії 4.0, цифрової промисловості і 3D друку.

**Медичні технології 3D-друку:** біопрінтинг – відтворення об'ємних моделей тканин і органів, створення тривимірних васкуляризованих органів, індивідуалізованих імплантатів і протезів, синтетичної шкіри, кісток, заміни частин черепа; здешевлення технології протезування, розроблення анатомічних моделей для підготовки хірургів, тестових хірургічних операцій, медичного обладнання; виготовлення датчиків із заданим набором характеристик, створення унікальних лікарських препаратів із індивідуальними дозуваннями; складних багатокomпонентних лікарських засобів.

**Сфери застосування:** матеріали та обладнання для медицини і стоматології, роботизовані системи на основі біологічних прототипів, роботизовані захватні пристрої, будівельні матеріали, прес-форми, моделі і прототипи в архітектурі, моделювання реальних об'єктів, прототипування, сфера візуального мистецтва, текстильна промисловість, цифрові заводи, додатки та матеріали для архітектурного моделювання, промислові зразки і матеріали, створення харчових продуктів, технології художньої обробки матеріалів, методи моделювання та сканування і т.п.

**Цифрова індустрія:** великі дані, штучний інтелект, життєвий цикл цифрових технологій, приводні механізми датчиків, розширена реальність, візуалізація, моделювання систем, бездротовий зв'язок, IT-безпека, електронна комерція, блокчейн технології, безпека даних, автономні роботи, системна інтеграція, інтернет речей, кібербезпека, хмарні обчислення, цифрове виробництво.

**Дизайн, моделювання і аналіз:** моделювання для 3D друку, екструдера; розробка різноманітних продуктів, проектування систем керамічного виробництва, удосконалення технології виробництва харчових продуктів, проектування предметів меблів, електронних компонентів, механічних деталей, стандартних компонентів і т.п.

**Механічні властивості ниток:** полімерні матеріали, гнучкі матеріали, біоматеріали, вироби з металу і деревини, композиційні матеріали.

**Технології управління додатками:** контрольні програми, проектні програми, технології 3D-сканування, технології DMLS, SLA, SLS, FDM, цифрові технології виробництва, інші технології 3D-друку і т.п.

Періодичність виходу журналу – 3 рази на рік:

1-й випуск – січень-квітень;

2-й випуск – травень-серпень;

3-й випуск – вересень-грудень.

ISSN 2602-3350

Web-site: <http://dergipark.gov.tr/ij3dptdi>

E-mail: [korayozsoy32@gmail.com](mailto:korayozsoy32@gmail.com)



# ULUSLARARASI 3B YAZICI TEKNOLOJİLERİ VE DİJİTAL ENDÜSTRİ DERGİSİ

Cilt:9 Sayı: 1 Yıl: 2025

## INTERNATIONAL JOURNAL OF 3D PRINTING TECHNOLOGIES AND DIGITAL INDUSTRY

Volume:9 Number: 1 Year: 2025

ISSN: 2602-3350

Yazıların tüm bilimsel sorumluluğu yazar(lar)a aittir. Editör, yardımcı editör ve yayıncı dergide yayımlanan yazılar için herhangi bir sorumluluk kabul etmez. Bu dergi, aşağıda listelenen veri tabanları tarafından taranmaktadır. All the scientific responsibilities of the manuscripts belong to the authors (s). The editor, assistant editor and publisher accept no responsibility for the articles published in the journal. The Journal is indexed by the following abstracting and indexing databases.

TR Dizin, Google Scholar, ResearchBib, Index Copernicus, Asos indeks

TR Dizin



INDEX COPERNICUS  
INTERNATIONAL

ASOS  
indeks

<http://dergipark.gov.tr/ij3dptdi>



# Uluslararası 3B Yazıcı Teknolojileri ve Dijital Endüstri Dergisi / International Journal of 3D Printing Technologies and Digital Industry

**Vol: 9, No:1 (2025)**

**Cilt: 9, Sayı:1 (2025)**

## **Editörler ve Kurullar / Editors and Boards**

### **Yayın Kurulu Başkanı / Publication Board Manager**

Dr. Kerim ÇETİNKAYA, Antalya BELEK Üniversitesi, Sanat ve Tasarım Fakültesi, TÜRKİYE

### **Baş Editörler / Editor(s)-in-Chief**

Dr. Kerim ÇETİNKAYA, Antalya BELEK Üniversitesi, Sanat ve Tasarım Fakültesi, TÜRKİYE

Dr. Koray ÖZSOY, Isparta Uygulamalı Bilimler Üniversitesi, Isparta OSB MYO, Makine ve Metal Teknolojileri Bölümü, TÜRKİYE

### **Editörler Kurulu / Editorial Board**

Dr. Kerim ÇETİNKAYA, Antalya BELEK Üniversitesi, Sanat ve Tasarım Fakültesi, TÜRKİYE

Dr. Kerim ÇETİNKAYA, Antalya BELEK Üniversitesi, Sanat ve Tasarım Fakültesi, TÜRKİYE

Dr. Burhan DUMAN, Isparta Uygulamalı Bilimler Üniversitesi, Teknoloji Fakültesi, Bilgisayar Mühendisliği Bölümü, TÜRKİYE

Dr. Ahu ÇELEBİ, Celal Bayar Üniversitesi, Mühendislik Fakültesi, Malzeme Mühendisliği Bölümü, TÜRKİYE

Dr. Hatice EVLEN, Karabük Üniversitesi, Teknoloji Fakültesi, Endüstriyel Tasarım Mühendisliği Bölümü, TÜRKİYE

Dr. Murat Aydın, Karabük Üniversitesi, Teknoloji Fakültesi, Endüstriyel Tasarım Mühendisliği Bölümü, TÜRKİYE

Dr. Hanane ZERMANE, Batna 2 Üniversitesi, Endüstri Mühendisliği Bölümü, CEZAYİR

Dr. Serhii Yevseiev, Simon Kuznets Kharkiv Ulusal Ekonomi Üniversitesi, Siber Güvenlik ve Bilgi Teknolojileri Bölümü, UKRAYNA

Dr. Pınar DEMİRCİOĞLU, Aydın Adnan Menderes Üniversitesi, Mühendislik Fakültesi, Makine Mühendisliği Bölümü, TÜRKİYE

Dr. Bekir AKSOY, Isparta Uygulamalı Bilimler Üniversitesi, Teknoloji Fakültesi, Mekatronik Mühendisliği Bölümü, TÜRKİYE

Dr. İshak ERTUĞRUL, Muş Alparslan Üniversitesi, Teknik Bilimler MYO, Mekatronik Programı, TÜRKİYE

Dr. Levent AYDIN, Kocaeli Üniversitesi, Sağlık Hizmetleri MYO, Sağlık Bakım Hizmetleri Bölümü, TÜRKİYE



Dr. Kıyas KAYAALP, Isparta Uygulamalı Bilimler Üniversitesi, Teknoloji Fakültesi, Bilgisayar Mühendisliği Bölümü, TÜRKİYE

Dr. İbrahim KARAAĞAÇ, İmalat Mühendisliği, Teknoloji Fakültesi, Gazi Üniversitesi, TÜRKİYE

Dr. Yasin HAMARAT, Biyoteknoloji, Kaunas University Of Technology, LİTVANYA

Dr. Binnur SAĞBAŞ, Yıldız Teknik Üniversitesi, Makine Fakültesi, Makine Mühendisliği Bölümü, TÜRKİYE

Dr. Heshham A. Hegazi, German University, Department of Design and Production Engineering, CAIRO

#### **Mizanpaj Editörü/ Layout Editor**

Mehmet YÜCEL, Isparta Uygulamalı Bilimler Üniversitesi, Teknoloji Fakültesi, Mekatronik Mühendisliği Bölümü, TÜRKİYE

Arda PAZARCIKCI, Isparta Uygulamalı Bilimler Üniversitesi, Teknoloji Fakültesi, Mekatronik Mühendisliği Bölümü, TÜRKİYE

#### **Danışma Kurulu / Advisory Board**

Dr. Hüseyin Rıza BÖRKLÜ, GAZİ ÜNİVERSİTESİ, TR

Dr. Mustafa BOZDEMİR KIRIKKALE ÜNİVERSİTESİ, TR

Dr. Savaş DİLİBAL, İSTANBUL GEDİK ÜNİVERSİTESİ, TR

Dr. Cem Bülent ÜSTÜNDAĞ, YILDIZ TEKNİK ÜNİVERSİTESİ, TR

Dr. Ahmet CAN, NECMETTİN ERBAKAN ÜNİVERSİTESİ, TR

Dr. Fuat KARTAL, KASTAMONU ÜNİVERSİTESİ, TR

Dr. İhsan TOKTAŞ, YILDIRIM BEYAZIT ÜNİVERSİTESİ, TR

Dr. Okan ORAL, AKDENİZ ÜNİVERSİTESİ, TR

Dr. Mustafa Aydın, KÜTAHYA DÜMLUPINAR ÜNİVERSİTESİ, TR

Dr. Serap ÇELEN, EGE ÜNİVERSİTESİ, TR

Dr. İsmail BÖĞREKÇİ, AYDIN ADNAN MENDERES ÜNİVERSİTESİ, TR

Dr. Samsun M. BAŞARICI, AYDIN ADNAN MENDERES ÜNİVERSİTESİ, TR

Dr. Serkan ŞENDAĞ, MERSİN ÜNİVERSİTESİ, TR

**ISSN 2602-3350**



Vol:9, No:1 (2025)

Cilt:9, Sayı:1 (2025)

<b>İçindekiler /Table of Contents</b>	<b>Sayfa /Pages</b>
<b>Araştırma Makaleleri/Research Articles</b>	
<b>SHAPE'S IMPACT ON DIMENSIONAL PRECISION IN 3D PRINTED COMPONENTS</b>	<b>1-8</b>
Hilmi Saygin SUCUOGLU <sup>a</sup> , Ismail BOGREKCI <sup>a</sup> , Pinar DEMIRCIOGLU <sup>a,b</sup>	
<b>INVESTIGATION OF THE EFFECTS OF PROCESS PARAMETERS ON MACHINING PERFORMANCE IN LASER CUTTING OF 3D-PRINTED PLA</b>	<b>9-20</b>
Oguzhan Der <sup>a</sup> , Gokhan Basar <sup>b</sup>	
<b>ALZHEİMER HASTALIĞININ ERKEN TEŞHİSİ İÇİN MAKİNE ÖĞRENİMİ TABANLI UZMAN SİSTEM GELİŞTİRİLMESİ</b>	<b>21-35</b>
Osamah Khaled Musleh SALMAN <sup>a</sup> , Sema ÇAYIR <sup>a</sup> , Mustafa Melikşah ÖZMEN <sup>a</sup> , Enes AÇIKGÖZOĞLU <sup>b</sup>	
<b>COMPARATIVE ANALYSIS OF BCCZZ LATTICE STRUCTURE COMPRESSION BEHAVIOR: EXPERIMENTAL, NUMERICAL, AND MACHINE LEARNING APPROACHES</b>	<b>36-44</b>
Deniz Aktürk <sup>a,b,*</sup> , Muhammed Taha Yıldız <sup>a,b</sup> , Nazim Babacan <sup>a</sup>	
<b>INVESTIGATING THE EFFECT OF UNIT CELL ORIENTATION ON MECHANICAL PROPERTIES OF GYROID-BASED LATTICE STRUCTURES</b>	<b>45-52</b>
Golbarg Nikaein <sup>a</sup> , Binnur Sagbas <sup>b</sup> , Maryam Jamshidi <sup>a</sup> , Mohammad Hossein Sadeghi <sup>a</sup>	
<b>PREDICTION OF HARDNESS VALUES OF AGED SELECTIVE LASER MELTED AlSi10Mg ALLOY DATA WITH MACHINE LEARNING METHODS</b>	<b>53-62</b>
Murat İnce <sup>a</sup> , Hatice Varol Özkavak <sup>b</sup>	
<b>EFFECT OF GEOMETRIC MODIFICATIONS ON THE COMPRESSIVE STRENGTH AND MECHANICAL PERFORMANCE OF GYROID-BASED BONE SCAFFOLDS</b>	<b>63-72</b>
Muhammet Mevlüt Karaca <sup>a</sup> , İzel Ekinci <sup>b</sup> , Daver Ali <sup>b</sup>	
<b>3D MEDICAL IMAGE SEGMENTATION WITH DEEP LEARNING METHODS</b>	<b>73-91</b>
Sezin Barın <sup>a</sup> , Uçman Ergün <sup>a</sup> , Gür Emre Güraksın <sup>b</sup>	
<b>BIBLIOMETRIC OF BLOCKCHAIN PUBLICATIONS IN SCIENCE CITATION INDEX EXPANDED FROM 1991 TO 2022</b>	<b>92-113</b>
Yuh-Shan Ho <sup>a</sup> , Samia Aitouche <sup>b*</sup>	



<b>FINITE ELEMENT ANALYSIS AND PRODUCTION OF A BALANCE ROBOT DESIGNED TO BE USED IN THE FIELD OF ADVERTISING</b>	<b>114-121</b>
Yusuf Coşkun <sup>a</sup>  , Diyar Can Aydın <sup>a</sup>  , Halil Aktoz <sup>a</sup>  , Lale Özyılmaz <sup>a</sup> 	
<b>INVESTIGATION TO THE V-I CHARACTERISTICS OF ROGOWSKI COILS WITH MAGNETIC FILAMENTS BY REGRESSION ANALYSIS</b>	<b>122-128</b>
Gizem Merve Aydın <sup>a</sup>  , Gülsüm Yıldırım <sup>b</sup>  , Emin Yıldırım <sup>c</sup> 	
<b>ROBOTİK KOL ENTEGRELİ MOBİL ARAMA VE KURTARMA ROBOTUNUN TASARIMI VE UYGULAMASI</b>	<b>129-141</b>
Cemal Beik <sup>a</sup>  , Merdan Özkahraman <sup>a</sup> 	





ULUSLARARASI 3B YAZICI TEKNOLOJİLERİ  
VE DİJİTAL ENDÜSTRİ DERGİSİ

INTERNATIONAL JOURNAL OF 3D PRINTING  
TECHNOLOGIES AND DIGITAL INDUSTRY

ISSN:2602-3350 (Online)

URL: <https://dergipark.org.tr/ij3dptdi>

## SHAPE'S IMPACT ON DIMENSIONAL PRECISION IN 3D PRINTED COMPONENTS

**Yazarlar (Authors):** Hilmi Saygin SUCUOGLU , Ismail BOGREKCI , Pinar DEMIRCIOGLU 

**Bu makaleye şu şekilde atıfta bulunabilirsiniz (To cite to this article):** Sucuoglu H. S., Bogrekci I., Demircioglu P., "Shape's Impact on Dimensional Precision in 3D Printed Components" *Int. J. of 3D Printing Tech. Dig. Ind.*, 9(1): 1-8, (2025).

DOI: 10.46519/ij3dptdi.1417150

Araştırma Makale/ Research Article

Erişim Linki: (To link to this article): <https://dergipark.org.tr/en/pub/ij3dptdi/archive>

# SHAPE'S IMPACT ON DIMENSIONAL PRECISION IN 3D PRINTED COMPONENTS

Hilmi Saygin SUCUOGLU<sup>a</sup> , Ismail BOGREKCI<sup>a</sup> , Pinar DEMIRCIOGLU<sup>a,b</sup> 

<sup>a</sup>Aydın Adnan Menderes University, Faculty of Engineering, Mechanical Engineering Department, Aydın, TURKEY

<sup>b</sup>Technical University of Munich, TUM School of Engineering and Design, Institute of Materials Science, GERMANY

\* Corresponding Author: [hilmisucuoglu@adu.edu.tr](mailto:hilmisucuoglu@adu.edu.tr)

(Received: 09.01.24; Revised: 04.04.24; Accepted: 16.04.24)

---

## ABSTRACT

In this comprehensive exploration, the study explores the relationship between shape and the dimensional accuracy of components manufactured through additive manufacturing processes. The methodology involves the adept utilization of Autodesk Inventor Software, strategically embossing capital letters from A to O onto a rectangular plate. The resulting models are exported in STL format, laying the foundation for rapid prototyping. The investigation unfolds with the application of a Prusa I3 desktop 3D printer, where specific settings, including layer height (ranging from 90 to 300 microns), 20% infill density, and a heated bed temperature of 60 °C, are scrupulously chosen. Three different embossing methods are examined in this study to see how each affects dimensional correctness. These methods are join, cut half, and cut through. Through a meticulous comparative analysis, facilitated by high-resolution image acquisition and advanced processing techniques like binarizing and edge detection, the study discerns that embossing with join yields shapes characterized by higher dimensional accuracy, a conclusion substantiated by correlation coefficient analysis. This research stands as a significant contribution, offering valuable insights into optimizing additive manufacturing processes and elevating dimensional precision in 3D printed components.

**Keywords:** Additive Manufacturing, Shape Effects, Image Processing, Edge Detection, Dimensional Accuracy, STL Format.

---

## 1. INTRODUCTION

### 1.1. Advancements in Melt Extrusion

The details of the conventional melt extrusion additive manufacturing (AM) process, depicted in Figure 1, involve a systematic conveyance of filament feedstock to the system through an electric motor-controlled pinch roller mechanism. This complicated mechanism plays an important role in facilitating the precise delivery of the filament, ensuring a controlled and uniform flow. Central to this process is the predominant use of amorphous thermoplastics, where materials such as acrylonitrile butadiene styrene (ABS) or polylactic acid (PLA) are ideal choices for feedstock filament. The selection of these materials is vital, as they exhibit properties conducive to the extrusion and layering process, ultimately contributing to the successful fabrication of sophisticated and precise three-

dimensional structures. This initial phase sets the stage for the subsequent stages of melting, deposition, and layering, highlighting the significance of material choice in the additive manufacturing workflow.

At the base of the extrusion AM system resides the heated liquefier, a critical component where the filament undergoes the crucial phase of melting. The resulting molten material is then thoroughly propelled through a small print nozzle by the liquefier, forming what is commonly referred to as a road or bead as it exits the nozzle. The liquefier head assembly undergoes systematic maneuvers throughout the build environment, propelled by stepper motors. This orchestrated interplay of planar, x-y motion of the print head, synchronized with the z-motion of the build stage, lays the foundation for the layer-

by-layer construction of intricate 3D structures [1-2]. This intricate dance of components in the extrusion process exemplifies the precision and complexity inherent in additive manufacturing methodologies.

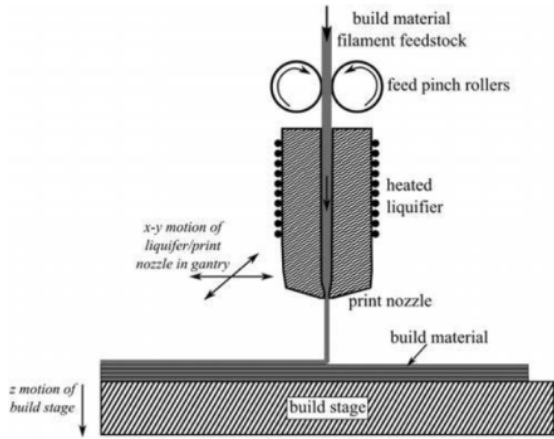


Figure 1. Typical extrusion based AM process [2].

The trajectory traced by the print head along the gantry is commonly known as the tool path, representing a critical design variable in the implementation of extrusion-based additive processes for part production. Achieving a consistent surface involves the typical printing of a contour or road along the part's perimeter. Internally, a lattice of roads is deposited, with each layer usually oriented at a fixed raster angle relative to the layer beneath it. The thickness of contours and roads assumes vital significance in shaping the dimensional accuracy and surface roughness of the final parts, as illustrated in Figure 2.

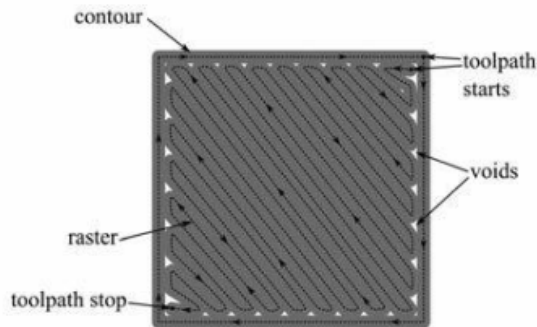


Figure 2. Typical toolpath with a single contour [2].

### 1.2. Optimizing Design and Product Characteristics in Melt Extrusion Additive Manufacturing

Dimensional accuracy, resolution and surface roughness are closely related to performance

parameters and product design. The main factors affecting performance and production results are equipment track design, water and ambient temperature, and heating rate. Also, the control algorithms that control filament feed speed, path width, wafer thickness, and air gap are important considerations. The dimensions of the road, especially the width and thickness specified in the x-y plane of the build plate, play an important role in defining the basic limits of dimensional accuracy in the manufacturing process. These parameters directly affect the possible resolution of the printed object. In addition, the space between adjacent roads, known as the air gap, is an important factor affecting the correct size [3]. These important considerations highlight the importance of shaping the final product of the manufacturing process and providing a basis for understanding and optimizing the resolution and accuracy of printed parts. In additive manufacturing (AM) design software, a positive air gap means that two adjacent roads do not touch, while a negative air gap refers to a distance less than the distance between the centers of two adjacent roads (Figure 3).

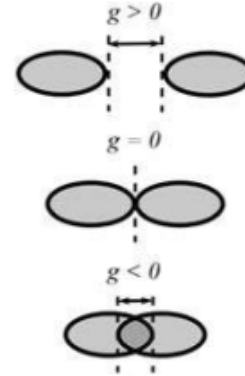


Figure 3. The positive, zero and negative air gap [4].

Implementing a minimum negative void is considered a strategy to reduce the void ratio between roads and increase the bounding area. However, this approach should be carefully considered as it can degrade the physical appearance of the part. Computer control of construction direction and raster model is important because it has a significant impact on construction time and mechanical properties. Critical process parameters such as liquefaction temperature, manufacturing environment temperature, and filament feed rate are critical determinants in ensuring the quality of manufactured components. Thermal stresses built up in a part during

drying and cooling, influenced by the temperature of the manufacturing environment, can cause instability and distortion. In addition, other parameters that affect the dimensional accuracy are the materials selected, the nominal dimensions (small, medium, or large), the construction, the geometric characteristics of the laboratory and the topology (open or closed). The choice between thick-walled parts, such as frame or solid, and post-processing methods will have a significant impact on the final parts of the manufactured part.

Hannon et al. [5], studied the effects of printing parameters on the dimensional accuracy of the sample in the (Fused Deposition Modelling) FDM 3D printing. They produced cylindrical and dog bone tensile specimens with different process parameters such as orientation, mesh orientation angle, and layer thickness. They found that the layer thickness parameter had a significant impact on accuracy and that the grid orientation angle was not an important factor. Akbas et al. [6], researched the effects feed rate and die temperature for dimensional accuracy of FDM polymer parts. They printed 30 strips with the same width as the diameter of the nozzle for each sample. Using calipers to measure ribbon width at five locations, they created a linear regression model to find the relation between deviation and parameters. They found that polylactic acid (PLA) samples were more accurate than acrylonitrile butadiene styrene (ABS) samples. Bora and Negabola [7], aimed to use the Taguchi method to optimize the printing parameters (layer height, printing direction and exposure time) of a mask stereolithography (MSLA) tool. They performed analysis of variance (ANOVA) to determine the most effective factors and used regression equations to predict outcomes. They observed a significant effect of exposure time on production measures. Resende et. al [8], used the stereolithography (SLA) method to evaluate the accuracy of 3D printed castings. They produced samples using 3D layers with different thicknesses of 25, 50 and 100 micrometers. They found no significant difference in accuracy between layer thickness. Zarian et al. [9] studied the effect of printing parameters (orientation and position) on mechanical properties using polyetheretherketone (PEEK) biomaterials and the material extrusion (MEX) method. They classify the specimens based on their orientation and location. They

observed no significant difference in mechanical strength between top and bottom printed samples and vertically and horizontally oriented samples.

Akincioğlu et al. [10] investigated the effect of infill density (25%, 50%, and 75%) on the wear properties of gyroid-patterned ABS samples. Their main objective was to determine the coefficient of friction values and to present the impact of infill density on wear and friction performance. They evaluated several performance indicators such as diameter deviation, hardness, surface roughness, test temperature, friction coefficient, weight loss, and wearing surface results. Their results indicated that infill density significantly affects the tribological and heating characteristics of ABS samples. Specifically, increasing infill density leads to higher friction and heat in the samples.

Norani et al. [11] studied the coefficient of friction and wear properties of ABS material by determining the optimal parameters for 3d printing process. They analyzed the dependent variables (friction coefficient and wear rate) as functions of the nozzle temperature, layer height and printing pattern. As a result of study, they found that layer height of 0.10 mm and nozzle temperature of 234 °C with triangle infill pattern is optimal to minimize the coefficient of friction and wear rate.

Chand et al. [12] studied the dimensional accuracy and surface roughness of 3D printed parts fabricated in different orientations. They explored four different part orientations to analyze the variations in dimensional deviation and SR. Additionally, fabricated parts were analyzed using scanning electron microscopy (SEM). The results showed that there was a variation in dimensional accuracy and SR with different part orientations.

Irene and Figueras [13], conducted a research for a comparison of the dimensional accuracy and form errors of Fused Filament Fabrication (FFF) 3D printed spur gears made from two different polymeric materials: PLA and Nylon-PA6. They designed and printed two types of gears with different module and teeth number printed. They used the sector span method to determine the base circular thickness and pitch of the gears. They measured the root and tip di-

ameters to determine the roundness and concentricity errors. The results indicated that PLA generally provides better dimensional accuracy than Nylon.

Moradi et al. [14], investigated the additive manufacturing of ABS using statistical analysis and optimization methods. They considered the impact of layer thickness, infill percentage and contours number on the maximum failure load and elastic modulus of the final ABS product. They used both artificial neural network (ANN) and response surface method (RSM) to assess the impact of additive manufacturing parameters on build quality. They extracted main effect plots and 3D plots from the artificial neural network (ANN) and response surface methodology (RSM) models to analyze the process. They reported, although ANN is better, those two models are efficient for prediction of mechanical properties.

Zhao et al. [15] proposed a 3d machine vision method to detect the 3d printing defects. They reported from their experimental tests, method is accurate and robust for both potential defect region extraction and accurate defect detection.

Purpose of this study is to investigate the relationship between shape and the dimensional accuracy of components manufactured through additive manufacturing. The investigation focused on the influence of shape on the dimensional accuracy of components manufactured through additive manufacturing. Capital letters from A to O were embossed on a rectangular plate using extrusion through join, cut to half the plate thickness, and cut through options with Autodesk Inventor Software. Capital letters have been selected as each of them has their own geometric features such as straight-line end and curved edges. By this way the effects of the geometric features were also measured. High-resolution images of the specimens were captured using a 20.2 Megapixels CCD camera. These images underwent various image processing techniques, including binarizing, edge detection, edge enhancement, and image correlation. The dimensional errors in the manufactured components were identified through correlation of the images of the three replicated parts embossed with join, cut half, and cut through.

## 2. MATERIAL AND METHOD

### 2.1. Specimen Design and Manufacturing

Models were created to precise dimensional measurements using CAD (Autodesk Inventor) software using joining, cutting and semi-deep cutting techniques. A diagram with capital letters A to O mounted on a square plate 150 mm long, 100 mm high and 3 mm thick. The text size of 15 mm was chosen to improve the resolution and quality of the text. The carefully designed model is then exported to the STL file format, which lays the foundation for 3D printing. The work continued with the printing of prototypes for accurate measurement of dimensions using a Prusa I3 desktop 3D machine (Figure 3) with a layer height of 90 to 300 microns and a diameter of 1.75 mm. Complex printing parameters were carefully configured using Simplified3D software (Figure 4).



Figure 3. Prusa I3 desktop 3D machine.

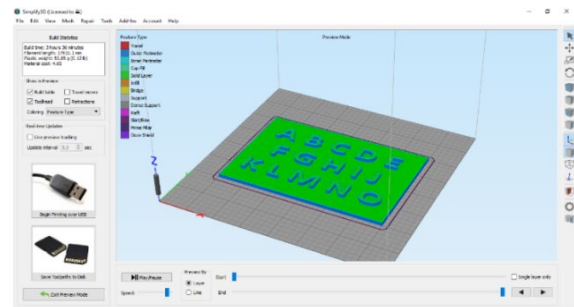


Figure 4. Printing settings of measurement samples [16].

The 3D printer's specifications include crucial parameters such as layer resolution, defining the thickness of each printed layer; build volume, determining the maximum print dimensions; XY positioning precision, ensuring accuracy in

the horizontal plane; Z positioning precision, affecting vertical layer alignment; filament diameter, indicating the material thickness used for printing; extruder temperature, specifying the temperature range for material extrusion; and print material, denoting the type of material employed. These specifications collectively influence the printer's capabilities, precision, and suitability for diverse applications, emphasizing the importance of understanding and optimizing each parameter for achieving desired 3D printing outcomes. In the scope of material versatility, the Prusa I3 3D printer showcases its capability by adeptly producing parts with both PLA and ABS materials. The printing process were meticulously managed, with a heated bed temperature of 60 °C strategically chosen to elevate bonding and enhance surface quality, complemented by an extruder temperature set precisely at 195 °C. The structural composition of the specimens was carefully designed, featuring a shell thickness of 0.8 mm, a layer height of 0.2 mm, and the incorporation of two shells to ensure robustness. The deliberate selection of a print speed at 80 mm/s further attests to the optimization of efficiency in the manufacturing process. Figure 6 visually encapsulates the tangible outcomes of three distinct manufacturing methods: (a) join, (b) cut, and (c) cut half. To explore the details of dimensional accuracy, the acquired images of replicated parts embossed with join, cut half, and cut through underwent a comprehensive analysis using various image processing techniques, such as binarizing and edge detection. This was followed by a correlation analysis aimed at identifying and understanding any potential dimensional errors within the manufactured components.



(a)



(b)



(c)

**Figure 5.** The produced samples (a) join (b) cut (c) cut half methods.

## 2.2. Dimensional Accuracy Assessment Through Image Processing Techniques

Edge detection, within the domain of digital image processing, serves as a cornerstone in image analysis by systematically identifying boundaries and transitions in image features. The underlying principle involves the recognition of intensity variations in image points, where distinct changes signify the presence of edges. The procedural steps in edge detection are integral to extracting valuable information from images, encompassing the acquisition of a color image, refinement to minimize noise while preserving authentic edges, intensification to enhance edge quality, thresholding to eliminate noisy edges based on magnitude, localization to estimate edge locations and pixel spacing, and the final retrieval of the processed image. In the context of digital image processing, an edge reflects alterations in light, color, and texture, providing essential cues for defining characteristics such as depth, size, orientation, and surface properties. This selectivity enables the selective identification of key edge points, making edge detection indispensable in applications like feature detection and extraction within the broader landscape of image processing [16 - 18]. Figure 6 serves as a schematic representation, delineating the sequential flow of the edge detection process. This academic discourse underscores the pivotal role of edge detection in extracting meaningful insights from digital images, contributing to advancements in fields ranging from computer vision to medical imaging.

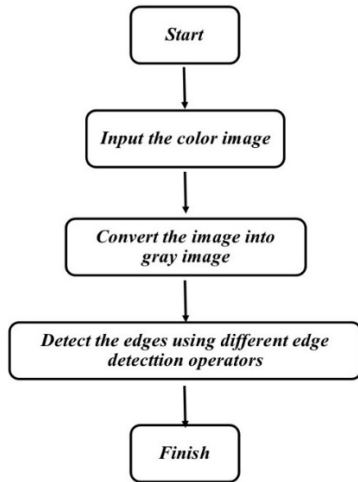


Figure 6. Flowchart of edge detection [16].

### 2.3. Image Correlation

For the image correlation, sample images were obtained from printed boards (printed through join, cut and cut to half depth of the plate thickness methods) and design environment of Autodesk Inventor (designed through join, cut and cut to half depth of the plate thickness with emboss) (Figure 7).

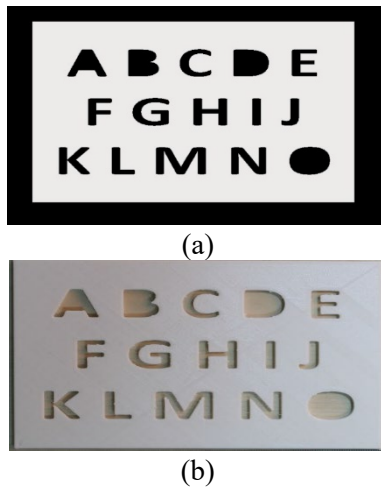


Figure 7. The images obtained from (a) design environment and (b) printer.

The images derived from edge-detected and enhanced images underwent a correlation process with the images acquired from the design environment and the physical parts produced through additive manufacturing. This correlation analysis serves as a crucial step in validating the fidelity and accuracy of the image processing techniques applied. By comparing the processed images with the original design and the tangible manufactured components, this correlation effort aims to assess the alignment

and congruence between the digital representation and the physical realization. The correlation results provide insights into the effectiveness of the edge detection and enhancement procedures in faithfully representing the intended design and the subsequent additive manufacturing outcomes.

### 3. RESULTS AND DISCUSSION

The images obtained from the additive manufacturing process and the design environment for specimens embossed with join, cut, and cut half are displayed in Figure 8.



Figure 8. Images from design environment and additive manufacturing from top to bottom for embossed with join, cut and cut half, respectively.

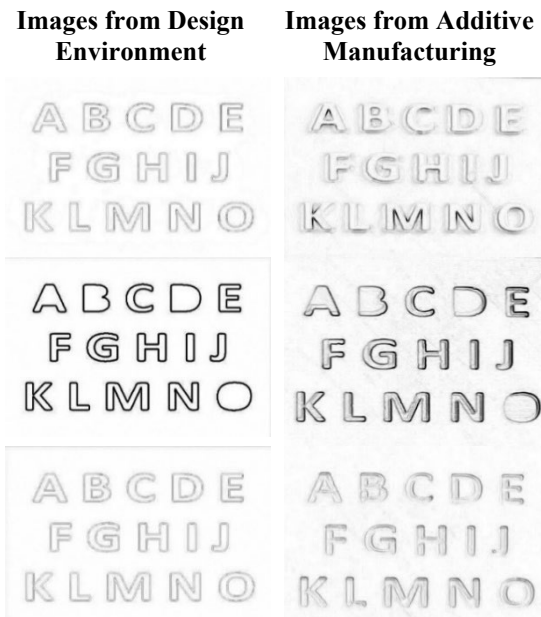


Figure 9. Images processed with edge detection from top to bottom for embossed with join, cut and cut-half, respectively.

The images processed using Sobel Edge filter from both the design environment and additive manufacturing for embossed with join, cut and cut-half, respectively are given in Figure 10. The correlation coefficients, computed using Matlab, were found to be 0.50, 0.28, and 0.37 for join, cut, and cut-half, respectively. The calculation of correlation coefficients was based on the entire plate, which included fifteen letters with different shapes. It is noteworthy that since each letter introduces a small amount of error, the accumulation of these errors contributes to a lower overall correlation coefficient.

#### 4. CONCLUSION

The study has contributed valuable insights into the intricate relationship between shape and dimensional accuracy in additive manufacturing. The computation of overall correlation coefficients, with values of 0.50, 0.28, and 0.37 for join, cut, and cut half, respectively, underscores the varying degrees of accuracy associated with different embossing techniques. Notably, the designed images exhibited near-perfect dimensions, highlighting the fidelity of the initial digital representation. In contrast, images derived from additive manufacturing showed more pronounced distortions, suggesting the presence of inherent challenges in achieving perfect replication through the manufacturing process.

Furthermore, the observed loss of information during resizing and transformation to gray level underscores the need for careful consideration in preprocessing steps to retain dimensional accuracy. The differential correlation coefficients between join, cut, and cut half emphasize the distinct impact of each embossing technique on the overall accuracy of the manufactured components.

As the research progresses, additional image processing and analyses are planned to explore deeper the specific influence of each letter in the images. This granular investigation aims to resolve the shape effects on dimensional accuracy, providing a comprehensive understanding that can inform optimization strategies for additive manufacturing processes. The outcomes of these forthcoming analyses are anticipated to contribute significantly to the refinement and enhancement of dimensional precision in 3D printed components.

#### ACKNOWLEDGES

This study was presented in " 4th International Congress on 3D Printing (Additive Manufacturing) Technologies " Congress. We declare special thanks to the board of congress.

#### REFERENCES

1. Turner, N., Strong, B. and Gold, S.A., "Review of melt extrusion additive manufacturing processes: I. Process design and modeling", *Rapid Prototyping Journal*, Vol. 20, Issue 3, Pages 192-204, 2014.
2. Turner, B.N and Gold, S.A., "A review of melt extrusion additive manufacturing processes: II. Materials, dimensional accuracy, and surface roughness", *Rapid Prototyping Journal*, Vol. 2, Issue 3, Pages 250-261, 2015.
3. Ahn, S.H., Montero, M., Odell, D., Roundy., S and Wright, P.K., "Anisotropic material properties of fused deposition modeling ABS", *Rapid prototyping journal*, Vol. 8, Issue 4, Pages 248-257, 2002.
4. Rodríguez, J.F., Thomas, J.P and Renaud, J.E., "Mechanical behavior of acrylonitrile butadiene styrene (ABS) fused deposition materials. Experimental investigation", *Rapid Prototyping Journal*, Vol. 7, Issue 3, Pages 148-158, 2001.
5. Hanon, M., László Z. and Quanjin M., "Accuracy investigation of 3D printed PLA with various process parameters and different colors", *Materials Today: Proceedings*, Vol. 42, Pages 3089-3096, 2021.
6. Akbaş, O. E., Hıra, O., Hervan, S. Z., Samankan, S. and Altınkaynak A., "A. Dimensional accuracy of FDM-printed polymer parts", *Rapid Prototyping Journal*, Vol. 26, Issue 2, Pages 288-298, 2020.
7. Borra N. and Venkata N., "Parametric optimization for dimensional correctness of 3D printed part using masked stereolithography: Taguchi method", *Rapid Prototyping Journal*, Vol. 29, Issue 1, Pages 166-184, 2023.
8. Resende, C. C. D., Barbosa, T. A. Q., Moura, G. F., Rizzante, F. A. P., Mendonça, G., Zancopé, K., and Neves, F. D., "Cost and effectiveness of 3-dimensionally printed model using three different printing layer parameters and two resins", *The Journal of Prosthetic Dentistry*, Vol. 129, Issue 2, Pages 350-353, 2023.
9. Zarean, P., Malgaroli, P., Zarean, P., Seiler, D., de Wild, M., Thieringer, F. M. and Sharma, N., "Effect of printing parameters on mechanical performance of material-extrusion 3D-printed PEEK specimens at the Point-of-care", *Applied Sciences*, Vol.13, Issue 3, 2023.

10. Akıncıoğlu G, Şirin E, Aslan E., “Tribological characteristics of ABS structures with different infill densities tested by pin-on-disc”, Proceedings of the Institution of Mechanical Engineers, Part J: Journal of Engineering Tribology. 2023 Vol. 237, Issue 5, Pages 1224-1234,2023.
11. Norani M.N, Abdollah M.F, Abdullah M.I, Amiruddin H, Ramli F.R, Tamaldin N, “3D printing parameters of acrylonitrile butadiene styrene polymer for friction and wear analysis using response surface methodology”, Proceedings of the Institution of Mechanical Engineers, Part J: Journal of Engineering Tribology, Vol.235, Issue 2, Pages 468-477, 2021.
12. Chand R., Sharma V.S., Trehan R., Gupta M.K., Sarikaya M., “Investigating the dimensional accuracy and surface roughness for 3D printed parts using a multi-jet printer”, Journal of Materials Engineering and Performance, Vol.32 Issue 3, Pages 1145-1159, 2023.
13. Buj-Corral I., Zayas-Figueras E.E., “Comparative study about dimensional accuracy and form errors of FFF printed spur gears using PLA and Nylon. Polymer Testing”, Vol. 117:107862,2023.
14. Moradi M., Beygi R., Mohd. Yusof N., Amiri A., da Silva L.F., Sharif S.,”3D printing of acrylonitrile butadiene styrene by fused deposition modeling: Artificial neural network and response surface method analyses” Journal of Materials Engineering and Performance, Vol.32, Issue 4 Pages 2016-2023,2023.
15. Zhao X., Li Q., Xiao M., He Z., “Defect detection of 3D printing surface based on geometric local domain features”, “The International Journal of Advanced Manufacturing Technology, Vol. 125, Pages 183-194, 2023.
16. Sucuoglu, H. S., Bogrekci, I. and Demircioglu, P., “The Effect of Shape on the Dimensional Accuracy for 3d Printed Parts”, In: 4th International Congress on 3d Printing (Additive Manufacturing) Technologies and Digital Industry, Pages 11-14, Antalya, Turkey, 2019.
17. Dharampal, M.V., “Methods of Image Edge Detection: A Review”, Journal of Electrical & Electronic Systems, Vol. 4, Issue 2, 2015.
18. Melin, P., González, C., Castro, J., Mendoza, O. and Castillo, O., “Edge detection method for image processing based on generalized type-2 fuzzy logic”, IEEE Transactions on Fuzzy Systems, Vol. 22, Pages 1515-1525, 2013.



ULUSLARARASI 3B YAZICI TEKNOLOJİLERİ  
VE DİJİTAL ENDÜSTRİ DERGİSİ

INTERNATIONAL JOURNAL OF 3D PRINTING  
TECHNOLOGIES AND DIGITAL INDUSTRY

ISSN:2602-3350 (Online)

URL: <https://dergipark.org.tr/ij3dptdi>

# INVESTIGATION OF THE EFFECTS OF PROCESS PARAMETERS ON MACHINING PERFORMANCE IN LASER CUTTING OF 3D-PRINTED PLA

**Yazarlar (Authors):** Oguzhan Der , Gokhan Basar 

***Bu makaleye şu şekilde atıfta bulunabilirsiniz (To cite to this article):*** Der O., Basar G., “Investigation of the Effects of Process Parameters on Machining Performance in Laser Cutting of 3D-Printed PLA” *Int. J. of 3D Printing Tech. Dig. Ind.*, 9(1): 9-20, (2025).

DOI: 10.46519/ij3dptdi.1581618

Araştırma Makale/ Research Article

Erişim Linki: (To link to this article): <https://dergipark.org.tr/en/pub/ij3dptdi/archive>

# INVESTIGATION OF THE EFFECTS OF PROCESS PARAMETERS ON MACHINING PERFORMANCE IN LASER CUTTING OF 3D-PRINTED PLA

Oguzhan Der<sup>a</sup> , Gokhan Basar<sup>b</sup> 

<sup>a</sup>Bandirma Onyedi Eylul University, Maritime Faculty, Marine Vehicles Management Engineering Department, TÜRKİYE

<sup>b</sup>Osmaniye Korkut Ata University, Engineering and Natural Sciences of Faculty, Industrial Engineering Department, TÜRKİYE

\* Corresponding Author: [oder@bandirma.edu.tr](mailto:oder@bandirma.edu.tr)

(Received: 08.11.24; Revised: 02.01.25; Accepted: 06.01.25)

---

## ABSTRACT

In the current research, the influences of process parameters on surface roughness and kerf width in CO<sub>2</sub> laser cutting of PLA plates produced by the fused filament fabrication method were experimentally investigated. Laser cutting was performed using three plate thicknesses (2, 3, and 4 mm), three cutting speeds (3, 6, and 9 mm/s), and three laser power levels (90, 95, and 100 W). Surface roughness was determined with a surface roughness tester, and kerf widths were evaluated using a digital microscope. The findings indicate that higher cutting speeds and lower laser power lead to a reduction in both surface roughness and kerf width. Higher cutting speeds combined with lower laser power decreased the thermal effect during cutting by reducing the interaction between the laser and material, resulting in lower surface roughness and narrower kerf width. The effect of plate thickness on surface roughness and kerf width was complex, varying with cutting speed and laser power. The lowest surface roughness (0.951 μm) and kerf width (0.793 mm) values were achieved with a plate thickness of 3 mm, a cutting speed of 9 mm/s, and a laser power of 90 W. This study provides valuable insights into how laser cutting parameters affect the surface quality and dimensional accuracy of PLA plates, contributing to quality improvements in industrial applications. The results highlight the essential influence of cutting speed and laser power on managing surface roughness and kerf width, thus aiding in optimizing the process.

**Keywords:** Laser cutting, Fused filament fabrication, PLA, Surface roughness, Kerf width.

---

## 1. INTRODUCTION

Polylactic Acid (PLA) is a biodegradable thermoplastic polymer sourced from renewable materials like cornstarch, sugarcane, and tapioca roots. Unlike petroleum-based plastics, PLA offers environmental sustainability due to its ability to decompose under industrial composting conditions [1]. Its desirable properties, including mechanical strength, stiffness, and thermal stability, make PLA suitable for diverse applications, such as packaging, biomedical devices, automotive parts, and 3D printing. Additionally, its relatively low melting point and ease of processing have led to widespread adoption in industries aiming to reduce environmental impact [2].

Recently, the use of PLA in additive manufacturing, particularly in Fused Filament Fabrication (FFF), has expanded significantly. Additive manufacturing, or 3D printing, enables the layer-by-layer creation of complex geometries that would be challenging or costly to produce through traditional subtractive methods [3]. In the FFF process, a heated thermoplastic filament, such as PLA, is extruded to form parts from a digital model. This technique provides high design flexibility and minimizes material waste, making it ideal for rapid prototyping and low-volume production [4]. PLA's characteristics—low shrinkage, high dimensional stability, and strong layer adhesion—make it a preferred material for FFF applications [5]. Its ease of handling and relatively low cost further increase

its accessibility for both industrial and consumer-level users [6].

Laser cutting has emerged as an essential post-processing technique for materials produced through additive manufacturing, especially for achieving precise and clean cuts [7]. Laser cutting uses a high-energy laser beam to vaporize or melt the material along a specified path, producing clean, accurate cuts with minimal contact. This non-mechanical approach is particularly advantageous for fragile or intricate 3D-printed parts, where traditional cutting methods may introduce stress or damage. For PLA, laser cutting maintains edge quality and dimensional accuracy, reducing the heat-affected zone and minimizing thermal distortion [8]. Additionally, laser cutting facilitates the rapid processing of complex patterns, making it ideal for components with fine details. By preserving both mechanical properties and aesthetic appearance, laser cutting is invaluable for producing functional prototypes and final products [9].

Research on laser cutting as a post-processing method for 3D-printed materials has focused heavily on PLA due to its precision and surface quality enhancement. For instance, Kechagias et al. explored the influence of laser power and cutting speed on surface roughness (Ra) and kerf angle of 3D-printed PLA plates, finding that lower cutting speeds improved surface quality while both speed and power affected kerf geometry significantly [10-11]. Similarly, Moradi et al. [12] optimized the laser cutting process for FDM-printed PLA, analyzing kerf width, taper ratio, and the effects of focal plane position, laser power, and cutting speed. Fountas et al. [10] applied neural networks to predict optimal process settings, examining the effects of laser parameters on kerf angle and Ra in PLA/wood composites. In a related study, Kechagias et al. [13] employed genetic algorithms and neural networks to optimize kerf geometry and Ra during CO<sub>2</sub> laser cutting of PLA, developing predictive models for industrial applications. More recently, Tsiolikas et al. [14] introduced a hybrid approach combining fuzzy logic and grey relational analysis to enhance surface quality and dimensional accuracy in 3D-printed parts.

This study aims to experimentally investigate the impact of process parameters on Ra and kerf width during CO<sub>2</sub> laser cutting of PLA materials produced via fused filament fabrication. It serves as a pioneering contribution to scientific research by examining the effects of cutting conditions to achieve precise and high-quality cuts in the laser processing of 3D-printed PLA materials.

## 2. MATERIALS AND METHODS

The PLA filament used in this study was supplied by Filameon, featuring a 1.75 mm diameter and recognized for its excellent printability and mechanical properties. Samples were produced using FFF technology on a TEIRA3D 3D printer. The printing settings were as follows: a nozzle temperature of 215°C, a bed temperature of 60°C, a printing speed of 40 mm/s, and a layer height of 0.24 mm. The infill density was set to 100%, with four shell layers applied to both the top and bottom surfaces. The samples, designed in SolidWorks 2020 CAD software, measured 130 × 130 mm and varied in thickness (2, 3, and 4 mm). G-codes for 3D printing were generated using PrusaSlicer 2.6.1. The manufacturing process flow of PLA materials via fused filament fabrication is illustrated in Figure 1.

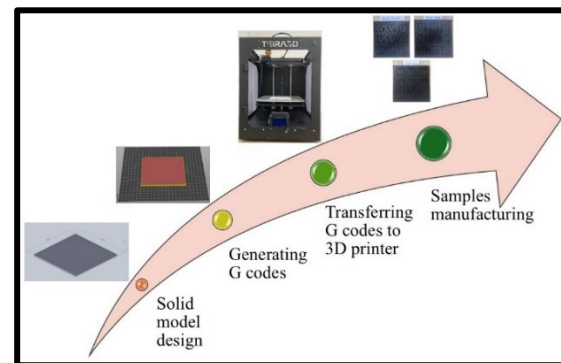


**Figure 1.** Manufacturing flow of 3D printed PLA with fused filament fabrication.

The CO<sub>2</sub> laser cutting process was conducted using a LazerFix LF7010 Laser Cutting Machine (Figure 2). For all experiments, the laser nozzle was positioned 7 mm above the workpiece. Compressed air was used to expel molten material and to protect the optics from debris. Plate thickness, cutting speed, and power were selected as the experimental parameters for the laser cutting process. Table 1 presents the experimental parameters and their levels. To ensure stability during the process,

the samples were securely fixed to the laser cutting table using polypropylene material.



**Figure 2.** CO<sub>2</sub> laser cutting device.

Laser power levels of 90, 95, and 100 W were chosen based on preliminary experiments to ensure effective cutting of PLA plates across all thicknesses without causing excessive thermal damage. Furthermore, similar power levels have been reported in previous studies [11-12] to yield favorable results for cutting thermoplastic materials, further validating their selection for this study. These selected levels are also relevant to industrial practices, representing typical power settings for CO<sub>2</sub> laser cutting of thermoplastics.

**Table 1.** Parameters and levels utilized in the laser cutting process.

Factor	Level	Level	Level
	1	2	3
Plate thickness (mm)	2	3	4
Cutting speed (mm/s)	3	6	9
Power (W)	90	95	100

Following a full factorial experimental design, 27 experiments were performed. For each plate thickness shown in Figure 3, nine laser cutting trials were carried out on 3D-printed PLA materials, with three different cutting speeds and three power levels. A full factorial experimental design was employed to evaluate the effects of laser power, cutting speed, and plate thickness on kerf width and surface roughness. This design systematically examines all possible combinations of the selected parameters, ensuring a comprehensive analysis of their individual and interaction effects. By testing each combination, the study achieves high statistical reliability and robust

conclusions regarding the influence of process parameters. Additionally, the factorial design facilitates the optimization of laser cutting parameters for improving both dimensional accuracy and surface quality, making the findings broadly applicable to various industrial applications.

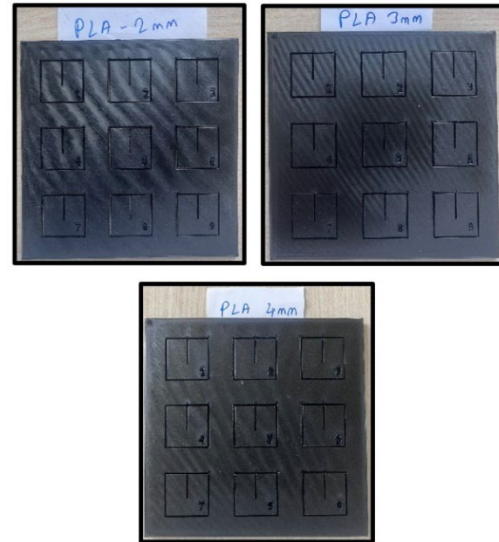


**Figure 3.** 3D printed PLA materials cut by laser.

Upon completion of the cutting process, the surface roughness (Ra) and kerf width of the cut samples were measured to evaluate the impact of the parameters. Precision instruments were employed to ensure accurate assessments of cut quality. Ra was measured on the cut surfaces using a DAILYAID DR100 model device, with nine readings taken for each experimental condition to calculate an average value. Kerf width was measured using a digital microscope (Dino-Lite AM4113T), with four measurements taken per condition, followed by calculating an average value. Figure 4 shows the surface roughness measurement device and the digital microscope.

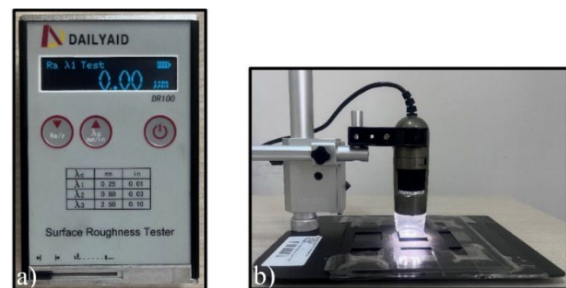


**Figure 4.** Devices used in measurements a) Surface roughness device b) Digital microscope.

### 3. RESULTS AND DISCUSSION

#### 3.1. Evaluation of Surface Roughness

The Ra values obtained at a laser power of 90 W, with different plate thicknesses (2, 3, and 4 mm) and cutting speeds (3, 6, and 9 mm/s), are shown in Figure 5. Overall, an increase in cutting speed resulted in a decrease in Ra. This reduction is attributed to the shortened interaction time between the laser and material at higher speeds, which reduces energy accumulation and contributes to a smoother surface [12, 14]. For instance, at a plate thickness of 2 mm, raising the cutting speed from 3 mm/s to 6 mm/s led to an 18.48% reduction in Ra, decreasing from 2.506  $\mu\text{m}$  to 2.043  $\mu\text{m}$ . Increasing the speed further to 9 mm/s lowered Ra by an additional 27.70%, reducing it to 1.477  $\mu\text{m}$ . The reduction in surface roughness at higher cutting speeds can be attributed to the shorter interaction time between the laser beam and the material surface. This limits the accumulation of thermal energy, preventing excessive melting and the formation of surface irregularities. Furthermore, higher speeds reduce the HAZ and material swelling caused by prolonged thermal exposure, resulting in a smoother and more homogeneous surface. These findings align with observations from previous studies [14], which indicate that faster cutting speeds improve surface quality by reducing thermal degradation. By increasing the speed, this localized overheating effect is diminished, resulting in improved surface

homogeneity and lower surface roughness. Likewise, for a 3 mm thick plate, Ra at 3 mm/s cutting speed was 2.352  $\mu\text{m}$ ; raising the speed to 6 mm/s led to a 47.87% reduction to 1.226  $\mu\text{m}$ , and at 9 mm/s, Ra further decreased by 59.57% to 0.951  $\mu\text{m}$ . These results indicate that increased speed reduces the interaction time between the laser and material, thus decreasing surface roughness and providing a more homogeneous surface. Moradi et al. [12] also observed a decrease in surface roughness with higher laser speeds, achieving optimal cutting quality. For the 4 mm thick plate, surface roughness at 3 mm/s cutting speed was 2.118  $\mu\text{m}$ ; increasing the speed to 6 mm/s reduced surface roughness by 37.87% to 1.316  $\mu\text{m}$ , and further to 1.167  $\mu\text{m}$  at 9 mm/s, marking a 44.90% reduction. These findings demonstrate that increasing laser cutting speed reduces surface roughness and minimizes thermal effects during cutting, resulting in a smoother surface. The effect of plate thickness on surface roughness is also noteworthy. In general, thinner plates (2 mm) exhibited higher surface roughness, while increasing thickness resulted in reduced surface roughness values. For instance, at a cutting speed of 3 mm/s, a 3 mm thick plate showed a 6.15% lower surface roughness (2.352  $\mu\text{m}$  compared to 2.506  $\mu\text{m}$  for the 2 mm plate).

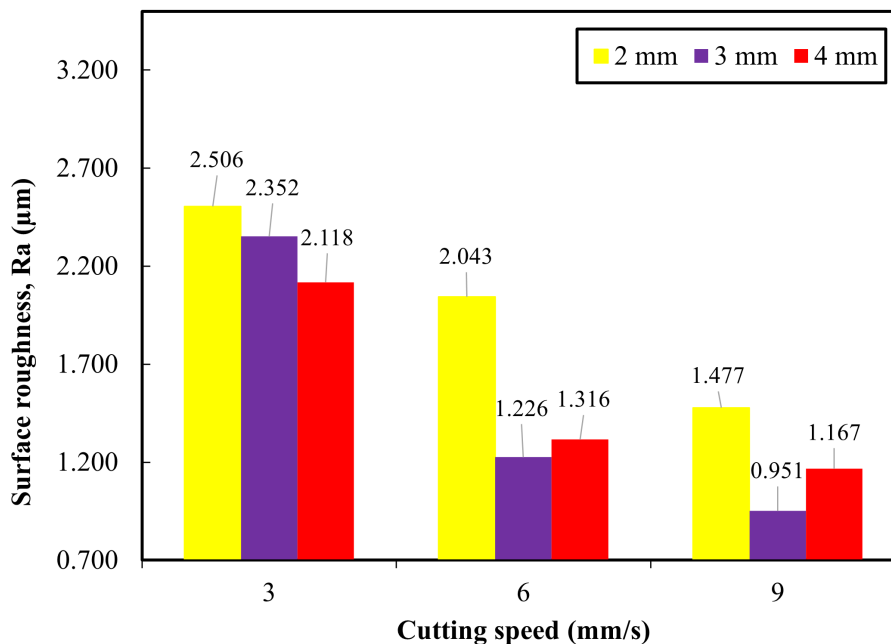
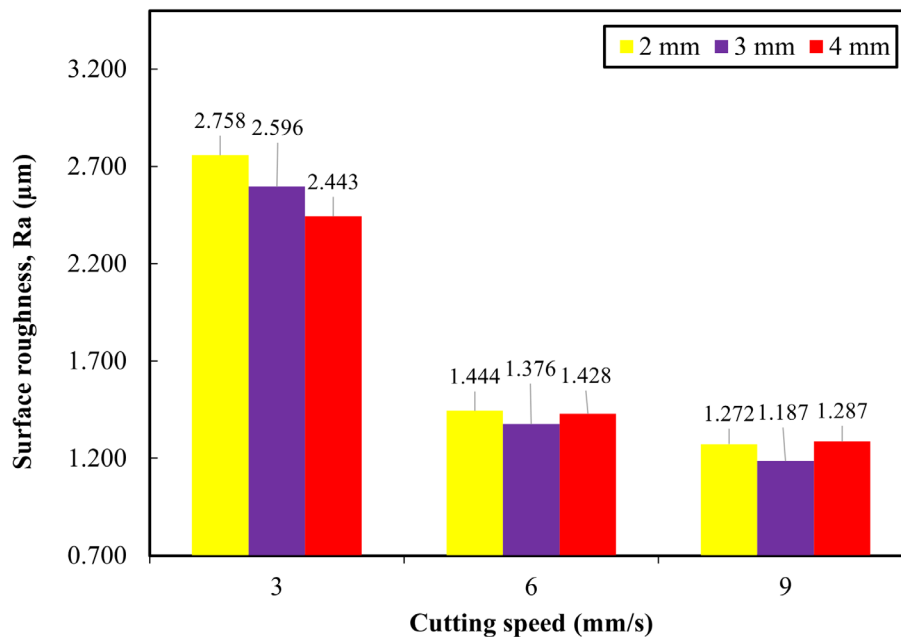


Figure 5. Surface roughness depending on cutting speed and plate thickness at 90 W power.

Similarly, for a 4 mm thick plate at the same speed, surface roughness further decreased by 9.95% to 2.118  $\mu\text{m}$ , providing a smoother surface. At a cutting speed of 6 mm/s, surface roughness for a 2 mm thick plate decreased by 18.48%, from 2.506  $\mu\text{m}$  to 2.043  $\mu\text{m}$ . A 3 mm thick plate showed a 47.87% reduction (from 2.352  $\mu\text{m}$  to 1.226  $\mu\text{m}$ ), achieving a lower surface roughness. For the 4 mm thick plate, surface roughness decreased by 37.87% from 2.118  $\mu\text{m}$  to 1.316  $\mu\text{m}$ . At the highest cutting speed (9 mm/s), surface roughness for a 2 mm thick plate dropped by 41.06%, from 2.506  $\mu\text{m}$  to 1.477  $\mu\text{m}$ , while a 3 mm thick plate achieved a 59.57% lower surface roughness (2.352  $\mu\text{m}$  to 0.951  $\mu\text{m}$ ). For a 4 mm thick plate, surface roughness decreased by 44.90%, from 2.118  $\mu\text{m}$  to 1.167  $\mu\text{m}$ . This trend suggests that thicker plates produce a more uniform cut when interacting with the laser beam. As noted by Tsiolikas et al. [14], thicker plates processed by laser tend to exhibit lower surface roughness due to more homogeneous energy distribution and transfer. Moradi et al. [12] also emphasized that energy absorption in thicker materials is more uniform, resulting in reduced surface roughness. Surface roughness values obtained at a laser power of 95 W across different plate thicknesses (2, 3, and 4 mm) and cutting speeds (3, 6, and 9 mm/s) are shown in Figure 6. A clear reduction in surface roughness was observed as cutting speed increased.

For instance, with a 2 mm thick plate, increasing the cutting speed from 3 mm/s to 6 mm/s resulted in a 47.64% decrease in surface roughness, from 2.758  $\mu\text{m}$  to 1.444  $\mu\text{m}$ . Further raising the speed to 9 mm/s reduced surface roughness by an additional 11.91%, bringing it down to 1.272  $\mu\text{m}$ . For a 3 mm thick plate, the surface roughness at 3 mm/s was 2.596  $\mu\text{m}$ . Increasing the speed to 6 mm/s led to a 47% reduction to 1.376  $\mu\text{m}$ , and at 9 mm/s, surface roughness further dropped by 54.28% to 1.187  $\mu\text{m}$ . For the 4 mm thick plate, surface roughness at 3 mm/s was 2.443  $\mu\text{m}$ . Increasing the speed to 6 mm/s reduced it by 41.55% to 1.428  $\mu\text{m}$ , and at 9 mm/s, it further decreased by 47.32% to 1.287  $\mu\text{m}$ . The impact of plate thickness on surface roughness is also noteworthy. In general, thinner plates (2 mm) exhibited higher surface roughness, while an increase in thickness tended to result in lower surface roughness values. For instance, at a cutting speed of 3 mm/s, a 3 mm thick plate achieved a 5.87% lower surface roughness (2.596  $\mu\text{m}$  compared to 2.758  $\mu\text{m}$  for the 2 mm plate). Similarly, a 4 mm thick plate showed an additional 5.89% reduction in Ra (from 2.596  $\mu\text{m}$  to 2.443  $\mu\text{m}$ ), producing a smoother surface. When the cutting speed was set to 6 mm/s, surface roughness values for the 2-, 3- and 4-mm plates were measured at 1.444  $\mu\text{m}$ , 1.376  $\mu\text{m}$ , and 1.428  $\mu\text{m}$ , respectively, with the 3 mm plate exhibiting the lowest surface roughness.



**Figure 6.** Surface roughness depending on cutting speed and plate thickness at 95 W power.

At an increased cutting speed of 9 mm/s, surface roughness further decreased across all thicknesses, with values recorded at 1.272  $\mu\text{m}$  for the 2 mm plate, 1.187  $\mu\text{m}$  for the 3 mm plate, and 1.287  $\mu\text{m}$  for the 4 mm plate. These results indicate that increasing laser cutting speed reduces surface roughness, contributing to a smoother finish by minimizing thermal effects during cutting. Additionally, the trend of decreasing surface roughness with increasing plate thickness suggests that thicker plates allow for a more uniform surface under the laser beam, thereby enhancing surface quality. Figure 7 shows the Ra values measured for 3D-printed PLA materials at a constant laser power of 100 W with varying parameters. Surface roughness decreased with increasing cutting speed. For instance, with a 2 mm thick plate, increasing the cutting speed from 3 mm/s to 6 mm/s reduced Ra by 43.95%, from 2.983  $\mu\text{m}$  to 1.672  $\mu\text{m}$ . A further increase in speed to 9 mm/s lowered surface roughness by an additional 8.07%, reaching 1.537  $\mu\text{m}$ . Similarly, for a 3 mm thick plate, surface roughness at 3 mm/s was 2.758  $\mu\text{m}$ ; raising the speed to 6 mm/s resulted in a 41.44% reduction to 1.615  $\mu\text{m}$ , and at 9 mm/s, Ra decreased by 49.60% to 1.390  $\mu\text{m}$ . For a 4 mm thick plate, surface roughness at a cutting speed of 3 mm/s was 2.691  $\mu\text{m}$ ; increasing the speed to 6 mm/s reduced it by 41.32% to 1.579  $\mu\text{m}$ , and at 9 mm/s, Ra was further reduced by 51.77% to 1.298  $\mu\text{m}$ .

The influence of plate thickness on surface roughness is evident when evaluated alongside cutting speed. In general, thinner plates (2 mm) exhibited higher surface roughness, while an increase in plate thickness correlated with lower surface roughness values. For example, at a cutting speed of 9 mm/s, comparing Ra values for the 2 mm and 3 mm thick plates showed a reduction of 9.56%, from 1.537  $\mu\text{m}$  to 1.390  $\mu\text{m}$ . Similarly, comparing the 3 mm and 4 mm thick plates at the same speed, the 4 mm thickness showed an additional 6.62% reduction in Ra, from 1.390  $\mu\text{m}$  to 1.298  $\mu\text{m}$ . These results suggest that thicker plates and higher cutting speeds enable a more uniform interaction with the laser beam, thereby enhancing surface quality. Figure 8 shows cross-sectional images of surfaces obtained at different cutting speeds with a plate thickness of 3 mm and a laser power of 90 W. The images reveal a noticeable improvement in surface quality as cutting speed increases. At the lowest cutting speed of 3 mm/s, distinct irregularities and surface unevenness are observed. Due to the longer interaction time between the laser and the material at this speed, energy accumulation on the surface increases, resulting in a higher Ra of 2.352  $\mu\text{m}$ . At a cutting speed of 6 mm/s, there is a moderate improvement in surface quality, as the shorter interaction time reduces energy accumulation on the surface, bringing the surface roughness down to 1.226  $\mu\text{m}$ .

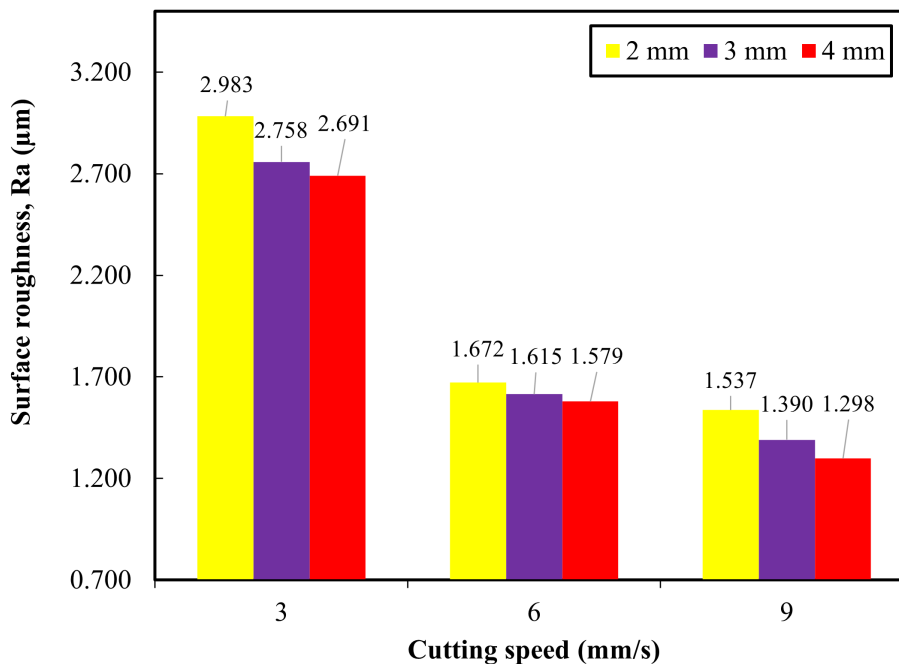
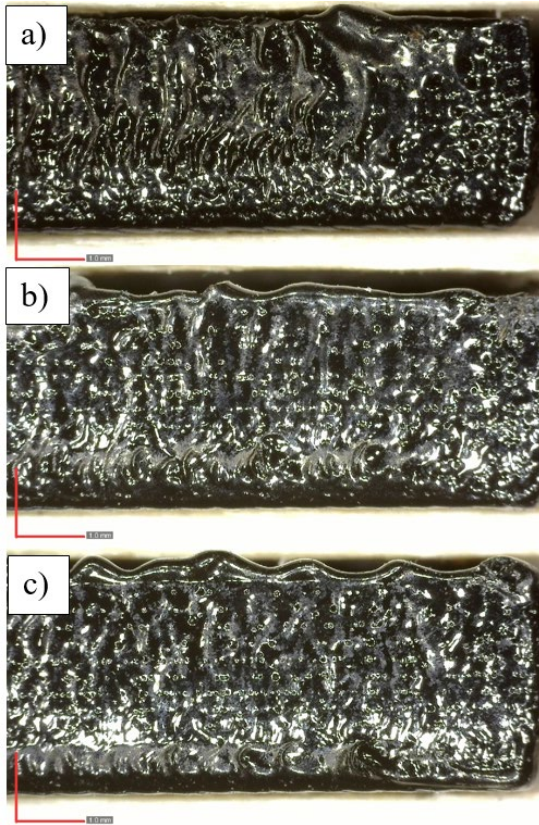


Figure 7. Surface roughness depending on cutting speed and plate thickness at 100 W power.

At the highest speed of 9 mm/s, surface quality reaches its optimal level; the brief contact between the laser and the material results in minimal energy build-up and reduced thermal impact, lowering surface roughness to its minimum level of 0.951  $\mu\text{m}$ . These observations align with previous findings, confirming that increased cutting speed reduces surface roughness and enhances surface quality.



**Figure 8.** Laser cutting at different speeds for 3 mm thickness and 90 W power a) 3 mm/s, b) 6 mm/s and c) 9 mm/s.

Figure 9 illustrates the effect of laser power (90, 95, and 100 W) on average surface roughness. A notable increase in Ra was observed with rising laser power. For example, the average Ra at 90 W was 1.684  $\mu\text{m}$ , which increased by 4.22% to 1.755  $\mu\text{m}$  at 95 W and further by 10.94% to 1.947  $\mu\text{m}$  at 100 W. These findings indicate that higher laser power leads to greater energy density on the surface, resulting in more pronounced melting and surface irregularities in the material. Increased laser power causes greater energy accumulation on the surface, which raises the extent of melting and leads to a significant increase in surface roughness. These results demonstrate that higher laser power reduces surface quality, as the increased energy density negatively impacts surface roughness.

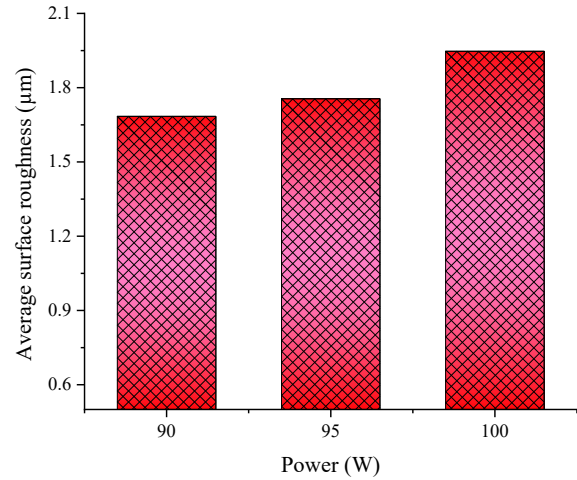


**Figure 9.** Average surface roughness at different powers.

### 3.2. Evaluation of Kerf Width

The kerf widths of 3D-printed PLA material were examined by cutting it at 90 W power with three different plate thicknesses and three different cutting speeds; the results are shown in Figure 10. The highest kerf width, measured at 1.071 mm, was observed with a plate thickness of 2 mm and a cutting speed of 3 mm/s. When the cutting speed was increased to 6 mm/s and 9 mm/s, the kerf width for the 2 mm thick plate decreased by 12.89% and 24.09%, respectively. At the same laser power, the kerf width for a 3 mm thick plate at a cutting speed of 3 mm/s was 0.979 mm, reaching the lowest value of 0.793 mm at 9 mm/s. At lower cutting speeds, the prolonged interaction time between the laser and the material allows for significant heat accumulation, particularly in thicker plates. This increased heat transfer leads to a wider kerf width due to greater melting of the material. In contrast, thinner plates exhibit narrower kerf widths at the same cutting speed, as the heat dissipates more quickly. As the cutting speed increases, the interaction time decreases, limiting heat accumulation and minimizing the influence of plate thickness on kerf width. These trends highlight the critical role of optimizing cutting speed and thickness to achieve precise kerf dimensions. In general, increasing the cutting speed for all plate thicknesses reduced the energy transfer in the cutting zone by decreasing the interaction time between the laser beam and material, which in turn reduced melting and led to narrower kerf widths [15-16]. At a low cutting speed (3 mm/s), variations in kerf width were observed with increasing plate thickness.

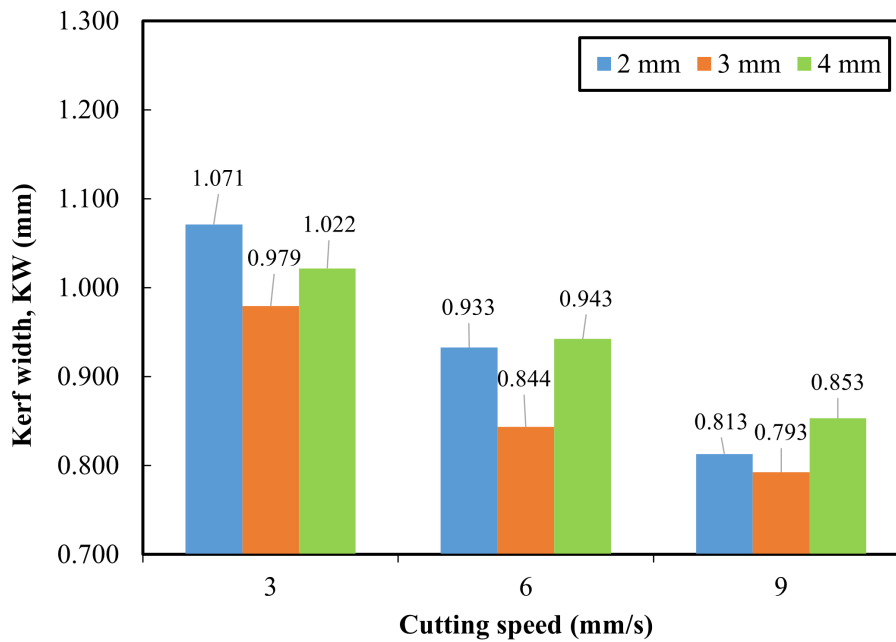


**Figure 10.** Kerf widths depending on cutting speed and plate thickness at 90 W power.

As the plate thickness rose from 2 to 3 mm, the kerf width contracted by 8.59%. However, when the thickness advanced further from 3 to 4 mm, the kerf width expanded by 4.39%. These findings align with literature suggesting that thicker plates at lower cutting speeds absorb more heat, leading to increased melting [11]. At cutting speeds of 6-9 mm/s, the widest kerf values were observed for 4 mm thick plates [12, 17]. This trend of increasing kerf width with plate thickness at lower speeds can be attributed to thicker plates spreading the laser beam's effect over a larger area, enhancing heat distribution. It is emphasized that laser processing parameters have a significant impact on cutting operations and should be optimized according to plate thickness and cutting speed [12, 18]. These results indicate that careful selection of process parameters is critical to improve laser cutting quality. Figure 11 presents the kerf widths obtained at a laser power of 95 W for three different plate thicknesses and cutting speeds. A clear reduction in kerf width was observed across all plate thicknesses as cutting speed increased. For example, with a 2 mm thick plate, increasing the cutting speed from 3 mm/s to 6 mm/s reduced the kerf width by 14.47%, from 1.099 mm to 0.940 mm. Further increasing the speed to 9 mm/s led to an additional 21.20% reduction, yielding a kerf width of 0.866 mm. Similarly, for a 3 mm thick plate, increasing the cutting speed from 3 mm/s to 6 mm/s reduced the kerf width by 10.57%, from 0.946 mm to 0.846 mm,

and further increasing the speed to 9 mm/s resulted in a 12.05% reduction, reaching 0.832 mm. For a 4 mm thick plate, the kerf width was 1.043 mm at a cutting speed of 3 mm/s. Raising the speed to 6 mm/s decreased the kerf width by 6.33%, bringing it to 0.977 mm, and further increasing to 9 mm/s led to a 15.34% reduction, resulting in a kerf width of 0.883 mm. At a low cutting speed (3 mm/s), variations in kerf width were observed with increasing plate thickness. Increasing the thickness from 2 to 3 mm led to a 13.92% decrease in kerf width (from 1.099 mm to 0.946 mm), while increasing thickness from 3 mm to 4 mm caused a 10.25% rise, reaching 1.043 mm. These results indicate an overall trend of decreasing kerf width with higher cutting speeds; however, variations in kerf width were seen at lower speeds depending on plate thickness. This can be attributed to the laser's larger area of influence on thicker materials and the extended interaction time at lower speeds, resulting in a wider kerf. Figure 12 shows the kerf widths obtained from the laser cutting process conducted at a power level of 100 W, using different plate thicknesses and cutting speeds. Generally, an increase in cutting speed led to a reduction in kerf width. For instance, for a 2 mm thick plate, increasing the cutting speed from 3 mm/s to 6 mm/s reduced the kerf width by 18.64%, from 1.164 mm to 0.947 mm. Further increasing the speed to 9 mm/s decreased the kerf width by an additional 22.34%, resulting in a final width of 0.904 mm.

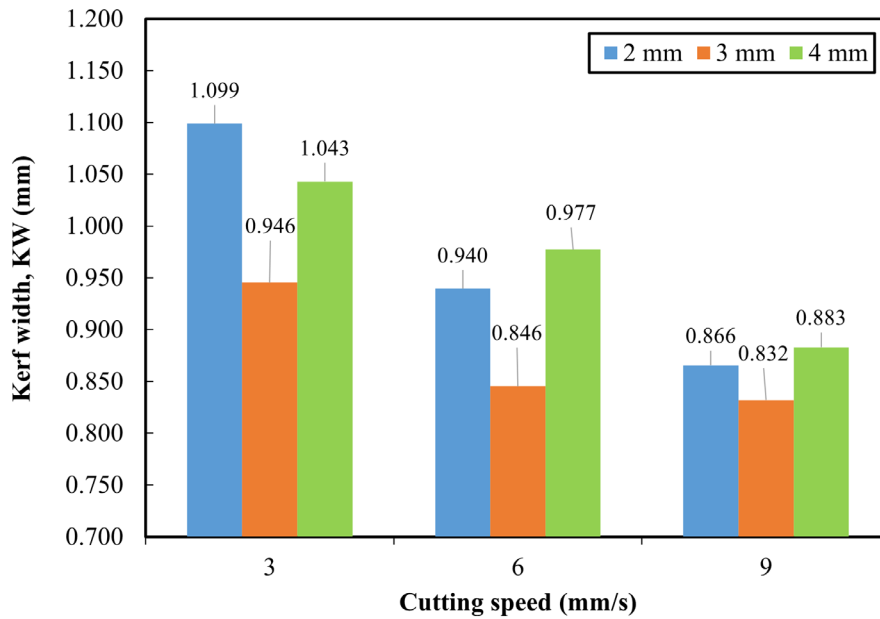


**Figure 11.** Kerf widths depending on cutting speed and plate thickness at 95 W power.

For a 3 mm thick plate, the kerf width at a cutting speed of 3 mm/s was 0.938 mm; raising the speed to 6 mm/s reduced the kerf width by 10.55% to 0.839 mm, and a further increase to 9 mm/s reduced it by 12.05%, bringing it down to 0.825 mm. For a 4 mm thick plate, the kerf width measured 1.030 mm at a cutting speed of 3 mm/s. Increasing the speed to 6 mm/s lowered the kerf width by 6.89%, reducing it to 0.959 mm, while a further increase to 9 mm/s resulted in a 16.70% reduction, bringing the kerf width down to 0.858 mm. Overall, at a laser power of 100 W, higher cutting speeds resulted in narrower kerf widths across all plate thicknesses.

This outcome can be attributed to the reduced interaction time between the laser beam and the material, which decreases the amount of melting and produces a narrower kerf. Additionally, an increase in kerf width was observed with greater plate thicknesses at lower cutting speeds, likely due to higher heat absorption in thicker plates. Figure 13 shows the microscope images and measurement pictures of the kerf widths after laser cutting at 2 mm plate thickness, 90 W power and three different cutting speeds (3, 6 and 9 mm/s).

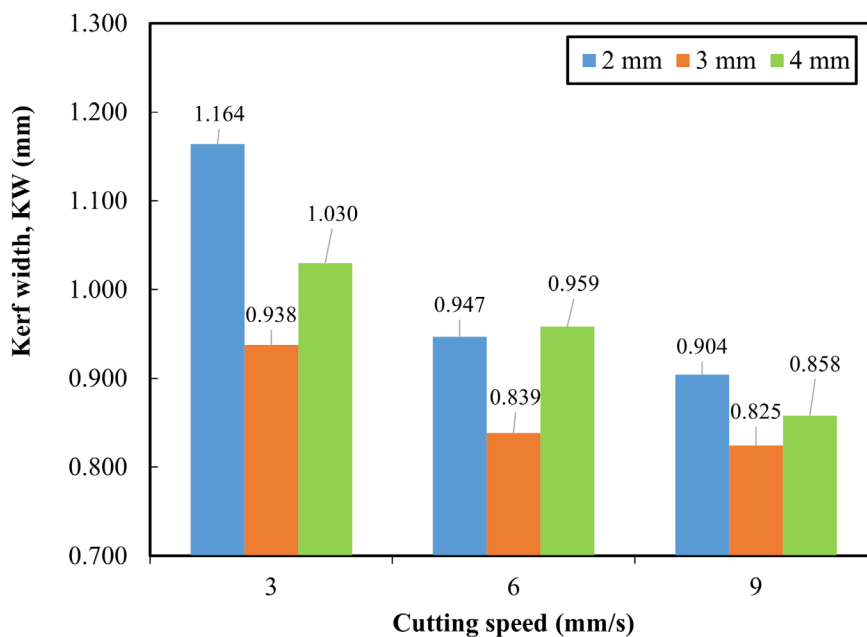


**Figure 12.** Kerf widths depending on cutting speed and plate thickness at 100 W power.

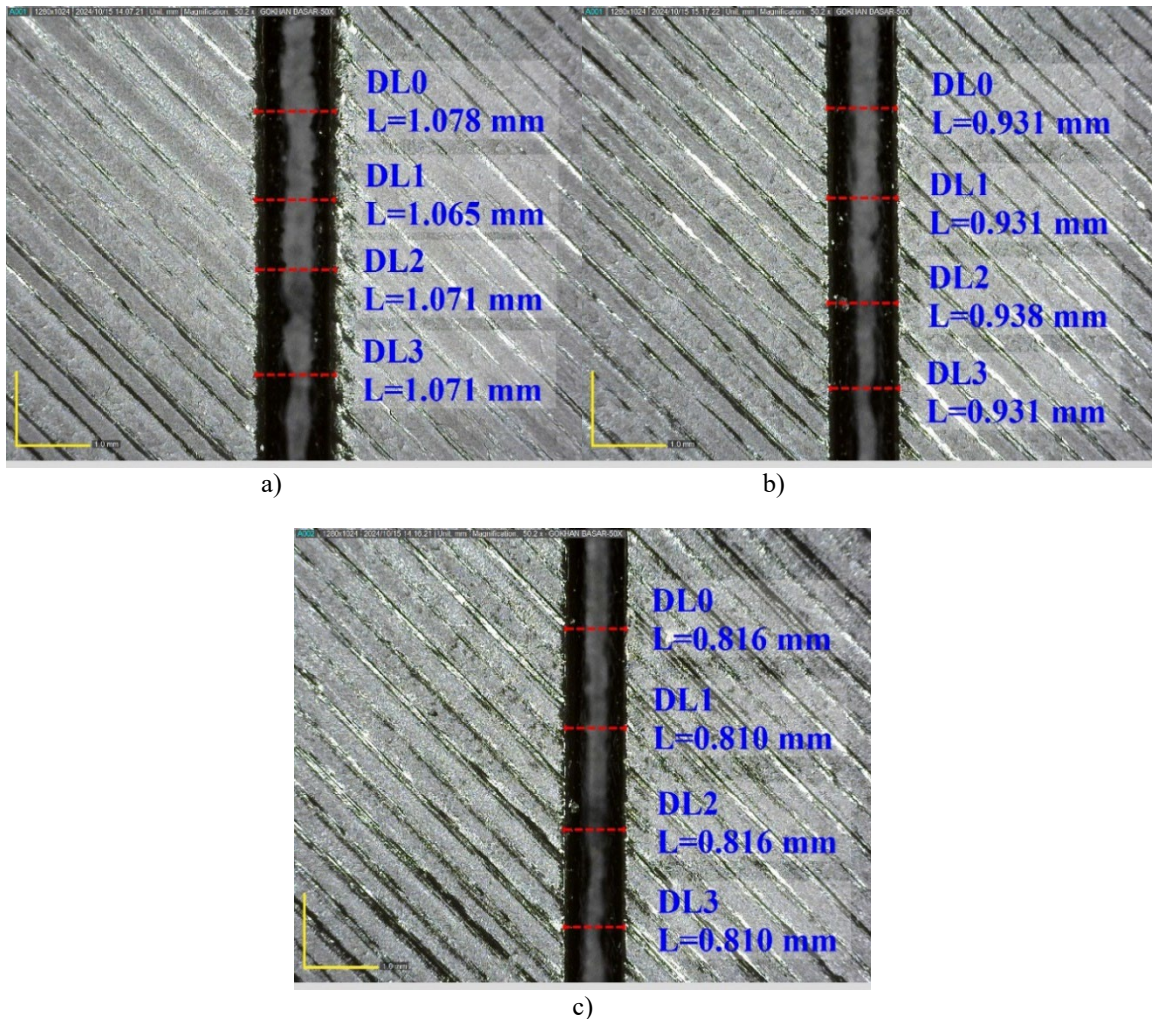


**Figure 13.** Laser cutting at different speeds for 2 mm thickness and 90 W power  
a) 3 mm/s, b) 6 mm/s and c) 9 mm/s.

An examination of the figure shows that kerf widths decrease as the speed rises. In the first image, kerf width measurements for a speed of 3 mm/s range from 1.078 mm to 1.071 mm, reflecting the relatively wide kerf width expected at low speeds. As the cutting speed increased, the kerf width consistently declined, as illustrated in the second image (6 mm/s), where the kerf width fell between 0.931 mm and 0.938 mm, and in the third image (9 mm/s), where it ranged from 0.810 mm to 0.816 mm. These trends are consistent with the literature where studies by Kechagias et al. [11] and Sabri et al. [19] similarly reported that increasing cutting speeds resulted in more consistent and narrower kerf widths. Figure 14 shows the average kerf widths resulting from laser cutting at different power levels. The average kerf widths for 3D-printed PLA cut at 90, 95, and 100 W were calculated as 0.917, 0.937, and 0.940 mm, respectively. An increase in kerf width was observed with rising power levels, with the lowest kerf width occurring at 90 W

and the highest at 100 W. However, the increase in kerf width with higher power levels was not significant, suggesting that the limited laser cutting time, combined with a certain level of energy density, was sufficient to achieve adequate melting without further widening the kerf. While an upward trend in average kerf width was observed with increasing laser power, this increase was minimal. This result can be attributed to the accumulation of more energy on the material surface as laser power increases, leading to a greater amount of melted material. The increase in the amount of melting widens the kerf. These findings align with other studies on the effect of laser power on kerf width and are consistent with the work by Moradi et al., which also examined the relationship between laser power and kerf width [12].

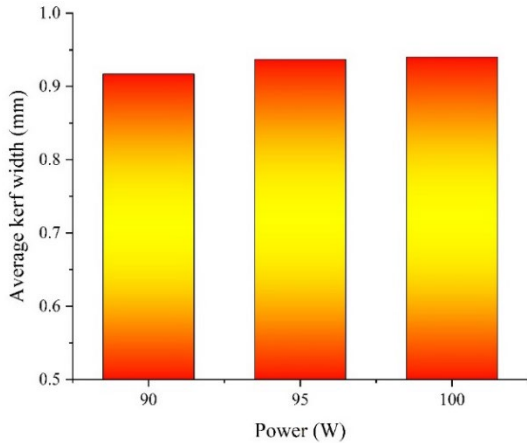


**Figure 14.** Average kerf widths at different powers.

#### 4. CONCLUSIONS

The influence of cutting parameters—plate thickness, cutting speed, and laser power—on surface roughness and kerf width in CO<sub>2</sub> laser cutting of PLA materials made by fused filament fabrication was examined through experimental investigation. The findings obtained from the investigation are summarized below:

- At the lowest cutting speed (3 mm/s), the smallest kerf width was achieved with a 2 mm plate thickness regardless of laser power. Under these conditions, kerf width increased as laser power increased.
  - When all cutting conditions are considered, kerf width decreased when plate thickness increased from 2 mm to 3 mm, whereas a further increase in plate thickness to 4 mm resulted in an increase in kerf width.
  - Under all laser cutting conditions, the minimum kerf width of 0.793 mm was achieved with a 3 mm plate thickness, a cutting speed of 9 mm/s, and a laser power of 90 W. In contrast, the maximum kerf width of 1.164 mm occurred with a 2 mm plate thickness, a cutting speed of 3 mm/s, and a laser power of 100 W.
- Ra reduced with rising cutting speed at for all laser power levels.
  - In laser cutting operations performed at low cutting speeds, Ra decreased as plate thickness increased. Moreover, at these low cutting speeds, surface roughness values rose with an increase in laser power.
  - The lowest Ra (2.118 μm) at low cutting speed (3 mm/s) was measured with a plate thickness of 4 mm and the lowest laser power (90 W).
  - The lowest surface roughness observed in laser cutting processes conducted at 90 and 95 W laser power and cutting speeds of 6 and 9 mm/s was achieved with a plate thickness of 4 mm.
  - Across all laser cutting conditions, the lowest surface roughness (0.951 μm) was achieved with a plate thickness of 3 mm, cutting speed of 9 mm/s, and laser power of 90 W, whereas the highest surface roughness (2.983 μm) was obtained with a plate thickness of 2 mm, cutting speed of 3 mm/s, and laser power of 100 W.
  - Kerf width was reduced with higher cutting speeds and lower laser power across all plate thicknesses.

This study demonstrates the importance of carefully selecting cutting parameters to achieve optimal surface quality and minimum kerf width in CO<sub>2</sub> laser cutting. Increasing cutting speed, adjusting laser power, and optimizing plate thickness play critical roles in achieving high precision and quality surfaces in industrial applications. The findings of this study hold significant potential for various industrial applications. In rapid prototyping and additive manufacturing, the optimized laser cutting parameters enable precise and high-quality processing of 3D-printed PLA components, reducing post-processing needs. In biomedical applications, the results facilitate the accurate fabrication of complex geometries, critical for implants and custom prosthetics. Additionally, the packaging industry can use these findings to enhance the efficiency of eco-friendly PLA product manufacturing. By reducing kerf width and surface roughness, the study's optimized parameters improve manufacturing efficiency, minimize material waste, and lower production costs, making the approach applicable across multiple industries requiring precision and sustainability.

#### ACKNOWLEDGMENTS

This work was supported by Scientific Research Projects Coordination Unit of Bandırma Onyedi Eylül University under Project Number: BAP-24-1003-003.

## REFERENCES

1. Altan, M., Eryildiz, M., Gumus, B., Kahraman, Y., "Effects of process parameters on the quality of PLA products fabricated by fused deposition modeling (FDM): Surface roughness and tensile strength", *Materials Testing*, Vol. 60, Issue 5, Pages 471-477, 2018.
2. Mushtaq, R.T., Iqbal, A., Wang, Y., Khan, A.M., Petra, M.I., "Advancing PLA 3D printing with laser polishing: Improving mechanical strength, sustainability, and surface quality", *Crystals*, Vol. 13, Issue 4, 626, 2023.
3. Eryildiz, M., "Comparison of notch fabrication methods on the impact strength of FDM-3D-printed PLA specimens", *Materials Testing*, Vol. 65, Issue 3, Pages 423-430, 2023.
4. Alabd, M.U., Temiz, A., "Optimization of annealing and 3D printing process parameters of PLA parts", *International Journal of 3D Printing Technologies and Digital Industry*, Vol. 8, Issue 2, Pages 185-201, 2024.
5. Arslan, O., Selvi, O., Totuk, O.H., "Characterization of 3D printed conductive flexible materials for soft robotic applications", *International Journal of 3D Printing Technologies and Digital Industry*, Vol. 8, Issue 1, Pages 1-7, 2024.
6. Kechagias, J.D., Vidakis, N., Petousis, M., Mountakis, N., "A multi-parametric process evaluation of the mechanical response of PLA in FFF 3D printing", *Materials and Manufacturing Processes*, Vol. 38, Issue 8, Pages 941-953, 2023.
7. Der, O., Marengo, M., Bertola, V., "A low cost, flexible pulsating heat pipe technology", *Proceeding of 3rd Thermal and Fluids Engineering Conference (TFEC)*, Pages 321-327, Fort Lauderdale, 2018.
8. Der, O., Edwardson, S., Marengo, M., Bertola, V., "Engineered composite polymer sheets with enhanced thermal conductivity", *IOP Conference Series: Materials Science and Engineering*, Vol. 613, Issue 1, 012008, 2019.
9. Davim, J.P., Oliveira, C., Barricas, N., Conceição, M., "Evaluation of cutting quality of PMMA using CO<sub>2</sub> lasers", *The International Journal of Advanced Manufacturing Technology*, Vol. 35, Issues 9-10, Pages 875-879, 2008.
10. Fountas, N. A., Ninikas, K., Chaidas, D., Kechagias, J., Vaxevanidis, N.M., "Neural networks for predicting kerf characteristics of CO<sub>2</sub> laser-machined FFF PLA/WF plates", *MATEC Web of Conferences*, Vol. 368, 01010, 2022.
11. Kechagias, J.D., Ninikas, K., Petousis, M., Vidakis, N., Vaxevanidis, N., "An investigation of surface quality characteristics of 3D printed PLA plates cut by CO<sub>2</sub> laser using experimental design", *Materials and Manufacturing Processes*, Vol. 36, Issue 13, Pages 1544-1553, 2021.
12. Moradi, M., Karami Moghadam, M., Shamsborhan, M., Bodaghi, M., Falavandi, H., "Post-processing of FDM 3D-printed polylactic acid parts by laser beam cutting", *Polymers*, Vol. 12, Issue 3, 550, 2020.
13. Kechagias, J.D., Fountas, N.A., Ninikas, K., Vaxevanidis, N.M., "Kerf geometry and surface roughness optimization in CO<sub>2</sub> laser processing of FFF plates utilizing neural networks and genetic algorithms approaches", *Journal of Manufacturing and Materials Processing*, Vol. 7, Issue 2, 77, 2023.
14. Tsiolikas, A., Kechagias, J.D., Zaoutsos, S.P., "Hybrid fuzzy logic approach for multi-objective optimisation in laser-based processes", *International Journal of Mechatronics and Manufacturing Systems*, Vol. 17, Issue 1, Pages 1-20, 2024.
15. Kechagias, J.D., Ninikas, K., Salonitis, K., "An experimental study of laser cutting of PLA-wood flour 3D printed plates using a modified Taguchi design", *International Journal of Experimental Design and Process Optimisation*, Vol. 7, Issue 1, Pages 62-75, 2022.
16. Petousis, M., Ninikas, K., Vidakis, N., Mountakis, N., Kechagias, J.D., "Multifunctional PLA/CNTs nanocomposites hybrid 3D printing integrating material extrusion and CO<sub>2</sub> laser cutting", *Journal of Manufacturing Processes*, Vol. 86, Pages 237-252, 2023.
17. Kechagias, J.D., Vidakis, N., Ninikas, K., Petousis, M., Vaxevanidis, N.M., "Hybrid 3D printing of multifunctional polylactic acid/carbon black nanocomposites made with material extrusion and post-processed with CO<sub>2</sub> laser cutting", *The International Journal of Advanced Manufacturing Technology*, Vol. 124, Pages 1843-1861, 2023.
18. Kechagias, J.D., Ninikas, K., Petousis, M., Vidakis, N., "Laser cutting of 3D printed acrylonitrile butadiene styrene plates for dimensional and surface roughness optimization", *The International Journal of Advanced Manufacturing Technology*, Vol. 119, Pages 2301-2315, 2022.
19. Sabri, H., Mehrabi, O., Khoran, M., Moradi, M., "Leveraging CO<sub>2</sub> laser cutting for enhancing fused deposition modeling (FDM) 3D printed PETG parts through postprocessing", *Proceedings of the Institution of Mechanical Engineers, Part E: Journal of Process Mechanical Engineering*, 2024.



ULUSLARARASI 3B YAZICI TEKNOLOJİLERİ  
VE DİJİTAL ENDÜSTRİ DERGİSİ

INTERNATIONAL JOURNAL OF 3D PRINTING  
TECHNOLOGIES AND DIGITAL INDUSTRY

ISSN:2602-3350 (Online)

URL: <https://dergipark.org.tr/ij3dptdi>

# ALZHEİMER HASTALIĞININ ERKEN TEŞHİSİNE YÖNELİK UZMAN SİSTEM GELİŞTİRİLMESİ

DEVELOPING A EXPERT SYSTEM FOR EARLY  
DIAGNOSIS OF ALZHEIMER'S DISEASE

**Yazarlar (Authors):** Osamah Khaled Musleh SALMAN <sup>ID</sup>, Sema ÇAYIR <sup>ID</sup>, Mustafa Melikşah ÖZMEN <sup>ID</sup>, Enes AÇIKGÖZOĞLU <sup>ID</sup>

**Bu makaleye şu şekilde atıfta bulunabilirsiniz (To cite to this article):** Salman O. K. M., Çayır S., Özmen M. M., Açıkgözoğlu E., "Alzheimer Hastalığının Erken Teşhisine Yönelik Uzman Sistem Geliştirilmesi" *Int. J. of 3D Printing Tech. Dig. Ind.*, 9(1): 21-35, (2025).

DOI: 10.46519/ij3dptdi.1418059

Araştırma Makale/ Research Article

Erişim Linki: (To link to this article): <https://dergipark.org.tr/en/pub/ij3dptdi/archive>

# ALZHEİMER HASTALIĞININ ERKEN TEŞHİSİ İÇİN MAKİNE ÖĞRENİMİ TABANLI UZMAN SİSTEM GELİŞTİRİLMESİ

Osamah Khaled Musleh SALMAN<sup>a</sup> <sup>\*</sup>, Sema ÇAYIR<sup>a</sup> , Mustafa Melikşah ÖZMEN<sup>a</sup> , Enes AÇIKGÖZOĞLU<sup>b</sup> 

<sup>a</sup>Isparta Uygulamalı Bilimler Üniversitesi, Teknoloji Fakültesi, Mekatronik Mühendisliği Bölümü, TÜRKİYE  
<sup>b</sup>Isparta Uygulamalı Bilimler Üniversitesi, Keçiborlu Meslek Yüksekokulu, Bilgisayar Teknolojileri Bölümü, TÜRKİYE

\* Sorumlu Yazar: [osamahkms1994@gmail.com](mailto:osamahkms1994@gmail.com)

(Geliş/Received: 11.01.24; Düzeltme/Revised: 10.12.24; Kabul/Accepted: 13.01.25)

## ÖZ

1990'ların başından bu yana internet kullanımının hızla yaygınlaşması, anlamlı analiz için gelişmiş araçlar gerektiren büyük veri kümelerinin oluşmasına yol açmıştır. Yapay zeka teknolojilerinin, özellikle erken teşhis ve hastalık tespitinde hataların azaltılması için kullanıldıkları sağlık hizmetlerinde bu konuda etkili olduğu kanıtlanmıştır. Bu çalışma, yaşlı bireyler arasında yaygın olan ilerleyici bir nörodejeneratif durum olan Alzheimer Hastalığının (AD) erken teşhisi için yapay zeka tabanlı bir uzman sistem geliştirmeye odaklanmaktadır. Çalışmada 174 örneklî DARWIN veri kümesi (89'u AD'li ve 85'i AD'siz) kullanılarak AdaBoost, Gradient Boost, VotingHard, Stack, Decision Trees, Random Forest, Naive Bayes ve 1D-CNN olmak üzere sekiz makine öğrenimi algoritması ile eğitilmiştir. Çalışmada kullanılan Stack modeli %91,43 doğruluk, %93,75 özgüllük, %94,44 duyarlılık, %89,47 kesinlik, %91,89 F-ölçümü ve %91,43 AUC değeri ile yüksek bir tahmin performansı elde ederek en etkili model olarak ortaya çıkmıştır. Orta düzeyde performans gösteren modeller arasında AdaBoost %88,57 doğruluk, %88,24 özgüllük, %88,89 duyarlılık, %88,89 kesinlik, %88,89 F-ölçümü ve %88,56 AUC değeri elde etmiştir. Buna karşılık, VotingHard modeli %80,00 doğruluk, %77,78 özgüllük, %77,78 duyarlılık, %82,35 hassasiyet, %80,00 F-ölçümü ve %80,00 AUC değeri ile en düşük performansı göstermiştir. Bu bulgular, Stack modelinin güvenilir erken evre AD teşhisi potansiyelini vurgulamakta ve algoritma performansına ilişkin karşılaştırmalı bir bakış açısı sağlamaktadır.

**Anahtar Kelimeler:** Alzheimer hastalığı erken Teşhisi, Yapay zekâ, Uzman sistem.

## DEVELOPING A EXPERT SYSTEM FOR EARLY DIAGNOSIS OF ALZHEIMER'S DISEASE

### ABSTRACT

The rapid expansion of Internet use since the early 1990s has led to the generation of massive datasets, necessitating advanced tools for meaningful analysis. Artificial intelligence (AI) technologies have proven instrumental in this regard, particularly in healthcare, where they are employed for early diagnosis and error reduction in disease detection. This study focuses on developing an AI-based expert system for the early diagnosis of Alzheimer's Disease (AD), a progressive neurodegenerative condition prevalent among elderly individuals. Utilizing the DARWIN dataset comprising 174 subjects (89 with AD and 85 without), eight machine learning algorithms were evaluated: AdaBoost, Gradient Boost, VotingHard, Stack, Decision Trees, Random Forest, Naive Bayes, and 1D-CNN. The Stack model emerged as the most effective, achieving a high predictive performance with 91.43% accuracy, 93.75% specificity, 94.44% sensitivity, 89.47% precision, an F-measure of 91.89%, and an AUC value of 91.43%. Among the models with moderate performance, AdaBoost achieved 88.57% accuracy, 88.24% specificity, 88.89% sensitivity, 88.89% precision, an F-measure of 88.89%, and an

AUC value of 88.56%. Conversely, the VotingHard model demonstrated the lowest performance, with 80.00% accuracy, 77.78% specificity, 77.78% sensitivity, 82.35% precision, an F-measure of 80.00%, and an AUC value of 80.00%. These findings highlight the Stack model's potential for reliable early-stage AD diagnosis and provide a comparative perspective on algorithmic performance.

**Keywords:** Early detection of Alzheimer's disease, Artificial intelligence, Expert system.

## 1. GİRİŞ

Alzheimer hastalığı (AH), genellikle orta ve ileri yaşlarda ortaya çıkan ve zamanla ilerleyen bir nörodejeneratif (sinir hücrelerindeki yapısal ve işlevsel dejenerasyon) hastalıktır. Hastalık, hafıza kaybı, bilişsel bozukluklar ve kişilik değişiklikleri gibi semptomlarla kendini gösterir. Alzheimer, beyindeki sinir hücrelerinin zamanla hasar görmesi ve ölmesi sonucu ortaya çıkar [1]. Bu nedenle, hastalığın seyri zamanla ilerleyerek bireyin günlük yaşamını etkiler [2]. Hastalığın tedavisinde hem farmakolojik hem de farmakolojik olmayan yöntemler kullanılmakta ve bu tedavilerin etkinlikleri üzerine araştırmalar sürmektedir. Günümüzde, egzersiz uygulamaları farmakolojik olmayan etkili bir tedavi yöntemi olarak ön plana çıkmaktadır [3]. Bu bağlamda, hastalığın erken tanı önlemlerinin zamanında alınması açısından kritik önem taşımaktadır. Alzheimer hastalığının tespiti için bir dizi uzman tarafından klinik değerlendirme ve testler yapılmaktadır [4]. Ancak, Alzheimer hastalığının kesin teşhisi ancak otopsi sonucu ile konulabilmektedir [5]. Bu durum, Alzheimer hastalığının tespiti için çalışmaların artırılması ve tanı sonuçlarının iyileştirilmesi gerekliliğini göstermektedir.

Günümüzde birçok hastalık tespitine yönelik yeni teknolojik uygulamalar gerçekleştirilmektedir ve çalışmaların sonuçları tartışılmaktadır. Son dönemlerde yapay zekâ ve makine öğrenme algoritmaları ile yapılan çalışmalarda artışlar gözlemlenmektedir [6]. Artışların en önemli sebeplerinden biri, sonuçları açısından değerlendirildiğinde yüksek doğrulukları ile sağlık alanında umut vaat eden bir alan olmaya başlamasıdır. Hoşgör (2022), sağlıkta yapay zekânın kullanımını 125 adet tez çalışması ile ele alarak incelemiştir. Hazırlanan makalede yapay zekâ ve makine öğrenme algoritmalarının kullanımı, hastalık teşhisinde güvenilir ve başarılı sonuçların elde edildiği tespit edilmiştir [7].

Li ve ark. Alzheimer hastaları ile hafif bilişsel bozukluk (MCI) hastalarının teşhisi için yaptıkları çalışmada dayanıklı ya da sağlam olarak ifade edilen Derin Öğrenme tekniğini geliştirmişlerdir. Çalışmanın deneysel sonuçlar, önerilen tekniğin AH tanısında çok etkili olduğunu ve sınıflandırma doğruluğunu klasik derin öğrenme yöntemlerine göre ortalama %5,9 artırdığını göstermiştir [8].

Benzer şekilde, Hu ve çalışma arkadaşları, Alzheimer hastalığını tahmin etmek için yenilikçi bir yöntem geliştirmiştir. İlk aşamada 90 farklı beyin bölgesine ait aktiviteleri bir matrise dönüştürmüşler ve ardından bu bölgeler arasındaki işlevsel bağlantıyı belirlemek için korelasyon hesaplamaları yapmışlardır. Daha sonra, oluşturulan korelasyon matrislerini sınıflandırmak amacıyla Otomatik Kodlayıcı (AE) adı verilen bir sinir ağı modeli kullanmışlardır. Deneysel sonuçlar, bu yöntemin geleneksel yöntemlere kıyasla daha başarılı olduğunu göstermiştir. Özellikle destek vektör makineleri (SVM) ile karşılaştırıldığında, tahmin doğruluğunda yaklaşık %25'lik bir iyileşme sağlanmıştır [9].

Karabay ve Çavaş çalışmalarında, hastalık teşhisi için AlexNet, MobileNetV2 mimarileri ve Evrişimsel Sinir Ağları (ESA) modeli kullanılmıştır. Çalışmada, 6400 adet manyetik rezonans (MR) görüntüsü kullanılmıştır. Her iki mimariden elde edilen özellikler birleştirilmiş ve bu özelliklerin seçiminde Komşuluk Bileşen Analizi (KBA) algoritması kullanılmıştır. Ardından, özelliklerin sınıflandırılması Destek Vektör Makineleri (DVM) ile gerçekleştirilmiş ve modelin %100 doğruluk oranına ulaştığı rapor edilmiştir [10].

Öziç vd., OASIS veri tabanından temin edilen 70 Alzheimer hastası ve 70 sağlıklı bireye ait 3B T1 ağırlıklı manyetik rezonans (MR) görüntülerini kullanmış ve bu görüntüler üzerinde 116 subkortikal bölgenin hacimsel ölçümlerini gerçekleştirebilen atlas tabanlı bir

hacim ölçüm ve sınıflandırma modeli geliştirmiştir. Ölçülen değerler, her bir denekte gri madde, parankim ve toplam beyin hacmi ile ilişkilendirilerek normalizasyon işlemine tabi tutulmuştur. Bu sayede, 140x116 matris boyutuna sahip dört farklı veri kümesi elde edilmiştir. Veri kümeleri, entropi, t-testi, ROC, Bhattacharyya ve Wilcoxon özellik derecelendirme yöntemleri kullanılarak en anlamlı özellikten en anlamsız özelliğe doğru sıralanmıştır. Sıralanan veriler, her bir döngüde birleştirilmiş ve Destek Vektör Makineleri (SVM) kullanılarak lineer ve RBF (Radial Basis Function) çekirdekleri ile 10 kat çapraz doğrulama yöntemiyle sınıflandırma işlemi gerçekleştirilmiştir. Tüm senaryolar ayrıntılı bir şekilde analiz edilerek, en az sayıda özellikle en iyi sonuçları sağlayan özellik derecelendirme ve sınıflandırma yöntemleri belirlenmiştir. Normalizasyon ve özellik derecelendirme yöntemlerinin sınıflandırma sonuçları üzerindeki etkisi detaylı bir şekilde incelenmiştir. Deney sonuçlarına göre, ROC tabanlı özellik derecelendirme yöntemiyle lineer SVM kullanıldığında toplam beyin hacmi normalizasyonu ile %95.71 hassasiyet, %94.29 özgüllük, %95.00 doğruluk ve 0.95 eğri altında kalan alan (AUC) değeri elde edilmiştir [11].

Nalçakan (2018) Alzheimer hastalığı teşhisi için, Alzheimer hastaları ile normal kontrol gruplarına ait manyetik rezonans görüntüleri içeren bir veri kümesi kullanılmış ve bu veri kümesi, üç boyutlu evrişimli sinir ağları (3D CNN) ile eğitim ve test verisi olarak işlenmiştir. Bu çalışma sonucunda geliştirilen yapay zeka modeli, test verileri üzerinde %90.6 doğruluk oranına ulaşarak Alzheimer hastalığının teşhisinde etkili bir performans sergilemiştir. [12].

Wang vd., Alzheimer hastalığının erken teşhisi için yapay sinir ağları kullanarak bir erken uyarı modeli geliştirmiştir. Erken uyarı modelini geliştirmek için Lojistik Regresyon, k-En Yakın Komşu (kNN) ve Destek Vektör Makinesi (SVM) modelleriyle karşılaştırılmıştır. Üç katmanlı geri yayımlı bir yapıya sahip olan modelin performansı, duyarlılık, özgüllük, doğruluk, pozitif ve negatif prognostik değer (PPV ve NPV) ve eğri altındaki alan (AUC) ölçütleriyle değerlendirilmiştir. YSA modeli, %92.13 doğruluk, %87.28 duyarlılık, %94.74 özgüllük

ve 0.897 AUC değeri ile en iyi sonuçları sağlamıştır [13].

Janghel ve Rathore, ADNI veri tabanını kullanarak Alzheimer hastalığının teşhisi için derin öğrenmeye dayalı bir yöntem sunmuştur. Veri setindeki fMRI ve PET görüntüleri, sağlıklı bireylerin verileriyle birlikte analiz edilmiştir. Görüntüler, önce 3D'den 2D'ye dönüştürülmüş ve ardından Konvolüsyonel Sinir Ağları'nın (CNN) VGG-16 mimarisi kullanılarak özellik çıkarımı yapılmıştır. Sınıflandırma işlemi SVM, Doğrusal Ayrım, K-ortalama Kümeleme ve Karar Ağaçları algoritmaları ile gerçekleştirilmiştir. Deney sonuçları, fMRI veri seti için %99.95, PET veri seti için ise %73.46 doğruluk oranı elde edildiğini göstermiştir [14].

Alzheimer DARWIN veri setini analiz etmek için Rastgele Orman (RF), Lojistik Regresyon (LR), K-en Yakın Komşu (KNN), Doğrusal Diskriminant Analizi (LDA), Gaussian Naive Bayes (GNB) ve SVM algoritmalarını kullanmıştır. Algoritmaların doğruluk oranları %77.14 ile %91.4 arasında değişmiştir [15]. Benzer şekilde, Subha ve arkadaşları (2022), aynı veri setini LR, KNN, SVM, Karar Ağaçları (DT), RF ve AdaBoost algoritmalarıyla eğitmiş ve %86.79 ile %90.57 arasında doğruluk oranları elde etmiştir [16]. Gattulli ve arkadaşları (2022), Alzheimer DARWIN veri seti üzerinde LR, KNN, SVM, DT, RF, LDA, GNB, Çok Katmanlı Perceptron (MLP) ve Öğrenme Vektörü Kantizasyonu (LVQ) algoritmalarını kullanmış, doğruluk oranlarının %71.2 ile %83.5 arasında olduğunu rapor etmiştir [17]. Önder ve arkadaşları (2023) ise XGBoost, AdaBoost, Gradient Boost ve Voting algoritmaları ile %75 ile %85 arasında değişen doğruluk oranlarına ulaşmıştır [18].

**Tablo 1.** Literatürde DARWIN veri seti üzerinde yapılan çalışmalar

Çalışma	Kullanılan Makine Öğrenmesi Algoritmaları	Doğruluk
Gregorio vd., [15]	RF, LR, KNN, LDA, G-NV, SVM	77,14% - 91,4%
Subha vd., [16]	LR, DT, KNN, RF, AdaBoost, SVM,	86,79%-90,57%

Gattulli vd., [17]	RF, LR, KNN, LDA, G-NV, SVM, DT, MLP, LVQ	71,2%-83,5%
Önder vd. [18]	XGBoost, AdaBoost, GradientBoost, Voting	75%-85%

### 1.1 Araştırma soruları/hipotezleri

Hipotez 1: Alzheimer hastalığının erken teşhisine yönelik kullanılan veri setiyle eğitilen makine öğrenimi modelleri, %90'ın üzerinde bir doğruluk oranı sağlayabilir mi?

Hipotez 2: Alzheimer teşhisinde kullanılan makine öğrenimi algoritmaları arasında en yüksek performans hangi algoritma ile elde edilebilir?

Hipotez 3: El yazısı verileri, Alzheimer hastalığının erken belirtilerini belirlemek için uygun maliyetli ve güvenilir biyobelirteçler olarak kullanılabilir mi?

## 2. MATERYAL VE METOT

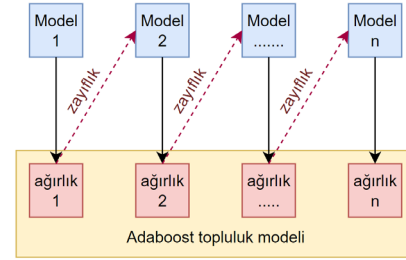
### 2.1. Materyal

Çalışmada kullanılan makine öğrenme algoritmaları bu bölümde detaylı olarak verilmiştir.

#### 2.1.1. AdaBoost

Adaboost (Adaptive Boosting), sınıflandırma ve regresyon gibi görevleri gerçekleştirmek için kullanılan bir makine öğrenme algoritmasıdır. İsmi “adaptive” (uyarlamalı) ve “boosting” (güçlendirme) terimlerinin birleşiminden alan Adaboost, zayıf sınıflandırma algoritmalarının performansını artırarak daha güçlü sınıflandırıcılar oluşturmak amacıyla kullanılmaktadır [19]. Bu algoritma, zayıf sınıflandırıcıların bir arada çalışmasıyla daha güçlü bir sınıflandırma algoritması oluşturmaktadır [20]. Adaboost algoritmasında, ilk olarak tüm verilere ait ağırlık değerleri eşit seçilir ve veriler eğitilir. Daha sonra zayıf olan sınıflandırıcı üzerinde örneklerin ağırlık değerleri artırılmaya başlanır. Sınıflandırıcı, her döngüde ağırlık değerini güncellemektedir. Böylece hatalı olan örneklerin önemi artmaktadır [19,20]. Ağırlıkları artırılmış olan örnekler, bir sonraki sınıflandırıcıda öne çıkarak seçilme olasılığını artırmış olur. Bu şekilde oluşturulan tüm sınıflandırıcıların bir araya getirilmesiyle daha

yüksek doğrulukla bir sınıflandırıcı elde edilmektedir. Algoritmaya ait şema, Şekil 1’de gösterilmektedir [19,20].



Şekil 1. Adaboost Algoritması [20].

#### 2.1.2. Gradient Boost

Gradient Boost algoritması, standart makine öğrenmesinden farklı olarak tahminleri sırayla yapan bir topluluk algoritmasıdır [21]. Algoritmanın temel amacı, düşük doğruluk değerindeki tahminleri yüksek doğrulukla tahminlere çevirmektir. Algoritmada ilk olarak tahminleri üretmek için  $y_i^p$  fonksiyonu oluşturulur. Tahminler ve hedef değer arasındaki farkın hesaplanması için ise bir “Loss” fonksiyonu oluşturulmaktadır. İlk iterasyondan sonra  $y_i^p$  ve “Loss” fonksiyonları birleştirilerek hedef değerle tahmin edilen değer arasındaki fark yeniden hesaplanır. Bu işlem tekrarlanarak  $y_i^p$  fonksiyonuna ait doğruluk değeri artırılmaya ve hedef değere olan uzaklık azaltılmaya çalışılmaktadır [21].

$$\text{Loss} = \text{MSE} = \sum (y_i - y_i^p)^2 \quad (1)$$

Denklemden  $y_i$  i. hedef değer,  $y_i^p$  ise i. tahmin edilen değeri, “Loss” ise kayıp fonksiyonunu temsil etmektedir. Elde edilen tahminlerin kayıp fonksiyonlarını minimum seviyede tutmak gerekmektedir. Gradyan inişi kullanılarak her iterasyonda öğrenme oranları güncellenir ve kayıp fonksiyonunun minimum değeri bulunur [22].

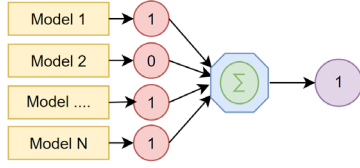
$$y_i^p = y_i^p - a * \delta \sum \frac{(y_i - y_i^p)^2}{\delta y_i^p} \quad (2)$$

$$y_i^p = y_i^p - a * 2 * \sum (y_i - y_i^p) \quad (3)$$

#### 2.1.3. Voting hard

Voting hard sınıflandırıcısı, tahmin doğruluğunun artırılabilmesi amacıyla birden çok sınıflandırma algoritmasını birleştiren bir yöntemdir [23]. Tek bir modele tahmin yaptırmak yerine, kullanılan tüm modellerin çıktısının oylama prensibine dayanmaktadır. Yani, birden çok modelin verdiği cevaba bakılarak en doğru sonuç hedeflenmektedir

[23,24]. Algoritmaya ait şema, Şekil 2'de gösterilmektedir.

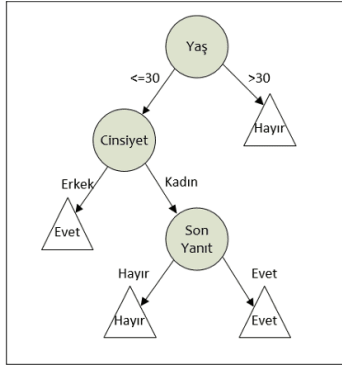


Şekil 2. VotingHard Modeli[24]

#### 2.1.4. Karar ağaçları

Karar ağaçları modeli, kararları veya muhtemel sonuçları göstermek amacıyla kullanılan ağaç benzeri bir modeldir [25]. Bu model, araştırma çalışmalarında gerçekleştirilen analizlerde bir sonuca ulaşabilmek için izlenmesi gereken yolu belirlemede kullanılmaktadır. Karar ağaçları temel olarak, iç düğümlerden, dallardan ve sonuç düğümünden meydana gelmektedir [25,26]. Algoritmaya ait şema, Şekil 3'te gösterilmektedir.

1. İç Düğüm: İç düğüm belirli bir özelliği değerlendirir ve test eder.
2. Dallar: İç düğümde yapılan değerlendirmelerin sonuçlarını göstermektedir.
3. Sonuç Düğümü: Çıktı olarak alınan kararı göstermektedir.



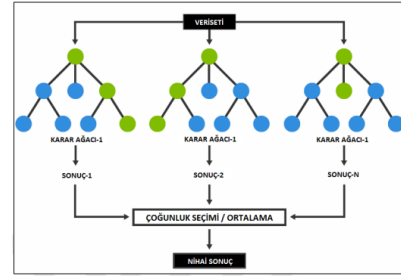
Şekil 3. Örnek karar ağacı yapısı [26].

#### 2.1.5. Rastgele Orman

Rastgele Orman(RO) algoritması temel olarak karar ağaçlarının birleşiminden oluşmaktadır. Karar ağaçlarının genel yapısı kök, düğümler, dallar ve yapraklardan oluşmaktadır. Kök ve düğümler kararların ölçütlerini, yapraklar verilen kararların durumlarını, dallar ise ölçütler ile kararlar arasındaki bağlantıyı temsil etmektedir [27,28]. RO algoritması, her bir düğümde rastgele olarak seçilmiş olan değişkenlerin en iyi olanını belirleyip düğümleri dallara ayırmaktadır. Ana veri setinde yaptığı değişikliklerle alt veri setleri

oluşturulmaktadır. Daha sonrasında rastgele özellikler seçilerek ağaçlar oluşturulur ve ağaçlarda budama yapılmaz. Orijinal eğitim veri setinin yaklaşık olarak %70'i ön yükleme örneklerini, %30'u ise hataları test etmek için kullanılır [27].

Rastgele Orman (RO) algoritması, her düğümde rastgele seçilen en iyi değişkeni belirleyerek dallara ayırır. Orijinal veri setinden küçük veri setleri oluşturulur ve bu veri setleriyle ağaçlar geliştirilir; ağaçlarda budama yapılmaz. Algoritma, her düğümde kullanılan değişken sayısını ( $m$ ) ve toplam ağaç sayısını ( $N$ ) ayarlayarak çalışır. Eğitim verisinin %67'si modeli eğitmek, %33'ü ise hataları test etmek için kullanılır. Algoritmanın şeması Şekil 4'te sunulmaktadır [28,29].



Şekil 4. RO Algoritması [29].

#### 2.1.6. Naive bayes

Bayes teoremi, 1701-1761 yılları arasında Thomas Bayes tarafından geliştirilmiş bir teoremdir. Bayes teoremi, bir değişken için koşullu olasılıklar ile marjinal olasılıklar arasındaki bağıntıyı göstermektedir. Herhangi bir olayın meydana gelmesinde birden fazla bağımsız neden varsa, bu nedenlerden birinin olayı meydana getirme olasılığını hesaplamada kolaylık sağlar [30]. Bayes teoremine ait denklem aşağıda verilmiştir. (Denklem 4).

$$P(A|B) = \frac{P(B|A)P(A)}{P(B)} \quad (4)$$

- $P(A)$ ; A için olasılık veya marjinal olasılık
- $P(A|B)$ ; verilen bir B olayında A olayının koşullu olasılığıdır. B olayı var ise A olayının gerçekleşme olasılığıdır.
- $P(B|A)$ ; A olayı gerçekleşmiş ise B olayının olma olasılığıdır.
- $P(B)$ ; B olayı için önsel olasılıktır.

Naive Bayes sınıflandırma modeli, Bayes teoreminin basitleştirilmiş bir halidir. Makine öğrenmesi uygulamalarında denetimli öğrenmenin bir alt sınıfıdır. Naive Bayes

modelinde, sınıflandırılması gereken veriler ve bu verilerin hangi kümeye ait olduğu belirlenmiştir. Bu kümelerden yararlanılarak daha sonrasında gelen bir verinin hangi sınıfa ait olduğu belirlenir [30].

### 2.1.7. Stack

Stack, birçok makine öğrenimi algoritmasının tahminlerini birleştirmek için kullanılan bir topluluk öğrenme tekniğidir [31]. İlk olarak, çeşitli temel algoritmalar veri kümesi üzerinde eğitilir ve tahminler üretir. Ardından, bu temel algoritmaların tahminleri, genellikle başka bir makine öğrenimi modeli olan bir meta-algoritma tarafından birleştirilir. Bu birleştirme süreci, daha iyi tahminler elde etmeyi amaçlar ve farklı modellerin güçlü yanlarını bir araya getirerek modelin genel performansını artırabilir. Stack, karmaşık problemlerde daha iyi sonuçlar elde etmek için yaygın olarak kullanılan bir tekniktir [32,33].

### 2.1.8. 1D-CNN

Tek boyutlu evrişimli sinir ağları (1D-CNN), derin öğrenme alanında önemli bir yere sahiptir ve çeşitli uygulamalarda etkili sonuçlar elde etmiştir [34,35]. Bu ağlar, özellikle görüntü işleme ve sınıflandırma görevlerinde yaygın olarak kullanılmaktadır. Tek boyutlu CNN'lerin temel avantajlarından biri, öznelik çıkarımını otomatik olarak gerçekleştirmeleri ve geleneksel yöntemlere göre daha genel çözümler sunmalarıdır [34]. Bu özellikleri, onları birçok farklı görev için uygun hale getirmektedir.

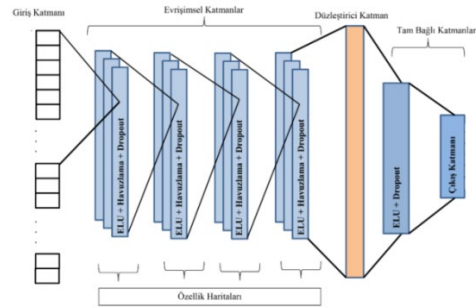
Tek boyutlu evrişimli sinir ağları, genellikle bir dizi ardışık katmandan oluşur. Bu katmanlar, giriş verilerinden özellikleri çıkarmak için filtreler kullanır ve bu filtrelerin ağırlıkları, geri yayılım algoritması ile güncellenir [34,35]. Özellikle, CNN'ler görüntü sınıflandırma, nesne tanıma ve segmentasyon gibi alanlarda yüksek başarı oranları ile dikkat çekmektedir [36,37]. Örneğin, U-Net mimarisi, tıbbi görüntü segmentasyonunda sıkça tercih edilmektedir ve bu alandaki başarıları ile literatürde önemli bir yer edinmiştir [37].

Ayrıca, tek boyutlu CNN'ler, finansal verilerin tahmin edilmesi gibi farklı alanlarda da kullanılmaktadır. Örneğin, bir çalışmada, tek boyutlu CNN'ler kullanılarak finansal piyasa hareketlerinin tahmin edilmesi üzerine başarılı sonuçlar elde edilmiştir [38]. Bu tür

uygulamalar, CNN'lerin çok yönlü kullanım potansiyelini göstermektedir.

Bu ağlar, verinin yerel bağıntılarını öğrenme konusunda makine öğrenme algoritmalarına göre üstünlük sağlar ve bu sayede karmaşık özellikleri tespit edebilmektedirler. Bunun yanında, basit makine öğrenme algoritmaları, genellikle daha az veri gerektiren ve daha hızlı çalışabilen modeller olarak avantaj sağlarlar. Ancak, 1D-CNN'ler karmaşık desenleri ve ilişkileri daha iyi öğrenebilirken, basit makine öğrenme algoritmaları daha az hesaplama gücü gerektiren ve yorumlanabilirliği yüksek çözümler sunar. Bu nedenle, problem türüne ve veri yapısına bağlı olarak her iki yaklaşımın da kendine özgü üstünlükleri vardır.

Sonuç olarak, tek boyutlu evrişimli sinir ağları, derin öğrenme alanında önemli bir yere sahiptir ve görüntü işleme, finansal tahminler gibi birçok alanda etkili bir şekilde kullanılmaktadır. Bu ağların otomatik öznelik çıkarımı yapabilme yetenekleri ve yüksek başarı oranları, onları günümüzdeki en popüler derin öğrenme yöntemlerinden biri haline getirmiştir [34-38]. 1D-CNN genel yapısı Şekil 5'te gösterilmektedir.



Şekil 5. 1D-CNN Yapısı [39].

## 2.2. Metot

Alzheimer hastalığının erken teşhisine yönelik geliştirilen makine öğrenme tabanlı uzman sistemi için açık kaynak erişimli DARWIN veri seti kullanılmıştır [40]. Kullanılan veri seti, 85 Alzheimer hastası olmayan ve 89 Alzheimer hastası olan toplam 174 veriden oluşmaktadır. Alınan veri setindeki 450 özellik için her bir kişiye, tıbbi tahliller kullanılarak bazı ölçümler yapılmıştır. Çalışmada kullanılan veri seti, AdaBoost, Gradient Boost, Voting Hard, Stack, Karar Ağaçları, Rastgele Orman, Naive Bayes ve tek boyutlu evrişimli sinir ağları olmak üzere 8 farklı makine öğrenme algoritmasıyla modellenmiştir. Elde

edilen modellerin doğruluk, özgüllük, duyarlılık, kesinlik, F-ölçüsü, AUC ve ROC eğrisi performans değerlendirme ölçütlerine göre değerlendirilmiş ve sonuçlar karşılaştırılmıştır. Çalışmadaki Alzheimer hastalığının erken teşhisine yönelik geliştirilen uzman sistemin pseudo kodu aşağıda verilmiştir.

DARWIN veri seti, 450 özelliğe sahip 174 örnekten oluşmakta olup, yüksek boyutlu verilerle çalışabilen ve karmaşık desenleri algılayabilen sağlam modellerin kullanımını gerektirmektedir. Bu bağlamda, stack modeli, üstün tahmin performansı sunma kapasitesi, yüksek hassasiyete ulaşma yeteneği ve yanlış negatifleri en aza indirerek erken teşhis sürecini destekleme potansiyeli nedeniyle tercih edilmiştir. Gradient Boost ve AdaBoost gibi yöntemlerin yanı sıra RO ve VotingHard gibi topluluk yaklaşımları, doğruluğu ve genelleştirilebilirliği artırmak amacıyla yanlış sınıflandırılmış örneklere odaklanma yetkinlikleri ve gürültüye karşı dirençleri ile dengesiz veri setlerinde sağlamlık sağlamaları nedeniyle seçilmiştir. Ayrıca, Karar Ağaçları ve Naive Bayes algoritmaları, veri setindeki farklı özellik türlerini işleyebilme kapasiteleri sayesinde yorumlanabilirlik ve kararlılık sunarken, aynı zamanda güvenilir tahminler yapabilmektedir. Tüm bu algoritmalar, doğruluğu optimize ederek, erken teşhis süreçlerinde yüksek hassasiyet sağlayarak ve Alzheimer hastalığının teşhisine yönelik makine öğrenimi yaklaşımlarının kapsamlı bir şekilde değerlendirilmesine katkıda bulunarak araştırma hedeflerini desteklemektedir.

#### **Algoritma: Uzman sistemin Pseudo Kodu**

<i>Veri seti</i>	<i>Alzheimer hastalığına dair veri seti toplama ve ön işleme: veri setinin standartlaştırılması, normalleştirilmesi, eksik değerlerin işlenmesi ve kategorik değişkenlerin kodlaması.</i>
<i>Seçme</i>	<i>Makine Öğrenme Algoritmaları (Sınıflandırma): AdaBoost, Gradient Boost, VotingHard, Stack, Karar Ağaçları, RO, Naive Bayes ve tek boyutlu evrişimli sinir ağıları.</i>
<i>Tanımla</i>	<i>En iyi modeli, kombinasyonu ve performansı saklamak için değişkenler tanımlanır</i>

<i>Ayrırma</i>	<i>Eğitim Veri Kümesini rastgele olarak eğitime ve teste ayırma</i>
<i>Döngü</i>	<i>Tüm makine öğrenme algoritmaları için:</i> <i>(1)Model tanımlama</i> <i>(2)Eğitim veri seti ile modeli eğitime</i> <i>(3)Eğitilen modelin test edilmesi</i> <i>(4)Modeli değerlendirme</i> <i>(5)Değerlendirme sonuçlarını saklama</i>
<i>Sonuç</i>	<i>En iyi modeli seçme</i>

### **3. ARAŞTIRMA BULGULARI**

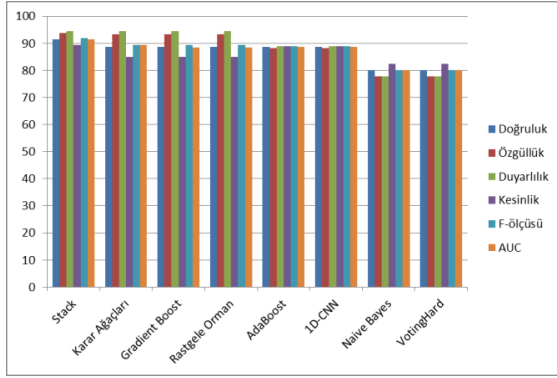
Çalışmada, Alzheimer hastalığının erken teşhisine yönelik makine öğrenme tabanlı bir uzman sistem geliştirilmiştir. Uzman sistemin geliştirilmesinde AdaBoost, Gradient Boost, VotingHard, Stack, Karar Ağaçları, Rastgele Orman, Naive Bayes ve 1D-CNN olmak üzere farklı makine öğrenme algoritması kullanılmıştır. Eğitilen modeller, test veri seti ile test edilerek doğruluk, özgüllük, duyarlılık, kesinlik, F-ölçüsü, AUC ve ROC eğrisi performans değerlendirme ölçütlerine göre değerlendirilmiştir.

Şekil 7’de 8 makine öğrenme modeli için karmaşıklık matrisleri verilmiştir. Matrislerdeki Gerçek Pozitifler (TP) doğru bir şekilde tanımlanmış Alzheimer vakalarını temsil ederken, Gerçek Negatifler (TN), doğru bir şekilde tanımlanmış Alzheimer olmayan vakalardır. Yanlış Pozitifler (FP) Alzheimer olmayan vakaların yanlış bir şekilde Alzheimer olarak sınıflandırılması durumunda meydana gelir ve Yanlış Negatifler (FN) yanlış bir şekilde Alzheimer olmayan olarak tanımlanmış Alzheimer vakalarıdır. Şekil 7 incelediğinde, modellerin 35 adet veri ile test edildiği ve 32 tanesinin doğru bir şekilde sınıflandırdığı görülmektedir; (d) Stack algoritması en başarılı modeldir. Ayrıca çalışmada eğitilen tüm modellerin ROC eğrisi Şekil 8’de verilmiştir. ROC eğrileri, her model için duyarlılık (Gerçek Pozitif Oranı) ve özgüllük (1 - Yanlış Pozitif Oranı) arasındaki dengeyi gösterir. Eğri altındaki alan (AUC), modellerin genel performansını niceliksel olarak belirler ve 1’e yakın değerler üstün sınıflandırma yeteneğini gösterir. Bu ölçüm, modelin duyarlılığı ve özgüllüğü etkili bir şekilde dengeleme yeteneğini vurgular. Tablo 2’de ve Şekil 6’da eğitilen tüm modellerin performans değerlendirme ölçütlerinin sonuçları

verilmiştir. Tablo 2 incelendiğinde, Stack modeli en başarılı modeldir.

**Tablo 2. Makine öğrenme modellerin performans değerlendirme ölçütlerinin sonuçları.**

Model	Doğruluk	Özgüllük	Duyarlılık	Kesinlik	F-ölçüsü	AUC
Stack	91,43	93,75	94,44	89,47	91,89	91,43
Karar Ağaçları	88,57	93,33	94,44	85,00	89,47	89,47
Gradient Boost	88,57	93,33	94,44	85,00	89,47	88,40
Rastgele Orman	88,57	93,33	94,44	85,00	89,47	88,40
AdaBoost	88,57	88,24	88,89	88,89	88,89	88,56
ID-CNN	88,57	88,24	88,89	88,89	88,89	88,56
Naive Bayes	80,00	77,78	77,78	82,35	80,00	80,07
VotingHard	80,00	77,78	77,78	82,35	80,00	80,00



**Şekil 6.** Makine öğrenme modellerin performans değerlendirme ölçütlerinin sonuçları

#### 4. TARTIŞMA

Literatür incelendiğinde, birçok çalışma, el yazısının kinematik, basınç ve zamansal özelliklerinin bilişsel gerilemeyi tespit etmek için potansiyel biyobelirteçler olarak hizmet edebileceğini göstermiştir. Garré-Olmo vd., (2017) hafif bilişsel bozukluğu (MCI), Alzheimer hastalığı ve sağlıklı kontrolleri olan hastalarda el yazısı kinematığı ve basıncının derinlemesine bir analizini yapmışlardır. Araştırmaları, üç grup arasında el yazısı desenlerinde önemli farklılıklar olduğunu göstermiş ve bu özelliklerin potansiyel olarak Alzheimer hastalığı için erken belirteçler olarak hizmet edebileceğini vurgulamışlardır. Bu durum, el yazısı analizinin klinik ortamlarda uygulanabilecek non-invaziv bir tanı aracı olarak faydasını vurgulamaktadır[41]. Ayrıca, Alzheimer hastalığı teşhisi için el yazısı analizindeki son gelişmeler, yeni veri kümeleri ve makine öğrenimi modelleri aracılığıyla elde edilmiştir. Cilia vd., (2022), özellikle Alzheimer hastalığının teşhisine yönelik çevrimiçi el yazısı analizi için yeni bir veri kümesi sunmuştur [42]. Öcal (2024) üçlü bir topluluk öğrenme modeli üzerine yaptığı araştırma, Alzheimer hastalarında ince motor becerilere

ve bunların bozulmasına odaklanarak literatüre daha fazla katkıda bulunmaktadır. Bu çalışma, el yazısı analizinde tanısal doğruluğu artırmak için çeşitli makine öğrenimi algoritmalarını birleştirmenin önemini vurgulamaktadır. Birden fazla modelin tahminlerini bir araya getiren topluluk yöntemlerinin, yığın modelinin en yüksek doğruluk ve hassasiyeti sağladığı bu çalışmada görüldüğü gibi, gelişmiş performans sunduğu gösterilmiştir[43]. Bu çalışmalar ışığında, el yazısı analizinin erken AD teşhisi için invazif olmayan, uygun maliyetli ve erişilebilir bir yöntem olarak önemli bir potansiyel sunduğu açıktır. Makine öğrenimi modellerinin bu verilere uygulanması, tanısal doğruluğu daha da artırabilir ve bu da onu gelecekteki araştırmalar için önemli bir alan haline getirir. Mevcut çalışmanın da gösterdiği gibi, Stack modeli diğer algoritmalarından daha iyi performans göstererek Alzheimer hastalığını tespit etmede yüksek düzeyde doğruluk elde etmiştir.

Makine öğrenimi tabanlı uzman sistemler, Alzheimer hastalığının erken teşhisinde sağlık hizmetlerine önemli katkılar sunabilir. Yüksek doğruluk ve hassasiyet oranlarıyla bu sistemler, erken tanı süreçlerini optimize ederek hastalık ilerlemesini yavaşlatacak müdahalelere olanak tanır. Özellikle Stack modeli gibi performansı yüksek algoritmalar, yanlış negatifleri en aza indirerek tedavi planlamasını daha etkin hale getirir. Bu yaklaşım, bireysel yaşam kalitesini artırmanın yanı sıra sağlık sistemlerinin verimliliğini ve mali sürdürülebilirliğini destekler.

Çalışmada, DARWIN veri seti kullanılarak Alzheimer hastalığının erken teşhisi için makine öğrenimi algoritmaları ile

modellenmiştir. Kullanılan algoritmaların performans ölçütleri bakımından avantajlar ve sınırlamalar sunmuştur.

Gerçekleştirilen deneylerde Stack modeli, %91,43 AUC değeri ile en yüksek performansı sergileyerek diğer tüm algoritmaları geride bırakmıştır. Bu üstün başarısı, topluluk öğrenmesi yaklaşımı sayesinde birden fazla modelin güçlü yönlerini bir araya getirmesine bağlanabilir. Modelin yüksek doğruluk, özgüllük ve duyarlılık değerleri, erken evre Alzheimer teşhisinde güvenilir bir araç olabileceğini göstermektedir. Ancak, modelin karmaşık yapısı ve yüksek hesaplama maliyeti, aşırı uyum riskini artırarak eğitim ve ayarlama süreçlerini zorlaştırmaktadır.

Karar Ağaçları modeli de, özellikle özgüllük ve duyarlılık metriklerinde yüksek değerler elde ederek dikkat çekmiştir. Modelin yorumlanabilir yapısı, tıbbi teşhislerde açıklanabilirliğin büyük önem taşıdığı düşünüldüğünde önemli bir avantaj sunmaktadır. Ancak, karar ağaçları karmaşık veri yapılarında aşırı uyum eğilimi gösterebilmekte ve tıbbi verilerde sıklıkla görülen doğrusal olmayan ilişkileri tam olarak yakalayamamaktadır.

Gradient Boosting ve AdaBoost gibi artırma algoritmaları, zayıf öğrencileri birleştirerek güçlü bir tahminci oluşturma prensibine dayanmaktadır. Bu algoritmalar, Alzheimer hastalığı gibi sınıflandırma problemlerinde başarılı sonuçlar vermektedir. Gradient Boosting, her adımda önceki adımdaki hataları minimize etmeye çalışarak daha iyi bir model oluşturur. AdaBoost ise hatalı sınıflandırılan örneklerin ağırlıklarını artırarak modelin bu örnekleri daha iyi öğrenmesini sağlar. Her iki algoritma da Alzheimer veri kümesinde %88.57 doğruluk oranına ulaşarak güçlü bir teşhis yeteneği sergilemiştir. Özellikle Gradient Boosting, yüksek özgüllük ve duyarlılık değerleriyle dengesiz veri kümelerinde etkili bir sınıflandırıcı olduğunu kanıtlamıştır. Ancak, aşırı uyum ve yüksek hesaplama maliyeti gibi dezavantajları da bulunmaktadır.

Rastgele Orman algoritması, birden fazla karar ağacının tahminlerinin ortalamasını alarak karar veren bir topluluk öğrenme yöntemidir. Bu sayede aşırı uyum riskini azaltır ve daha

genelleyici bir model oluşturur. Alzheimer veri kümesinde %88.57 doğruluk oranıyla Gradient Boosting ile benzer bir performans göstermiştir. Ancak, tek bir karar ağacı kadar yorumlanabilir değildir ve büyük veri kümeleri için hesaplama maliyeti yüksek olabilir.

1D-CNN, sıralı verilerden otomatik olarak özellik çıkarma yeteneği sayesinde Alzheimer hastalığının teşhisinde başarılı sonuçlar elde etmiştir. Bu model, Alzheimer hastalığına özgü karmaşık örüntüleri etkili bir şekilde öğrenerek AdaBoost ile benzer bir performans göstermiştir. Ancak, derin öğrenme modelleri genellikle büyük miktarda veri ve hesaplama kaynağı gerektirmektedir. Özellikle küçük veri kümelerinde aşırı uyum riski bulunmaktadır.

Naive Bayes, hesaplama açısından verimli ve basit yapısıyla bilinir. Bu çalışmada, Alzheimer hastalığının teşhisinde %80,00 doğruluk ve %82,35 kesinlik oranlarına ulaşılmıştır. Ancak, modelin tüm özniteliklerin birbirinden bağımsız olduğu varsayımı, gerçek dünyadaki verilerin karmaşık ilişkilerini tam olarak yakalamada yetersiz kalmıştır.

VotingHard, tüm algoritmalar arasında en düşük performansı sergileyerek %80,00 doğruluk oranına ulaşmıştır. Gelişmiş bir optimizasyon stratejisi kullanılmadan farklı modellerin tahminlerinin birleştirilmesi, modelin genel performansını sınırlamıştır.

Alzheimer hastalığının teşhisi için makine öğrenmesi algoritmalarının kullanımı, hastalığın erken teşhisinde önemli bir adım olarak değerlendirilmektedir. Ancak, her bir algoritmanın kendine özgü avantajları ve dezavantajları bulunmaktadır. Bu nedenle, farklı algoritmaların performanslarının karşılaştırılması ve veri setinin özelliklerine göre en uygun modelin seçilmesi önemlidir.

## 5. SONUÇLAR

Alzheimer hastalığının erken teşhisine yönelik uzman sistemlerin geliştirilmesi önemli bir sağlık hedefidir. Bu tür bir uzman sistem, bireylerin risk faktörlerini, semptomlarını ve genetik yatkınlıklarını dikkate alarak erken teşhis ve müdahale için daha iyi bir yol sunabilir. Yapay zekâ ve derin öğrenme teknolojilerinin gelişimi, büyük miktarda veri analizi ve nörolojik göstergelerin daha iyi anlaşılmasıyla bu hedefe ulaşmada önemli bir

rol oynamaktadır. Bu çalışmada Alzheimer hastalığının erken teşhisi için makine öğrenme tabanlı bir uzman sistemi geliştirilmiştir. Çalışmada kullanılan açık erişimli veri seti, AdaBoost, Gradient Boost, VotingHard, Stack, Karar Ağaçları, Rastgele Orman, Naive Bayes ve 1D-CNN olmak üzere 8 farklı makine öğrenme algoritmasıyla modellenmiştir. Elde edilen modellerin doğruluk, özgüllük, duyarlılık, kesinlik, F-ölçüsü, ROC eğrisi ve ROC eğrisinin altındaki alan (Ardea Under Curve ve AUC) performans değerlendirme ölçütlerine göre değerlendirilmiş ve sonuçlar karşılaştırılmıştır. Elde edilen sonuçlar aşağıda maddeler halinde verilmiştir.

- Tüm değerlendirme kriterlerine göre en başarılı model Stack olmuştur. Stack'in değerlendirme sonucunda %91.43 doğruluk, %93.75 özgüllük, %94.44 duyarlılık, %89.47 kesinlik, %91.89 F-ölçüsü ve %91.43 AUC değeri ile başarılı tahmin gerçekleştirdiği belirlenmiştir.
- Tüm değerlendirme kriterlerine göre en başarısız model VotingHard olmuştur. VotingHard'in değerlendirme sonucunda %80.00 doğruluk, %77.78 özgüllük, %77.78 duyarlılık, %82.35 kesinlik, %80.00 F-ölçüsü ve %80.00 AUC değeri ile başarılı tahmin gerçekleştirdiği belirlenmiştir.

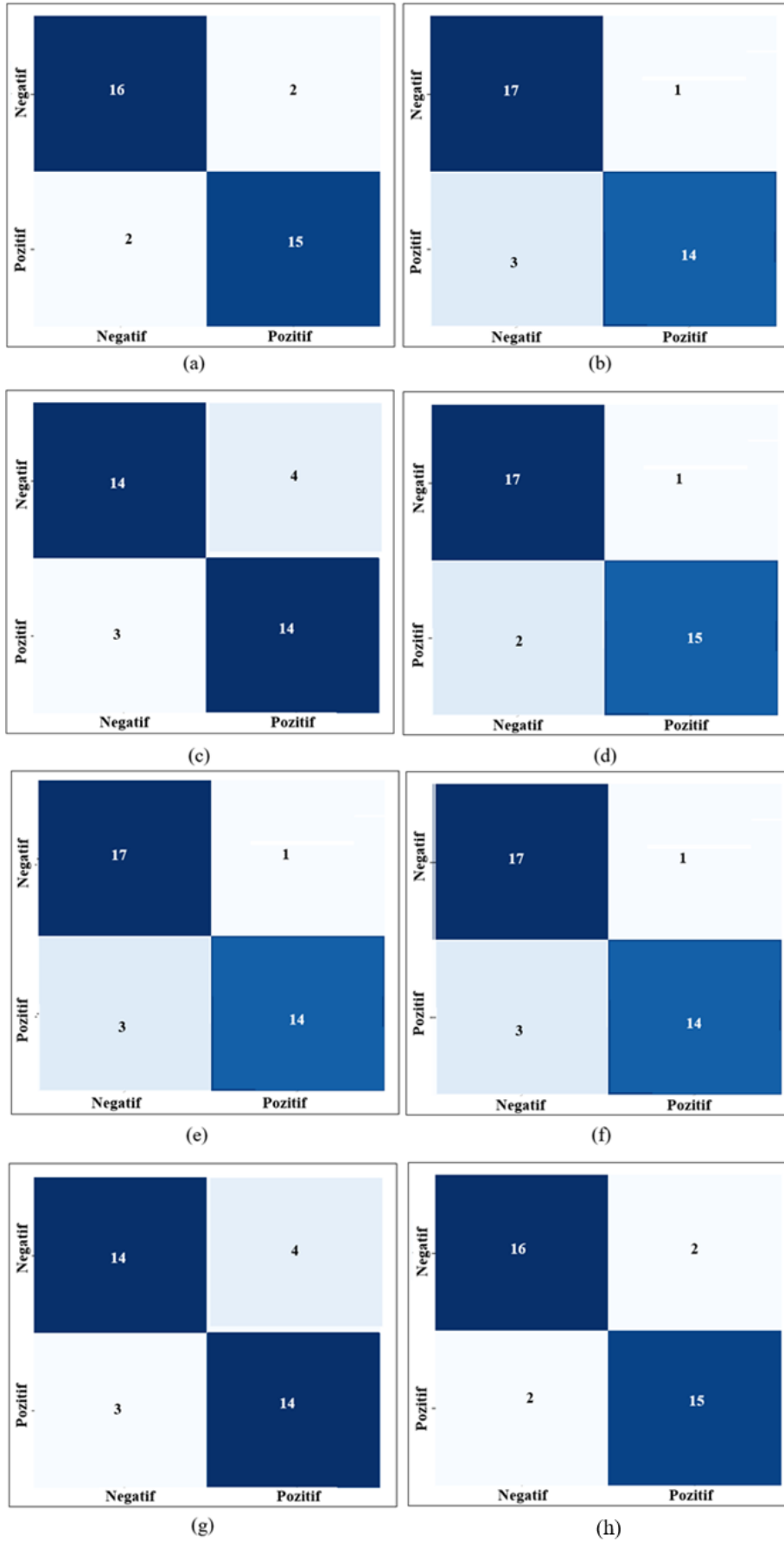
Ayrıca araştırma soruları için öngörülen sonuçlar şu şekilde ifade edilebilir.

**Hipotez 1 Sonucu:** Çalışmadaki veri seti ve algoritmalar, Alzheimer hastalığının erken teşhisinde %90'ın üzerinde doğruluk sağlamış; Stack modeli %91.43 doğrulukla en yüksek başarıyı göstermiştir.

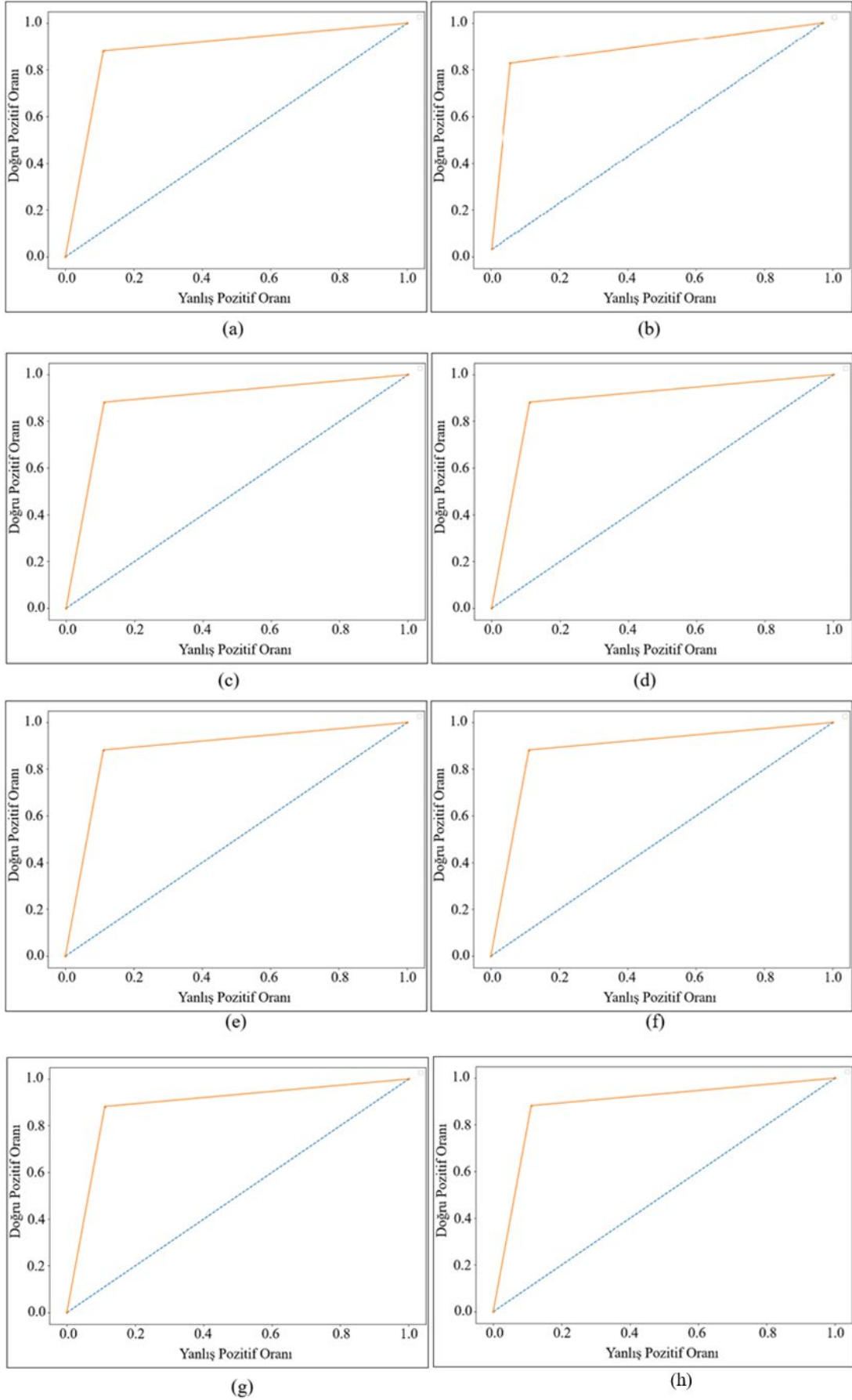
**Hipotez 2 Sonucu:** Stack modeli, diğer algoritmalarından daha yüksek doğruluk, özgüllük ve duyarlılık ile Alzheimer teşhisinde en başarılı yöntem olmuştur

**Hipotez 3 Sonucu:** El yazısı verileri, Alzheimer hastalığının erken belirtilerini tespit etmek için düşük maliyetli, güvenilir bir biyobelirteç olarak umut vaat etmektedir; bu veriler, hastalığın non-invaziv teşhisinde potansiyel sunmaktadır.

Sonuç olarak yapay zekâ ile Alzheimer hastalığı tespitinde en iyi modelin Stack olduğu belirlenmiştir. İleride yapılacak çalışmalarda daha büyük veri setleri ve farklı yapay zekâ yöntemleri kullanılarak doğruluk oranının artırılmasının mümkün olacağı düşünülmektedir.



Şekil 7. Karmaşıklık Matrisleri: (a) AdaBoost (b) Gradient Boost (c) VotingHard (d) Stack (e) Karar Ağaçları (f) Rastgele Orman (g) Naive Bayes (h) ID-CNN



Şekil 8. Karmaşıklık Matrisleri: (a) AdaBoost (b) Gradient Boost (c) VotingHard (d) Stack (e) Karar Ağaçları (f) Rastgele Orman (g) Naive Bayes (h) 1D-CNN

**TEŞEKKÜR**

Çalışma 5. Uluslararası Mühendislikte Yapay Zekâ ve Uygulamalı Matematik Konferansı'nda özet metin olarak sunulmuştur. Ayrıca çalışmada DARWIN veri setini açık kaynak erişime açan kişi/kişilere teşekkürlerimizi sunarız

**KAYNAKLAR**

1. Demir, Z., and Türkan, F. “Asetilkolinesteraz ve Bütirikolinesteraz Enzimlerinin Alzheimer Hastalığı ile İlişkisi”. *Journal of the Institute of Science and Technology*, Vol. 12, Issue 4, Pages 2386-2395, 2020.
2. Kara, G. and Kılınç, G.E. “Alzheimer hastalığında ketojenik diyet tedavisi”. *İstanbul Gelişim Üniversitesi Sağlık Bilimleri Dergisi*, Vol. 15, Pages 630-638, 2021.
3. Keleş, E., and Özalevli, S. “Alzheimer hastalığı ve tedavi yaklaşımları”. *İzmir Kâtip Çelebi Üniversitesi Sağlık Bilimleri Fakültesi Dergisi*, Vol. 3, Issue 2, Pages 39-42, 2018.
4. Tekin, S., “Alzheimer Hastalığı Klinik Göstergeleri”, In Keskin A, O., UYSAL, A., Özge, A., Yener, G., Kırbaş, D., Sağlık Kurulunda Demans, Pages 28-36, Türk Nöroloji Derneği. Ankara, 2022.
5. Mutluer, M., “Devinime ilişkin kortikal potansiyellerin hafif bilişsel bozukluk ve orta evre alzheimer hastalığını değerlendirmede nöropsikolojik testler ile korelasyonu”, *Tıpta Uzmanlık Tezi*, Necmettin Erbakan Üniversitesi, Konya, 2009.
6. Saphioğlu, K., and Uzundurukan, S. “Bilimsel çalışmalarda kullanılan bazı yapay zeka uygulamalarının ve trendlerinin incelenmesi”. *Dicle Üniversitesi Mühendislik Fakültesi Mühendislik Dergisi*, Vol. 10, Issue 1, Pages 249-262, 2019
7. Hoşgör, H., and Güngördü, H. “Sağlıkta Yapay Zekanın Kullanım Alanları Üzerine Nitel Bir Araştırma”. *Avrupa Bilim ve Teknoloji Dergisi*, Vol. 35, Pages 395-407, 2022
8. Li, F., Tran, L., Thung, K.H., Ji, S., Shen, D., Li, J. “A robust deep model for improved classification of ad/mci patients”, *IEEE J. Biomed. Health Inform.* Vol. 19, Issue 5, 1610–1616, 2015
9. Hu, C., Ju, R., Shen, Y., Zhou, P., Li, Q. “Clinical decision support for alzheimer's disease based on deep learning and brain network”, 2016 IEEE International Conference on Communications (ICC), Kuala Lumpur, Pages 1-6, 2016
10. Karabay, G. S. and Çavaş, M. “Derin Öğrenme Yöntemiyle Alzheimer Hastalığının Tespiti” . *Firat Üniversitesi Mühendislik Bilimleri Dergisi*, Vol. 34, Issue 2, Pages 879-887, 2022.
11. Öziç, M. Ü. , Ekmekci, H. , Özşen, S. , Barstuğan, M. & Yıldıoğan, A. “3B T1 Ağırlıklı MR Görüntülerinde Atlas Tabanlı Hacim Ölçüm Yöntemini Kullanarak Alzheimer Hastalığının Teşhisi” . *Politeknik Dergisi* , Vol. 25, Issue 1 , Pages 47-58, 2022
12. Nalçakan, Y., “Derin Öğrenme ile Alzheimer Hastalığının Teşhisi”, *Yüksek Lisans Tezi*, İstanbul Üniversitesi-Cerrahpaşa Lisansüstü Eğitim Enstitüsü, İstanbul, 2018.
13. Wang, N., Chen, J., Xiao, H. et al., “Yapay sinir ağı modelinin Alzheimer hastalığının tanısında uygulanması”. *BMC Neurol*, Vol. 19 , Issue 154, 2019.
14. Janghel, R. R., & Rathore, Y. K. “Deep convolution neural network based system for early diagnosis of Alzheimer's disease”. *Irbm*, Vol. 42, Issue4, Pages 258-267, 2021.
15. De Gregorio, G., Desiato, D., Marcelli, A., & Polese, G. “A multi classifier approach for supporting Alzheimer's diagnosis based on handwriting analysis. In *Pattern Recognition*”, ICPR International Workshops and Challenges: Virtual Event, January 10–15, 2021, Proceedings, Part I , pages 559-574, Springer International Publishing.
16. Subha, R., Nayana, B. R., & Selvadass, M. “Hybrid Machine Learning Model Using Particle Swarm Optimization for Effectual Diagnosis of Alzheimer's Disease from Handwriting”, In 2022 4th International Conference on Circuits, Control, Communication and Computing (I4C), 2022, December, Pages 491-495, IEEE.
17. Gattulli, V., Impedovo, D., Pirlo, G., & Semeraro, G. “Handwriting Task-Selection based on the Analysis of Patterns in Classification Results on Alzheimer Dataset”, In *DSTNDS*, pages 18-29, 2023
18. Önder, M., Şentürk, Ü., Polat, K., & Paulraj, D. “Diagnosis of Alzheimer's Disease Using Boosting Classification Algorithms”, In 2023 International Conference on Research Methodologies in Knowledge Management, Artificial Intelligence and Telecommunication Engineering (RMKMATE), 2023, Pages 1-5, IEEE.

19. Schapire, R.E. “explain Adaboost”. In: Schölkopf, B., Luo, Z., Vovk, V. (eds) Empirical Inference, Pages 37-52, Heidelberg: Springer Berlin Heidelberg, Berlin, 2013.
20. “Alma Better”, <https://www.almabetter.com/bytes/tutorials/data-science/adaboost-algorithm>, Ocak 05, 2024.
21. Keleş, M. B., Keleş, A., & Keleş, A. “Makine Öğrenmesi Yöntemleri İle Uçuş Fiyatlarının Tahmini”. Euroasia Journal of Mathematics, Engineering, Natural & Medical Sciences, Vol. 7, Issue 11, Pages 72-78, 2020.
22. Gültekin, M., “Makine öğrenmesi tabanlı yazılım maliyet tahmini yöntemlerinin karşılaştırmalı analizi”, Doktora Tezi, Yıldız Teknik Üniversitesi, İstanbul, 2019.
23. Delgado, R. “A semi-hard voting combiner scheme to ensemble multi-class probabilistic classifiers”. Applied Intelligence, Vol. 52, Issue 4, Pages 3653-3677, 2022.
24. Koptur, M., “Makine Öğrenimi”, <https://makineogrenimi.wordpress.com/2017/06/14/modellerin-birlestirilmesi-ensemble-learning/>, Ocak 05, 2024.
25. Uysal, M., and Güyer, T. “İstatistiksel veri analizine ilişkin genişleyebilir bir karar ağacı tasarımı”. Bilişim Teknolojileri Dergisi, Vol. 7, Issue 3, Pages 33-43, 2014.
26. Kuzey, C., “Veri madenciliğinde destek vektör makinaları ve karar ağaçları yöntemlerini kullanarak bilgi çalışanlarının kurum performansı üzerine etkisinin ölçülmesi ve bir uygulama”, Yayımlanmamış Doktora Tezi, İstanbul Üniversitesi Sosyal Bilimler Enstitüsü, İstanbul, 2012.
27. Aytuğ, O. “Şirket iflaslarının tahminlenmesinde karar ağacı algoritmalarının karşılaştırmalı başarımlarını”. Bilişim Teknolojileri Dergisi, Vol. 8, Issue 1, Pages 9-19, 2015.
28. Özlem, A. & Güngör, O. “Rastgele orman algoritması kullanılarak çok bantlı görüntülerin sınıflandırılması”. Jeodezi ve Jeoinformasyon Dergisi, Issue 106, Pages 139-146, 2012.
29. Emhan Ö., & Mehmet, A. “Filtreleme tabanlı öznelik seçme yöntemlerinin anomali tabanlı ağ saldırısı tespit sistemlerine etkisi”. Dicle Üniversitesi Mühendislik Fakültesi Mühendislik Dergisi, Vol. 10, Issue 2, Pages 549-559, 2019.
30. Gülcü, Ş. “Bilgisayar ağ güvenliğinde naive bayes algoritmasının kullanımı”. Kilis 7 Aralık Üniversitesi Fen ve Mühendislik Dergisi, Vol. 3, Issue 1, , 2019.
31. Farzaliyev, E., Saihood, Q., and Sonuç, E. “Çocuklarda Anemi Hastalığının Teşhisinde Topluluk Öğrenme Yöntemlerinin Kullanılması”. In International Conference on Recent Academic Studies Vol. 1, Pages. 129-135, 2023.
32. Sikora, R. “A modified stacking ensemble machine learning algorithm using genetic algorithms”. In Handbook of research on organizational transformations through big data analytics, Pages 43-53, IGI Global, 2015.
33. Dou, J., Yunus, A. P., Bui, D. T., Merghadi, A., Sahana, M., Zhu, Z., ... and Pham, B. T. “Improved landslide assessment using support vector machine with bagging, boosting, and stacking ensemble machine learning framework in a mountainous watershed”, Japan. Landslides, Vol. 17, Pages 641-658, 2020.
34. Doğan, G. and Ergen, B. “İmobilenet cnn yaklaşımları ve özellik seçme yöntemleri kullanarak araç türlerini sınıflandırma”. Süleyman Demirel Üniversitesi Fen Bilimleri Enstitüsü Dergisi, Vol. 25, Issue 3, Pages 618-628, 2021.
35. Elmas, B. “Türkiye'deki kelebek türlerinin basamaklı evrişimli sinir ağları ile sınıflandırılması”. Konya Journal of Engineering Sciences, Vol. 9, Issue 3, 568-587, 2021.
36. Uçar, M. “Glokom hastalığının evrişimli sinir ağı mimarileri ile tespiti”. Deu Mühendislik Fakültesi Fen Ve Mühendislik, Vol. 23, Issue 68, Pages 521-529, 2021.
37. Gökçe, E., Demiral, M. F., Işık, A. H., & Bilen, M. “Evrişimli sinir ağlarında beyin tümörü segmentasyonu”. El-Cezeri Fen Ve Mühendislik Dergisi. Vol. 9, Issue 4, Pages 1518-1528, 2022.
38. Kantar, O. and Kilimci, Z. H. “Derin öğrenme temelli hibrid altın endeksi (xau/usd) yön tahmin modeli”. Gazi Üniversitesi Mühendislik Mimarlık Fakültesi Dergisi, Vol. 38, Issue 2, Pages 1117-1128, 2022.
39. Özen, G., Sultanov, R., Özen, Y., & Güneş, Z. Y. “A Convolutional Neural Network Based on Raw Single Channel EEG for Automatic Sleep Staging”. Sakarya University Journal of Computer and Information Sciences, Vol. 3, Issue 3, pages149-158, 2020.

40. Cilia, N. D., De Gregorio, G., De Stefano, C., Fontanella, F., Marcelli, A., and Parziale, A. "Diagnosing Alzheimer's disease from on-line handwriting: a novel dataset and performance benchmarking". *Engineering Applications of Artificial Intelligence*, Vol. 111, 104822, 2022.

41. Garré-Olmo, J., Faundez-Zanuy, M., Ipiña, K. L. d., Calvó-Perxas, L., & Turró-Garriga, O. "Kinematic and pressure features of handwriting and drawing: preliminary results between patients with mild cognitive impairment, alzheimer disease and healthy controls". *Current Alzheimer Research*, Vol. 14, Issue 9, Pages 960-968, 2017.

42. Cilia, N. D., Stefano, C. D., Fontanella, F., Marcelli, A., & Parziale, A. "Diagnosing alzheimer's disease from on-line handwriting: a novel dataset and performance benchmarking". *Engineering Applications of Artificial Intelligence*, Vo. 111, 104822, 2022.

43. Öcal, H. "A novel approach to detection of alzheimer's disease from handwriting: triple ensemble learning model". *Gazi Üniversitesi Fen Bilimleri Dergisi Part C: Tasarım Ve Teknoloji*, Vol. 12, Issu 1, Pages 214-223, 2024.



ULUSLARARASI 3B YAZICI TEKNOLOJİLERİ  
VE DİJİTAL ENDÜSTRİ DERGİSİ

INTERNATIONAL JOURNAL OF 3D PRINTING  
TECHNOLOGIES AND DIGITAL INDUSTRY

ISSN:2602-3350 (Online)

URL: <https://dergipark.org.tr/ij3dptdi>

# COMPARATIVE ANALYSIS OF BCCZZ LATTICE STRUCTURE COMPRESSION BEHAVIOR: EXPERIMENTAL, NUMERICAL, AND MACHINE LEARNING APPROACHES

**Yazarlar (Authors):** Deniz Aktürk \*, Muhammed Taha Yıldız , Nazim Babacan 

**Bu makaleye şu şekilde atıfta bulunabilirsiniz (To cite to this article):** Aktürk D., Yıldız M. T., Babacan N., “Comparative Analysis of BCCZZ Lattice Structure Compression Behavior: Experimental, Numerical, and Machine Learning Approaches” *Int. J. of 3D Printing Tech. Dig. Ind.*, 9(1): 36-44, (2025).

DOI: 10.46519/ij3dptdi.1490522

Araştırma Makale/ Research Article

Erişim Linki: (To link to this article): <https://dergipark.org.tr/en/pub/ij3dptdi/archive>

# COMPARATIVE ANALYSIS OF BCCZZ LATTICE STRUCTURE COMPRESSION BEHAVIOR: EXPERIMENTAL, NUMERICAL, AND MACHINE LEARNING APPROACHES

Deniz Aktürk<sup>ID a, b, \*</sup>, Muhammed Taha Yıldız<sup>ID a, b</sup>, Nazim Babacan<sup>ID a</sup>

<sup>a</sup> Department of Mechanical Engineering, Sivas University of Science and Technology, TÜRKİYE

<sup>b</sup> Institute of Defence Technologies, Sivas University of Science and Technology, TÜRKİYE

\* Corresponding Author: [dakturk@sivas.edu.tr](mailto:dakturk@sivas.edu.tr)

(Received: 27.05.24; Revised: 07.10.24; Accepted: 12.02.25)

---

## ABSTRACT

In this study, the compression behavior of the body-centered cubic with exterior and interior vertical struts (BCCZZ) lattice structure produced with Polylactic Acid (PLA) has been investigated using experimental, numerical, and machine-learning algorithms. When comparing digital image correlation and the ANSYS Static Structural numerical module, the measurements of deformation in the -Y direction taken from the top-right, top-left, middle-right, and middle-left points of the lattice structure are closely matched, with differences of 3.5%, 0.66%, 22.3%, and 12.69%, respectively. However, measurements from the bottom-left and bottom-right points show discrepancies of 49.17% and 58.91%, respectively. The lack of agreement between numerical and digital image correlation (DIC) analyses at the bottom-left and bottom-right points of the lattice structure is attributed to deformation in the lower section observed in the experimental study. The numerical study, modeling only elastic deformation, fails to account for broken regions' deformation adequately. Furthermore, the elastic deformation region has been comparatively investigated using experimental, numerical, and multilinear regression (MLR) models. Despite the MLR algorithm being trained with data from the compression test and achieving an  $R^2$  value of 0.97, numerical modeling is closer to the experimental results. Thus, for the first time in the literature, the compression behavior of the BCCZZ lattice structure made from PLA+ has been comparatively investigated using experimental, numerical, and machine learning methods.

**Keywords:** Additive Manufacturing, Lattice Structure, Digital Image Correlation, Numerical Modeling, Machine Learning, Compression Behavior.

---

## 1. INTRODUCTION

In recent years, the popularity of additive manufacturing methods has increased due to rapid prototyping, allowing the production of materials with desired tolerance and complexity [1, 2]. This manufacturing technique was first implemented in 1986 through the stereolithography technique, and over years of development, it has continued to evolve with techniques such as selective laser melting and fused deposition modeling (FDM) [3-5]. These methods are utilized in numerous sectors, including the aerospace, automotive, medical implants, and the defense industry [6-9].

FDM technology has emerged as the foremost additive manufacturing method for producing polymeric components, owing to its ease of implementation and cost-effectiveness [10]. In terms of polymer materials, polylactic acid (PLA) and acrylonitrile butadiene styrene (ABS) are the most commonly utilized, facilitating additive manufacturing in practical applications [11]. These thermoplastics, prized for their lightweight nature and affordability, are extensively favored in engineering and medical sectors [12]. PLA has earned its popularity in various applications due to its exceptional qualities, including

biocompatibility, biodegradability, mechanical strength, and processability [13].

In many engineering applications, lattice structures, which can be manufactured by additive manufacturing methods such as FDM technology, have become increasingly important due to their energy absorption capabilities and lightweight properties [14, 15]. Lattice structures are configurations created by connecting struts with three-dimensional geometry to nodes in a repeating cell pattern [16]. These structures are referred to by different names based on their arrangements, with the most commonly used being body-centered cubic (BCC) and face-centered cubic (FCC) structures [17]. These structures are referred to as BCCZ and FCCZ with the addition of vertical z-struts. The inclusion of these z-struts enhances the resistance to yielding and deformation in both BCC and FCC configurations [18-21]. Zhou et al. [22] have numerically and experimentally investigated the compression behavior of four different lattice geometries produced with PLA. They found that BCCZ and FCCZ lattice structures have a higher load-bearing capacity compared to BCC structures. In a recent study [23], the novel BCCZZ structure, featuring extra z-struts situated at the mid-span of oblique struts, was examined. It was found that the additional vertical struts in the BCCZ structures offer greater advantages for load-bearing applications, as they result in higher relative density and relative strength compared to the reference BCCZ structure.

To understand the behavior of lattice structures in load-bearing applications, experimental, analytical, and numerical methods are available [24, 25]. An ideal technique for measuring strain and revealing the deformation and failure mechanisms in lattice structures is a non-contact strain measurement method such as digital image correlation (DIC) [26, 27]. In addition, further insights into the deformation behavior and local strain values of lattice structures can be gained by the finite element method [28]. Moreover, machine learning algorithms, such as multiple linear regression (MLR) algorithm, can predict the behavior of the material under compression based on the features obtained from the compression test data. Once this algorithm

developed and validated, the model can be applied to predict the stress-strain data of the similar materials or structures.

Previous studies investigating compression behavior in lattice structures have typically relied on individual approaches like experiments, numerical simulations, or analytical methods, or a combination of two of these methods [27, 29-34]. This study uniquely addresses this gap by comparatively analyzing the compression behavior of a novel BCCZZ lattice structure through using a combined approach of digital image correlation (DIC), numerical method, and machine learning algorithm. Overall, the novelty of the study lies in the integration of multiple approaches to achieve a comprehensive understanding of a lattice structure's compressive behavior and deformation mechanism. It is believed that this integration enhances prediction accuracy, aids in design optimization, and improves the efficiency of engineering analysis processes.

## 2. MATERIAL AND METHODS

### 2.1. Experimental Analysis

The productions were performed with an FDM 3D printer (Ender-3 S1-Pro, Creality) at a nozzle temperature of 205 °C and a bed temperature of 65 °C. The lattice structure was made from polylactic acid (PLA+, eSUN) polymer. The dimensions of the produced lattice specimen were designed to be 62.5 x 62.5 x 60 mm<sup>3</sup> with strut diameters of 2.5 mm using the SolidWorks program. The drawing of the model is shown in Figure 1. It was then sliced in the Creality Slicer CAM program and converted into a G-code file for printing with a 10% infill density.

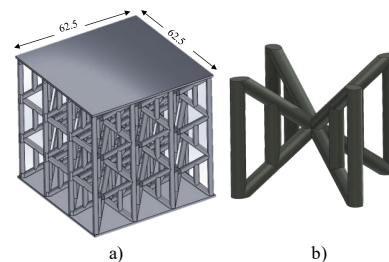


**Figure 1.** a) The model of the BCCZZ lattice structure and b) A view of the unit BCCZZ cell.

The compression test was conducted using a Shimadzu AG-S 50 kN universal testing machine

at a 1 mm/min deformation rate. Three specimens of the BCCZZ lattice structure have been produced, and compression tests have been conducted for each sample. A DIC system (EduDIC, Dantec) was used during the compression test to monitor the strain values in real-time and allow for later comparison with numerical analysis. The sample was sprayed with black speckles in a stochastic pattern. The images were captured at 100 Hz with the DIC system, and experimental data was examined through deformation of 2.5 mm. Figure 2 presents the compression test setup with DIC system. Datasets for numerical and machine learning algorithm analyses were generated from the compression test data.

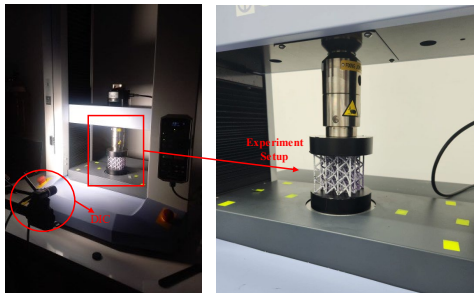


Figure 2. Compression Test Setup with DIC.

## 2.2. Numerical Analysis

In this study, the compression test of the BCCZZ lattice structure, produced with eSUN: PLA+ material, was numerically modeled. The ANSYS Static Structural module, which utilizes the finite element method for computation, has been used for numerical modeling.

To model the lattice structure produced with eSUN: PLA+, the material parameters shown in Table 1, was used.

Table 1. eSUN: PLA+ Ansys Engineering Data Parameters [35].

Parameters	Value
Density	1.23 g/cm <sup>3</sup>
Thermal Expansion Coefficient	0.00135 1/°C
Young Modulus	2.3 GPa
Poisson Ratio	0.3
Bulk Modulus	1.91 GPa

Shear Modulus

8.84 GPa

After conducting a mesh dependency study for element sizes of 0.75, 1, and 1.25 mm, a tetrahedral mesh structure with an element size chosen as 1 mm was utilized for the lattice structure. Figure 3 depicts the details and visual representation of the mesh structure.

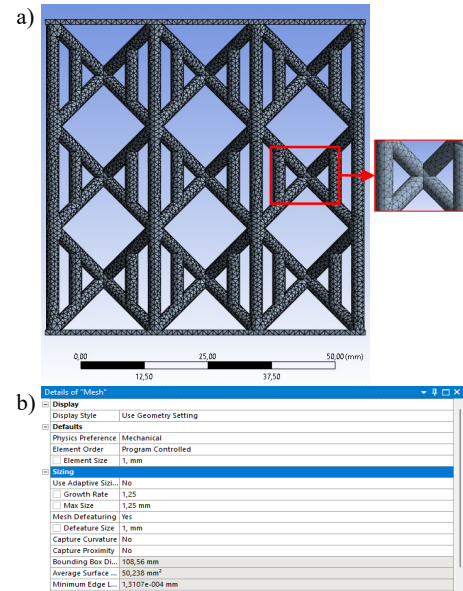


Figure 3. a) BCCZZ Mesh structure and b) Detail of the Mesh.

The compression analysis employed specific boundary conditions: a fixed support at the material's base and a displacement in the -Y direction at the top, set to 2.5 mm. The analysis involved measuring total deformation, total stress, force reaction, and directional deformation at six specific points. These points, depicted in Figure 4, had their directional deformation values measured across compression levels of 0.5, 1, 1.5, 2, and 2.5 mm.

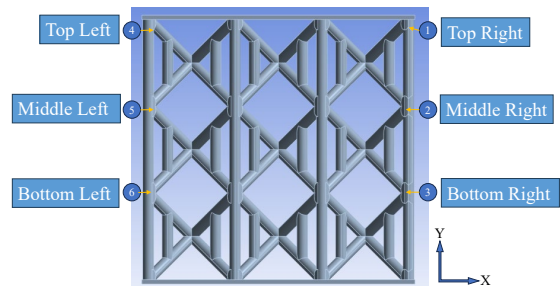


Figure 4. Deformation measurement points at the front face.

### 2.3. Multilinear Regression Algorithm

Multiple linear regression (MLR), a traditional prediction method, is an algorithm that attempts to predict a target variable based on one input variable [36, 37]. The MLR method possesses a simple, efficient, and data noise-resistant algorithm for predicting data with a linear distribution [38]. The MLR algorithm is shown in Equation (1). "Y" and "x<sub>i</sub>" represent the response and predictor variables, respectively, "b<sub>i</sub>" and "ε" denote the regression and residual coefficients, respectively, and "a" indicates the intercept [39].

$$\begin{aligned}
 Y &= a + \sum_{i=1}^n b_i x_i + \varepsilon \\
 &= b_1 x_1 + b_2 x_2 + \dots \\
 &\quad + b_i x_i + \varepsilon
 \end{aligned} \quad (1)$$

The necessary data for MLR were obtained from the elastic deformation region of compression test results. A test size of 0.2 was determined, and the data were trained. In the MLR method, Scikit-learn, Pandas, Matplotlib, Seaborn, and NumPy libraries were used. Analyses were performed using Python 3.11 programming language, with Spyder 5.4.3 IDE. The results obtained with MLR have been comparatively examined with experimental data.

### 3.RESULTS AND DISCUSSIONS

In this study, the deformation of the BCCZZ lattice structure under compressive loading was investigated using experimental, numerical, and machine learning methods. The DIC results obtained from the experimental analysis were compared with numerical analyses. Furthermore, a machine learning algorithm was trained using the results obtained from the experimental data, and the experimental, numerical, and machine learning results were comparatively analyzed.

Figure 5 displays the total deformation contour images obtained from numerical and DIC analysis

results. These images depict various deformation values ranging from 0.5 to 2.5 mm, with intervals of 0.5 mm. Table 2 presents the deformation values in the (-Y) direction at the relevant points (indicated in Figure 4) obtained from numerical test and experimental DIC analysis, as well as their relative differences. Throughout all deformation steps in numerical analyses, the base is experienced minimum deformation, due to the fixed deformation. However, in all deformation steps analyzed using DIC, deformation was observed on the ground. This discrepancy arises because, in the numerical analysis, defining the part as fixed to the ground prevents any deformation on the surface of the part or the ground. In contrast, experimental analyses conducted with DIC have shown deformation on the ground. At 0.5 and 1 mm, neither numerical nor DIC analyses show significant bending in struts. In addition, the BCCZZ lattice structure undergoes transverse expansion and longitudinal shortening while absorbing the force.

In the numerical analyses (Figure 5(e)), the maximum deformation is observed in the bent struts labeled as 1 and 3. Conversely, in the DIC tests (Figure 5(f)), maximum deformation primarily concentrates at the upper regions of the lattice structure, with heightened deformation observed at points where strut bending commences. Similar deformation patterns are noted in the struts within designated regions under deformation points of 1.5, 2, and 2.5 mm, as observed in both numerical and DIC analyses. Furthermore, it is seen that there is no significant shape change in the struts in the central region of the lattice structure in both analyses. This occurs because the presence of neighboring struts in the central region allows the load to be distributed more evenly to the struts at the center point. Thus, it has been observed that contour graphs are highly consistent throughout all deformation steps.

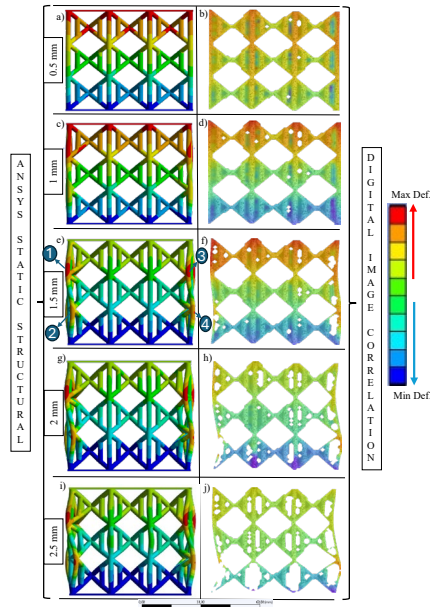


**Figure 5.** Contour images of the total deformation values from Ansys Static Structural (on the left) and DIC results (on the right).

Table 2 presents the deformation measurements at the points indicated in Figure 4 through numerical and DIC analyses, showing both deformation values and the percentage of absolute relative difference. Meanwhile, Table 3 presents the average percentages of absolute relative differences (ARD) separately. From these findings, it is apparent that the values at the top right, top left, middle right, and middle left points are relatively close to each other, with respective percentages of 3.5%, 0.66%, 22.3%, and 12.69%. However, a discrepancy is observed between the values at the bottom right and bottom left points, which are 58.91% and 49.17%, respectively. This can be attributed to the fact that in numerical analyses, the ground is fixed with fixed support, meaning the lattice structure does not undergo any movement on the surface, while in DIC analyses, the deformation caused by the force applied by the compression device also results in significant deformation of the ground. Additionally, due to fractures occurring in the struts during DIC analysis, the mesh structure that the analysis can track (randomly painted surface) is disrupted, resulting in the inability to capture the deformation at the bottom left, as seen in Figure 5(j).

**Table 2.** Deformation and ARD (%) values for Ansys Static Structural and DIC

Deformation	Measured Point	Ansys Static Structural	DIC	Absolute Relative Difference (%)
0.5 mm	Top Right	0.485	0.492	1.42
	Middle Right	0.337	0.471	28.45
	Bottom Right	0.172	0.439	60.82
	Top Left	0.485	0.489	0.81
	Middle Left	0.335	0.458	26.85
	Bottom Left	0.172	0.428	59.81
1 mm	Top Right	0.951	0.989	3.84
	Middle Right	0.657	0.838	21.59
	Bottom Right	0.324	0.660	50.90
	Top Left	0.982	0.976	0.61
	Middle Left	0.684	0.815	16.07
	Bottom Left	0.344	0.650	47.07
1.5 mm	Top Right	1.417	1.471	3.67
	Middle Right	1.006	1.228	18.07
	Bottom Right	0.403	0.890	54.71
	Top Left	1.532	1.510	1.45
	Middle Left	1.136	1.157	1.81
	Bottom Left	0.488	0.848	42.45
2 mm	Top Right	1.895	1.972	3.90
	Middle Right	1.377	1.711	19.52
	Bottom Right	0.496	1.304	61.96
	Top Left	2.059	2.041	0.88
	Middle Left	1.576	1.700	7.29
	Bottom Left	0.628	1.086	42.17
2.5 mm	Top Right	2.367	2.483	4.67
	Middle Right	1.713	2.250	23.86
	Bottom Right	0.605	1.788	66.16
	Top Left	2.570	2.540	1.18
	Middle Left	2.001	2.260	11.46
	Bottom Left	0.764	1.674	54.36

**Table 3.** Average relative difference (ARD) for deformation measurement points.

Measured Point	Average ARD (%)	Max ARD (%)	Min ARD (%)
Top Right	3.5	4.67	1.42
Top Left	0.66	1.45	0.61
Middle Right	22.3	28.45	18.07
Middle Left	12.69	26.85	1.81
Bottom Right	58.91	66.16	50.90
Bottom Left	49.17	59.81	42.17

The force-displacement curve for experimental and numerical analyses was obtained from the compression test, as shown in Figure 6. After examining the three experimental studies, it was observed that yielding began around a force of 5750 N and a deformation of 1.4 mm. Numerical simulations exclusively simulated the elastic region, demonstrating elastic deformation up to 2.5 mm. Upon comparing the elastic portions, it is evident that the elastic curves have similar slopes, yet the limits of the elastic region are different. The yielding observed at around 1.4 mm deformation in the experimental studies is likely due to the disadvantages associated with FDM printers [40-42]. In the FDM process, porosity occurs in the material due to the inability to control thermal variation and humidity content [43, 44]. Among these disadvantages, the most significant reason is the decrease in the material's density and consequently its strength due to porosity [45].

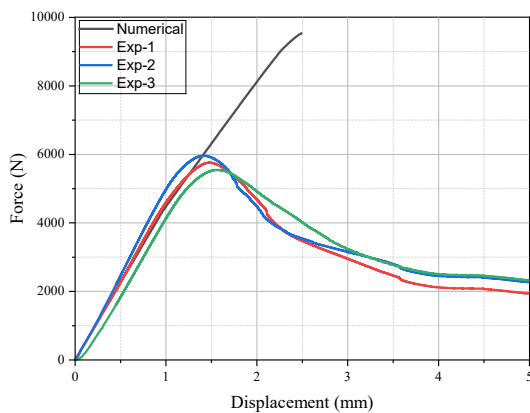


**Figure 6.** Experimental and numerical force-displacement curves for the BCCZZ lattice structure.

In the final step of the study, the results of experimental, numerical, and machine learning algorithms were comparatively analyzed in the elastic deformation region. Thus, it was determined which approach, the machine learning-based algorithm or the numerical model, aligns more closely with the experimental data. The MLR algorithm was trained using data obtained from compression test analyses conducted in Experiment 1 (Exp-1). Figure 7(a) presents a comparative analysis of the force values up to 1.5 mm deformation from experimental, numerical analyses and the MLR algorithm. In the MLR algorithm, the values of

$R^2$ , RMSE (Root Mean Square Error), MAE (Mean Absolute Error), and MAPE (Mean Absolute Percentage Error) are 0.97, 185.63, 158.25, and 4.38, respectively. Upon examining Figure 7(a), it was observed that the experimental and numerical data coincide regarding elastic deformation, while the MLR algorithm exhibited poorer performance compared to the numerical data. When analyzing the force-deformation graph, the experimental and numerical data almost align up to 0.6 mm, whereas the MLR algorithm has made a more distant prediction. The MLR algorithm, which constructs a linear regression line based on the training data, failed to accurately identify these points. Beyond 1.4 mm, as yielding began in the experimental data, neither the numerical analysis nor the MLR algorithm could predict the plastic deformation. This is because experimental data exhibit logarithmic variations, which the MLR algorithm inherently fails to capture due to its linear nature. To address this limitation, advanced algorithms such as polynomial regression, decision trees, or gradient boosting methods could be employed for better accuracy in modeling logarithmic changes.

The prediction error distribution of the MLR algorithm, depicted in Figure 7(b), reveals that the majority of errors cluster between -100 and 200, implying that most predictions closely approximate the actual values. However, due to the peaks in the 100-200 range, the errors deviate from a Gaussian normal distribution, indicating predictions further from the actual values. Therefore, the MLR algorithm has been less successful in the elastic region than the numerical method.

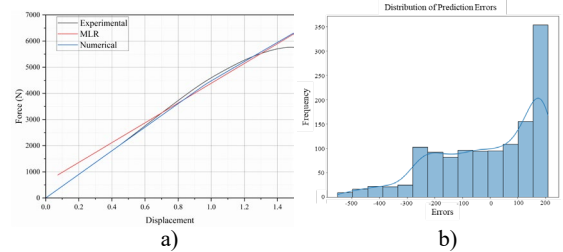


**Figure 7.** a) Comparison of experimental, numerical, and MLR results in the elastic deformation region, b) Error distribution graph of the MLR algorithm.

#### 4.CONCLUSIONS

In this study, the compression behavior of the BCCZZ lattice structure produced with eSUN PLA+ has been investigated through experimental, numerical, and MLR algorithms. The experimental analysis was compared with DIC analysis and numerical results. Additionally, the numerical results were compared with a machine learning algorithm developed using data obtained from the experimental study. The findings from the study are presented as follows:

- The error rates for the direction-dependent (-Y) deformation values measured at the top-right, top-left, middle-right, and middle-left points of the BCCZZ lattice structure subjected to the compression test were calculated to be 3.5%, 0.66%, 22.3%, and 12.69%, respectively. The measurements performed at these points have similar values when comparing DIC and numerical results.
- The error rates obtained at the bottom-right and bottom-left points were calculated as 58.91% and 49.17%, respectively. This is due to the specimen undergoing plastic deformation and failure at the bottom-right and bottom-left points under the applied force during the experiment measured with DIC. Since only elastic deformation is numerically modeled, high error rates have been observed at the lower points located on the base.
- The compression test results for elastic region deformation have been compared using experimental, numerical, and MLR algorithm analyses. Despite the MLR algorithm's  $R^2$  value of 0.97, the numerical results correspond more closely with the experimental data in the elastic region deformation.
- Although the experimental findings align with the numerical and machine learning algorithms in the elastic region, this agreement does not extend to the plastic region. The early onset of plastic deformation in the experimental study compared to the numerical analysis is attributed to section narrowing and the tendency for easy separation between layers, which are drawbacks associated with FDM technology.

#### REFERENCES

1. Hirschberg, C., Larsen, M.S., Bøtker, J.P., Rantanen, J., "Additive manufacturing of prototype elements with process interfaces for continuously operating manufacturing lines", *Asian journal of pharmaceutical sciences*, Vol. 13, Issue 6, Pages 575-583, 2018.
2. Ngo, T.D., Kashani, A., Imbalzano, G., Nguyen, K.T., Hui, D., "Additive manufacturing (3D printing): A review of materials, methods, applications and challenges", *Composites Part B: Engineering*, Vol. 143, Pages 172-196, 2018.
3. Wang, Y., Zhou, Y., Lin, L., Corker, J., Fan, M., "Overview of 3D additive manufacturing (AM) and corresponding AM composites", *Composites Part A: Applied Science and Manufacturing*, Vol. 139, Pages 106114, 2020.
4. Hanzl, P., Zetek, M., Bakša, T., Kroupa, T., "The influence of processing parameters on the mechanical properties of SLM parts", *Procedia Engineering*, Vol. 100, Pages 1405-1413, 2015.
5. Ning, F., Cong, W., Qiu, J., Wei, J., Wang, S., "Additive manufacturing of carbon fiber reinforced thermoplastic composites using fused deposition modeling", *Composites Part B: Engineering*, Vol. 80, Pages 369-378, 2015.
6. Seabra, M., Azevedo, J., Araújo, A., Reis, L., Pinto, E., Alves, N., Santos, R., Mortágua, J.P., "Selective laser melting (SLM) and topology optimization for lighter aerospace components", *Procedia Structural Integrity*, Vol. 1, Pages 289-296, 2016.
7. Yuan, L., Ding, S., Wen, C., "Additive manufacturing technology for porous metal implant applications and triple minimal surface structures: A review", *Bioactive materials*, Vol. 4, Pages 56-70, 2019.
8. Karayel, E., Bozkurt, Y., "Additive manufacturing method and different welding applications", *Journal of Materials Research and Technology*, Vol. 9, Issue 5, Pages 11424-11438, 2020.
9. Delic, M., Evers, D.R., "The effect of additive manufacturing adoption on supply chain flexibility and performance: An empirical analysis from the automotive industry", *International Journal of Production Economics*, Vol. 228, Pages 107689, 2020.

10. Tang, C., Liu, J., Yang, Y., Liu, Y., Jiang, S., Hao, W., "Effect of process parameters on mechanical properties of 3D printed PLA lattice structures", *Composites Part C: Open Access*. Vol. 3, Pages 100076, 2020.
11. Luo, J., Luo, Q., Zhang, G., Li, Q., Sun, G., "On strain rate and temperature dependent mechanical properties and constitutive models for additively manufactured polylactic acid (PLA) materials", *Thin-Walled Structures*. Vol. 179, Pages 109624, 2022.
12. Samykano, M., "Mechanical property and prediction model for FDM-3D printed polylactic acid (PLA)", *Arabian Journal for Science and Engineering*, Vol. 46, Pages 7875-7892, 2021.
13. Singhvi, M., Zinjarde, S., Gokhale, D., "Polylactic acid: Synthesis and biomedical applications", *Journal of applied microbiology*. Vol. 127, Issue 6, Pages 1612-1626, 2019.
14. Sharma, D., Hiremath, S.S., "Experimental and FEM study on the in-plane and out-plane loaded reversible dual-material bio-inspired lattice structures with improved energy absorption performance", *Composite Structures*, Vol. 303, Pages 116353, 2023.
15. Takaichi, A., Kajima, Y., Kittikundecha, N., Htat, H.L., Cho, H.H.W., Hanawa, T., Yoneyama, T., Wakabayashi, N., "Effect of heat treatment on the anisotropic microstructural and mechanical properties of Co-Cr-Mo alloys produced by selective laser melting", *Journal of the Mechanical Behavior of Biomedical Materials*, Vol. 102, Pages 103496, 2020.
16. Babamiri, B.B., Barnes, B., Soltani-Tehrani, A., Shamsaei, N., Hazeli, K., "Designing additively manufactured lattice structures based on deformation mechanisms", *Additive Manufacturing*, Vol. 46, Pages 102143, 2021.
17. Maconachie, T., Leary, M., Lozanovski, B., Zhang, X., Qian, M., Faruque, O., Brandt, M., "SLM lattice structures: Properties, performance, applications and challenges", *Materials & Design*, Vol. 183, Pages 108137, 2019.
18. Wu, W., Xia, R., Qian, G., Liu, Z., Razavi, N., Berto, F., Gao, H., "Mechanostructures: Rational mechanical design, fabrication, performance evaluation, and industrial application of advanced structures", *Progress in Materials Science*, Vol. 131, Pages 101021, 2023.
19. Köhnen, P., Haase, C., Bültmann, J., Ziegler, S., Schleifenbaum, J.H., Bleck, W., "Mechanical properties and deformation behavior of additively manufactured lattice structures of stainless steel", *Materials & Design*, Vol. 145, Pages 205-217, 2018.
20. Mines, R., Tsopanos, S., Shen, Y., Hasan, R., McKown, S., "Drop weight impact behaviour of sandwich panels with metallic micro lattice cores", *International Journal of Impact Engineering*, Vol. 60, Pages 120-132, 2013.
21. Wang, W., Wang, T.Y., Yang, Z., Liu, L., Tong, X., Tong, W., Deng, J., Chen, F., Liu, X., "Cost-effective printing of 3D objects with skin-frame structures", *ACM Transactions on Graphics (ToG)*, Vol. 32, Issue 6, Pages 1-10, 2013.
22. Zhou, X., Qu, C., Luo, Y., Heise, R., Bao, G., "Compression behavior and impact energy absorption characteristics of 3D printed polymer lattices and their hybrid sandwich structures", *Journal of Materials Engineering and Performance*, Vol. 30, Pages 8763-8770, 2021.
23. Seremet, H., Babacan, N., "Compressive properties of AlSi10Mg lattice structures with novel BCCZZ and FCCZZ configurations fabricated by selective laser melting", *Rapid Prototyping Journal*, Vol. 30, Issue 4, Pages 770-781, 2024.
24. Ramos, H., Pickering, E., AlMahri, S., Krishnan, K., Oyebanji, J., Guan, Z., Langdon, G., Santiago, R., "Experimental evaluation of hybrid lattice structures subjected to blast loading". *Additive Manufacturing*. Vol. 76, Pages 103751, 2023.
25. Araghi, M., Rokhgireh, H., Nayebi, A., "Experimental and FEM investigation of BCC lattice structure under compression test by using continuum damage mechanics with micro-defect closure effect". *Materials & Design*. Vol. 232, Pages 112125, 2023.
26. Gonabadi, H., Yadav, A., Bull, S., "The effect of processing parameters on the mechanical characteristics of PLA produced by a 3D FFF printer", *The International Journal of Advanced Manufacturing Technology*, Vol. 111, Pages 695-709, 2020.
27. Song, J., Wang, Y., Zhou, W., Fan, R., Yu, B., Lu, Y., Li, L., "Topology optimization-guided lattice composites and their mechanical characterizations", *Composites Part B: Engineering*, Vol. 160, Pages 402-411, 2019.

28. Drücker, S., Lüdeker, J.K., Blecken, M., Kurt, A., Betz, K., Kriegesmann, B., Fiedler, B., "Probabilistic analysis of additively manufactured polymer lattice structures", *Materials & Design*, Vol. 213, Pages 110300, 2022.
29. Kolken, H., Garcia, A.F., Du Plessis, A., Meynen, A., Rans, C., Scheys, L., Mirzaali, M., Zadpoor, A., "Mechanisms of fatigue crack initiation and propagation in auxetic meta-biomaterials", *Acta biomaterialia*, Vol. 138, Pages 398-409, 2022.
30. Hedayati, R., Sadighi, M., Mohammadi-Aghdam, M., Zadpoor, A., "Analytical relationships for the mechanical properties of additively manufactured porous biomaterials based on octahedral unit cells", *Applied Mathematical Modelling*, Vol. 46, Pages 408-422, 2017.
31. Yavas, D., Liu, Q., Zhang, Z., Wu, D., "Design and fabrication of architected multi-material lattices with tunable stiffness, strength, and energy absorption", *Materials & Design*, Vol. 217, Pages 110613, 2022.
32. Liu, C., Lertthanasarn, J., Pham, M.-S., "The origin of the boundary strengthening in polycrystal-inspired architected materials". *Nature Communications*, Vol. 12, Issue 1, Pages 4600, 2021.
33. Mostafa, K.G., Momesso, G.A., Li, X., Nobes, D.S., Qureshi, A.J., "Dual graded lattice structures: generation framework and mechanical properties characterization", *Polymers*, Vol. 13, Issue 9, Pages 1528, 2021.
34. Saleh, M., Anwar, S., Al-Ahmari, A.M., Alfaify, A., "Compression performance and failure analysis of 3D-printed carbon fiber/PLA composite TPMS lattice structures", *Polymers*, Vol. 14, Issue 21, Pages 4595, 2022.
35. *eSUN PLA+ filament*, <https://www.esun3d.com/pla-pro-product/>, May 5, 2024.
36. Hauswirth, S.M., Bierkens, M.F., Beijik, V., Wanders, N., "The potential of data driven approaches for quantifying hydrological extremes", *Advances in Water Resources*, Vol. 155, Pages 104017, 2021.
37. Zhao, X., Zhang, R., Chen, F., Maisupova, B., Kirillov, V., Mambetov, B., Yu, S., He, Q., Dosmanbetov, D., Kelgenbayev, N., "Reconstructed summertime (June–July) streamflow dating back to 1788 CE in the Kazakh Uplands as inferred from tree rings", *Journal of Hydrology: Regional Studies*, Vol. 40, Pages 101007, 2022.
38. Ren, X., Mi, Z., Georgopoulos, P.G., "Comparison of Machine Learning and Land Use Regression for fine scale spatiotemporal estimation of ambient air pollution: Modeling ozone concentrations across the contiguous United States". *Environment international*, Vol. 142, Pages 105827, 2020.
39. Xie, X., Wu, T., Zhu, M., Jiang, G., Xu, Y., Wang, X., Pu, L., "Comparison of random forest and multiple linear regression models for estimation of soil extracellular enzyme activities in agricultural reclaimed coastal saline land", *Ecological Indicators*, Vol. 120, Pages 106925, 2021.
40. Baechle-Clayton, M., Loos, E., Taheri, M., Taheri, H., "Failures and flaws in fused deposition modeling (FDM) additively manufactured polymers and composites", *Journal of Composites Science*, Vol. 6, Issue 7, Pages 202, 2022.
41. Moradi, M., Karami Moghadam, M., Shamsborhan, M., Bodaghi, M., "The synergic effects of FDM 3D printing parameters on mechanical behaviors of bronze poly lactic acid composites", *Journal of Composites Science*, Vol. 4, Issue 1, Pages 17, 2020.
42. Khosravani, M.R., Božić, Ž., Zolfagharian, A., Reinicke, T., "Failure analysis of 3D-printed PLA components: Impact of manufacturing defects and thermal ageing", *Engineering Failure Analysis*, Vol. 136, Pages 106214, 2022.
43. Bhagia, S., Bornani, K., Agrawal, R., Satlewal, A., Đurković, J., Lagaña, R., Bhagia, M., Yoo, C.G., Zhao, X., Kunc, V., "Critical review of FDM 3D printing of PLA biocomposites filled with biomass resources, characterization, biodegradability, upcycling and opportunities for biorefineries", *Applied Materials Today*, Vol. 24, Pages 101078, 2021.
44. Swetham, T., Reddy, K.M.M., Huggi, A., Kumar, M.N., "A Critical Review on of 3D Printing Materials and Details of Materials used in FDM", *Int. J. Sci. Res. Sci. Eng. Technol.*, Vol. 3, Issue 2, Pages 353-361, 2017.
45. Triyono, J., Sukanto, H., Saputra, R.M., Smaradhana, D.F., "The effect of nozzle hole diameter of 3D printing on porosity and tensile strength parts using polylactic acid material", *Open Engineering*. Vol. 10, Issue 1, Pages 762-768, 2020.



ULUSLARARASI 3B YAZICI TEKNOLOJİLERİ  
VE DİJİTAL ENDÜSTRİ DERGİSİ

INTERNATIONAL JOURNAL OF 3D PRINTING  
TECHNOLOGIES AND DIGITAL INDUSTRY

ISSN:2602-3350 (Online)

URL: <https://dergipark.org.tr/ij3dptdi>

# INVESTIGATING THE EFFECT OF UNIT CELL ORIENTATION ON MECHANICAL PROPERTIES OF GYROID-BASED LATTICE STRUCTURES

**Yazarlar (Authors):** Golbarg Nikaein <sup>ID</sup>, Binnur Sagbas <sup>ID</sup>, Maryam Jamshidi <sup>ID</sup>, Mohammad Hossein Sadeghi <sup>ID\*</sup>

**Bu makaleye şu şekilde atıfta bulunabilirsiniz (To cite to this article):** Nikaein G., Sagbas B., Jamshidi M., Sadeghi M. H., "Investigating The Effect of Unit Cell Orientation on Mechanical Properties of Gyroid-Based Lattice Structures" *Int. J. of 3D Printing Tech. Dig. Ind.*, 9(1): 45-52, (2025).

DOI: 10.46519/ij3dptdi.1542438

Araştırma Makale/ Research Article

Erişim Linki: (To link to this article): <https://dergipark.org.tr/en/pub/ij3dptdi/archive>

# INVESTIGATING THE EFFECT OF UNIT CELL ORIENTATION ON MECHANICAL PROPERTIES OF GYROID-BASED LATTICE STRUCTURES

Golbarg Nikaein<sup>a</sup>, Binnur Sagbas<sup>b</sup>, Maryam Jamshidi<sup>a</sup>, Mohammad Hossein Sadeghi<sup>a\*</sup>

<sup>a</sup> Tarbiat Modares University, Mechanical Engineering Faculty, Mechanical Engineering Department, IRAN

<sup>b</sup> Yildiz Technical University, Mechanical Engineering Faculty, Mechanical Engineering Department, TURKIYE

\* Corresponding Author: [sadeghim@modares.ac.ir](mailto:sadeghim@modares.ac.ir)

(Received: 12.07.24; Revised: 07.02.25; Accepted: 04.03.25)

---

## ABSTRACT

Today, lattice bone scaffolds are highly regarded due to their controllable mechanical properties and biological performance. However, lattice structures often exhibit anisotropy because of the non-uniform distribution of the constitutive material in the tessellated unit cells, leading to variations in mechanical response based on loading direction. Loads applied to a lattice bone scaffold may not align with the main axes of the arranged unit cells. Therefore, optimizing the unit cell orientation angle seems necessary for achieving superior mechanical performance. This study investigates the mechanical properties of Gyroid-based lattice structures with varying unit cell orientations. Numerical analyses were conducted on five Gyroid-based lattice models with different cell orientations, and their compressive Young's moduli were determined. These findings were validated through mechanical compression experiments on corresponding 3D printed samples. The results indicate that the compressive Young's modulus in the least stiff direction is 18.99% lower than that along the stiffest direction. This is an advantage for the development of Gyroid-based bone regeneration scaffolds, particularly in scenarios where loading directions are not known in advance.

**Keywords:** Gyroid Lattice Structure, Unit Cell Orientation, Lattice Bone Scaffolds.

---

## 1. INTRODUCTION

Architected lattice structures are two or three-dimensional arrangements of repetitive units called unit cells. Generally, the properties of such structures are predominantly influenced by their microstructural geometry, in addition to the material they are made from [1]. In other words, changing the geometrical parameters of the microstructure will change the properties and behavior of the macrostructure. Therefore, by assigning appropriate values to each of the geometrical parameters, the behavior of the structure can be controlled in a way that the requirements will be met. Recent advancements in additive manufacturing (AM) have facilitated the precise creation of such complicated structures with fine features. Controllable properties and ease of manufacturing have caused an increasing interest in using such structures in various fields of engineering. However, the more advanced use of such

structures can be found in biomedical engineering fields, especially in developing orthopedic implants and bone scaffolds, where both mechanical and biological requirements should be considered. Luckily, architected lattice structures can make it possible to adjust mechanical properties and biological performance simultaneously. These structures can reduce the stiffness of a metal bone scaffold to that of the host bone tissue, hence the risk reduction of stress shielding phenomenon. They can also provide an environment where bone ingrowth happens. It has been suggested that a fully interconnected porous scaffold with a porosity of more than 50% and pore size of 100  $\mu\text{m}$  to 700  $\mu\text{m}$ , results in an ideal osseointegration [2]. However, increasing the porosity to reduce the stiffness and enhance the osseointegration, causes a decrease in mechanical strength [3] and fatigue life [4]. By keeping these in mind, the design parameters of

a lattice (i.e., geometric parameters of the constituent unit-cells as well as the arrangement of the cells in the structure) should be chosen intellectually to satisfy all the requirements.

Lattices derived from triply periodic minimal surfaces (TPMS) are promising candidates for developing orthopedic implants, given their favourable characteristics, which include a high surface-to-volume ratio, appropriate stiffness, and high manufacturability [5]. Among the different types of TPMS structures, Gyroid structure has been of great interest and so far, many studies have been conducted to investigate its properties [6-10] or to compare them with the properties of other TPMS lattices [11-13]. Moreover, many bone implants and scaffolds have been designed based on this unit cell type as can be mentioned in [14-16].

When evaluating the mechanical properties of lattice structures, it's worth knowing that such structures often exhibit anisotropy because of the non-uniform distribution of the constitutive material in the tessellated unit cells, leading to different mechanical properties based on loading direction. Furthermore, in the case of lattice scaffolds, applied loads are not necessarily aligned with the main axes of the tessellated unit cells. Since a scaffold must be able to withstand complex loading conditions, achieving anisotropic properties of its structure is of great importance, which can also be used later in the optimal design process. In this regard, Barber et al. [17] studied the effect of cell orientation on the compressive mechanical properties of three different lattice structures, including sheet-based Gyroid, sheet-based Schwartz-D, and strut-based Diamond structures. The difference in the peak compressive strength between the strongest and weakest orientations in truss-based Diamond, sheet-based Schwartz-D and sheet-based Gyroid structures was 49%, 21%, and 18%, respectively, which showed that the sheet-based TPMS structures are less anisotropic than the truss-based one. In a study conducted by Caiazzo et al. [18] it was shown that until geometrical expansion is not applied along the sheet-based Gyroid axes, the mechanical response of the structure is not significantly affected by the orientation of unit cells. However, according to [19], in a sheet-based Gyroid structure, the maximum and minimum values of elastic modulus are obtained in

diagonal and axial cell orientation, respectively. In the case of truss-based Diamond lattices, Cutolo et al. [20] showed that mechanical properties, except for energy absorption, increase by changing the loading direction from [001]. It was shown that the increased stiffness in [011] direction makes the resulting structure one with a high strength-to-weight ratio, applicable in orthopedic devices.

This study aims to investigate the compressive Young's modulus of a Gyroid-based lattice structure under different loading directions. The methodology of the present work is discussed in the next section. In that section, the process of design, manufacturing, and evaluation is presented. In the third section, the obtained results will be presented and discussed. Finally, in the fourth section, a conclusion is drawn regarding the use of Gyroid structures as bone regeneration scaffolds. Suggestions for further research will be given as well.

## 2. MATERIAL AND METHOD

The complicated topology of a sheet-based Gyroid unit cell is shown in Figure 1. Like other TPMS cells, this one is also described using a trigonometric equation as follows:

$$\cos x \sin y + \cos y \sin z + \cos z \sin x = P \quad (1)$$

Where  $P$  is the offset parameter that controls the wall thickness.

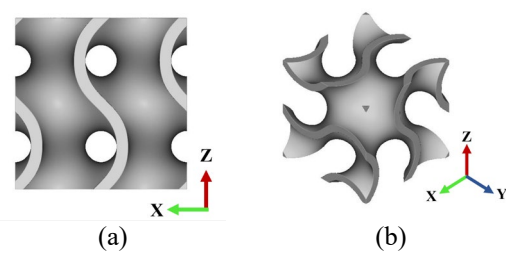


**Figure 1.** Computer-aided design model of a sheet-based Gyroid unit cell from (a) side view and (b) isometric view. The model is obtained through nTopology design software.

As previously mentioned, the study aims to investigate the compressive Young's modulus of a Gyroid structure under different loading directions. Since it requires changes in the test setup to apply load in different directions, it was decided to keep the applied load direction constant and change the orientation angle of the

tessellated unit cells instead. Here, five orientation angles in the x-z plane were considered. These orientation angles are 0,  $\arctan(0.5)$ , 45,  $\arctan(2)$ , and 90 degrees. For convenience, these orientations are also represented by [001], [102], [101], [201], and [100], respectively. [001] is considered as the principal orientation. Therefore, if it is assumed that there is a large lattice box containing unit cells along this principal direction, the other oriented lattices will be obtained by extracting samples along any of the above-mentioned angles from that box. Figure 2 shows the extracted oriented models.

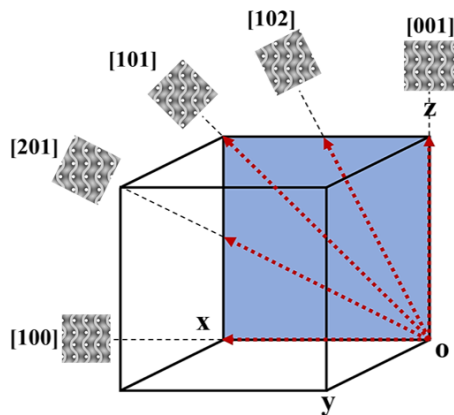


**Figure 2.** Rotation plane (shown in blue) in which the desired cell orientations are defined.

In the following, numerical and experimental evaluations will be conducted to see how different cell orientations affect the Young's modulus of a Gyroid structure.

### 2.1. Preparing Gyroid structures

Five cylindrical Gyroid-based lattice models were designed using nTopology design software. Each model corresponded to one specific cell orientation. The orientations were along the [001], [102], [101], [201], and [100]

directions (as previously shown in Figure 2). These orientations were selected to find out how the stiffness will change when cell orientation deviates from the main initial orientation, i.e. [001]. All the cylindrical models were 15 mm in diameter and 20 mm in height. Cell size and wall thickness were set at 5 mm and 0.45 mm, respectively. These geometrical characteristics create lattices with a nominal porosity of almost 76.4%, which is suitable for a bone scaffold in order to provide good osseointegration. The designed models are shown in Figure 3. As evident from the figure, a change in cell orientation angle, changes the topology of the lateral surface of the structure.

All the samples were additively manufactured using liquid crystal display (LCD) 3D printing technology with an ANYCUBIC Photon Mono X (4k) printer with a layer thickness of 50 microns. The constitutive material was ANYCUBIC Colored UV Resin, which was a commercial material made up of polyurethane acrylate, acrylate monomer, and photoinitiator. Immediately after manufacturing, each sample was exposed to high-intensity visible light for an hour. Here, to check the repeatability of the experimental results, three samples were made for each designed model. Besides the lattice samples, three fully solid samples were also made for two reasons: First, to measure the density of the constitutive material which will be used later in measuring the porosity of each manufactured lattice sample. Second, to determine the Young's modulus of the constitutive material, which might be changed depending on the manufacturing and post-curing parameters. This quantity will be used in determining the effective Young's moduli of the lattices in the numerical solution. Figure 4 displays the manufactured samples.

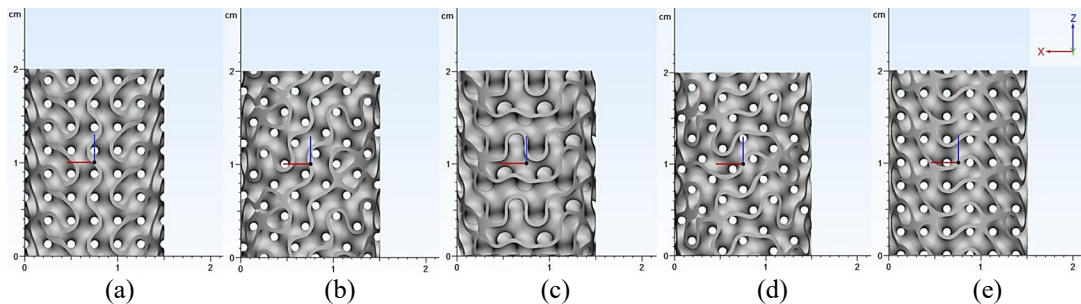


**Figure 3.** Designed lattice models with cell orientations along (a) [001], (b) [102], (c) [101], (d) [201], and (e) [100] directions.

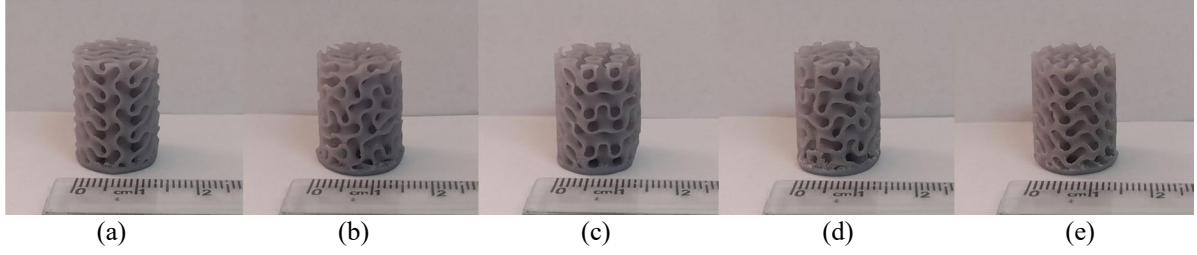


**Figure 4.** Manufactured lattice samples with cell orientations along (a) [001], (b) [102], (c) [101], (d) [201], and (e) [100] directions.

In order to evaluate the manufacturing quality, the overall porosities of the manufactured lattice samples were measured and compared with those of the designed ones. The porosity of each manufactured sample can be measured as follows:

$$P = 1 - \left(\frac{V^*}{V}\right) \quad (2)$$

Where  $P$  is the porosity of the manufactured lattice,  $V^*$  and  $V$  are the volume of the lattice and the volume of its surrounding box, respectively.  $V$  can be easily obtained by measuring the dimensions of the manufactured sample with a calliper, while  $V^*$  is obtained as follows:

$$V^* = \frac{m^*}{\rho} \quad (3)$$

Where  $m^*$  is the mass of the manufactured lattice which can be measured using an analytical balance, and  $\rho$  is the density of the constitutive material, which can be measured by dividing the mass of the fully solid sample by its volume.

## 2.2. Numerical Solution

Numerical analysis of the structures was done in the Abaqus finite element software. After importing each model to the Abaqus, two rigid planes were added at the top and at the bottom of the cylindrical structure to imitate the compression plates in a compression testing machine. The rigid plane at the bottom was fixed in all directions while the one at the top was allowed to translate along the Z-axis by  $-0.3$  mm. Tetrahedron elements were used to mesh the structure. The derived force-displacement data was converted to a stress-strain curve by dividing the force and the displacement by the cross-sectional area and the initial height of the cylindrical lattice, respectively. The compressive Young's

modulus of the lattice structure is determined by the slope of the linear segment of the curve.

## 2.3. Experimental Evaluation

Experiments were undertaken to characterize the effective Young's moduli of the lattice structures, thereby validating the numerical solution results. Samples were tested in a universal testing machine (Gotech, GT-TCS-2000) with 1000 kgf maximum load capacity (Figure 5). The test speed was set at 1 mm/min. Force-displacement curves were recorded and converted later to stress-strain curves. The linear segment of the stress-strain curve corresponds to the elastic region, where the slope of this segment indicates the Young's modulus.



**Figure 5.** Demonstration of the Gotech universal testing machine utilized for conducting the simple compression tests.

## 3. RESULTS AND DISCUSSION

In the current section, the effect of cell orientation on the Young's modulus of a Gyroid-based lattice structure is presented and discussed regarding the numerical and experimental findings. As mentioned in section 2.1, to measure the porosity of the manufactured samples, it is essential to determine the density

of the constituent resin material. The density was determined by dividing the mass of the fully solid samples, measured with an analytical balance with a precision of 0.0001 g readability, by their volume, which was obtained using a calliper. This calculation resulted in an average density of 1.260 g/cm<sup>3</sup>. The porosity of the manufactured samples was then determined using Equations (2) and (3) and represented in Table 1. The porosity of the manufactured lattice samples is on average 5.66% lower than

that of the designed models. This amount of difference between the porosities is not abnormal. Such a difference has also been reported in other similar works [2]. Because the designed models have complicated geometric details with fine features, the 3D printer is not capable of perfectly creating them. For example, the dimensions of the manufactured features do not completely match with those of the CAD models. This, in turn, can be enough to explain this discrepancy.

**Table 1.** Porosity and Young’s modulus of the designed and manufactured Gyroid lattices.

Cell orientation	Porosity (%)			Young’s modulus (MPa)		
	Designed	Manufactured	error (%)	Simulation	Experiment	error (%)
[001]	76.3	72.1±0.99	5.50	50.62	43.36±2.92	16.74
[102]	76.3	71.5±0.70	6.29	53.73	49.46±3.15	8.63
[101]	76.5	72.5±1.35	5.23	57.28	53.52±5.40	7.02
[201]	76.4	72.1±0.57	5.63	54.82	47.53±4.29	15.34
[100]	76.3	72.0±1.65	5.64	50.60	44.62±3.93	13.40

As mentioned before, the compressive Young’s modulus of the constitutive resin material should be obtained from the solid samples through the compression tests. Figure 6 illustrates the stress-strain curves for the solid samples.

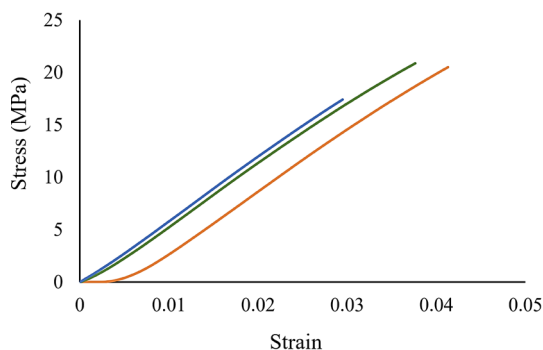


**Figure 6.** Stress-Strain curves of three solid samples obtained from compression tests.

The Young's modulus of the solid samples was obtained to be 617.45 MPa on average. This represents the elastic modulus of the resin material. The compressive Young’s modulus of the lattices was then obtained through numerical and experimental methods. As it can be seen in Table 1, the results of both methods are in good

agreement. As it turns out, by changing the orientation angle of the cells from [001] to [100] in the lattice structure, the value of the compressive Young's modulus increases at first and then decreases again. It can be clearly observed that the maximum value of the compressive Young’s modulus belongs to the structure with the cell orientation along [101], while the minimum value occurs along [001] and [100]. In the two latter orientations, Gyroid samples become completely the same and that’s why their results match with each other. This agrees with the findings of Khaleghi et al. [19] and Chen et al. [21]. Here, the value of the compressive Young’s modulus along the least stiff direction is 18.99% lower than that along the stiffest direction. However, this difference is for the considered lattice with a porosity of about 72.0%. By decreasing the porosity, the distribution of the material increases in the structure. Therefore, the lattice becomes more homogenous. So, it is expected that the difference between the compressive Young’s moduli along the stiffest and least stiff directions becomes less. The von Mises stress distribution for all the oriented Gyroid lattices is depicted in Figure 7.

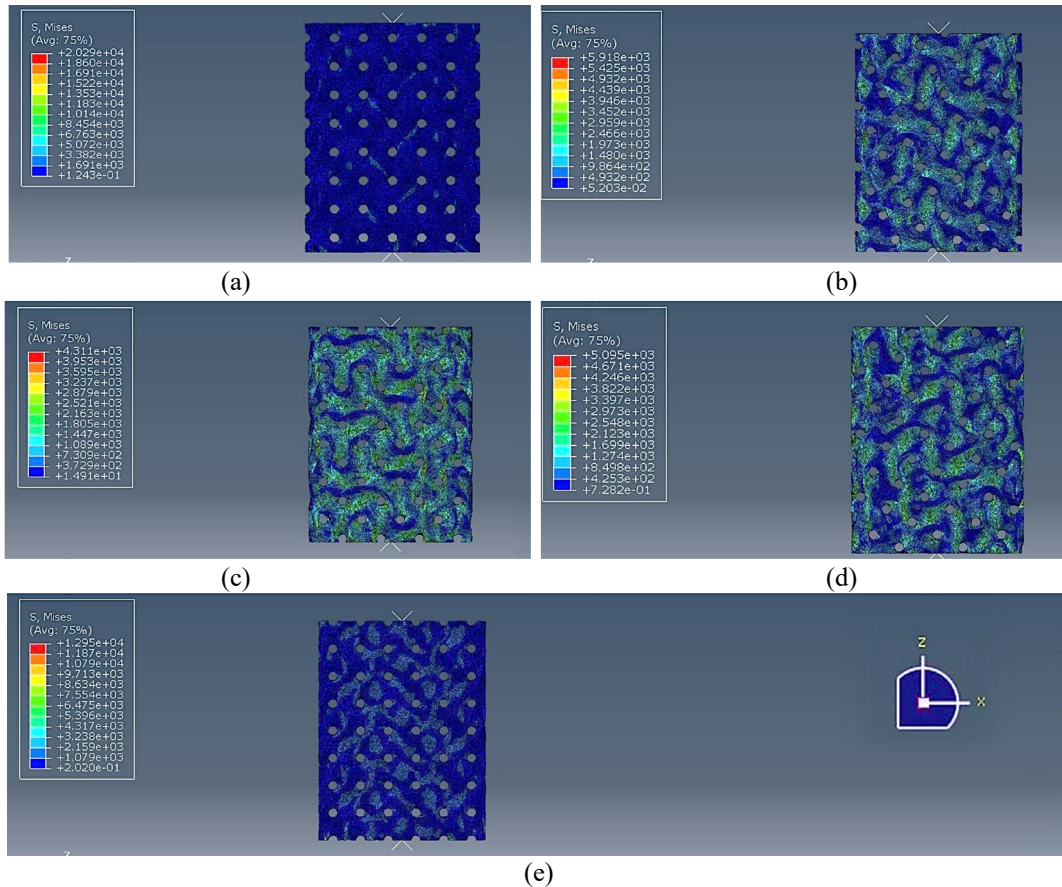


**Figure 7.** The von Mises stress distribution in the Gyroid designed models oriented along (a) [001], (b) [102], (c) [101], (d) [201], and (e) [100] directions.

In order to have a better visualization of the above findings, a bar graph is presented in Figure 8.

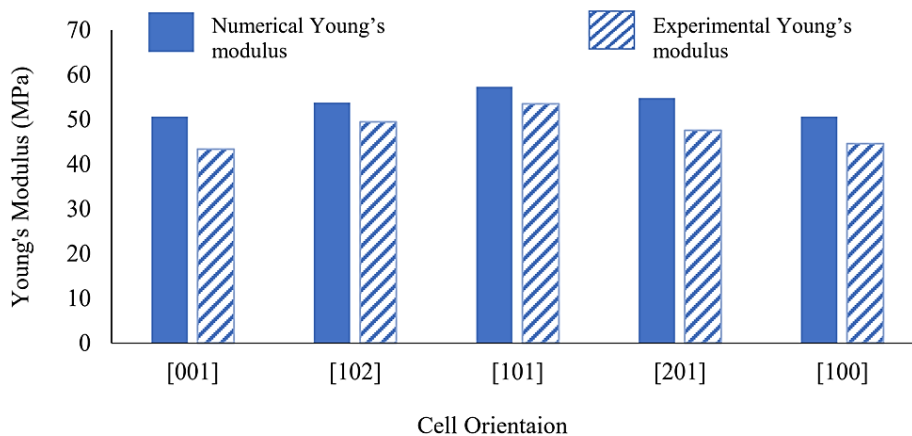


**Figure 8.** Compressive Young's modulus obtained through numerical analysis and experimental tests.

The approximate porosity of 72.0% in the considered Gyroid structure reduces the compressive Young's modulus along [001] and [101] directions to 7.02% and 8.67% of that of the fully solid sample, respectively. Furthermore, the compressive Young's moduli

obtained through experiments have lower values than the numerical results. The most important reason through which this can be explained is the mismatch between the designed models and the corresponding manufactured samples. Similar discrepancies between

numerical and experimental findings have also been observed in other studies within the field of lattice structures, as referenced in [22, 23]. There are some structural defects in the printed samples due to the limitations of the manufacturing process. For example, some features have not been printed well or even not been printed at all. Figure 9 presents two of the lattice samples with structural defects. As shown in the figure, cracks have formed in areas where the wall thickness is notably thin. This in turn can lead to a lower compressive Young's modulus for the manufactured samples compared to the designed ones.

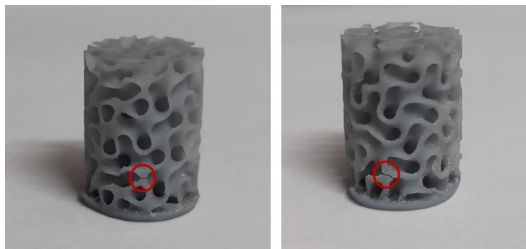


**Figure 9.** Structural defects (cracks) in the additively manufactured lattice samples due to the low thickness of the geometric features.

#### 4. CONCLUSION

In this research, the effect of five different cell orientations on the compressive Young's modulus of a Gyroid-based lattice structure was investigated through both numerical and experimental methods. Among the cell orientations considered in this study, [101] causes the maximum compressive Young's modulus. As the orientation angle moves away from that, the value of the Young's modulus decreases and finally reaches its minimum value along [001] and [100]. These results can be correctly interpreted as the results of investigating the effect of loading direction on the Young's modulus of the considered Gyroid-based lattice structure. Due to the relatively small differences in Young's modulus among different orientations, there will be no more concern about the cell orientation angle or the loading direction in sheet-based Gyroid structures. This makes this type of lattice suitable for use in a bone regeneration scaffold which might be subjected to unknown loadings. Designing such regeneration scaffold is a subject that can be addressed in our future works.

#### ACKNOWLEDGES

This article was presented orally at the 7th International 3D Printing Technologies and Digital Industry Congress and its abstract has been printed in the "Abstract Book".

#### REFERENCES

1. Moussa, A.E.A., "Topology Optimization of Cellular Materials: Application to Bone Replacement Implants", McGill University (Canada), 2020.
2. Zaharin, H.A., Abdul Rani, A.M., Azam, F.I., Ginta, T.L., Sallih, N., Ahmad, A., Yunus, N.A., Zulkifli, T.Z.A., "Effect of unit cell type and pore size on porosity and mechanical behavior of additively manufactured Ti6Al4V scaffolds", *Materials*, Vol. 11, Issue 12, Pages 2402, 2018.
3. Dabrowski, B., Swieszkowski, W., Godlinski, D., Kurzydowski, K.J., "Highly porous titanium scaffolds for orthopaedic applications", *Journal of Biomedical Materials Research Part B: Applied Biomaterials*, Vol. 95, Issue 1, Pages 53-61, 2010.
4. Yavari, S.A., Wauthle, R., van der Stok, J., Riemsdijk, A.C., Janssen, M., Mulier, M., Kruth, J.P., Schrooten, J., Weinans, H., Zadpoor, A.A., "Fatigue behavior of porous biomaterials manufactured using selective laser melting", *Materials Science and Engineering*, Vol. 33, Issue 8, Pages 4849-4858, 2013.
5. Lehder, E., Ashcroft, I., Wildman, R., Ruiz-Cantu, L., Maskery, I., "A multiscale optimisation method for bone growth scaffolds based on triply periodic minimal surfaces", *Biomechanics and modeling in mechanobiology*, Vol. 20, Pages 2085-2096, 2021.
6. Abueidda, D.W., Elhebeary, M., Shiang, C.-S.A., Pang, S., Al-Rub, R.K.A., Jasiuk, I.M., "Mechanical properties of 3D printed polymeric Gyroid cellular structures: Experimental and finite element study", *Materials & Design*, Vol. 165, Pages 107597, 2019.
7. Li, D., Liao, W., Dai, N., Xie, Y.M., "Comparison of mechanical properties and energy absorption of sheet-based and strut-based gyroid cellular structures with graded densities", *Materials*, Vol. 12, Issue 13, Pages 2183, 2019.
8. Wang, Y., Ren, X., Chen, Z., Jiang, Y., Cao, X., Fang, S., Zhao, T., Li, Y., Fang, D., "Numerical and experimental studies on compressive behavior of Gyroid lattice cylindrical shells", *Materials & Design*, Vol. 186, Pages 108340, 2020.
9. Yang, E., Leary, M., Lozanovski, B., Downing, D., Mazur, M., Sarker, A., Khorasani, A., Jones, A., Maconachie, T., Bateman, S., "Effect of geometry on

the mechanical properties of Ti-6Al-4V Gyroid structures fabricated via SLM: A numerical study", *Materials & Design*, Vol. 184, Pages 108165, 2019.

10. Maconachie, T., Tino, R., Lozanovski, B., Watson, M., Jones, A., Pandelidi, C., Alghamdi, A., Almalki, A., Downing, D., Brandt, M., "The compressive behaviour of ABS gyroid lattice structures manufactured by fused deposition modelling", *The International Journal of Advanced Manufacturing Technology*, Vol. 107, Pages 4449-4467, 2020.

11. Teng, F., Sun, Y., Guo, S., Gao, B., Yu, G., "Topological and Mechanical Properties of Different Lattice Structures Based on Additive Manufacturing", *Micromachines*, Vol. 13, Issue 7, Pages 1017, 2022.

12. Kladovasilakis, N., Tsongas, K., Kostavelis, I., Tzouvaras, D., Tzetzis, D., "Effective mechanical properties of additive manufactured triply periodic minimal surfaces: Experimental and finite element study", *The International Journal of Advanced Manufacturing Technology*, Vol. 121, Issue 11-12, Pages 7169-7189, 2022.

13. AlMahri, S., Santiago, R., Lee, D.-W., Ramos, H., Alabdouli, H., Alteneiji, M., Guan, Z., Cantwell, W., Alves, M., "Evaluation of the dynamic response of triply periodic minimal surfaces subjected to high strain-rate compression", *Additive Manufacturing*, Vol. 46, Pages 102220, 2021.

14. Xu, W., Yu, A., Jiang, Y., Li, Y., Zhang, C., Singh, H.-p., Liu, B., Hou, C., Zhang, Y., Tian, S., "Gyroid-based functionally graded porous titanium scaffolds for dental application: Design, simulation and characterizations", *Materials & Design*, Vol. 224, Pages 111300, 2022.

15. Kelly, C.N., Lin, A.S., Leguineche, K.E., Shekhar, S., Walsh, W.R., Guldborg, R.E., Gall, K., "Functional repair of critically sized femoral defects treated with bioinspired titanium gyroid-sheet scaffolds", *Journal of the Mechanical Behavior of Biomedical Materials*, Vol. 116, Pages 104380, 2021.

16. Eltlhawy, B., Fouda, N., Eldesouky, I., "Numerical evaluation of a porous tibial-knee implant using gyroid structure", *Journal of Biomedical Physics & Engineering*, Vol. 12, Issue 1, Pages 75, 2022.

17. Barber, H., Kelly, C.N., Nelson, K., Gall, K., "Compressive anisotropy of sheet and strut based porous Ti-6Al-4V scaffolds", *Journal of the Mechanical Behavior of Biomedical Materials*, Vol. 115, Pages 104243, 2021.

18. Caiazzo, F., Alfieri, V., Bujazha, B.D., "Additive manufacturing of biomorphic scaffolds for bone tissue engineering", *The International Journal of Advanced Manufacturing Technology*, Vol. 113, Pages 2909-2923, 2021.

19. Khaleghi, S., Dehnavi, F.N., Baghani, M., Safdari, M., Wang, K., Baniassadi, M., "On the directional elastic modulus of the TPMS structures and a novel hybridization method to control anisotropy", *Materials & Design*, Vol. 210, Pages 110074, 2021.

20. Cutolo, A., Engelen, B., Desmet, W., Van Hooreweder, B., "Mechanical properties of diamond lattice Ti-6Al-4V structures produced by laser powder bed fusion: On the effect of the load direction", *Journal of the Mechanical Behavior of Biomedical Materials*, Vol. 104, Pages 103656, 2020.

21. Chen, Z., Xie, Y.M., Wu, X., Wang, Z., Li, Q., Zhou, S., "On hybrid cellular materials based on triply periodic minimal surfaces with extreme mechanical properties", *Materials & design*, Vol. 183, Pages 108109, 2019.

22. Caiazzo, F., Alfieri, V., Guillen, D.G., Fabbriatore, A., "Metal functionally graded gyroids: additive manufacturing, mechanical properties, and simulation", *The International Journal of Advanced Manufacturing Technology*, Vol. 123, Pages 2501-2518, 2022.

23. Di Caprio, F., Franchitti, S., Borrelli, R., Bellini, C., Di Cocco, V., Sorrentino, L., "Ti-6Al-4V octet-truss lattice structures under bending load conditions: numerical and experimental results", *Metals*, Vol. 12, Pages 410, 2022.



ULUSLARARASI 3B YAZICI TEKNOLOJİLERİ  
VE DİJİTAL ENDÜSTRİ DERGİSİ

INTERNATIONAL JOURNAL OF 3D PRINTING  
TECHNOLOGIES AND DIGITAL INDUSTRY

ISSN:2602-3350 (Online)

URL: <https://dergipark.org.tr/ij3dptdi>

# PREDICTION OF HARDNESS VALUES OF AGED SELECTIVE LASER MELTED AISi10Mg ALLOY DATA WITH MACHINE LEARNING METHODS

**Yazarlar (Authors):** Murat İnce , Hatice Varol Özkavak 

**Bu makaleye şu şekilde atıfta bulunabilirsiniz (To cite to this article):** İnce M., Özkavak Varol H., "Prediction of Hardness Values of Aged Selective Laser Melted AISi10Mg Alloy Data With Machine Learning Methods" *Int. J. of 3D Printing Tech. Dig. Ind.*, 9(1): 53-62, (2025).

DOI: 10.46519/ij3dptdi.1610116

Araştırma Makale/ Research Article

Erişim Linki: (To link to this article): <https://dergipark.org.tr/en/pub/ij3dptdi/archive>

# PREDICTION OF HARDNESS VALUES OF AGED SELECTIVE LASER MELTED AISi10Mg ALLOY DATA WITH MACHINE LEARNING METHODS

Murat İnce<sup>a</sup> , Hatice Varol Özkavak<sup>b</sup> 

<sup>a</sup> Isparta University of Applied Sciences, Technical Sciences Vocational School, Computer Technologies Department, TURKEY

<sup>b</sup> Isparta University of Applied Sciences, Technical Sciences Vocational School, Mechanical and Metal Technology Department, TURKEY

\* Corresponding Author: [haticevarol@isparta.edu.tr](mailto:haticevarol@isparta.edu.tr)

(Received: 03.01.25; Revised: 21.02.25; Accepted: 12.03.25)

---

## ABSTRACT

Aluminum manufactured with the Selective Laser Melting (SLM) method has been the subject of many research due to the benefits it provides, especially when used in the automotive and aviation industries. Therefore, it is important to examine and improve the mechanical properties of Al parts produced by the SLM method. Many experiments are needed to examine and improve the mechanical properties of SLM Al materials. This situation causes losses in terms of both time and cost. In this study, aims to estimate the hardness values of SLM AISi10Mg materials that have been aged. For this purpose, aging processes were applied to SLM AISi10Mg materials at different times and temperatures, and different machine learning methods were used to predict the hardness values using the hardness values obtained because of the process. Random Forest Regression (RFR) algorithm and Artificial Neural Network (ANN) were used in the study. As a result of the study, it was determined that the hardness values estimated by the ANN ( $R^2$  0.9276) method were close to the real hardness values. This is proof that it is possible to predict hardness values using the machine learning method.

**Keywords:** SLM, AISi10Mg, Aging, Artificial Neural Networks, Machine Learning, Regression

---

## 1. INTRODUCTION

Additive Manufacturing (AM), unlike other manufacturing methods, is used to create machine parts by adding materials step by step and covers all 3D manufacturing methods [1]. 3D manufacturing technology has developed considerably in recent years due to the increased need for personalized production, lightweight structure design and smart production [2-5]. In addition, the 3D manufacturing method offers design freedom and low-cost opportunities due to low material loss [6]. Selective Laser Melting (SLM) method, one of the 3D manufacturing methods, attracts attention due to its production accuracy and high designability [7-9]. Due to these features, the SLM method is used in industrial applications that require advanced technology such as automotive, aviation and shipbuilding [10-12]. Steel, nickel, titanium and aluminum alloys are preferred as materials in the SLM method. AISi10Mg materials have

many outstanding properties such as excellent corrosion resistance, thermal conductivity, impressive strength-to-weight ratio. Having these properties, this alloy is preferred in areas where high performance and lightness are important. In addition, AISi10Mg alloys are preferred in complex designs due to their surface quality and superior stability properties. In addition to all these features, it is compatible with metal 3D printing methods and selective laser melting (SLM) method. For this reason, it has become the preferred material in 3D manufacturing [13,14]. The mechanical properties of AISi10Mg parts produced by the SLM method are significantly improved compared to the parts produced by the high-pressure casting and die casting methods [15-17]. The mechanical properties of SLM parts were improved by heat treatment [18-21]. Li and his colleagues determined that elongation and the tensile strength can be improved by

controlling the morphology of Si by applying a special heat treatment to the parts manufactured by the AM method [22]. Thermal processes applied to Al-Si-Mg alloys are solution, quenching, natural or artificial aging, operations [23]. If the solution process is applied to these alloys, spheroidization and structure become homogeneous in the Si phase [24]. In their study, Zhuo et al. determined that there was an increase in the elongation and a decrease in the strength of SLM samples subjected to stress relief annealing at 300 °C [8]. In their study, Maamoun et al. concluded that high temperature solid solution heat-treatment worsened the hardness values of the samples applied [25]. When literature is examined, it is seen that controlling the process temperature and waiting time is important during heat treatment of the samples manufactured by the SLM method. Considering this situation, the importance of optimizing the aging process temperature, time and cooling environment to improve the mechanical properties of AlSi10Mg parts manufactured by the SLM method emerges. Many experiments are needed for optimization. For this reason, many researchers have used various machine learning

techniques in their studies to better understand input relationships and identify factors in obtaining an optimized prediction model [26]. Many researchers have successfully employed ANN, a machine learning technique noted for its excellent reliability and prediction capability [17-29]. For this purpose in this study, aging processes were applied to SLM AlSi10Mg materials at different times and temperatures, and different machine learning methods were used to predict the hardness values using the hardness values obtained because of the process.

The rest of the paper is organized as follows; the materials and methods utilized in the study are described in Section 2. The application and assessment of machine learning techniques on the experimental study data are described in Section 3. The last part concludes the study.

## 2. MATERIAL AND METHOD

### 2.1. Experimental Procedure

In this study, 20-70mm spherical AlSi10Mg powder was used. The chemical properties of the powder used in the study are given in Table 1.

**Table 1.** Chemical Composition of AlSi10Mg

Element(%w)	Al	Si	Fe	Cu	Mn	Mg	Zn	Ti	Ni	Sn
	The rest	9-11	≤0.55	≤0.05	≤0.45	0,2-0.45	≤0.1	≤0..5	≤0.05	≤0.05

In this study, samples of AlSi10Mg material were manufactured by the SLM method. SLM samples were produced in a 250mmx250mmx325mm production room using Yb-fiber laser on the EOS M 290 system. 400W laser power, 7m/s scan speed, 100µm focus diameter and 100psi compressed air application were selected as process parameters in sample production. A prismatic sample with dimensions of 10\*10\*5 mm was used in the study.

In this study, it was aimed to determine the effect of the aging process on the hardness of samples produced by the SLM method. For this purpose, the aging processes applied to the samples are given in Table 2.

**Table 2.** Heat treatment parameters applied to the samples

Process	Parameter
Solution Heat Treatment	415°C 2 h solution HT + that water-cooled
	415°C 2 h solution HT + air cooling
	515°C 1.5 solution HT after that water cooling
	540°C 1 h solution HT after that water cooling
Solution Heat Treatment + aging treatment	515°C 1 h water cooling + 160°C 10h air cooling
	515°C 1 h water cooling + 160°C 14h air cooling
	515°C 1 h water cooling + 160°C 18h air cooling
	515°C 1 h water cooling + 160°C 10h indoor cooling
	515°C 1 h water cooling + 160°C 14h indoor cooling
	515°C 1 h water cooling + 160°C 18h indoor cooling
	540°C 1 h water cooling + 180°C 8h air cooling
	540°C 1 h water cooling + 180°C 12h air cooling
	540°C 1 h water cooling + 180°C 16h air cooling
	540°C 1 h water cooling + 180°C 8h indoor cooling
	540°C 1 h water cooling + 180°C 12h indoor cooling
	540°C 1 h water cooling + 180°C 16h indoor cooling

The workflow of the study and aging process applied for the study is given in Figure 1.

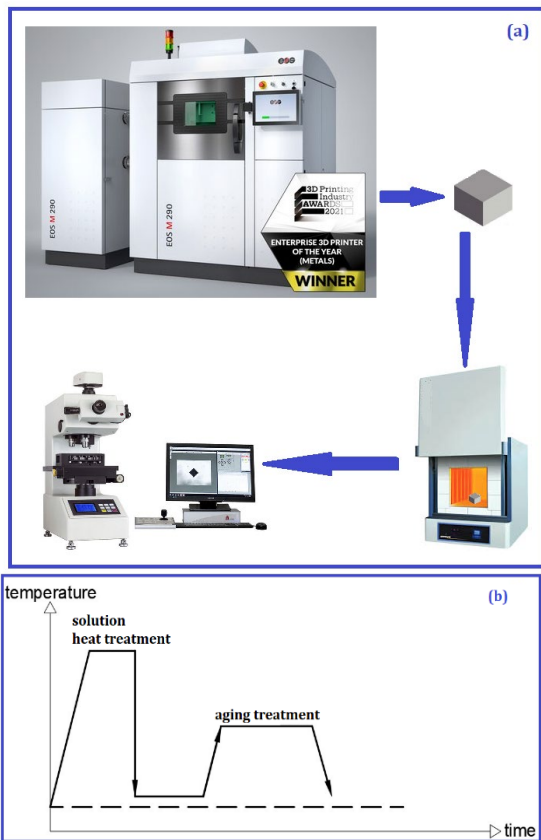


**Figure 1.** (a) Workflow of the study (b) Heat treatment procedure applied to AlSi10Mg samples

In the experimental work, Protherm HLF100 type heat treatment furnace was used for the aging process. In order to determine the change in the hardness of the samples after the aging process, the hardness values of the samples were measured using the TTS Matsuzawa

HWMMT-X3 micro hardness device with an applied load of 10 g for 10 s.5 measurements were made on each sample and the arithmetic average was taken. Microstructural examinations were carried out on samples with and without the aging process. Before microstructural examinations, the samples were polished and then etched using Keller reagent [30]. FEI QUANTA FEG 250 Scanning electron Microscope (SEM) was used for surface investigations.

## 2.2. Machine Learning Methods

In this study, aging processes were applied to SLM AlSi10Mg materials at different times and temperatures were used to predict the hardness values. For this purpose, Artificial Neural Network (ANN) and Random Forest Regressor (RFR) methods, popular machine learning methods, were used. Inspired by the human brain, artificial neural networks (ANNs) are computer models that can identify patterns and make decisions in a manner akin to that of biological neurons [31]. They can learn from data and generalize effectively to new cases, which makes them useful in domains like multivariable regression analyzes [32] and image recognition [33]. The input layer, hidden layers, and output layer are the three types of ANNs (Figure 2). First, data is received at the input layer and is processed using activation functions through hidden layers. The outcome of the classification or prediction is generated by the output layer. Complex computations are carried out via input layers, where each neuron applies a non-linear activation function after a linear translation. The model's prediction is

produced by the final output layer, which is typically a single neuron with linear activation for regression tasks [34] or a softmax layer for classification tasks [35]. Another popular algorithm for regression problems is an ensemble learning technique called the Random Forest Regressor (RFR)(Figure 3). During training, RFR entails creating many decision trees and combining their predictions to increase the robustness and performance of the model [36]. This method improves the model's capacity for generalization while lowering overfitting. Bootstrap sampling, random feature selection, and aggregate prediction are the main elements of a random forest. A random portion of the training data is used to train each tree, and the total of all the trees' predictions is the final forecast [35]. The performance of the model is affected by the number of trees, the maximum depth of the trees, and the minimum number of samples required to split a node.

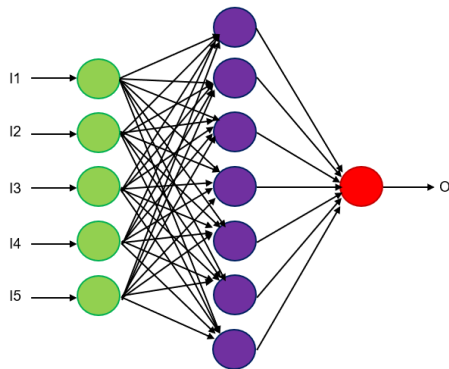


**Figure 2.** ANN structure of the study

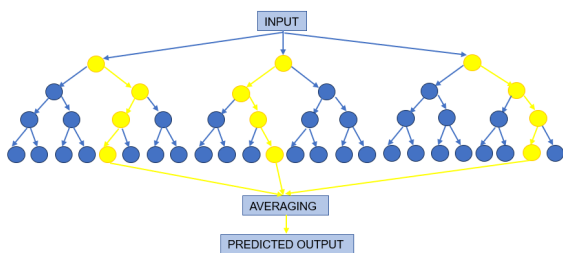


**Figure 3.** RFR structure of the study

ANNs are efficient in learning detailed patterns and interactions between features, making them useful in complex, non-linear data contexts like speech and image recognition [37]. On the other hand, RFRs work better with structured data that has distinct feature importance and relationships, and they are more efficient with simpler, piecewise linear data [38]. Additionally, they can manage missing values

without requiring a lot of preprocessing and are resistant to overfitting. ANNs, however, are computationally demanding and need a large amount of memory and processing power with numerous layers and parameters [39]. (Distributed computers and GPUs can speed up ANN training, however RFRs are easier to train and can be parallelized effectively [40]. ANNs or RFRs are chosen based on the particular task requirements, data type, and resource availability.

### 2.3. Evaluation Metrics

Regression model performance in machine learning is assessed using a number of metrics, such as Root Mean Squared Error (RMSE), Mean Absolute Error (MAE), and R-squared ( $R^2$ ). These measures shed light on the accuracy and error distribution of the model. The percentage of the dependent variable's variation that can be predicted from the independent variables is shown by  $R^2$ , sometimes referred to as the coefficient of determination [41]. Higher values of the ratio, which goes from 0 to 1, denote greater match. The average size of errors in a set of predictions, without considering their direction, is measured by the MAE. It offers an intuitive sense of the model's prediction accuracy in the same units as the target variable, making it simple to comprehend and apply [42]. The magnitude of the data, however, can have an impact on MAE, which does not penalize greater errors more than smaller ones. The average magnitude of the error is measured by the quadratic scoring procedure known as RMSE. The square root of the average of the squared discrepancies between the actual observation and the prediction is what it is. Because each term is squared before being averaged and the square root is taken, RMSE emphasizes greater errors more than smaller ones [43]. Because it is sensitive to outliers and penalizes greater errors more severely, it is often utilized in situations where large errors are especially undesirable.

When selecting amongst R-squared, MAE, and RMSE to assess the effectiveness of a regression model, it is crucial to take the particular context and data type into account.  $R^2$  is helpful in determining the percentage of variance that the model explains, but as it doesn't take into consideration the size of the mistakes, it should be used in conjunction with other metrics [44]. In actual use, reporting a

variety of metrics is frequently advantageous in order to have a thorough grasp of the model's performance. One can determine whether the model's mistakes are consistently minimal or if there are major outliers by combining the analysis of MAE and RMSE. To sum up,  $R^2$ , MAE, and RMSE are useful metrics for assessing regression model performance in machine learning.

### 3. RESULTS AND EVALUATION

#### 3.1. Experimental Results

The aim of this study was to estimate the change in hardness during the aging process at different temperatures, durations and cooling environments. In addition, different solution temperatures were selected. For this purpose, AlSi10Mg samples manufactured by the SLM method were subjected to the aging process. While determining the solution temperatures for the study, the Al-Si binary phase diagram in the work of Silvia et al. was used and the binary phase diagram is given in Figure 4. [45]. These temperatures were chosen as 415, 515 and 540 °C below the eutectic point and agree with the literature [46].

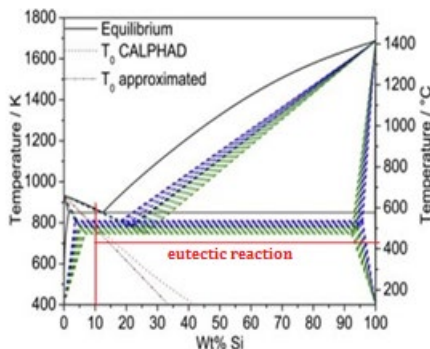


Figure 4. Phase diagram for Al-Si alloys [45]

The hardness values of the samples without aging were determined as 65HV. The solution temperature was 415°C, and the hardness values for the samples selected for both air cooling and water cooling were determined as 52 HRB (95HV). 53HV was obtained for the samples whose solution temperature was 540°C and the cooling environment in water was selected. The highest hardness value was measured as 57 HRB (102 HV) in the samples where the solution temperature was 515°C and the cooling medium was selected in water. After the solution process, Si particles and coarsening of the grain structure occurred. Additionally, during the solution process, the amount of

dissolved Si in Al decreased, which agrees with the literature [47-48]. The coarsening in the microstructure and the decrease in the amount of Si caused a decrease in the hardness of the AlSi10Mg alloy manufactured by the SLM method after the solution process. The decrease in Si content in Al and the coarsened microstructure will lead to a decrease in the hardness of the SLM AlSi10Mg alloy after solution processing. In addition, the samples were taken into solution for 1 hour at 515 °C and 540 °C, and then aged at 160 °C for 10h, 14h and 18h. After the aging process, air and indoor were chosen as the cooling medium. When the samples in which water was used as the cooling medium were examined, it was determined that the highest hardness value was 86 HV in the samples with 14h aging process. These samples were followed by samples aged 18 h with a hardness value of 78 HRB (150 HV) and 10 h with a hardness value of 74 HRB (139 HV). When the hardness values were examined, the decrease in the hardness value with increasing processing time was determined to be a result of excessive aging. Additionally, with the quenching process, Si particles become spherical [49]. The quenching process causes rapid cooling and precipitation is stopped. The precipitates resulting from the solution process are thus stopped. During the aging process, these precipitates grow in the Al matrix and are evenly distributed in the matrix [14]. This allows us to adjust the mechanical properties of the AlSi10Mg alloy produced by SLM [50,51]. When the samples in which the cooling medium was selected as a indoor were examined, it was determined that the highest hardness value was 73 HRB (137 HV) in the samples with 10h aging process. These samples were followed by samples that were aged for 18h with a hardness value of 68 HRB (122 HV) and 14h with a hardness value of 64 HRB (112 HV). If the cooling medium was selected as a indoor, the hardness values obtained were lower than when cooled in air. Uncontrolled cooling process causes the formation of undesirable precipitate phases. These precipitations will cause a decrease in hardness. Additionally, this can be explained because of over aging. A correct cooling process should be as slow as possible and as fast as necessary [50]. When the hardness values of the samples, where the solution temperature was selected as 540°C and air cooling was applied after aging at 160°C for 8h, 12h and 16h, were examined, the hardness

values were obtained as 67 HRB (120 HV), 62 HRB (110 HV) and 57 HRB (100 HV) at 12h, 16h and 8h processing times, respectively. has been made. This situation is similar to the samples that were subjected to solution at 515

°C. When the hardness values of the samples whose solution temperature was selected as 540°C and which were cooled in the indoor after aging at 160°C for 8h, 12h and 16h were

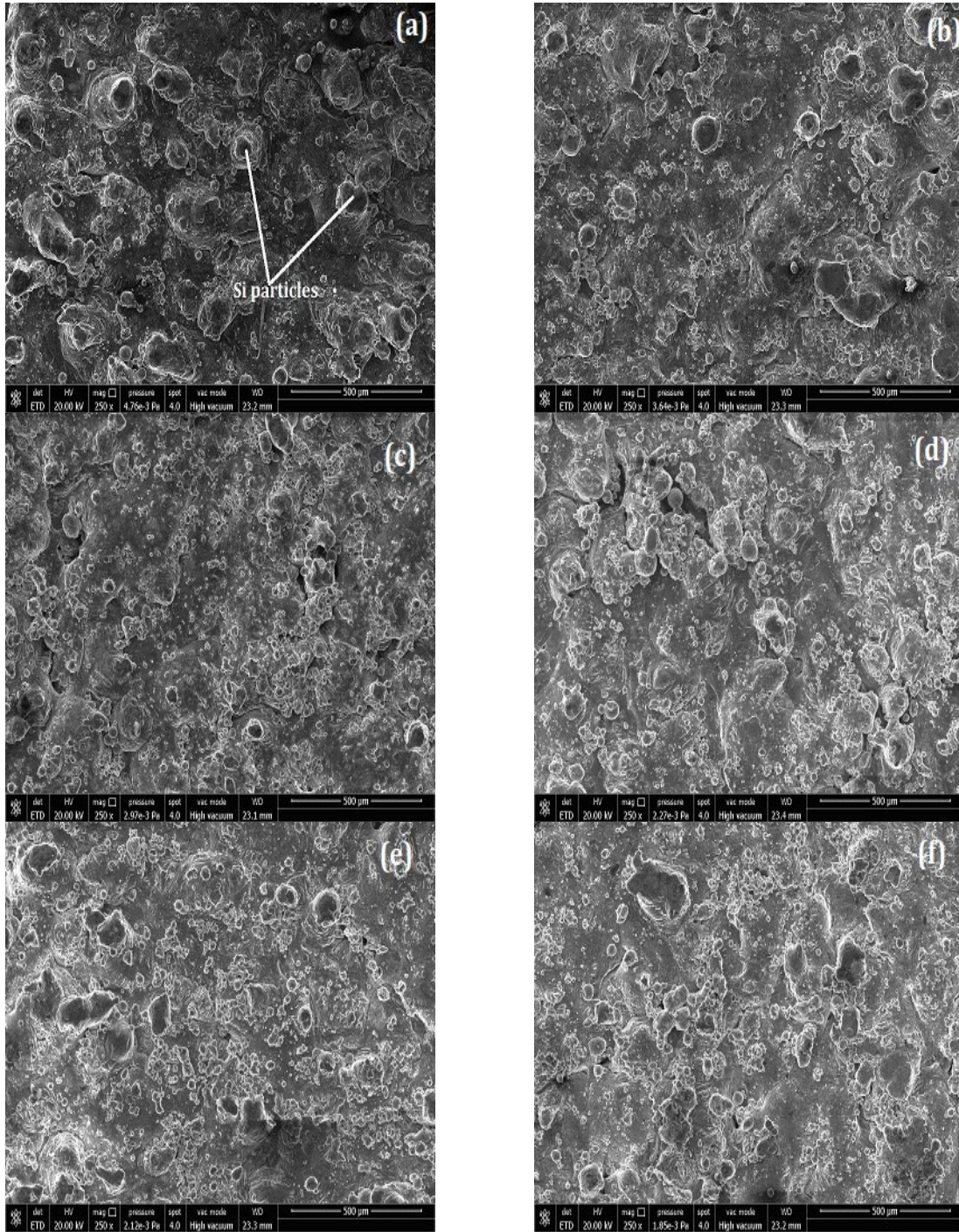


**Figure 5.** SEM images of the samples subjected to at different solution treatment, aging temperature and time (a) 515°C 1 h water cooling + 160°C 18h indoor cooling (b) 515°C 1 h water cooling + 160°C 14h indoor cooling (c) 540°C 1 h water cooling + 180°C 16h air cooling (d) 415°C 2 h water cooling (e) 515°C 1 h water cooling + 160°C 14h air cooling (f) 540°C 1 h water cooling + 180°C 12h air cooling

examined, it was determined that the highest hardness value was obtained in the samples with 16h aging (59 HRB (105 HV)). The slow cooling rate in the indoor cooling process increased precipitation formation and caused a decrease in hardness. Microstructure examinations of AlSi10Mg samples, which were manufactured by the SLM method and then aged by solution at different temperatures and times, were examined. SEM images of the samples subjected to at different solution treatment, aging temperature and time are shown in Figure 5 is given. With the solution taking process, coarsening occurred in the Si grain structure. Si particles have a fish-scale and column-shaped structure. However, it was determined that this Si structure was disrupted after the solution process. Additionally, as the processing time increased, the hardness increased. However, as the processing time increased further, the grains became coarser and the equilibrium solubility decreased, resulting in a decrease in hardness.

### 3.2. Dataset

In this paper, it is aimed to estimate the hardness values of SLM AlSi10Mg materials that have aged with different temperatures and time. The experimental measurement data consists of solution heat treatment temperature (I1), solution treatment process time (I2), aging treatment temperature (I3), aging process time (I4) and environment (I5) are used as inputs, while hardness value (O) is used as an output. For SLM AlSi10Mg examples, 12 distinct measurement data are available. Different training-test percentages was analyzed and then best results was founded as 80% of this data for training and the rest of the data for test.

### 3.3. Implementation Details

The suggested machine learning techniques in the study's application section were implemented using Python. GridSearchCV [63] was used to run algorithms and tune parameters on a computer system equipped with an Intel Core i7 13650HX Turbo Boost 4.9 GHz CPU and 16 GB RAM. The hidden layer of the ANN algorithm contains 1024 units. Batch size is 50, learning rate is 0.01, epoch is 100, and activation function is linear. The settings of the RFR method are as follows: random\_state = 20, max\_depth = 5, squared\_error = criteria, and n\_estimators = 100.

### 3.4. Testing and Evaluation

To use machine learning techniques, it is essential to correctly identify the features in the dataset. Consequently, the developed model can predict the properties of various combinations of aluminum materials that have not yet been developed, speeding up the search for workable materials with hardness values. Given this, the study proposed that machine learning models can be used to generate high-performing materials. Furthermore, ML techniques' ability to estimate data is significantly influenced by the quantity and caliber of the input dataset. Furthermore, the variety and breadth of input features can fully describe the underlying mechanisms. Using ML models to determine the hardness value, the algorithms' performance was evaluated in terms of  $R^2$ , RMSE, and MAE values (Table 3).  $R^2$  0.9276, RMSE 0.0804, and MAE 0.0626 were the best outcomes for the ANN algorithm (Figure 6).

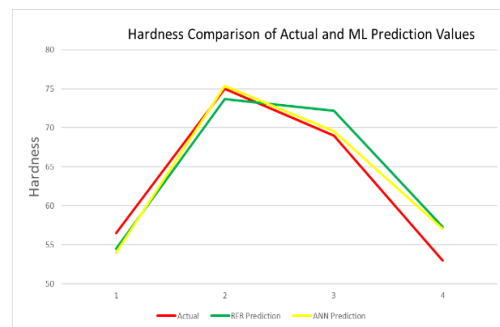


**Figure 6.** Comparison of actual and predicted values

**Table 3.** Estimation performances ML algorithms for hardness value estimation of different aluminum materials

Evaluation Metrics	ANN	RFR
$R^2$	0.9276	0.8930
RMSE	0.0804	0.0978
MAE	0.0626	0.090

The results show that in order to obtain the aluminum material with the highest hardness value, the ML algorithms produce results that significantly not different from the actual test data. The potential costs and waste of experiment time are decreased when machine learning algorithms are used for prediction tasks.

## 4. RESULTS

Aluminum metals are frequently used in many areas. Experiments are being carried out to obtain a durable and hard aluminum, and conducting many experiments creates a burden

in terms of time and cost. For this reason, trying to obtain experimental results using machine learning methods from a certain number of experimental data without further experiments is a frequently used method. In this paper, the hardness values of aluminum materials that were aged for different periods of time in different environments were tried to be estimated by using ANN and RFR methods, which are well-known machine learning methods. When the experimental results were examined, a 26% increase in hardness was obtained in the samples subjected to 515 solution soaking and 160 14-hour aging processes. The results obtained were evaluated with performance measurement metrics such as  $R^2$ , RMSE and MAE, and it was shown that the ANN algorithm gave the best results and machine learning methods can be used successfully in satisfying the hardness values of aluminum materials. Therefore, it has been determined that being able to estimate aluminum materials without trying each time is advantageous in terms of time and cost.

#### ACKNOWLEDGES

The authors report no conflict of interest.

#### REFERENCES

- Gibson I., Rosen D.W., Stucker B., "Additive Manufacturing Technologies - Rapid Prototyping to Direct Digital Manufacturing", Pages 1-625, USA,2015.
- J.H. Martin, B.D. Yahata, J.M. Hundley, J.A. Mayer, T.A. Schaedler, and T.M. Pollock, "3D Printing Of High-Strength Aluminium Alloys", Nature, Vol. 549, Pages 365-369. 2017,
- A. Hadadzadeh, B.S. Amirkhiz, S. Shakerin, J. Kelly, J. Li, and M. Mohammadi, "Microstructural Investigation and Mechanical Behavior of a Two-Material Component Fabricated through Selective Laser Melting of AlSi10Mg on an Al-Cu-Ni-Fe-Mg Cast Alloy Substrate", Addit. Manuf.,Vol. 31, Pages 100937,2020.
- A.G. Demir and C.A. Biffi, "Micro Laser Metal Wire Deposition Of Thin-Walled Al Alloy Components: Process And Material Characterization", J. Manuf. Process., Vol. 37, Pages 362-369,2019.
- Q. Yan, B. Song, and Y. Shi, "Comparative Study Of Performance Comparison Of AlSi10mg Alloy Prepared By Selective Laser Melting And Casting", J. Mater. Sci. Technol., Vol. 41, Pages 199-208,2020.
- Y. Cao, X. Lin, Q.Z. Wang, S.Q. Shi, L. Ma, N. Kang, and W.D. Huang, "Microstructure Evolution And Mechanical Properties at High Temperature of Selective Laser Melted AlSi10Mg", J. Mater. Sci. Technol., Vol. 62, Pages 162-172, 2021,
- N.O. Larrosa, W. Wang, N. Read, M.H. Loretto, C. Evans, J. Carr, U. Tradowsky, M.M. Attallah, and P.J. Withers, "Linking Microstructure and Processing Defects to Mechanical Properties of Selectively Laser Melted AlSi10Mg Alloy", Theor. Appl. Fract. Mech., Vol. 98, Pages 123-133, 2018.
- L. Zhuo, Z. Wang, H. Zhang, E. Yin, Y. Wang, T. Xu, and C. Li, "Effect of Post-Process Heat Treatment on Microstructure and Properties of Selective Laser Melted AlSi10Mg Alloy", Mater. Lett., Vol. 234, Pages 196-200, 2019.
- J. Bi, Z. Lei, Y. Chen, X. Chen, N. Lu, Z. Tian, and X. Qin," An Additively Manufactured Al-14.1 Mg-0.47 Si-0.31 Sc-0.17 Zr Alloy with High Specific Strength, Good Thermal Stability and Excellent Corrosion Resistance", J. Mater. Sci. Technol., Vol. 67, Pages23-35, 2021,
- A. Heinz, A. Haszler, C. Keidel, S. Moldenhauer, R. Benedictus, and W.S. Miller, "Recent Development in aluminium Alloys for Aerospace Applications", Mater. Sci. Eng. A, Vol. 280, Pages 102-107,2000.
- F. Calignano, "Design Optimization of Supports for Overhanging Structures in Aluminum and Titanium Alloys by Selective Laser Melting", Mater. Des., Vol. 64, Pages 203-213,2014.
- L. Thijs, K. Kempen, J.P. Kruth, and J. Van Humbeeck, "Fine-structured Aluminium Products with Controllable Texture by Selective Laser Melting of Pre-alloyed AlSi10Mg Powder", Acta Mater., Vol. 61, Pages 1809-1819, 2013.
- N.T. Aboulkhair, M. Simonelli, L. Parry, I. Ashcroft, C. Tuck, and R. Hague, "Prog. 3D Printing of Aluminium Alloys: Additive Manufacturing of Aluminium Alloys using Selective Laser Melting", Mater. Sci., Vol. 106, Pages 100578, 2019.

14. E. Brandl, U. Heckenberger, V. Holzinger, and D. Buchbinder, "Additive Manufactured AlSi10Mg Samples using Selective Laser Melting (SLM): Microstructure, High Cycle Fatigue, and Fracture Behavior", *Mater. Des.*, Vol. 34, Pages 159-169,2012.
15. K. Kempen, L. Thijs, J. Van Humbeeck, and J.P. Kruth, "Processing AlSi10Mg by Selective Laser Melting: parameter optimisation and material characterisation", *Mater. Sci. Technol.*, Vol. 31, Pages 917-923,2015.
16. N. Takata, H. Kodaira, K. Sekizawa, A. Suzuki, and M. Kobashi, "Change in Microstructure of Selectively Laser Melted AlSi10Mg Alloy with Heat Treatments", *Mater. Sci. Eng. A.*, Vol. 704, Pages 218-228,2017.
17. R. Casati, M. Hamidi Nasab, M. Coduri, V. Tirelli, and M. Vedani, "Effects of Platform Pre-Heating and Thermal-Treatment Strategies on Properties of AlSi10Mg Alloy Processed by Selective Laser Melting", *Met., Basel*, Vol. 8, Pages 954,2018.
18. I. Rosenthal, R. Shneck, and A. Stern, "Heat Treatment Effect on the Mechanical Properties and Fracture Mechanism in Alsi10Mg Fabricated by Additive Manufacturing Selective Laser Melting Process", *Mater. Sci. Eng. A.*, Vol. 729, Pages 310-322,2018.
19. Q. Han and Y. Jiao," Effect of Heat Treatment and Laser Surface Remelting on Alsi10Mg Alloy Fabricated by Selective Laser Melting", *Int. J. Adv. Manuf. Technol.*, Vol. 102, Pages 3315-3324,2019.
20. L.F. Wang, J. Sun, X.L. Yu, Y. Shi, X.G. Zhu, L.Y. Cheng, H.H. Liang, B. Yan, and L.J. Guo, "Enhancement in Mechanical Properties of Selectively Laser-Melted Alsi10mg Aluminum Alloys by T6-Like Heat Treatment", *Mater. Sci. Eng. A.*,Vol. 734, Pages 299-310,2018.
21. W. Li, S. Li, J. Liu, A. Zhang, Y. Zhou, Q. Wei, C. Yan, and Y. Shi, "Effect of Heat Treatment on Alsi10Mg Alloy Fabricated by Selective Laser Melting: Microstructure Evolution, Mechanical Properties And Fracture Mechanism", *Mater. Sci. Eng. A.*, Vol. 663, Pages 116-125,2016.
22. X. Li, X. Wang, M. Saunders, A. Suvorova, L. Zhang, Y. Liu, M. Fang, Z. Huang, and T.B. Sercombe, "A Selective Laser Melting and Solution Heat Treatment Refined Al-12si Alloy with a Controllable Ultrafine Eutectic Microstructure and 25% Tensile Ductility", *Acta Mater.*,Vol. 95, Pages 74-82,2015.
23. E. Sjölander and S. Seifeddine, The Heat Treatment of Al-Si-Cu-Mg Casting Alloys, *J. Mater. Process. Technol.*, Vol. 210, Pages 1249-1259,2010.
24. M. Moustafa, F. Samuel, and H. Doty, "Effect of Solution Heat Treatment and Additives on the Microstructure of Al-Si (A413. 1) Automotive Alloys", *J. Mater. Sci.*, Vol. 38, Pages 4507-4522,2003.
25. A.H. Maamoun, M. Elbestawi, G.K. Dosbaeva, and S.C. Veldhuis, "Thermal Post-Processing of Alsi10Mg Parts Produced by Selective Laser Melting using Recycled Powder", *Addit. Manuf.*, Vol. 21, Pages 234-247,2018.
26. U.M.R. Paturi, S. Cheruku, V.P.K. Pasunuri, S. Salike, N.S. Reddy, and S. Cheruku, "Machine Learning and Statistical Approach in Modeling and Optimization of Surface Roughness in Wire Electrical Discharge Machining", *Mach. Learn. Appl.*, Vol. 6, Pages 100099,2021.
27. U.M.R. Paturi, D.G. Vanga, R.B. Duggem, N. Kotkunde, N.S. Reddy, and S. Dutta, "Estimation of Surface Roughness of Direct Metal Laser Sintered Alsi10Mg using Artificial Neural Networks and Response Surface Methodology", *Mater. Manuf. Process.*,Vol. 38, Issue 14, Pages 1798-1808,2023.
28. Z. Zhan, N. Ao, Y. Hu, and C. Liu, Defect-Induced Fatigue Scattering and Assessment of Additively Manufactured 300M-AerMet100 Steel: An Investigation Based on Experiments and Machine Learning, *Eng. Fract. Mech.*, Vol. 264, Pages 108352, 2022.
29. M. Marrey, E. Malekipour, H. El-Mounayri, and E.J. Faierson, A Framework for Optimizing Process Parameters in Powder Bed Fusion (PBF) Process Using Artificial Neural Network (ANN), *Proc. Manuf.*, Vol. 34, Pages 505-515,2019.
30. G.F.V. Voort, *Metallography: Principles & Practice*, ASM International, United States of America, 1999.
31. K. Upreti, M. Verma, M. Agrawal, J. Garg, R. Kaushik, C. Agrawa, D. Singh, R. Narayanasamy, "Prediction of Mechanical Strength by using an Artificial Neural Network and Random Forest Algorithm", *J. Nanomaterials*, Vol. 1, Pages 7791582,2021.
32. U. Atici, "Prediction of the Strength of Mineral Admixture Concrete using Multivariable Regression Analysis and an Artificial Neural Network", *Expert Sys. Appl.*, Vol. 38, Issue 8, Pages 9609-9618,2011.

33. J. Al-Azzeh, Z. Alqadi, and M. Abuzalata, "Performance Analysis of Artificial Neural Networks used for Color Image Recognition and Retrieving", *Inter. J. Comput. Sci. Mobile Comput.*, Vol. 8, Issue 2, Pages 20-33,2019.
34. H.V.T. Mai, T.A. Nguyen, H.B. Ly, and V.Q. Tran, "Investigation of ANN Model Containing One Hidden Layer for Predicting Compressive Strength of Concrete with Blast-Furnace Slag and Fly Ash", *Adv. Mater. Sci. Eng.*, Vol. 1, Pages 5540853,2021.
35. X. Zhou, P. Lu, Z. Zheng, D. Tolliver, and A. Keramati, "Accident Prediction Accuracy Assessment for Highway-Rail Grade Crossings using Random Forest Algorithm Compared with Decision Tree", *Reliability Eng. Sys. Safety*, Vol. 200, Pages 106931, 2020.
36. Z.N. Nemer, "Oil and Gas Production Forecasting Using Decision Trees, Random Forst, and XGBoost", *J. Al-Qadisiyah Comput. Sci. Math.*, Vol. 16, Issue 1, Pages 9-20,2024.
37. M.G. Abdolrasol, S.S. Hussain, T.S. Ustun, M.R. Sarker, MA. Hannan, R. Mohamed, A. Milad, *Artificial Neural Networks Based Optimization Techniques: a Review*, *Electronics*, Vol. 10, Issue 21, Pages 2689,2021.
38. S.B. Torrisi, M.R. Carbone, B.A. Rohr, J.H. Montoya, Y. Ha, J. Yano, and L. Hung," Random Forest Machine Learning Models For Interpretable X-Ray Absorption Near-Edge Structure Spectrum-Property Relationships", *npj Comput. Mater.*, Vol. 6, Issue 1,Pages 109,2020.
39. T. Guillod, P. Papamanolis, and J.W. Kolar, "Artificial neural network (ANN) based Fast and Accurate Inductor Modeling and Design", *IEEE Open J Power Electron.*, Vol. 1, Pages 284-299,2020.
40. J.R.S. Iruela, L.G.B. Ruiz, M.C. Pegalajar, and M.I. Capel, "A Parallel Solution with GPU Technology to Predict Energy Consumption in Spatially Distributed Buildings using Evolutionary Optimization and Artificial Neural Networks", *Energy Conv. Manag.*, Vol. 207, Pages 112535,2020.
41. S. Menard, "Coefficients of Determination for Multiple Logistic Regression Analysis", *American Stat.*, Vol. 54, Issue 1, Pages 17-24, 2000.
42. T.O. Hodson, "Root Mean Square Error (RMSE) or Mean Absolute Error (MAE): when to use them or not", *Geosci. Model Dev.*, Vol. 15, Pages 5481-5487,2022.
43. P.E. Dennison and D.A. Roberts, "Endmember Selection for Multiple Endmember Spectral Mixture Analysis using Endmember Average RMSE," *Remote Sens Environment*, Vol. 87, Issue 2-3, Pages 123-135,2003.
44. D. Chicco, M.J. Warrens, and G. Jurman, "The Coefficient of Determination R-Squared is more Informative than SMAPE, MAE, MAPE, MSE and RMSE in Regression Analysis Evaluation", *Peerj Comput. Sci.*, Vol. 5, Issue 7, Pages 623,2021.
45. S. Marola, D. M. Gianluca Fiore, M.G. Poletti, M. Lombardi, P. Fino, and L. Battezzati, "A Comparison of Selective Laser Melting with bulk Rapid Solidification of AlSi10Mg alloy", *J Alloys Compounds*, Vol.742, Pages 271-279,2018.
46. K.G. Prashanth, S. Scudino, H.J. Klauss, K.B. Surreddi, L. Lober, Z. Wang, A.K. Chaubey, U. Kühn, and J. Eckert," Microstructure and Mechanical Properties of Al-12Si Produced by Selective Laser Melting: Effect of Heat Treatment", *Mater. Sci. Eng. A*, Vol. 590, Pages 153-160, 2014.
47. L. Zhou, A. Mehta, E. Schulz, B. McWilliams, K. Cho, and Y. Sohn, "Microstructure, Precipitates and Hardness of Selectively Laser MELTED ALSI10MG Alloy before and after Heat Treatment", *Mater Char.*, Vol. 143, Pages 5-17,2018.
48. J. Murray and A. McAlister, *The Al-Si (Aluminum-Silicon) System*, *J. Phase Equilib.*, Vol. 5, Pages 74-84,1984.
49. M. Moustafa, F. Samuel, and H. Doty, "Effect of Solution Heat Treatment and Additives on the Microstructure of Al-Si (A413. 1) Automotive Alloys", *J. Mater. Sci.*, Vol. 38, Pages 4507-4522,2003.
50. A.H. Demirci, "Malzeme Bilgisi ve Malzeme Muayenesi: Seçilmiş Temel Kavramlar ve Endüstriyel Uygulamalar (Materials Information and Materials Inspection: Selected Basic Concepts and Industrial Applications)", Alfa Publishing, İstanbul (in Turkish), 2004.
51. N. Suroor, A. Jaiswal, and N. Sachdeva, "Stack Ensemble Oriented Parkinson Disease Prediction Using Machine Learning Approaches Utilizing GridSearchCV-Based Hyper Parameter Tuning", *Critical Review. Biomedical Eng.*, Vol. 50, Issue 5, Pages 39-58, 2022.



ULUSLARARASI 3B YAZICI TEKNOLOJİLERİ  
VE DİJİTAL ENDÜSTRİ DERGİSİ

INTERNATIONAL JOURNAL OF 3D PRINTING  
TECHNOLOGIES AND DIGITAL INDUSTRY

ISSN:2602-3350 (Online)

URL: <https://dergipark.org.tr/ij3dptdi>

# EFFECT OF GEOMETRIC MODIFICATIONS ON THE COMPRESSIVE STRENGTH AND MECHANICAL PERFORMANCE OF GYROID- BASED BONE SCAFFOLDS

**Yazarlar (Authors):** Muhammet Mevlüt Karaca \*, İzel Ekinci , Daver Ali 

**Bu makaleye şu şekilde atıfta bulunabilirsiniz (To cite to this article):** Karaca M. M., Ekinci İ., Ali D., “Effect of Geometric Modifications on the Compressive Strength and Mechanical Performance of Gyroid-Based Bone Scaffolds” *Int. J. of 3D Printing Tech. Dig. Ind.*, 9(1): 63-72, (2025).

DOI: 10.46519/ij3dptdi.1609933

Araştırma Makale/ Research Article

Erişim Linki: (To link to this article): <https://dergipark.org.tr/en/pub/ij3dptdi/archive>

# EFFECT OF GEOMETRIC MODIFICATIONS ON THE COMPRESSIVE STRENGTH AND MECHANICAL PERFORMANCE OF GYROID-BASED BONE SCAFFOLDS

Muhammet Mevlüt Karaca<sup>a\*</sup> , İzel Ekinci<sup>b</sup> , Daver Ali<sup>b</sup> 

<sup>a</sup>Karabuk University, Engineering Faculty, Mechanical Engineering Department, KARABUK

<sup>b</sup>Karabuk University, Engineering Faculty, Biomedical Engineering Department, KARABUK

\* Corresponding Author: [mmevlutkaraca@karabuk.edu.tr](mailto:mmevlutkaraca@karabuk.edu.tr)

(Received: 30.12.24; Revised: 08.03.25; Accepted: 15.03.25)

---

## ABSTRACT

Porous structures are of great interest in biomedical and engineering applications due to their light weight, high mechanical strength, and biological compatibility. In this study, based on the widespread use of gyroid structures in bone scaffolds and their potential to adapt to the heterogeneous mechanical properties of bone tissue, the effect of geometric arrangements on mechanical strength was investigated. Using the tri-periodic minimal surface trigonometric function, the reference model G(0) with 80% porosity was taken as a basis, and three different geometries were created by reducing the unit cell of the gyroid on the y-axis by 25% (G(-25)), keeping it constant (G(0)), and enlarging it by 25% (G(+25)). Using the biomaterial PLA, these non-isotropic structures were fabricated through Fused Deposition Modeling (FDM) and 3D printed in the longitudinal and lateral axes, then subjected to compression tests. The compression test results showed that the printing direction and loading direction play a decisive role in mechanical strength. Especially when the printing and loading directions were the same, an increase in strength was observed, with the G(-25) model exhibiting 37.8% higher strength than G(0) in the PLt-CLt (Printed Lateral – Compression Lateral) configuration. Conversely, increasing the pore size resulted in a 14.7% reduction in strength for G(-25) compared to G(0). Furthermore, when the printing and loading directions were aligned, the lateral axis exhibited 38.4% higher strength than the longitudinal axis in the G(-25) model. It was found that the arrangement of the pores parallel to the load direction minimized strength loss, and the increase in porosity did not significantly affect mechanical strength. In addition, the structure of the compression layers before and after the test was examined in detail by SEM analysis. The findings show that the geometrical arrangements of the gyroid structures have a significant effect on mechanical strength and that these structures can be optimized and used in biomedical applications.

**Keywords:** FDM, PLA, Gyroid Structure, Porosity, Bone Scaffold, Anisotropic Structure.

---

## 1. INTRODUCTION

Porous structures are of great interest in biomedical and engineering applications due to their properties such as light weight, high mechanical strength and biocompatibility. In particular, Triply Periodic Minimal Surface (TPMS) have become an important focus for scaffold design in biomedical applications. The unique geometric properties of TPMS structures allow them to mimic the mechanical behavior of natural bone, making them promising candidates for bone tissue engineering [1-2]. These surfaces are characterized by zero mean curvature, high surface-to-volume ratio, and

interconnected porous structure, and offer a favorable environment for bone regeneration by promoting cell adhesion and proliferation [3-4]. Gyroid structures represent an important subgroup of TPMS and are widely used in tissue engineering, implant design and other biomedical applications. Their interconnected porous network facilitates essential biological processes such as cell infiltration, vascularization, and nutrient transport, which are critical for the regeneration of both bone and soft tissues. These properties enhance osteointegration by promoting osteoblast adhesion and proliferation, ultimately

improving implant stability [5-6]. Furthermore, studies indicate that gyroid scaffolds provide a more uniform stress distribution compared to conventional strut-based lattice structures, leading to enhanced mechanical performance and reduced stress concentrations [7-8]. Gyroid structures offer an ideal option for load-bearing implants due to their unique mechanical performance and biocompatibility. For example, Eltlhawy et al. [9] demonstrated that gyroid cellular titanium is compatible with the mechanical properties of human bone and exhibits a 70% stiffness reduction, increasing the potential for successful integration in orthopedic applications. Pore size and porosity also significantly affect the performance of these structures. In the same study, a pore size of 500  $\mu\text{m}$  and a porosity of approximately 77% were reported to promote bone growth and increase bone-implant fixation stability. The advantages of gyroid structures in terms of stress distribution are noted for their lower stress concentrations compared to conventional support-based lattice structures. Hayashi et al. [8] showed that stress distribution in gyroid scaffolds is more homogeneous and that these structures outperform conventional scaffolds in terms of both strength and bone regeneration capabilities. In Ali's study [10], it was shown that the anisotropic properties of gyroid structures adapt to the mechanical and biological behavior of the bone structure. In the study, elastic modulus and permeability analyses were performed on gyroid scaffolds designed using different geometric variations and it was determined that these structures exhibit bone-like properties. The energy absorption capacity of gyroid structures is also superior to other porous structures. Hayashi et al. [8] determined that gyroid structures exhibit three times more specific energy absorption under pressure compared to other lattice structures.

The role of porosity and pore size in the design of gyroid and similar scaffolds is critical. Pore sizes have direct effects on cell infiltration, nutrient transport and mechanical strength [11-12]. Naghavi et al. [13] showed that gyroid structures with porosity between 52% and 66% exhibited hardness (4-5.8 GPa) and yield strength (120-225 MPa) similar to cortical bone. This was confirmed by Musthafa's study [14], which showed that structures with pore sizes smaller than 800  $\mu$  can offer mechanical

properties in the range of cortical bone. When the effect of pore size on mechanical strength was examined, Wu et al. [15] reported that smaller pore sizes increase compressive strength and there is an inverse relationship between pore size and mechanical strength. Caiazzo et al. [16] showed that the mechanical properties of Gyroid structures can be tuned by varying unit cell sizes and porosity ratios, thus optimizing the elastic modulus and compressive strength.

The mechanical properties of additively manufactured lattice structures show significant changes depending on parameters such as unit cell size and loading direction. For example, when the unit cell size is increased from 2 mm to 8 mm in 316L stainless steel gyroid lattice structures, the yield strength and elastic modulus decrease by 63.43% and 63.74%, respectively [17]. Similarly, the compressive modulus and compressive strength decrease by 10.33% and 29.45%, respectively [18]. Significant differences were also observed depending on the loading direction, and the elastic modulus of gyroid trusses produced in perpendicular direction was found to be 22.95% higher than those produced in parallel direction [17]. These data show that unit cell size and loading direction play a critical role in the design process of lattice structures and the mechanical properties should be optimized according to the targeted application.

Cellular structures are essential in engineering and biomedical applications due to their high specific strength, energy absorption capacity, and material efficiency [19]. TPMS structures ensure homogeneous stress distribution and superior mechanical performance, offering advantages over traditional lattices [18-19]. Conventional manufacturing methods are inadequate for producing such complex geometries, whereas additive manufacturing (AM) optimizes material usage, reduces production time, and minimizes waste. Among AM techniques, Selective Laser Melting (SLM) and Fused Deposition Modeling (FDM) excel in fabricating intricate cellular architectures with precise control over porosity and mechanical properties [18]. These advancements expand applications in aerospace, biomedical, and automotive industries.

In this study, the reference model G(0) was designed with a constant porosity of 80%, and three different geometries were obtained by reducing the unit cell of the gyroid structure on one axis by 25% (G(-25)), keeping it constant (G(0)) and enlarging it by 25% (G(+25)). The structures were 3D printed in two different directions in the longitudinal and lateral axes using the biomaterial Polylactic acid (PLA) and subjected to compression tests. The effect of printing direction, loading direction and porosity orientation on the mechanical properties of the obtained models were investigated. In addition, Scanning Electron Microscopy (SEM) images of the samples were taken after the mechanical tests and the adhesion and delamination between the printing layers were examined.

**2. MATERIALS AND METHODS**

**2.1. Modeling and Geometric Structure**

The basic surfaces of the skeletons were designed using the program K3Dsurf (k3dsurf.sourceforge.net). This design is based on the trigonometric function  $\cos(x) \sin(\alpha y) +$

$\cos(\alpha y) \sin(z) + \cos(z) \sin(x) = 0$ . For each model, the unit cells were repeated four times on three axes (x, y and z) to obtain a cube structure with a total of 64-unit cells. Information about the model unit cells and geometric parameters are given in Figure 1 and Table 1. The unit cell length was obtained in x, y, z on the boundary  $[-\pi, \pi]$ . For the models with scaling coefficients defined as -25%, 0% and 25%,  $\alpha$  values were set as 0.75, 1 and 1.25, respectively. These models are named G(-25), G(0) and G(+25) according to the scaling percentage. SolidWorks software was used to thicken the surfaces and create solid models. The thickness of the scaffold walls was determined as 400  $\mu\text{m}$ , and these structures were fabricated using Fused Deposition Modeling (FDM), a widely used additive manufacturing technique. FDM was chosen due to its capability to produce complex porous structures with high accuracy using PLA material. These structures can be easily manufactured with additive manufacturing technologies [20].

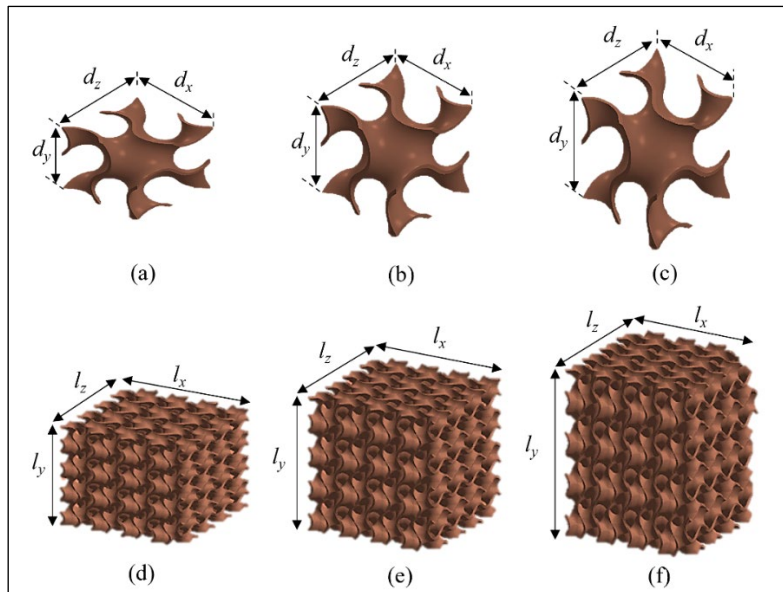


**Figure 1.** Unit cells of the designed gyroid structures: (a) G(-25), (b) G(0), (c) G(+25); full models: (d) G(-25), (e) G(0), (f) G(+25).

**Table 1.** Dimensions of the unit cell and the corresponding scaffold model (mm).

	Model		
Dimensions	G(-25)	G(0)	G(+25)
dx and dz	6,20	6,20	6,20
dy	4,58	6,20	7,72
Lx and Lz	25,54	25,55	25,33
Ly	19,09	25,32	31,54

**2.2. Production of Samples**

In this study, PLA filament was chosen for sample production due to its biocompatibility, biodegradability, and non-toxic degradation products. Widely used in scaffolds, drug delivery, and tissue engineering, PLA supports cell adhesion and reduces inflammation, as

shown in both in vitro and in vivo studies [21-23]. The properties of the Flashforge PLA Pro filament are listed in Table 2.

**Table 2.** Mechanical and physical properties of PLA Pro filament used [24].

Property	Test Method	Units	Typical Value
Density	ISO 1183	g/cm <sup>3</sup>	1.25~1.26
Tensile Strength	ISO 527	MPa	45.5~49
Elongation at Break	ISO 527	%	14.5~16.5
Modulus of Elasticity	ISO 527	MPa	950~1050
Izod Impact Strength	ISO 180	KJ/m <sup>2</sup>	9.5~10.5

The samples were produced using the Flash Forge Creator 3 Pro printer in accordance with the parameters specified in Table 3.

**Table 3.** Printing Parameters.

Parameters	Flash Forge - Creator 3 Pro
Material	PLA
Nozzle Diameter	0,4 mm
Printing Precision	0,1 mm
Extruder Temperature	210 °C
Bed Temperature	60 °C
Infill Density	% 100
Layer Thickness	0,18 mm
Print Speed	60 mm/s
Infill Pattern	Lines
Number of Wall Lines	3

In order to evaluate the effect of printing direction on mechanical properties, the specimens were printed in two different axes. As shown in Figure 2, the designed specimens were first printed in the longitudinal axis, then rotated 90° around the y-axis and printed in the lateral axis.

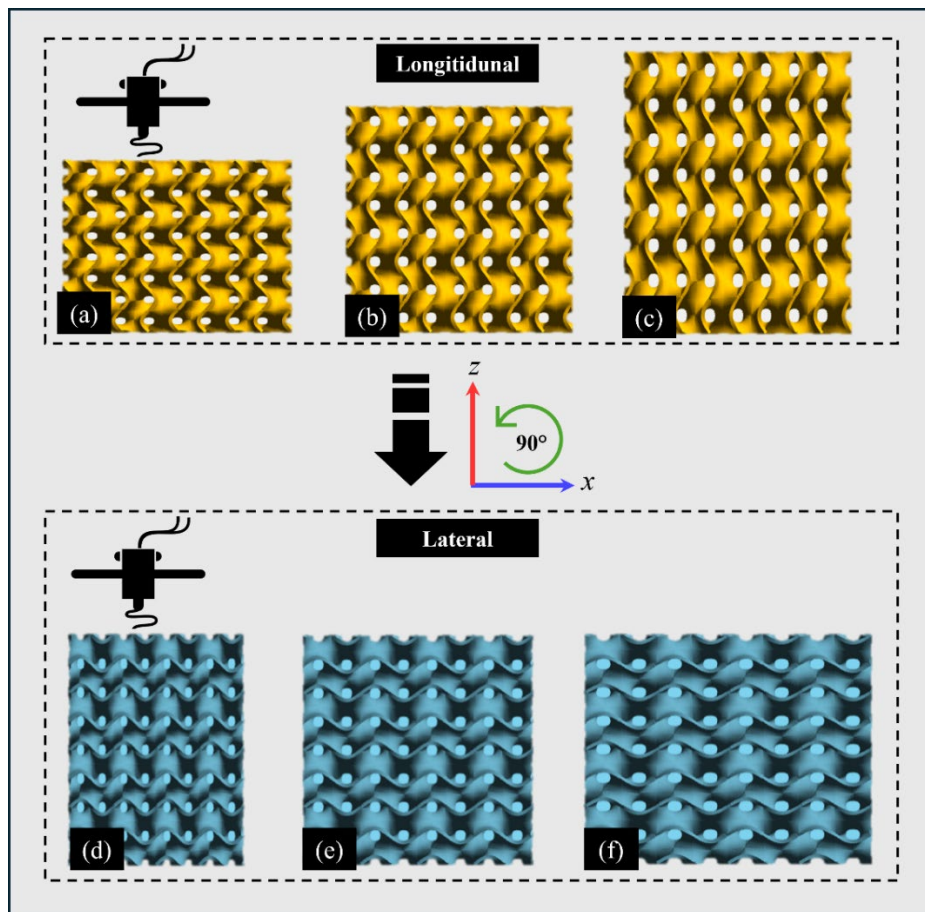


**Figure 2.** Gyroid structures produced in the longitudinal compression direction: (a) G(-25), (b) G(0) and (c) G(+25). Gyroid structures produced in the lateral compression direction: (d) G(-25), (e) G(0) and (f) G(+25).

### 2.3. Experimental Studies

Compression tests were performed on the successfully manufactured specimens. The sample specimens produced in the lateral direction are shown in Figure 3(a). The compression tests were conducted using a Zwick Z600 (Figure 3(b)) testing machine, with the test speed set to 2 mm/min in accordance with the ISO 604 standard. During the test, a deformation of 5 mm was applied to the specimens. Before and after the compression test, the structure of the specimens was examined by SEM. During the examinations, low levels of filamentation and porosity formation were observed in some areas, but it was observed that these formations were not significant and were not at a density that would adversely affect the mechanical performance. In addition, there was no visible delamination between the printing layers as a result of printing or detectable by SEM (Figure 3(c) and Figure 3(d)).

Analysis of the post-compression images revealed that the observed fracture behavior was

predominantly planar, with failure occurring along planes parallel to the compression direction. The narrowing effect observed under loading, as indicated in Figure 3(b), suggests localized stress concentrations that led to structural failure along these planes. The schematic representation within the figure further illustrates the deformation mechanism, showing that structural collapse primarily followed the interconnected porous architecture of the gyroid structure. No significant orthogonal fractures were detected, as no cracks propagating perpendicularly to the compression axis were observed.

The stringing behavior can be affected by printing parameters such as nozzle temperature, print speed and retraction settings. To solve this problem, strategies such as decreasing the nozzle temperature, increasing the printing speed and optimizing the retraction settings have been proposed [25-27].

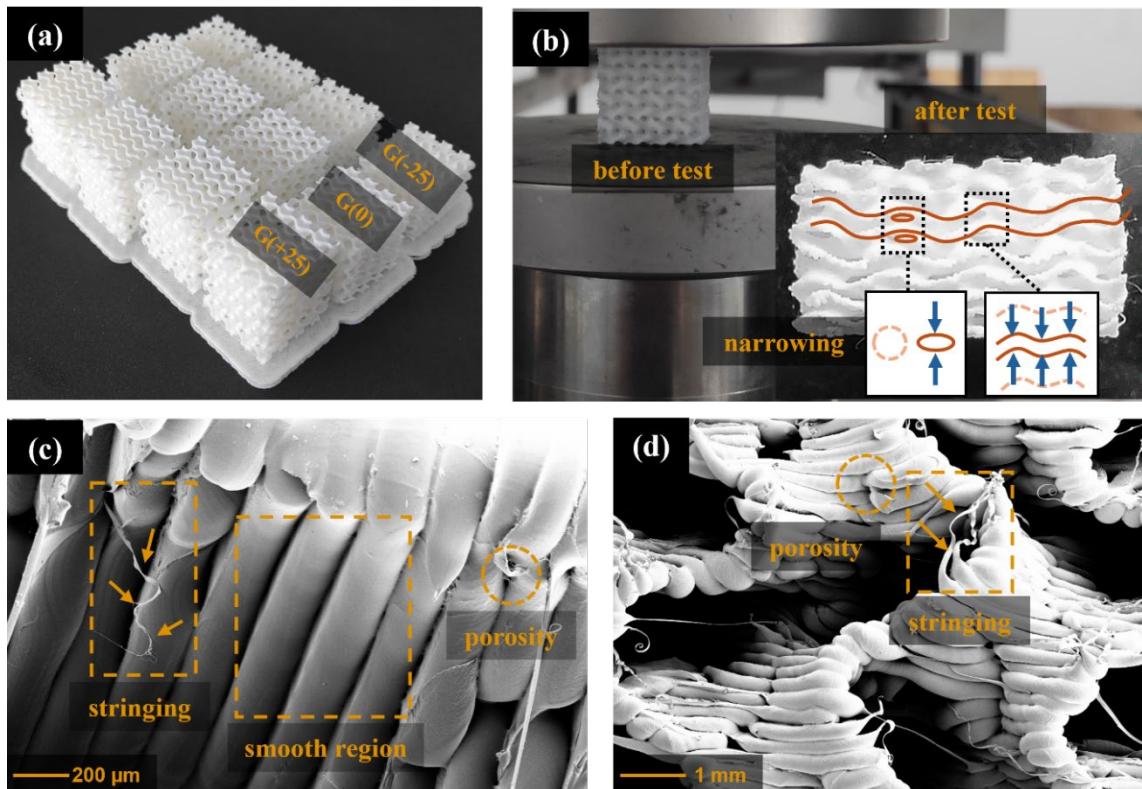


**Figure 3.** (a) 3D printed G(-25), G(0) and G(+25) samples, (b) Compression test of the gyroid scaffold samples before and after loading, (c) 200 µm scale SEM image, (d) 1 mm scale SEM image.

The compression test result graphs are given in Figure 4. The graphs compare the engineering stress-strain behavior (Figures 4a-4d), ultimate

compressive strength (Figure 4e) and deformation at maximum force (Figure 4f) of gyroid specimens of three different structures

(G(-25), G(0), G(+25)) under compression (PLo: Printed Longitudinal, PLt: Printed Lateral) and loading (CLo: Compression Longitudinal, CLt: Compression Lateral) conditions in different directions.

In Figures 4a and 4c, G(+25) specimens exhibited higher yield strength and ultimate compressive strength under PLo-CLo and PLa-CLt conditions, followed by G(0) and G(-25), respectively. Figure 4b and Figure 4d show that G(-25) specimens exhibited higher yield strength and ultimate compressive strength, followed by G(0) and G(+25), respectively.

According to Figure 4e, the highest ultimate compressive strength was observed in the PLt-

CLt G(-25) sample. This result was followed by PLo-CLo G(+25) and PLo-CLo G(0) samples, respectively. These findings reveal that when the printing direction and the test direction are the same, the material shows higher strength compared to other conditions. Similar results have been reported in the literature. Studies show that mechanical properties such as tensile, compressive and flexural strength increase significantly when the loading occurs in the same direction as the compression direction[28-31].

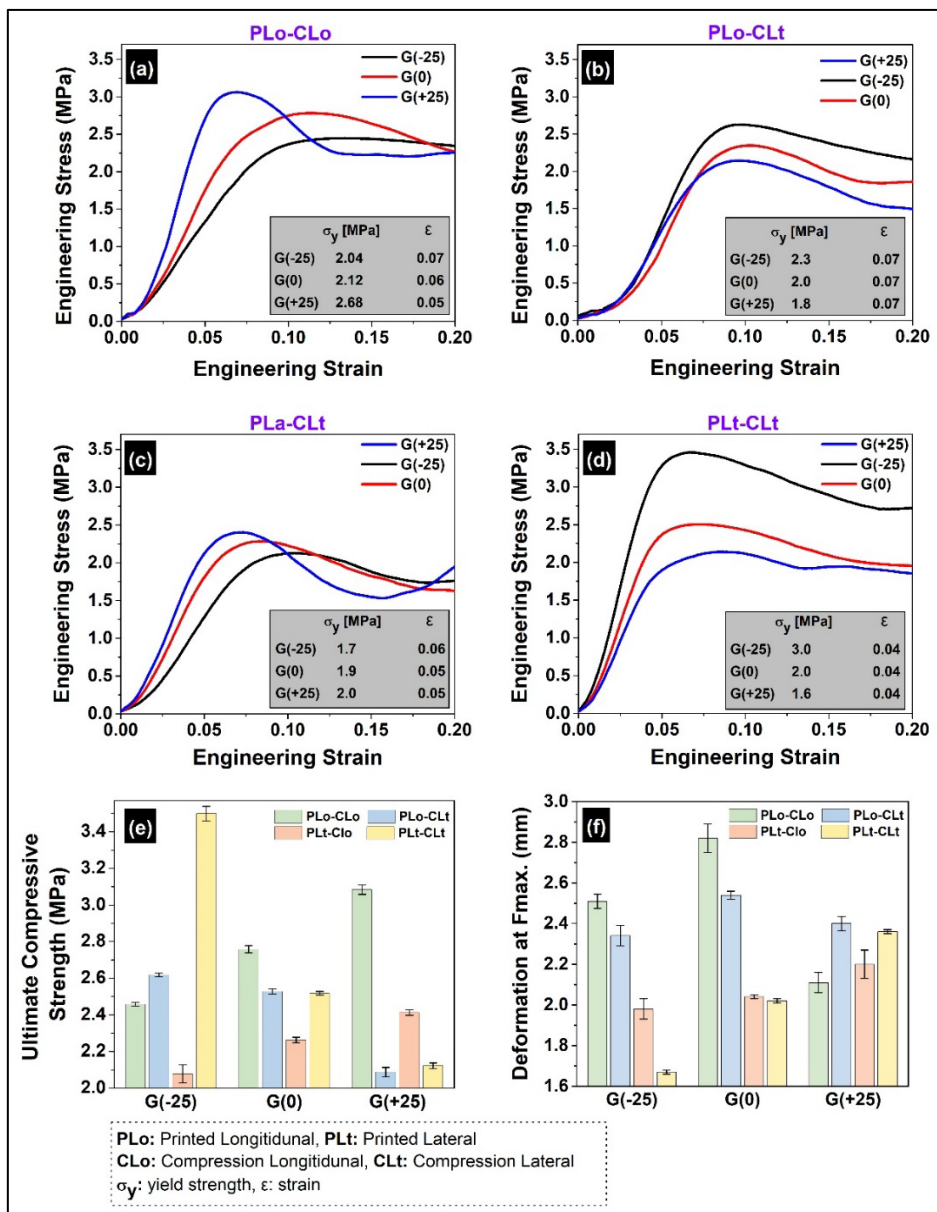


**Figure 4.** Engineering stress-strain curves and mechanical properties of compression tests at different compression and loading directions: (a) PLo-CLo, (b) PLo-CLt, (c) PLa-CLo, (d) stress-strain curves for PLa-CLo cases, (e) Ultimate compressive strength and (f) Deformation values at maximum force.

When PLt-CLt and PLo-CLt specimens are examined in Figures 4(b) and 4(d), the highest strength was observed at G(-25), followed by G(0) and G(+25), respectively. This is in line with the literature and can be explained by the effect of porosity on mechanical strength. The decrease in porosity improved the mechanical properties [32-33]. However, this result was reversed in PLo-CLo and PLt-CLo specimens. The probable reason for this is that the parallel arrangement of the pores to the load direction minimizes the strength loss and the increase in pores does not significantly affect the mechanical strength since the load carrying paths are not completely broken. Figure 5 shows the porosity distribution and dimensions of the specimens in the longitudinal and lateral directions. In the longitudinal direction, the width of the pores remained constant while the size of the pores changed. In the lateral direction, the heights of the pores are constant and the widths change. When these changes were analyzed, it was observed that the porosity widths in the longitudinal direction remained constant and were 1.16 mm. However, there were differences in the height values; the height

was measured as 0.78 mm for the G(-25) model, 1.16 mm for the G(0) model and 1.56 mm for the G(+25) model. In the lateral direction, the height values remained constant and were determined as 1.16 units. On the other hand, the width values changed and were measured as 0.78 mm for the G(-25) model, 1.16 mm for the G(0) model and 1.56 mm for the G(+25) model. Similar studies have shown that the mechanical strength of the material is higher when the pores are arranged parallel to the load direction. This is because the pores do not completely break the load carrying paths and minimize the strength loss[34-36]. In this case, the increase in porosity does not significantly affect the mechanical strength. On the other hand, in alignments perpendicular to the load direction, the pores interfere with load transfer and cause a decrease in strength. These findings indicate that pore orientation and loading direction play an important role in the mechanical properties of the material. In general, structure orientation and compression direction in scaffolds lead to significant differences in mechanical strength and deformation behavior.

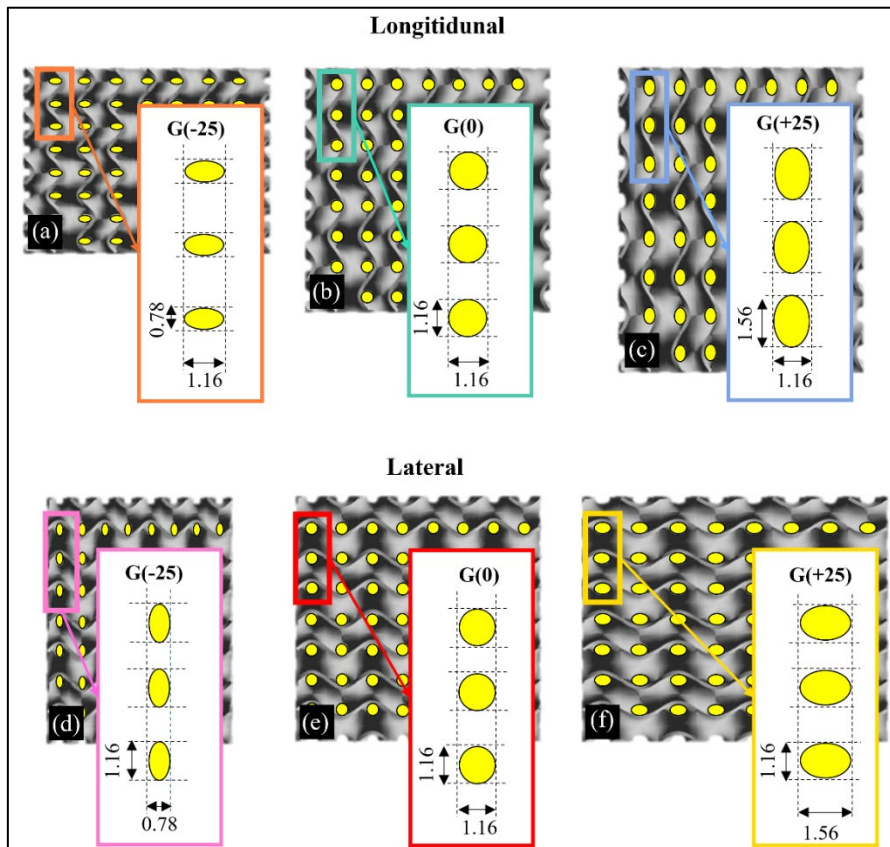


**Figure 5.** Pore shape and size of the specimens (mm): Longitudinal direction (a) G(-25), (b) G(0) and (c) G(+25); Lateral direction (d) G(-25), (e) G(0) and (f) G(+25).

### 3. CONCLUSIONS

In this study, the effect of geometric variations and compression-loading directions on the mechanical strength of gyroid structures is investigated in detail. Taking the G(0) model with constant 80% porosity as a reference, three different geometries with 25% reduction (G(-25)) and 25% enlargement (G(+25)) of the unit cell on the y-axis were evaluated. The findings are summarized as follows:

- Strength increased when the compression direction and loading direction were the same: Overlapping the loading direction with the compression direction improved the load carrying capacity by increasing the interlayer integrity. The G(-25) geometry showed the highest strength in the longitudinal direction.
- The strength differed in the longitudinal and lateral axes: Specimens produced in the longitudinal direction exhibited higher strength than those produced in the lateral direction due to the alignment of the filaments in the load direction.
- The reduction in pore size increased the mechanical strength: Smaller pore sizes improved the strength by making deformation of the scaffold structure more difficult. The G(-25) geometry therefore provided the best performance.
- The alignment of the pores parallel to the load direction improved the strength: Alignment of the pores parallel to the load direction minimized the strength loss, while alignment perpendicular to the load direction resulted in a decrease in mechanical strength.

In conclusion, this study revealed that geometrical optimization of gyroid structures, compression-loading directions and pore distribution significantly affect the mechanical strength. The usability of these structures in biomedical applications such as bone tissue engineering can be enhanced by accurately optimizing the geometric parameters. The results of this study further emphasize that

gyroid and similar architectural scaffolds are good alternatives for non-isometric bone.

### ACKNOWLEDGMENTS

This research received funding from the Scientific and Technological Research Council of Turkey (TUBITAK) under the project number 124M262. The study was conducted in the laboratories of Karabuk University, Material Research and Development Centre, with their support gratefully acknowledged.

### REFERENCES

1. Lehder, E. F., Ashcroft, I. A., Wildman, R. D., Ruiz-Cantu, L. A., and Maskery, I., "A multiscale optimisation method for bone growth scaffolds based on triply periodic minimal surfaces", *Biomechanics and Modeling in Mechanobiology*, Vol. 20, Issue 6, 2085-2096, 2021.
2. Zhang, Q., Ma, L., Ji, X., He, Y., Cui, Y., Liu, X., Xuan, C., Wang, Z., Yang, W., Chai, M., and Shi, X., "High-Strength Hydroxyapatite Scaffolds with Minimal Surface Macrostructures for Load-Bearing Bone Regeneration", *Advanced Functional Materials*, Vol. 32, Issue 33, 2022.
3. Noroozi, R., Shamekhi, M. A., Mahmoudi, R., Zolfagharian, A., Asgari, F., Mousavizadeh, A., Bodaghi, M., Hadi, A., and Haghhighipour, "In vitro static and dynamic cell culture study of novel bone scaffolds based on 3D-printed PLA and cell-laden alginate hydrogel", *Biomedical Materials*, Vol. 17, Issue 4, 2022.
4. Wang, Z., Liao, B., Liu, Y., Liao, Y., Zhou, Y., and Li, W., "Influence of structural parameters of 3D-printed triply periodic minimal surface gyroid porous scaffolds on compression performance, cell response, and bone regeneration", *Journal of Biomedical Materials Research Part B*, Vol. 112, Issue 1, 2024.
5. Charbonnier, B., Manassero, M., Bourguignon, M., Decambron, A., El-Hafci, H., Morin, C., Leon D., Bensedoum M., Corsia, S., Petite H., Marchat D., Potier, E., "Custom-made macroporous bioceramic implants based on triply-periodic minimal surfaces for bone defects in load-bearing sites", *Acta Biomaterialia*, Vol. 109, 254-266, 2020.
6. Verisqa, F., Park, J. H., Mandakhbayar, N., Cha, J. R., Nguyen, L., Kim, H. W., Knowles, J. C., "In vivo osteogenic and angiogenic properties of a 3d-printed isosorbide-based gyroid scaffold manufactured via digital light processing", *Biomedicines*, Vol. 12, Issue 3, 1-15, 2024.

7. Baumer, V., Isaacson, N., Kanakamedala, S., McGee, D., Kaze, I., Prawel, D. A., “Comparing ceramic fischer-koch-s and gyroid tpms scaffolds for potential in bone tissue engineering”, *Frontiers in Bioengineering and Biotechnology*, Vol. 12, 1-13, 2024.
8. Hayashi, K., Kishida, R., Tsuchiya, A., & Ishikawa, K., “Periodic Minimal Surface Gyroid Structure to Strut-Based Grid Structure in Both Strength and Bone Regeneration”, *ACS Applied Materials & Interfaces*, Vol. 15, Issue 29, 34570-34577, 2023.
9. Elthawy, B., “Numerical Evaluation of a Porous Tibial-Knee Implant using Gyroid Structure”, *Journal of Biomedical Physics and Engineering*, Vol. 12, Issue 1, 75-82, 2022.
10. Ali, D., “Mimicking Bone Anisotropic Structure with Modified Gyroid Scaffolds; A Finite Element Analysis”, *Politeknik Dergisi*, Vol. 24, Issue 4, 1637-1646, 2021.
11. Baumer, V., Gunn, E., Riegle, V., Bailey, C., Shonkwiler, C., and Prawel, D., “Robocasting of Ceramic Fischer–Koch S Scaffolds for Bone Tissue Engineering”, *Journal of Functional Biomaterials*, Vol. 14, Issue 5, 1-20, 2023.
12. Cubo-Mateo, N., and Rodríguez-Lorenzo, L. M., “Design of Thermoplastic 3D-Printed Scaffolds for Bone Tissue Engineering: Influence of Parameters of “Hidden” Importance in the Physical Properties of Scaffolds”, *Polymers*, Vol. 12, Issue 7, 1-14, 2020.
13. Naghavi, S. A., Tamaddon, M., Marghoub, A., Wang, K., Babamiri, B. B., Hazeli, K., Xu, W., Lu, X., Sun, C., Wang, L., Moazen, M., Wang, L., Li, D., and Liu, C., “Mechanical Characterisation and Numerical Modelling of TPMS-Based Gyroid and Diamond Ti6Al4V Scaffolds for Bone Implants: An Integrated Approach for Translational Consideration”, *Bioengineering*, Vol. 9, Issue 10, 1-25, 2022.
14. N. Musthafa, H.-S., Walker, J., Rahman, T., Bjørkum, A., Mustafa, K., & Velauthapillai, D., “In-Silico Prediction of Mechanical Behaviour of Uniform Gyroid Scaffolds Affected by Its Design Parameters for Bone Tissue Engineering Applications”, *Computation*, Vol. 11, Issue 9, 1-28, 2023.
15. Wu, F., Yang, J., Ke, X., Ye, S., Bao, Z., Yang, X., Zhong, C., Shen, M., Xu, S., Zhang, L., Gou, Z., and Yang, G., “Integrating pore architectures to evaluate vascularization efficacy in silicate-based bioceramic scaffolds”, *Regenerative Biomaterials*, Vol. 9, 1-10, 2022.
16. Caiazza, F., Alfieri, V., Guillen, D. G., and Fabbriatore, A., “Metal functionally graded gyroids: additive manufacturing, mechanical properties, and simulation”, *The International Journal of Advanced Manufacturing Technology*, Vol. 123, Issue 7-8, 2501-2518, 2022.
17. Gülcan, O., “Eklemeli İmalatla Üretilen Kafes Yapıların Mekanik Özellikleri Üzerine Etki Eden Faktörler”, *Makina Tasarım ve İmalat Dergisi*, Vol. 19, Issue 2, 64-81, 2021.
18. Ergene B, Yalçın B, “Eriyik yığıma modelleme (EYM) ile üretilen çeşitli hücresel yapıların mekanik performanslarının incelenmesi”, *Gazi Üniversitesi Mühendislik Mimarlık Fakültesi Dergisi*, Vol. 38, Issue 1, 201-217, 2023.
19. Khan, N., Riccio, A., “A systematic review of design for additive manufacturing of aerospace lattice structures: Current trends and future directions”, *Progress in Aerospace Sciences*, Vol. 149, 1-34, 2024.
20. Burkhard, M., Fünstahl, P., and Farshad, M., “Three-dimensionally printed vertebrae with different bone densities for surgical training”, *European Spine Journal*, Vol. 28, Issue 4, 798-806, 2019.
21. Li, N., and Chen, J., “Advances in chemical modifications of polylactide biodegradable materials”, *3rd International Forum on Energy, Environment Science and Materials (IFEESM 2017)*, 1640-1643, Shenzhen, 2017.
22. Gonçalves, A. P. B., Barbosa, W. T., Vieira J. L., Barbosa, J. D. V., and Soares, M. B. P., “Production of the Scaffold Using 3D Bioprinting Applied to the Biomedical Area: A Bibliometric Study”, *Journal of Bioengineering, Technologies and Health*, Vol. 6, Issue 3, 244-251, 2023.
23. Shasteen, C., and Choy, Y. Bin., “Controlling degradation rate of poly(lactic acid) for its biomedical applications”, *Biomedical Engineering Letters*, Vol. 1, Issue 3, 163-167, 2011.
24. Flash Forge, “Technical Data Sheet”, [https://after-support.flashforge.jp/uploads/datasheet/tds/PLA\\_Pro\\_TDS\\_EN.pdf](https://after-support.flashforge.jp/uploads/datasheet/tds/PLA_Pro_TDS_EN.pdf), February 24, 2025.
25. Hergel, J., and Lefebvre, S., “Clean color: Improving multi-filament 3D prints”, *Computer Graphics Forum*, Vol. 33, Issue 2, 469-478, 2014.

26. Prasher, A., Shrivastava, R., Dahl, D., Sharma-Huynh, P., Maturavongsadit, P., Pridgen, T., Schorzman, A., Zamboni, W., Ban, J., Blikslager, A., Dellon, E. S., and Benhabbour, S. R., "Steroid Eluting Esophageal-Targeted Drug Delivery Devices for Treatment of Eosinophilic Esophagitis", *Polymers*, Vol. 13, Issue 4, 1-20, 2021.
27. Catana, D. I., Pop, M. A., and Brus, D. I., "Comparison between Tests and Simulations Regarding Bending Resistance of 3D Printed PLA Structures", *Polymers*, Vol. 13, Issue 24, 1-11, 2021.
28. Zohourkari, I., "Anisotropic Mechanical Properties of 3D Printed Poly-Lactic Acid Parts in the Plane Stress State", *International Journal of Research Publication and Reviews*, Vol. 4, Issue 3, 4943-4948, 2023.
29. Syaefudin, E. A., Kholil, A., Hakim, M., Wulandari, D. A., Riyadi, and Murtinugraha, E., "The effect of orientation on tensile strength 3D printing with ABS and PLA materials", *12th International Physics Seminar*, 1-7, Jakarta, 2023.
30. Spišák, E., Nováková-Marcinčinová, E., Nováková-Marcinčinová, L., Majerníková, J., & Mulidrán, P., "Investigation of the Manufacturing Orientation Impact on the Mechanical Properties of Composite Fiber-Reinforced Polymer Elements in the Fused Filament Fabrication Process", *Polymers*, Vol. 15, Issue 13, 1-17, 2023.
31. Shen, Y., Lin, L., Wei, S., Yan, J., and Xu, T., "Research on the Preparation and Mechanical Properties of Solidified 3D Printed Concrete Materials", *Buildings*, Vol. 12, Issue 12, 1-23, 2022.
32. Zaharin, H. A., Abdul Rani, A. M., Azam, F. I., Ginta, T. L., Sallih, N., Ahmad, A., Yunus, N. A., and Zulkifli, T. Z. A., "Effect of Unit Cell Type and Pore Size on Porosity and Mechanical Behavior of Additively Manufactured Ti6Al4V Scaffolds", *Materials*, Vol. 11, Issue 12, 1-15, 2018.
33. Isaacson, N., Lopez-Ambrosio, K., Chubb, L., Waanders, N., Hoffmann, E., Witt, C., James, S., and Prawel, D. A., "Compressive properties and failure behavior of photocast hydroxyapatite gyroid scaffolds vary with porosity", *Journal of Biomaterials Applications*, Vol. 37, Issue 1, 55-76, 2022.
34. Wolff, S., Lee, T., Faierson, E., Ehmann, K., and Cao, J., "Anisotropic properties of directed energy deposition (DED)-processed Ti-6Al-4V", *Journal of Manufacturing Processes*, Vol. 24, 397-405, 2016.
35. von Windheim, N., Collinson, D. W., Lau, T., Brinson, L. C., and Gall, K., "The influence of porosity, crystallinity and interlayer adhesion on the tensile strength of 3D printed polylactic acid (PLA)", *Rapid Prototyping Journal*, Vol. 27, Issue 7, 1327-1336, 2021.
36. Honda, S., Hashimoto, S., Nait-Ali, B., Smith, D. S., Daiko, Y., and Iwamoto, Y., "Characterization of anisotropic gas permeability and thermomechanical properties of highly textured porous alumina", *Journal of the American Ceramic Society*, Vol. 105, Issue 10, 6335-6344, 2022.



ULUSLARARASI 3B YAZICI TEKNOLOJİLERİ  
VE DİJİTAL ENDÜSTRİ DERGİSİ

INTERNATIONAL JOURNAL OF 3D PRINTING  
TECHNOLOGIES AND DIGITAL INDUSTRY

ISSN:2602-3350 (Online)

URL: <https://dergipark.org.tr/ij3dptdi>

## 3D MEDICAL IMAGE SEGMENTATION WITH DEEP LEARNING METHODS

**Yazarlar (Authors):** Sezin Barın <sup>ID\*</sup>, Uçman Ergün <sup>ID</sup>, Gür Emre Güraksın <sup>ID</sup>

**Bu makaleye şu şekilde atıfta bulunabilirsiniz (To cite to this article):** Barın S., Ergün U., Güraksın G. E., "3D Medical Image Segmentation with Deep Learning Methods" *Int. J. of 3D Printing Tech. Dig. Ind.*, 9(1): 73-91, (2025).

DOI: 10.46519/ij3dptdi.1571288

Araştırma Makale/ Research Article

Erişim Linki: (To link to this article): <https://dergipark.org.tr/en/pub/ij3dptdi/archive>

# 3D MEDICAL IMAGE SEGMENTATION WITH DEEP LEARNING METHODS

Sezin Barın<sup>a</sup> , Uçman Ergün<sup>a</sup> , Gür Emre Güraksın<sup>b</sup> 

<sup>a</sup> Afyon Kocatepe University, Engineering Faculty, Biomedical Engineering Department, Afyonkarahisar/Turkey

<sup>b</sup> Afyon Kocatepe University, Engineering Faculty, Computer Engineering Department, Afyonkarahisar/Turkey

\* Corresponding Author: [sbarin@aku.edu.tr](mailto:sbarin@aku.edu.tr)

(Received: 21.10.24; Revised: 05.02.25; Accepted: 19.03.25)

---

## ABSTRACT

With advancements in technology, three-dimensional (3D) medical imaging has become vital in modern medicine, contributing to more accurate diagnosis, treatment planning, and personalized medicine. However, segmenting abdominal organs remains a challenging task due to anatomical variations, limited labeled data, and image noise. This study investigates the impact of deep learning-based architectures and preprocessing techniques on 3D organ segmentation using the publicly available Multi-Atlas Labeling Beyond the Cranial Vault (BTCV) dataset. To achieve this, 3D U-Net, UNETR, and SwinUNETR models were employed, and the effects of various preprocessing techniques and loss functions, including Dice Loss, Focal Loss, and Cross-Entropy Loss, were systematically analyzed. The findings reveal that combining Dice Loss with Cross-Entropy Loss significantly enhances segmentation performance. Additionally, preprocessing techniques improved segmentation accuracy by 1.19%, further optimizing model performance. Among the evaluated models, 3D U-Net achieved the highest overall segmentation performance, with an average Dice score of 0.8397, outperforming SwinUNETR and UNETR. These findings underscore the importance of selecting appropriate preprocessing methods and loss functions in 3D medical image segmentation. The results contribute to more precise and efficient medical image analysis, with potential applications in clinical decision support systems. Future research should focus on optimizing hybrid architectures, integrating advanced augmentation strategies, and expanding evaluation across multiple datasets to improve the robustness and real-world applicability of automated segmentation methods.

**Keywords:** Deep Learning, Image Processing, 3D Image Segmentation, Medical Image Analysis, 3D U-Net, UNETR, SwinUNETR.

---

## 1. INTRODUCTION

Medical imaging systems and medical images have long been a fundamental part of medicine. Developments in medical imaging systems have enabled the development of new approaches in early diagnosis of diseases, treatment planning, and monitoring of the treatment process[1]. However, medical image analysis, interpretation, and reporting are usually time-consuming and require expertise. In particular, manual segmentation applications in medical images are labor-intensive, prone to inter-observer variability, and subject to inconsistencies[2]. For this reason, studies on automatic analysis of medical images have continued to be popular for years.

Advancements in artificial intelligence, particularly in deep learning, have led to significant progress in automatic image analysis[3]. Unlike traditional image processing and machine learning methods, deep learning techniques automatically extract distinctive features from images, making them highly effective in segmentation, classification, detection, and registration tasks[4]. Thanks to this advanced feature, deep learning models exhibit superior performance in challenging tasks such as segmentation, classification, detection, and registration of images. The success of deep learning in medical image analysis has led to an increasing number of studies applying these methods for automatic segmentation[3,5-6]. According to the

literature, segmentation studies have a small proportion compared to other tasks in the field of medical image analysis. Compared to tasks like classification and detection, medical image segmentation remains a less explored area due to challenges such as limited annotated datasets[7], high computational costs[6], the complexity of medical image features[3], evaluation difficulties[8], and the integration of automated methods into clinical workflows[9].

Segmentation is a process used to separate targeted anatomical structures (organs, lesions, etc.) from other structures in medical images[10]. This process is the most critical step in many clinical applications, such as disease diagnosis, treatment planning, surgical interventions, and monitoring of the disease process, providing quantitative and objective information[11]. Accurate segmentation facilitates better treatment decisions and enables more efficient monitoring of disease progression. While manual segmentation can be time-consuming and subjective, automatic segmentation methods reduce the workload and provide more consistent results[12]. Deep learning models, particularly Convolutional Neural Networks (CNNs) and their derivatives, have demonstrated superior performance over conventional segmentation approaches[13]. Accurate and reliable organ segmentation in medical images is important in clinical applications in disease diagnosis, treatment planning, treatment process monitoring, surgical planning, and navigation systems [14]. Despite their success, medical image segmentation models still face challenges, such as variations in organ shapes, poor image contrast, and noise-related artifacts. In organ segmentation, it is possible to analyze medical images in 2D and 3D. Literature studies show that 2D image analysis is more widely preferred than 3D. Possible reasons for this situation can be listed as follows [3,7,10,11,15];

- 2D images can be easily obtained, and therefore, data sets can be easily created,
- 2D image analysis has lower computational costs than 3D images,
- 3D images need more preprocessing,
- Ease of comparison due to testing old methods on 2D images,
- Ease of visualization and interpretation of 2D images

In addition, there are some advantages of segmenting medical images in 3D instead of 2D segmentation that provide more successful segmentation. For example[14,16,17];

- 3D segmentation methods provide more consistent and accurate segmentation by preserving volumetric information and spatial relationships between neighboring slices and using contextual information.
- Preserving contextual information between neighboring pixels increases segmentation performance in noisy or low-contrast regions .
- When 3D medical images are analyzed in 2D, errors caused by shifts between slices are not considered. More accurate results can be obtained by reducing projection effects with 3D segmentation methods. This is especially important in surgical planning or navigation systems .

Since 2D segmentation methods work independently for each slice, they need to be repeated on the 3D volume. This increases computational cost and is an inefficient process. 3D segmentation methods work directly on the 3D volume using efficient architectures such as 3D convolutional neural networks and significantly reduce computational time [18].

However, these advantages of 3D images bring some difficulties. Handling 3D data in parallel necessitates the use of high computation hardware. Moreover, 3D organ segmentation is challenging due to the large data size, variations in the shape and appearance of organs, and image noise and artifacts[10]. From another perspective, deep learning-based approaches have the potential to automatically learn meaningful features from 3D medical images and increase segmentation accuracy[9].

The primary purpose of this study is to perform high-performance 3D abdominal organ segmentation using deep learning methods. As mentioned, abdominal organ segmentation is an essential problem in medical image analysis. Still, it is a challenging task due to the complex anatomy of organs, image quality issues, and high variability between organs [14]. Existing 2D segmentation methods show limited

performance in 2D organ segmentation since they cannot fully capture 3D volumetric information. Therefore, 3D segmentation methods that take into account 3D contextual information and volumetric morphology of organs contribute to the development of existing automatic segmentation systems. In the scope of the study, the performances of 3D U-Net [16], UNETR [19], and SwinUNETR [20] models, which are deep learning-based 3D segmentation architectures that have been widely used in recent years, were comparatively evaluated. These models aim to perform organ segmentation by extracting meaningful volumetric features from 3D medical images using 3D convolutional neural networks (CNN) and transformer-based approaches. In addition to deep learning-based 3D segmentation architectures, the effects of morphological image preprocessing and different loss functions on segmentation performance were also investigated in the study. In addition, the impact of data augmentation techniques on 3D organ segmentation was also analyzed in the scope of the study. Data augmentation methods can increase the generalization ability of deep learning models, especially in cases with limited training examples. Therefore, the aim is to make the models robust against different variations by applying different data augmentation methods.

The rest of this paper is structured as follows: Section 2 presents the related work, summarizing previous research on 3D medical image segmentation and highlighting key advancements in deep learning-based approaches. Section 3 describes the materials and methods used in this study, detailing the dataset, preprocessing techniques, and model configurations. Section 4 presents the experimental results, comparing different segmentation approaches and analyzing their effectiveness. Finally, Section 5 concludes the paper by summarizing key findings and discussing potential future research directions.

## 2. RELATED WORKS

In recent years, deep learning-based approaches, especially convolutional neural networks (CNN) and transformer architectures, have shown impressive results in medical image segmentation [3, 5].

U-Net [13] and V-Net [21] are considered the leading CNN architectures in medical image

segmentation. Çiçek et al. [16] introduced 3D U-Net, an extension of the U-Net model, designed for volumetric medical image segmentation. The study aimed to improve segmentation performance in 3D medical imaging, particularly in cases with sparse annotations where manual labeling is limited. The proposed model replaces 2D convolutions with 3D convolutional layers, enabling better feature extraction for volumetric data. The model was evaluated on electron microscopy (EM) data for neuron segmentation and magnetic resonance imaging (MRI) data for brain tumor segmentation. Experimental results demonstrated that 3D U-Net significantly outperformed traditional 2D approaches, particularly in segmenting small and complex structures. The model achieved a Jaccard score (IoU) of 0.853 in neuron segmentation and a Dice Similarity Coefficient (DSC) of 0.897 in brain tumor segmentation. These results highlight the effectiveness of 3D U-Net in handling volumetric medical images, even when trained on limited labeled data, making it a valuable tool for automated medical image analysis.

Milletari et al. [21] introduced V-Net, a fully convolutional neural network (FCN) designed for volumetric medical image segmentation, particularly prostate segmentation in MRI scans. The study aimed to overcome the limitations of 2D CNNs by utilizing 3D convolutional layers, allowing the model to learn spatial context across entire volumetric images. A key innovation of V-Net is the introduction of a Dice loss function, which is optimized directly during training. This loss function effectively addresses the class imbalance issue, which is common in medical image segmentation, by prioritizing foreground voxels without requiring manual weighting. The model was trained and evaluated on the PROMISE12 [22] prostate MRI dataset, consisting of 50 training and 30 test volumes. The experimental results demonstrated that V-Net achieved a Dice similarity coefficient (DSC) of 0.869, outperforming standard CNN-based approaches. The study also highlighted that V-Net significantly reduced segmentation time, achieving inference in just 1 second per MRI volume, making it suitable for real-time clinical applications.

Recently, Transformer architectures have shown remarkable performance in medical

image segmentation. Hatamizadeh et al. [19] proposed UNETR, a transformer-based model for 3D medical image segmentation, addressing the limitations of CNNs in capturing long-range dependencies. Unlike traditional methods, UNETR employs a Vision Transformer (ViT) encoder, processing 3D volumes as sequential patches, which enhances global context understanding. The model connects the transformer encoder to a CNN-based decoder via skip connections for precise segmentation. Evaluated on BTCV and MSD datasets, UNETR achieved 0.856 Dice in BTCV multi-organ segmentation, 0.964 in spleen segmentation, and 0.711 in brain tumor segmentation, outperforming state-of-the-art CNN and hybrid models. These results highlight UNETR's superior performance in volumetric medical image segmentation, establishing it as a strong candidate for future transformer-based segmentation models.

Chen et al. [23] introduced TransUNet, a hybrid model combining CNNs and Transformers for medical image segmentation. The study aimed to overcome CNNs' limitations in capturing long-range dependencies while maintaining precise localization through U-Net-like skip connections. Evaluated on the Synapse multi-organ CT dataset, TransUNet achieved 77.48% Dice score, outperforming CNN-based and transformer-only methods. Similarly, on the ACDC cardiac segmentation dataset, it achieved 89.71% Dice score, surpassing competing models. These results highlight TransUNet's effectiveness in balancing global context understanding with fine-grained spatial details, making it a strong alternative to traditional FCN-based segmentation models.

Cao et al. [20] introduced SwinUNETR, a U-Net-like architecture incorporating Swin Transformer blocks to enhance medical image segmentation. The study aimed to overcome the locality limitations of CNNs while reducing the high computational cost of standard Transformers. Unlike conventional U-Net models, SwinUNETR leverages hierarchical shifted window attention to capture both local and global dependencies efficiently. The model was evaluated on Synapse multi-organ segmentation (CT) and ACDC cardiac segmentation (MRI) datasets. SwinUNETR achieved a Dice similarity coefficient (DSC) of 79.13% on Synapse and 90% on ACDC,

outperforming CNN-based U-Net variants and Transformer-based architectures. These results highlight SwinUNETR's effectiveness in balancing spatial precision and computational efficiency, making it a promising alternative for high-accuracy medical image segmentation.

Isensee et al. [18] introduced nnU-Net, a self-configuring deep learning framework for biomedical image segmentation, addressing the challenge of manually optimizing deep learning models for diverse datasets. Unlike conventional approaches, nnU-Net automatically adapts its preprocessing, network architecture, training strategies, and post-processing to any given segmentation task. It systematically categorizes parameters into fixed, rule-based, and empirical decisions, reducing the need for expert intervention. nnU-Net was extensively tested on 23 public datasets across 53 segmentation tasks, achieving state-of-the-art performance in most cases. Notably, it outperformed highly specialized models in numerous international biomedical segmentation challenges. This study demonstrates nnU-Net's effectiveness as an out-of-the-box solution, making high-quality segmentation accessible without requiring expert knowledge or extensive computational resources.

Recently, models such as U-Mamba [24] and SegMamba [25], called the Mamba family, have also attracted considerable attention in segmentation studies. Ma et al. [24] introduced U-Mamba, a hybrid CNN-State Space Model (SSM) architecture for biomedical image segmentation, aiming to enhance long-range dependency modeling while maintaining computational efficiency. Unlike CNNs, which struggle with global context, and Transformers, which are computationally expensive, U-Mamba integrates Mamba blocks (a variant of SSMs) to efficiently capture both local and global features. The model employs a self-configuring mechanism, similar to nnU-Net, allowing it to automatically adapt to various datasets without manual tuning. Evaluated on four diverse segmentation tasks—3D abdominal CT and MRI segmentation, endoscopy instrument segmentation, and microscopy cell segmentation—U-Mamba consistently outperformed state-of-the-art CNN-based (nnU-Net, SegResNet) and Transformer-based (UNETR, SwinUNETR)

models. Notably, in 3D abdominal CT segmentation, U-Mamba achieved a Dice score of 0.8683, surpassing nnU-Net (0.8615), and in 3D MRI segmentation, it achieved 0.8501, outperforming SwinUNETR and UNETR. These results demonstrate U-Mamba's ability to balance computational efficiency with high segmentation accuracy, positioning it as a promising alternative to existing deep learning architectures in biomedical imaging.

Xing et al. [25] introduced SegMamba, a novel 3D medical image segmentation model that integrates Mamba-based State Space Models (SSMs) to enhance long-range dependency modeling while maintaining computational efficiency. Unlike CNN-based methods, which struggle with global context, and Transformer-based models, which suffer from high computational costs, SegMamba employs Tri-orientated Spatial Mamba (ToM) blocks to effectively capture global information in volumetric medical images. The model also incorporates a Gated Spatial Convolution (GSC) module for improved spatial feature representation and a Feature-level Uncertainty Estimation (FUE) module to refine multi-scale feature integration. Evaluated on BraTS 2023 (brain tumor segmentation), AIIB 2023 (airway segmentation), and CRC-500 (colorectal cancer segmentation) datasets, SegMamba achieved Dice scores of 91.32% on BraTS 2023, 88.59% on AIIB 2023, and 48.02% on CRC-500, outperforming state-of-the-art CNN and Transformer models. These results demonstrate SegMamba's ability to efficiently model long-range dependencies while maintaining high segmentation accuracy, positioning it as a strong alternative to existing deep learning architectures in medical imaging.

Automatic preprocessing and data augmentation techniques also play an important role in 3D medical image segmentation. Zhao et al. [26] proposed a learning-based data augmentation method to address the challenge of one-shot medical image segmentation, where only a single labeled scan is available. Unlike traditional augmentation techniques that rely on random transformations, this method learns spatial and intensity transformations from unlabeled medical images and applies them to generate realistic synthetic training examples. The model captures anatomical and imaging variations by learning spatial deformation fields

and intensity mappings, enabling robust augmentation beyond simple rotations or flips. Evaluated on MRI brain segmentation, the proposed method significantly outperformed state-of-the-art one-shot segmentation approaches, including single-atlas segmentation and traditional augmentation-based supervised segmentation. The study demonstrated that using learned transformations improved Dice scores by up to 0.056, bringing performance closer to fully supervised models while requiring only minimal labeled data. These results highlight the potential of learning-based augmentation to enhance segmentation accuracy in low-data medical imaging scenarios.

Despite significant advancements, 3D medical image segmentation continues to face challenges, particularly in achieving high accuracy for small and complex anatomical structures. CNN-based models excel at capturing local spatial details but struggle with modeling long-range dependencies. On the other hand, Transformer-based architectures address this limitation effectively; however, they often demand substantial computational resources and large amounts of labeled data. Hybrid approaches, such as U-Mamba and SegMamba, propose alternative mechanisms to balance these limitations, yet their generalizability across diverse datasets remains uncertain.

In light of these challenges, this study aims to bridge existing gaps by developing a segmentation framework that balances local and global feature extraction while optimizing computational efficiency. Specifically, this research focuses on improving 3D abdominal organ segmentation performance by leveraging advanced deep learning models and tailored preprocessing techniques. Considering the inherent difficulties of medical image segmentation, such as anatomical variability, image noise, and limited training datasets, this study contributes to the field by systematically evaluating the effectiveness of different segmentation methodologies. By addressing key limitations in current approaches, this work provides valuable insights for optimizing deep learning architectures for medical imaging applications.

### 3. MATERIAL AND METHOD

This study comparatively evaluates the performances of three widely used deep learning architectures for 3D medical image segmentation: 3D U-Net [16], UNETR [19], and SwinUNETR [20]. The impact of image preprocessing, post-processing, and loss

functions on the performance of these models is systematically examined. The objective is to identify the optimal configuration that maximizes segmentation accuracy. The overall study workflow is illustrated in Figure 1.

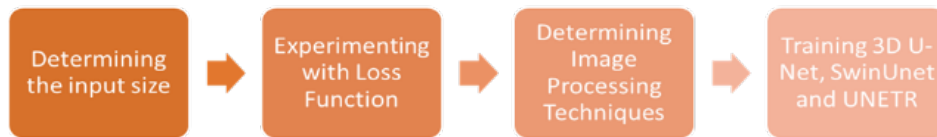


**Figure 1.** Flowchart of the Study

### 3.1. Dataset Used

The study utilizes the BTCV (Beyond the Cranial Vault) dataset [27], which was specifically designed for abdominal organ segmentation. The dataset was created for the "Multi-Atlas Labeling Beyond the Cranial Vault" competition held at the MICCAI 2015 conference. The images consist of 30 contrast-enhanced abdominal and pelvic CT scans. Each scan consists of 85 to 198 slices. The slice thickness is 2.5 mm, and the slice interval is 2.5 mm. The image size is 512 x 512 pixels. All scans were taken in the portal venous contrast phase. HU (Hounsfield Unit) values are in the

range of [-1024, 3071]. It is in NIFTI (.nii.gz) file format. Each CT scan in the dataset contains reference images manually segmented by expert radiologists. There are 13 segmented organs: spleen, right kidney, left kidney, gallbladder, esophagus, liver, stomach, aorta, inferior vena cava, portal vein and splenic vein, pancreas, retinitis adrenal gland, left adrenal gland. In the study, 24 of these 30 CT images were used for training, while six were used for validation and testing. Figure 2 shows a sample image from the dataset and the corresponding labeled image.

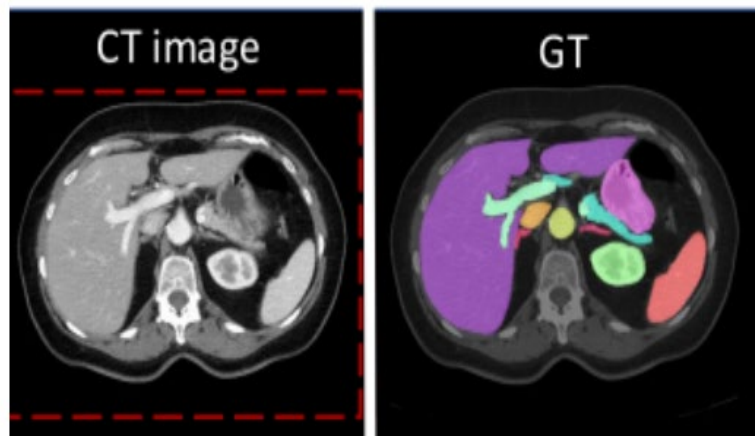


**Figure 2.** Dataset Sample Image and Ground Truth Image.

### 3.2. Applied Deep Learning Models

The study trained and compared three different deep-learning architectures with the dataset. First, the 3D U-Net architecture proposed by Çiçek et al. [16] was used. 3D U-Net was explicitly designed for volumetric medical image segmentation by extending the traditional U-Net architecture with three-dimensional convolutions. This architecture comprises an encoder with consecutive 3D convolutional layers, ReLU activations, and max pooling

operations, and a decoder with upsampling layers followed by 3D convolutions and ReLU activations. At each downsampling step, the number of feature channels is doubled. Skip connections from encoder to decoder enable low-level and high-level features to be effectively combined. This structure can produce detailed segmentation maps even in cases where there is limited training data. A standard 3D U-Net architecture is given in Figure 3. [16].

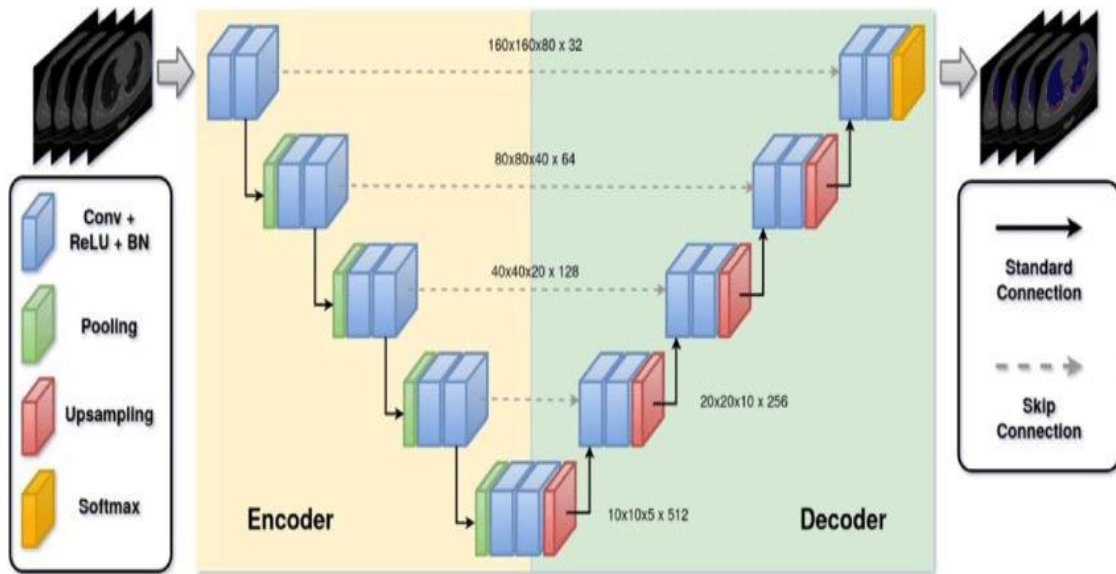


Figure 3. Standard 3D U-Net architecture

Secondly, the UNETR (UNet-Transformers) architecture developed by Hata-mizadeh et al. [19] is implemented. UNETR is a hybrid architecture that uses a transformer-based encoder and a CNN-based decoder. The encoder section first divides the 3D image into small volumetric patches with regular intervals and passes these patches through a linear projection layer. Then, position codings are added to these projections, and the resulting sequences are passed through a series of transformer blocks. Each transformer block has a multi-head self-attention mechanism and a feed-forward neural

network layer. This structure can effectively capture long-range spatial dependencies. The decoder section uses a CNN structure that combines features from different encoder layers and gradually amplifies them. This hybrid structure of UNETR combines the global context capturing ability of transformers with the local feature extraction power of CNNs, achieving successful results, especially for the segmentation of complex anatomical structures. Figure 4 shows a model showing the working flow of UNETR.

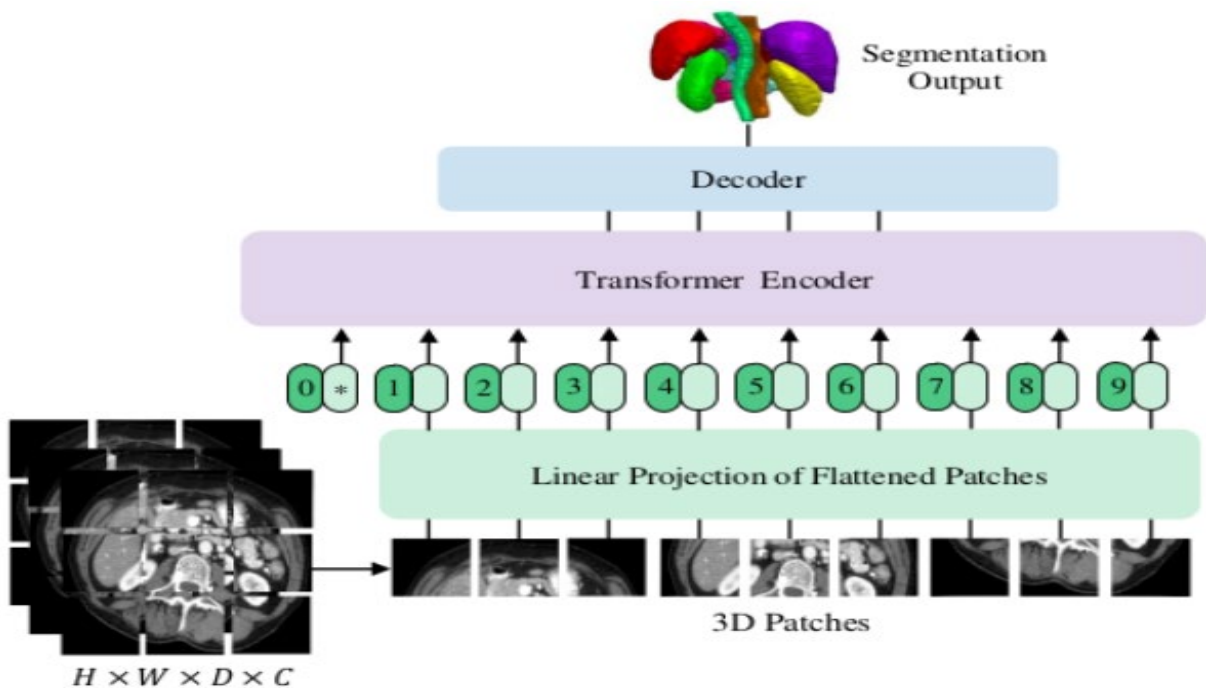


Figure 4. UNETR sample workflow [28]

Finally, the SwinUNETR architecture proposed by Cao et al.[20] is implemented. SwinUNETR is a model that uses Swin Transformer blocks in a U-Net-like architecture. The distinctive feature of the Swin Transformer is the shifted window approach. In this approach, self-attention calculations are first performed in small, non-overlapping windows, which are then shifted to establish connections between windows. This method effectively captures features at different scales while reducing computational complexity. The encoder section

of SwinUNETR consists of successive Swin Transformer blocks, and the number of channels increases while the feature resolution decreases in each block. The decoder section is a structure that gradually amplifies and combines the features coming from the encoder. This architecture is expected to perform highly, especially in abdominal organ segmentation, where extensive contextual information is important. Figure 5 shows the workflow of SwinUNETR.

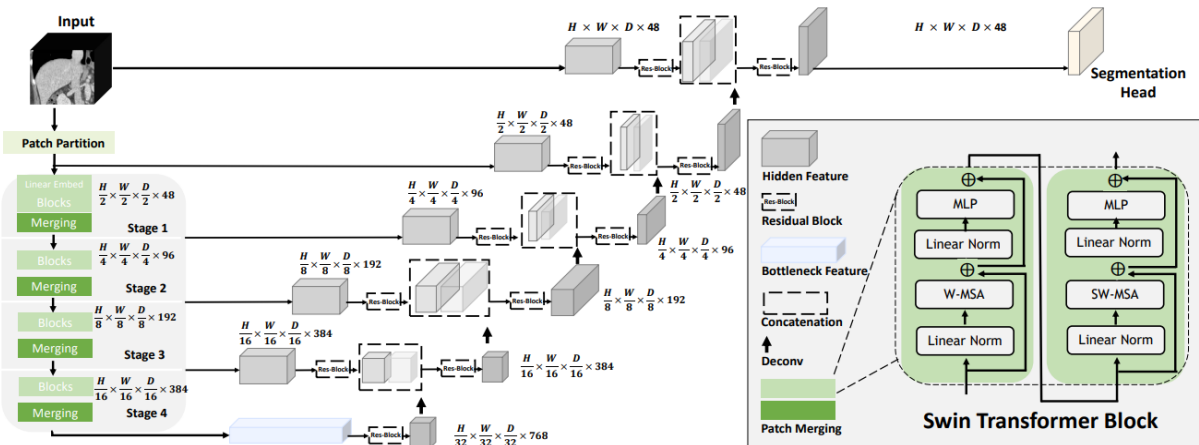


Figure 5. SwinUNETR sample study flow

### 3.3. Evaluated Loss Functions

The study further examined the effect of different loss functions on the model performance. The loss functions used include Dice Loss, Cross-Entropy Loss, Focal Loss, Dice+Cross-Entropy Loss, and Dice+Focal Loss.

Dice Loss was proposed by Milletari et al.[21]. Dice Loss is a loss function used primarily in medical image segmentation. It tries to maximize the overlap ratio between the estimated segmentation mask and the ground truth. Thus, it aims to increase the segmentation accuracy [29]. It is a popular choice, especially for imbalanced datasets, because it prevents the model from ignoring minority classes and can focus on the overlapping regions between the estimated and ground truth masks. The formula of Dice loss (Equation (1)) is;

$$L_{dice} = 1 - \frac{1}{c} \sum_{c=0}^{c-1} \frac{2 \sum_{n=1}^N t_n^c y_n^c}{\sum_{n=1}^N (t_n^c + y_n^c)} \quad (1)$$

Cross-entropy loss[30] is a common loss function that optimizes the correct classification

of each pixel. It measures the difference between two probability distributions for a random variable. It is used in segmentation tasks to measure how well the model's predictions match the target labels[29]. Cross-entropy loss is particularly effective in improving pixel-wise accuracy. The formula for Cross-Entropy loss (Equation (2)) is as follows;

$$L_{CE(y,t)} = - \sum_{n=1}^N \log(t_n \cdot y_n) \quad (2)$$

Focal loss, proposed by Lin et al. [31], is an improved version of the cross-entropy loss function that assigns different weights to easy and complex examples. Complex examples are those that are misclassified with a high probability, while easy examples are those that are correctly classified with a high probability. This helps balance the effect of easy and complex examples on the overall loss [29]. The formula for Focal loss (Equation (3)) is:

$$L_{focal(y,t,\gamma)} = - \sum_{n=1}^N (1 - t_n \cdot y_n)^\gamma \log(t_n \cdot y_n) \quad (3)$$

Here,  $\gamma$  is a non-adjustable positive hyperparameter. A flat cross-entropy loss is

obtained when  $\gamma$  is set to 0 for all samples. Focal loss is especially effective in cases where the imbalance between the background and the organ of interest is high. Dice + Focal loss, Focal+Cross-Entropy loss, and Dice + Cross-Entropy loss combinations were also used in the study. These hybrid loss functions aim to optimize both the overall shape similarity and pixel-based accuracy by combining the advantages of different loss functions. The formulas of these loss functions (Equations (4)-(5)) are as follows;

$$L_{DiceCE} = w_{ce} * L_{CE}(p, \gamma) + w_{dice} * (1 - L_{Dice}(p, \gamma)) \quad (4)$$

$$L_{DiceFocal} = L_{Focal}(p, \gamma) + \lambda * (1 - L_{Dice}(p, \gamma)) \quad (5)$$

The choice of loss functions directly impacts segmentation performance, particularly for imbalanced datasets. Dice Loss is preferred for its ability to mitigate class imbalance by maximizing region overlap, while Cross-Entropy Loss focuses on pixel-wise classification accuracy. Focal Loss enhances this by assigning higher weights to hard-to-classify samples, making it particularly effective for datasets where small anatomical structures are underrepresented. The study also evaluates hybrid loss functions (Dice+CE, Focal+CE, Dice+Focal) to balance spatial consistency and pixel-level accuracy

### 3.4. Applied Image Preprocessing Methods

The study investigated the effect of preprocessing applied to images in the dataset on the performance of trained models.

The intensity rescaling process linearly scales image intensities to a specific range. This process facilitates model training by normalizing the intensity differences between images from different scanners. Images obtained from a CT scanner have intensity values in Hounsfield Units (HU). Scale Intensity Ranged scales image intensity values to a specific range and thus reduces the intensity differences between different images.

The crop foreground process automatically determines the region containing the organ of interest by detecting non-zero voxels in the image and discards unnecessary background information. This increases computational

efficiency and allows the model to focus on the regions of interest.

The reorientation process is a preprocessing step used to align the orientation of the image and label data according to a standard coordinate system. Image orientations may differ in medical imaging due to different imaging devices or protocols. These differences can cause image processing errors and negatively impact the performance of deep learning models. This process standardizes the orientation of image and label data according to the "RAS" (Right-Anterior-Superior) coordinate system.

Spatial Resampling is a preprocessing step used to standardize an image's pixel dimensions (spacing) and label data to a certain value. In medical imaging, pixel dimensions may vary due to different imaging devices or protocols. This method reduces pixel size differences between different images by standardizing the spatial resolution of images.

Random Cropping Based on Positive and Negative Label Sampling is a data augmentation step that randomly cuts 3D patches from image and label data. The method helps alleviate the class imbalance problem by cutting equal numbers of patches from both positive (containing the target anatomical structure) and negative (not containing the target anatomical structure) regions. It was also used in the study to adjust the input dimensions.

Based on the conducted experiments, these methods have demonstrated successful outcomes and were deemed necessary at all stages of training, leading to their implementation throughout the entire process. The methods whose effects on performance are evaluated are as follows;

- Random Axis Flip is a data augmentation step that randomly flips images and labels data along specified axes. The primary purpose of this step is to expand the dataset and make the model more robust against rotational changes. Random 90-degree Rotation is a data augmentation step that randomly rotates the image and labels data by 90, 180, or 270 degrees.
- Random Intensity Shift is a data augmentation technique in which the

intensity of the image is randomly increased or decreased. It helps the model to be robust to different lighting conditions.

- Local Brightness Adjustment is a method that adjusts the brightness in some regions of an image. It is usually used to increase local details or to eliminate unbalanced lighting.
- Gaussian Noise Addition is a technique that adds random pixel changes to the image according to a Gaussian distribution. It increases the model's robustness to noisy data.
- Random Contrast Adjustment is a technique in which the difference between the bright and dark areas of the image is randomly adjusted. It increases the model's robustness to different lighting conditions.
- Gaussian Smoothing is a filter that blurs the image by averaging pixel values with their neighbors. It is used to reduce high-frequency noise.
- Gaussian Sharpening is a technique that highlights the edges and fine details in the image. It highlights essential features by increasing the pixel contrast at the edges.
- Random Cropping by Label Classes focuses on the areas of the image labeled with certain classes and performs random cropping in these parts. It has been tried as an alternative to the Random Cropping by Positive and Negative Labels method.

#### 4. RESULTS AND DISCUSSION

The loss functions and preprocessing methods used in the study were tested on 3D U-Net due to the low computational cost, and the successful results obtained were applied to SwinUNETR and UNETR models.

First, the loss functions were evaluated. In determining the loss functions, eight pieces of  $48 \times 48 \times 48$  images were created from each image for training the model. The Random Cropping Based on Positive and Negative Label Sampling algorithm was used for this. Table 1 shows the performance values obtained from 3D U-Net in different loss functions. When the table is examined, it is seen that the use of loss functions together has a positive effect on the model performance. When the performance values are examined, it is seen that the Cross-Entropy and Dice loss functions generally give the most successful results. The Cross-Entropy +

Dice(Dice+CE) loss function was used in the following steps of the study.

In the continuation of the study, the effect of input size on performance was investigated using the DiceCE loss function. For this purpose, the model was trained with different-sized image patches from each image, including eight images of  $48 \times 48 \times 48$ , eight images of  $96 \times 96 \times 96$ , and four images of  $96 \times 96 \times 96$ . The performance values obtained from the 3D-UNet model for different input sizes are presented in Table 2. When analyzing the obtained values, it is observed that the results are quite close to each other. However, overall, the model trained with four images of  $96 \times 96 \times 96$  achieved the best performance. Experiments conducted with larger input sizes (e.g.,  $128 \times 128 \times 128$ ) resulted in excessive memory consumption, particularly with SwinUNETR. To address this issue, alternative input sizes were explored, and it was determined that  $96 \times 96 \times 96$  provides the optimal balance between contextual information and computational efficiency. Similar strategies have been employed in previous studies. For instance, LoGoNet[32] adopts a patch-based segmentation approach, avoiding large input sizes to reduce computational overhead. These findings are consistent with the observations in this study, demonstrating that smaller patches improve memory efficiency while maintaining segmentation accuracy. Since achieving maximum performance is the priority in this study, all subsequent image preprocessing methods were applied using the most optimal input size of  $96 \times 96 \times 96$ .

In the continuation of the study, the effects of image preprocessing methods on model performance were examined. First, data augmentation methods were applied. For this, random and 90-degree rotation operations were applied to the images on the axes. As a result of the positive effect of this operation on performance, this operation was added to all subsequent preprocesses. The following operations differed in each training, and their effects on performance were examined. Table 3 shows the applied methods and their effects on segmentation studies. The numbers given to the applied preprocesses are as follows;

1. Data Augmentation(to increase training diversity and prevent overfitting)

- Random Flip (to introduce rotational invariance and improve robustness to anatomical variations)
  - 90-degree Rotation (to simulate different scanning orientations and improve generalization)
2. Local Brightness Adjustment (to compensate for scanner-specific intensity variations)
  3. Gaussian Noise Addition (to make the model more robust to imaging noise and artifacts)
  4. Random Contrast Adjustment (to enhance organ boundaries and improve segmentation clarity)
  5. Gaussian Smoothing (to reduce high-frequency noise and improve stability in predictions)
  6. Gaussian Sharpening (to enhance edge clarity and refine organ contours)
  7. Random Cropping by Label Classes (to focus learning on underrepresented structures and balance class distributions)

Table 3 confirms that data augmentation techniques significantly enhance segmentation accuracy by improving generalization. Additionally, Gaussian Sharpening and Random Contrast Adjustment contributed to performance gains by enhancing edge clarity and improving organ boundary delineation. However, Random Cropping by Label Classes produced inconsistent results, suggesting that targeted cropping does not always benefit segmentation performance. According to these findings, the most effective preprocessing methods were selected and applied to SwinUNETR and UNETR. The final preprocessing pipeline consisted of:

- Random Flip (to introduce rotational invariance)
- Random Intensity Shift (to improve robustness against intensity variations)
- Gaussian Sharpening (to enhance boundary clarity)

While preprocessing techniques generally improved segmentation performance, some models showed a slight decline in Dice scores of some classes after applying certain transformations. This effect was more prominent in Transformer-based architectures

such as SwinUNETR and UNETR, which are highly sensitive to intensity and contrast variations. Unlike CNN-based models, which primarily rely on local spatial details, Transformers incorporate long-range dependencies, making them more vulnerable to alterations in intensity distribution caused by preprocessing steps. Additionally, some augmentations, such as Gaussian Sharpening and Contrast Adjustment, may have unintentionally altered the natural organ boundaries, leading to minor segmentation inconsistencies in certain cases. These findings indicate that preprocessing strategies should be carefully tailored for different model architectures to ensure optimal performance.

The results indicate that 3D U-Net achieved the best trade-off between segmentation accuracy and computational efficiency. Although SwinUNETR produced comparable results to 3D U-Net, its training time was significantly longer (7298 sec vs. 3555 sec). Similarly, UNETR required 5564 sec for training but yielded slightly lower Dice scores. These findings suggest that CNN-based models like 3D U-Net are more computationally efficient than Transformer-based architectures (SwinUNETR and UNETR) for this segmentation task.

The comparative training times for each model were as follows:

- SwinUNETR: 7298.58 sec
- UNETR: 5564.40 sec
- 3D U-Net: 3555.69 sec

These results reinforce that while transformer-based models can capture long-range dependencies, they require significantly higher computational resources compared to CNN-based models.

Table 5 compares the segmentation performance of several methods, including 3D U-Net, Swin-UNETR, and UNETR tested in this study, against reference methods reported in the literature for 13 abdominal organs. The metrics are Dice scores, which indicate segmentation accuracy, and the last column presents the average performance across all organs.

The performance variability across organ types suggests that no single architecture universally outperforms others. Instead, combining specialized architectures, loss functions, and preprocessing techniques tailored to specific organs may yield optimal results. The findings reinforce the need to develop more robust methods for handling small organ segmentation, which is critical for applications requiring detailed anatomical analysis. This detailed comparison highlights the strengths and limitations of various deep learning models for 3D abdominal organ segmentation. The results show that CNN-based models such as 3D U-Net are computationally efficient and achieve competitive accuracy, while Transformer-based models such as UNETR are superior in capturing complex anatomical structures. However, the critical difference between the dice values of the UNETR model trained and tested on the same dataset by different researchers shows that the model has some problems with stabilization.

Also, the proposed 3D U-Net model demonstrates superior performance in pancreas segmentation, achieving a Dice score of 0.823, the highest reported value among all compared methods. This result highlights the effectiveness of the applied preprocessing techniques and model architecture in handling small and low-contrast structures. Given that pancreas segmentation remains a challenging task due to its anatomical variability and low contrast with surrounding tissues, this improvement is particularly significant.

In conclusion, the presented comparison table shows that all methods exhibit difficulties in segmentation of small organs and underlines the need for future research focusing on region-specific improvements and advanced magnification techniques.

Figure 6 presents sample segmentation results from the trained models. A detailed qualitative analysis was performed to evaluate segmentation accuracy, organ boundary preservation, and common misclassification patterns.

3D U-Net and SwinUNETR produced visually similar segmentation results, while UNETR showed slightly lower segmentation accuracy, particularly for small anatomical structures. All models generated false-positive organ segmentations in regions where no ground truth annotations exist. This issue was more pronounced in UNETR, suggesting that transformer-based architectures may introduce excessive spatial dependencies, leading to misclassifications in low-contrast areas.

3D U-Net exhibited the most stable segmentation boundaries across different organs, whereas SwinUNETR tended to capture more detailed structures at the cost of minor over-segmentation artifacts. Small organs such as the adrenal glands and gallbladder remained the most difficult to segment accurately across all models. The reduced contrast in these structures, along with their small size, likely contributed to the under-segmentation observed in multiple cases.

**Table 1.** The Effect of Loss Functions on Model Performance (a:IoU, b: Recall, c:Precision, d: Dice)

Loss Functions	Parameters	Background	Spleen	Right Kidney	Left Kidney	Gallbladder	Esophagus	Liver	Stomach	Aorta	Inferior Vena Cava	Portal Vein and Splenic Vein	Pancreas	Right Adrenal Gland	Left Adrenal Gland	Average
Cross Entropy Loss	d	0.9964	0.9018	0.918	0.9029	0.5597	0.6582	0.9588	0.8267	0.8779	0.7961	0.6769	0.7789	0.4731	0.5093	0.7739
	c	0.995	0.8771	0.9625	0.9222	0.7424	0.8081	0.9685	<b>0.9157</b>	0.9107	0.8827	0.7693	0.8277	<b>0.7472</b>	0.6825	0.858
	b	0.9978	0.9345	0.8785	0.8873	0.4677	0.5981	0.9495	0.7653	0.8501	0.7284	0.6133	0.7387	0.3736	0.4247	0.7291
	a	0.9928	0.8244	0.849	0.8259	0.358	0.497	0.9209	0.7099	0.7827	0.6625	0.5145	0.6382	0.3151	0.348	0.6599
Focal Loss	d	0.9963	0.9225	0.9272	0.9276	0.5991	0.5814	0.9467	0.8304	0.863	0.7898	0.6187	0.6935	0.4422	0.4208	0.7542
	c	0.9957	0.9041	0.9572	0.9581	0.595	0.8531	0.9281	0.8726	0.9307	0.8371	0.833	<b>0.9215</b>	0.702	<b>0.7663</b>	<b>0.861</b>
	b	0.9969	0.9455	0.8993	0.8992	0.5402	0.4602	<b>0.9666</b>	0.8009	0.8101	0.7565	0.5076	0.5596	0.3665	0.3117	0.7015
	a	0.9926	0.8579	0.8643	0.8653	0.4001	0.4161	0.8991	0.7165	0.7599	0.6545	0.4548	0.5339	0.2984	0.2718	0.6418
Dice Loss	d	0.9964	0.937	0.927	0.9183	0.5378	0.6603	0.9566	0.8234	0.8686	0.7959	0.6041	0.7453	0.4716	0.505	0.7677
	c	0.9952	0.9287	0.942	0.959	0.5723	0.7832	0.955	0.9099	0.9359	0.8609	0.8075	0.7945	0.6954	0.5807	0.8371
	b	0.9977	<b>0.9476</b>	0.9135	0.8812	0.5245	<b>0.6085</b>	0.9584	0.7689	0.8138	0.7457	0.4896	0.7079	0.3897	0.4838	0.7308
	a	0.9929	0.8824	0.8642	0.8492	0.3295	0.4945	0.9169	0.7086	0.7683	0.6618	0.4366	0.5965	0.3142	0.3439	0.6542
Focal+Cross Entropy Loss	d	0.9929	0.6477	0.7494	0.7673	0.4939	0.5735	0.8859	0.781	0.7926	0.5868	0.3156	0.6624	0.5145	0.4933	0.6612
	c	0.9901	0.5431	<b>0.9908</b>	<b>0.9875</b>	0.4435	0.7809	0.9678	0.8732	<b>0.9389</b>	<b>0.9131</b>	<b>0.8389</b>	0.8124	0.6252	0.5405	0.8033
	b	0.9957	0.8583	0.6095	0.6324	0.5022	0.4843	0.8253	0.7208	0.6983	0.4431	0.2066	0.5932	0.4763	0.4898	0.6097
	a	0.9859	0.4951	0.6058	0.6265	0.3067	0.4107	0.8026	0.646	0.6599	0.4225	0.1977	0.4991	0.3503	0.3395	0.5249
Dice + Cross Entropy Loss	d	<b>0.997</b>	<b>0.9386</b>	<b>0.9357</b>	<b>0.9331</b>	<b>0.6518</b>	<b>0.6768</b>	<b>0.9617</b>	<b>0.8592</b>	0.8855	0.8042	0.6342	<b>0.7931</b>	0.6406	0.5347	<b>0.8033</b>
	c	<b>0.9965</b>	<b>0.9481</b>	0.9386	0.939	0.5291	0.8206	0.9608	0.8687	0.9345	0.8958	0.8079	0.8302	0.657	0.7319	0.847
	b	0.9975	0.9307	<b>0.9333</b>	0.9273	<b>0.7343</b>	0.6042	0.9628	<b>0.8536</b>	0.8462	0.7336	0.5352	<b>0.7643</b>	<b>0.6352</b>	0.4348	<b>0.7781</b>
	a	<b>0.994</b>	<b>0.8851</b>	<b>0.8793</b>	<b>0.875</b>	<b>0.4265</b>	<b>0.5133</b>	<b>0.9263</b>	<b>0.759</b>	0.7956	0.6737	0.4721	<b>0.658</b>	0.4727	0.3714	<b>0.693</b>
Dice +Focal Loss	d	0.9966	0.903	0.8746	0.8921	0.5182	0.6599	0.9539	0.8022	<b>0.8973</b>	<b>0.8488</b>	<b>0.7221</b>	0.7824	<b>0.6642</b>	<b>0.6143</b>	0.795
	c	0.9951	0.9068	0.9379	0.8561	<b>0.7717</b>	<b>0.8963</b>	<b>0.9709</b>	0.9112	0.933	0.8682	0.7468	0.817	0.7331	0.7099	<b>0.861</b>
	b	<b>0.9981</b>	0.9037	0.833	<b>0.9401</b>	0.4236	0.5275	0.9382	0.7494	<b>0.8661</b>	<b>0.834</b>	<b>0.7032</b>	0.7568	0.6169	<b>0.5493</b>	0.76
	a	0.9933	0.8256	0.7886	0.8098	0.3389	0.4978	0.9122	0.6919	<b>0.8149</b>	<b>0.7381</b>	<b>0.5662</b>	0.6443	<b>0.4979</b>	<b>0.4552</b>	0.6839

**Table 2.** The Effect of Input Size on Model Performance (a:IoU, b: Recall, c:Precision, d: Dice)

Input Size	Parameter	Background	Spleen	Right Kidney	Left Kidney	Gallbladder	Esophagus	Liver	Stomach	Aorta	Inferior Vena Cava	Portal Vein and Splenic Vein	Pancreas	Right Adrenal Gland	Left Adrenal Gland	Average
48x48x48x8	d	<b>0.997</b>	0.9386	0.9357	0.9331	0.6518	0.6767	0.9617	<b>0.8592</b>	0.8855	0.8042	0.6342	0.7931	0.6406	0.5347	0.8033
	c	<b>0.9965</b>	0.9481	0.9386	<b>0.939</b>	0.5291	0.8205	0.9608	0.8687	<b>0.9345</b>	<b>0.8958</b>	<b>0.8079</b>	0.8302	0.657	0.7319	0.847
	b	0.9975	0.9307	0.9333	0.9273	<b>0.7344</b>	<b>0.6042</b>	0.9628	<b>0.8536</b>	0.8462	0.7336	0.5352	<b>0.7643</b>	<b>0.6352</b>	0.4348	0.7781
	a	<b>0.994</b>	0.8851	0.8793	0.875	0.4266	0.5133	0.9263	<b>0.759</b>	0.7956	0.6737	0.4721	0.658	0.4727	0.3714	0.693
96x96x96x8	d	0.9964	0.9195	0.9301	0.929	0.6866	0.672	0.9586	0.8003	0.8864	0.8113	0.6901	0.7644	0.5824	0.5664	0.7995
	c	0.9951	0.9212	<b>0.9402</b>	0.9305	0.5609	0.8133	<b>0.9691</b>	0.8883	0.9148	0.8337	0.7266	0.825	<b>0.7683</b>	0.6444	0.838
	b	0.9977	0.9221	0.9212	0.9279	0.7131	0.5797	0.9486	0.7604	0.8616	0.7999	0.6649	0.7204	0.4731	0.5277	0.7727
	a	0.9928	0.8527	0.8695	0.8677	0.4635	0.5069	0.9206	0.6828	0.7967	0.6844	0.5276	0.6204	0.4125	0.4028	0.6858
96x96x96x4	d	0.9968	<b>0.9483</b>	<b>0.9389</b>	<b>0.9367</b>	<b>0.7448</b>	<b>0.7035</b>	<b>0.9648</b>	0.8189	<b>0.9048</b>	<b>0.8406</b>	<b>0.7201</b>	<b>0.7963</b>	<b>0.664</b>	<b>0.6392</b>	<b>0.8298</b>
	c	0.9956	<b>0.9635</b>	0.9337	0.9329	<b>0.7352</b>	<b>0.8765</b>	0.9662	<b>0.9297</b>	0.9189	0.8733	0.771	<b>0.8561</b>	0.7304	<b>0.7755</b>	<b>0.8756</b>
	b	<b>0.9981</b>	<b>0.934</b>	<b>0.9452</b>	<b>0.9408</b>	0.6695	0.5969	<b>0.9636</b>	0.7588	<b>0.8927</b>	<b>0.8149</b>	<b>0.6795</b>	0.7512	0.6115	<b>0.5517</b>	<b>0.7934</b>
	a	0.9936	<b>0.9018</b>	<b>0.8851</b>	<b>0.8813</b>	<b>0.5078</b>	<b>0.5449</b>	<b>0.9321</b>	0.711	<b>0.8264</b>	<b>0.726</b>	<b>0.5645</b>	<b>0.6632</b>	<b>0.4976</b>	<b>0.4749</b>	<b>0.7222</b>

**Table 3.** The Effect of Image Preprocessing on Model Performance

Preprocess	Background	Spleen	Right Kidney	Left Kidney	Gallbladder	Esophagus	Liver	Stomach	Aorta	Inferior Vena Cava	Portal Vein and Splenic Vein	Pancreas	Right Adrenal Gland	Left Adrenal Gland	Average
Unprocessed	0.9968	0.9483	<b>0.9389</b>	0.9367	0.7448	0.7035	<b>0.9648</b>	0.8189	<b>0.9048</b>	0.8406	0.7201	0.7963	0.664	0.6392	0.8298
1	<b>0.9969</b>	0.9538	0.9355	0.937	<b>0.7731</b>	0.7528	0.964	<b>0.8423</b>	0.9036	<b>0.8584</b>	0.719	0.7769	0.6674	0.6304	<b>0.8365</b>
1_7	0.9966	<b>0.954</b>	0.9328	0.936	0.7478	<b>0.7539</b>	0.9613	0.8193	0.8945	0.8153	0.6988	0.7443	0.6495	0.6124	0.8226
1_3	0.9967	0.9312	0.9222	0.9289	0.7228	0.7435	0.957	0.8298	0.9008	0.8397	0.6678	0.7709	<b>0.6773</b>	<b>0.6741</b>	0.8259
1_2	0.9967	0.947	0.9361	0.9347	0.7118	0.74	0.9602	0.8138	0.8876	0.8529	0.7183	0.7928	0.6655	0.6155	0.8266
1_4	0.9969	0.9521	0.9384	0.9349	0.7402	0.7436	0.9622	0.8372	0.8904	0.8542	0.7119	0.8056	0.6491	0.6276	0.8317
1_5	0.9966	0.903	0.8746	0.8921	0.5182	0.6599	0.9539	0.8022	0.8973	0.8488	0.7221	0.7824	0.6642	0.6143	0.795
1_4_5	0.9967	0.9492	0.9343	<b>0.9374</b>	0.6315	0.7318	0.9581	0.8024	0.9006	0.8434	<b>0.7254</b>	<b>0.816</b>	0.6451	0.5896	0.8187
1_6	0.9968	0.9483	<b>0.9389</b>	0.9367	0.7448	0.7035	<b>0.9648</b>	0.8189	<b>0.9048</b>	0.8406	0.7201	0.7963	0.664	0.6392	0.8298
1_4_6	<b>0.9969</b>	0.9538	0.9355	0.937	<b>0.7731</b>	0.7528	0.964	<b>0.8423</b>	0.9036	<b>0.8584</b>	0.719	0.7769	0.6674	0.6304	<b>0.8365</b>

**Table 4.** Comparison of Model Dice Performance

Model	Preprocess	Background	Spleen	Right Kidney	Left Kidney	Gallbladder	Esophagus	Liver	Stomach	Aorta	Inferior Vena Cava	Portal Vein and Splenic Vein	Pancreas	Right Adrenal Gland	Left Adrenal Gland	Average
3D U-Net	Unprocessed	0.9968	0.9483	0.9389	0.9367	<b>0.7448</b>	0.7035	0.9648	0.8189	<b>0.9048</b>	0.8406	0.7201	0.7963	0.664	0.6392	0.8298
	Pre-Processed	<b>0.997</b>	<b>0.9595</b>	<b>0.9434</b>	<b>0.9422</b>	0.7225	<b>0.7419</b>	<b>0.9664</b>	0.7942	0.894	0.8456	<b>0.7604</b>	<b>0.8232</b>	<b>0.7126</b>	<b>0.6522</b>	<b>0.8397</b>
SwinUNETR	Unprocessed	0.9968	0.9447	0.9396	0.9373	0.6359	0.7043	0.9632	0.8009	0.8919	0.8462	0.7325	0.7958	0.6401	0.591	0.8157
	Pre-Processed	0.9969	0.9508	0.9379	0.9356	0.6812	0.7154	0.9657	<b>0.8247</b>	0.8872	<b>0.8493</b>	0.7306	0.8182	0.6891	0.6305	0.8295
UNETR	Unprocessed	0.9966	0.903	0.8746	0.8921	0.5182	0.6599	0.9539	0.8022	0.8973	0.8488	0.7221	0.7824	0.6642	0.6143	0.791
	Pre-Processed	0.9961	0.8326	0.9279	0.9161	0.6653	0.7332	0.9487	0.7942	0.8655	0.8147	0.6932	0.7489	0.6668	0.6057	0.8006

**Table 5.** Quantitative comparisons of the performance of segmentation studies with basic models on the BTCV dataset in the literature

Methods	Referans	Spleen	Right Kidney	Left Kidney	Gallbladder	Esophagus	Liver	Stomach	Aorta	Inferior Vena Cava	Portal Vein and Splenic Vein	Pancreas	Right Adrenal Gland	Left Adrenal Gland	Average
SETR+PUP	[33]	0,929	0,893	0,892	0,649	0,764	0,954	0,822	0,869	0,742	0,715	0,714	0,618	0,797	
nnUNet	[18]	0,942	0,894	0,910	0,704	0,723	0,948	0,824	0,877	0,782	0,720	0,680	0,616	0,802	
ASPP	[34]	0,935	0,892	0,914	0,689	0,760	0,953	0,812	0,918	0,807	0,695	0,720	0,629	0,811	
TransUNet	[23]	0,952	0,927	0,929	0,662	0,757	0,969	0,889	<b>0,920</b>	0,833	<b>0,791</b>	0,775	0,637	0,838	
UNETR	[19]	<b>0,968</b>	0,924	0,941	0,750	0,766	<b>0,971</b>	<b>0,913</b>	0,890	0,847	0,788	0,767	0,741	<b>0,856</b>	
UNETR	[32]	0,912	0,940	0,938	0,693	0,690	0,954	0,754	0,891	0,830	0,703	0,734	0,660	0,577	0,790
SwinUNETR	[32]	0,952	<b>0,947</b>	<b>0,945</b>	0,790	<b>0,770</b>	0,963	0,755	0,901	<b>0,850</b>	0,771	0,760	0,702	0,659	0,828
nnUNet	[32]	0,859	0,944	0,924	<b>0,796</b>	0,755	0,960	0,781	0,894	0,849	0,756	0,776	0,675	0,663	0,818
3D-Unet	Ours	0,960	0,943	0,942	0,723	0,742	0,966	0,794	0,894	0,846	0,760	<b>0,823</b>	0,713	0,652	0,840
SwinUNETR	Ours	0,951	0,938	0,936	0,681	0,715	0,966	0,825	0,887	0,849	0,731	0,818	0,689	0,631	0,830
UNETR	Ours	0,833	0,928	0,916	0,665	0,733	0,949	0,794	0,866	0,815	0,693	0,749	0,667	0,606	0,801

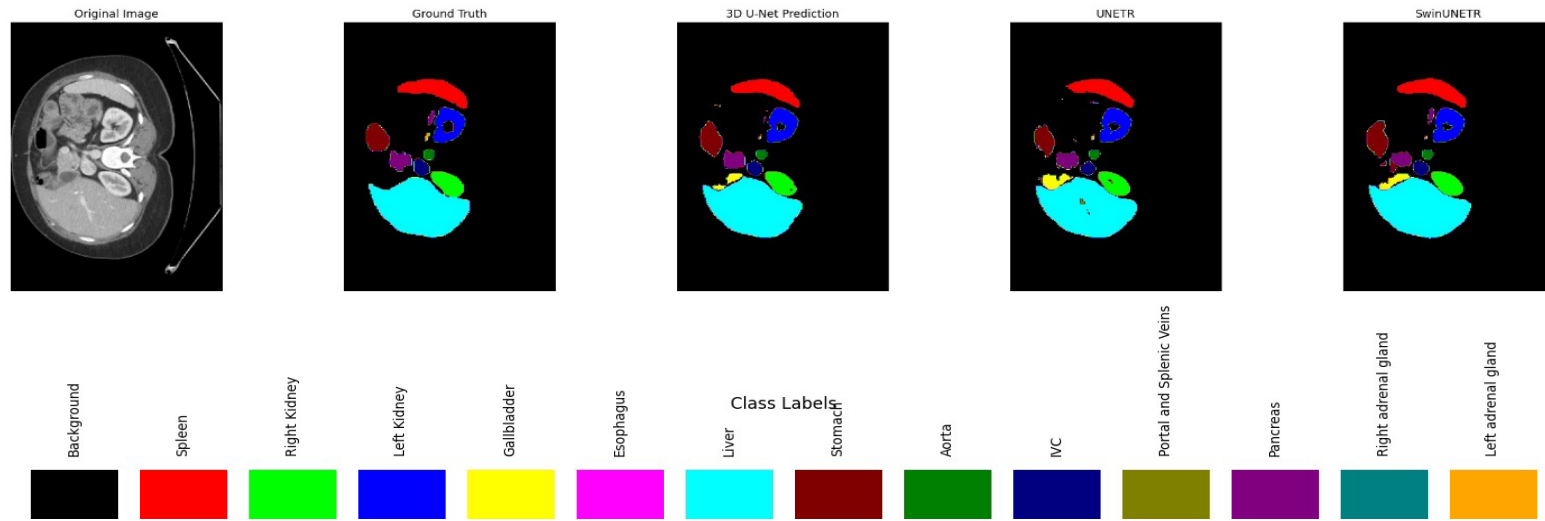


Figure 6. Segmentation results of the model

## 5. CONCLUSION AND FUTURE WORKS

Advancements in 3D medical imaging technology have significantly improved diagnosis, treatment planning, and patient monitoring. However, these advancements also introduce challenges in processing and analyzing large-scale medical data. Artificial intelligence, particularly deep learning-based approaches, has emerged as a transformative tool in medical imaging, demonstrating the ability to automate and enhance segmentation tasks, thereby reducing manual effort and improving diagnostic precision.

This study evaluated three deep learning architectures—CNN-based 3D U-Net, hybrid SwinUNETR, and Transformer-based UNETR—using the BTCV dataset for the segmentation of 13 different abdominal organs. Additionally, the impact of various preprocessing techniques and loss functions on model performance was analyzed. The findings highlight the importance of model architecture selection, preprocessing strategies, and loss function optimization in achieving high segmentation accuracy.

Among the models tested, 3D U-Net outperformed SwinUNETR and UNETR in both segmentation accuracy and efficiency. The highest Dice score was achieved with the  $96 \times 96 \times 96$  input size, balancing spatial context and memory constraints effectively. This result aligns with previous literature, reinforcing that moderate patch sizes maintain both computational feasibility and sufficient anatomical context. Preprocessing techniques such as Random Flip, Intensity Shift, and Gaussian Sharpening improved segmentation performance, enhancing robustness to variations in image acquisition. Despite these optimizations, the segmentation of small, mobile organs such as the adrenal glands and gallbladder remained a challenge, primarily due to their low contrast, anatomical variability, and limited training samples.

This study makes a significant contribution to the field of 3D medical image segmentation by systematically evaluating different architectures and preprocessing techniques, offering insights into their comparative advantages. This research provides a thorough evaluation of multiple architectures, preprocessing techniques, and input size optimization,

offering a detailed analysis of their combined effects on segmentation performance. By systematically assessing these factors, this study highlights key elements that contribute to improved segmentation accuracy and computational efficiency. Additionally, it bridges the gap between CNN-based and Transformer-based models, highlighting their respective strengths and limitations.

Although this study achieved promising results, several areas require further investigation. Small organ segmentation continues to be difficult due to factors such as low contrast, shape variability, and data imbalance. Future research should explore specialized refinement techniques tailored to small organs, such as region-aware loss functions or attention mechanisms, to improve segmentation accuracy. Additionally, incorporating multi-scale feature extraction approaches could provide finer detail representation, enhancing performance across different organ sizes.

Further research could explore several enhancements to mitigate false positives and improve the segmentation of small organs. Developing specialized segmentation refinements for challenging organs, such as the adrenal glands and gallbladder, may enhance model precision in these regions. Implementing anatomical and structural constraints in the segmentation process could improve the delineation of organ boundaries and reduce false positives. Additionally, region-aware data augmentation techniques could enhance model robustness for small anatomical structures by simulating realistic variations in medical imaging. Exploring more effective training paradigms, such as curriculum learning or self-supervised learning, could improve segmentation performance, particularly in underrepresented organ classes.

Expanding the dataset with more diverse imaging modalities, including MRI and PET scans, could improve model generalizability across different clinical applications. Integrating domain adaptation techniques or contrastive learning methods may further improve segmentation performance in cross-domain applications. The development of self-supervised learning frameworks could reduce reliance on extensive annotated datasets while maintaining model robustness.

By addressing these challenges, future advancements in deep learning-based 3D segmentation will help bridge the gap between automated medical image analysis and real-world clinical implementation. This study contributes to the growing body of literature by demonstrating the effectiveness of deep learning models in multi-organ segmentation while outlining key areas for further development, ultimately supporting improved patient outcomes and assisting medical professionals in their decision-making processes.

### ACKNOWLEDGES

This research was supported by the TÜBİTAK 2211-A and Afyon Kocatepe University BAP-24.FEN.BİL.02. Additionally, this article is derived from the PhD thesis titled 'Segmentation of Three-Dimensional Abdominal CT Images with Deep Learning Methods'.

### REFERENCES

- Rueckert D. and Schnabel J. A., "Model-Based and Data-Driven Strategies in Medical Image Computing," *Proceedings of the IEEE*, Vol. 108, Issue 1, Pages 110–124, 2020.
- Wachinger C., Reuter M. and Klein T., "DeepNAT: Deep convolutional neural network for segmenting neuroanatomy," *NeuroImage*, Vol. 170, Pages 434–445, 2018.
- Litjens G., Kooi T., Bejnordi B. E., Setio A. A. A., Ciompi F., Ghafoorian M., van der Laak J. A. W. M., van Ginneken B. and Sánchez C. I., "A survey on deep learning in medical image analysis," *Medical Image Analysis*, Vol. 42, Pages 60–88, 2017.
- Lecun Y., Bengio Y. and Hinton G., "Deep learning," *Nature*, Vol. 521, Issue 7553, Pages 436–444, 2015.
- Shen D., Wu G. and Suk H. II, "Deep Learning in Medical Image Analysis," *Annual Review of Biomedical Engineering*, Vol. 19, Issue Volume 19, 2017, Pages 221–248, 2017.
- Greenspan H., Van Ginneken B. and Summers R. M., "Guest Editorial Deep Learning in Medical Imaging: Overview and Future Promise of an Exciting New Technique," *IEEE Transactions on Medical Imaging*, Vol. 35, Issue 5, Pages 1153–1159, 2016.
- Tajbakhsh N., Jeyaseelan L., Li Q., Chiang J. N., Wu Z. and Ding X., "Embracing imperfect datasets: A review of deep learning solutions for medical image segmentation," *Medical Image Analysis*, Vol. 63, Page 101693, 2020.
- Taha A. A. and Hanbury A., "Metrics for evaluating 3D medical image segmentation: Analysis, selection, and tool," *BMC Medical Imaging*, Vol. 15, Issue 1, Pages 1–28, 2015.
- Asgari Taghanaki S., Abhishek K., Cohen J. P., Cohen-Adad J. and Hamarneh G., "Deep semantic segmentation of natural and medical images: a review," *Artificial Intelligence Review*, Vol. 54, Issue 1, Pages 137–178, 2021.
- Pham D. L., Xu C. and Prince J. L., "Current methods in medical image segmentation," *Annual Review of Biomedical Engineering*, Vol. 2, Issue 2000, Pages 315–337, 2000.
- Sharma N., Ray A. K., Shukla K. K., Sharma S., Pradhan S., Srivastva A. and Aggarwal L., "Automated medical image segmentation techniques," *Journal of Medical Physics*, Vol. 35, Issue 1, Pages 3–14, 2010.
- Norouzi A., Rahim M. S. M., Altameem A., Saba T., Rad A. E., Rehman A. and Uddin M., "Medical Image Segmentation Methods, Algorithms, and Applications," *IETE Technical Review*, Vol. 31, Issue 3, Pages 199–213, 2014.
- Ronneberger O., Fischer P. and Brox T., "U-Net: Convolutional Networks for Biomedical Image Segmentation," *Lecture Notes in Computer Science (including subseries Lecture Notes in Artificial Intelligence and Lecture Notes in Bioinformatics)*, Vol. 9351, Pages 234–241, 2015.
- Roth H. R., Shen C., Oda H., Sugino T., Oda M., Hayashi Y., Misawa K. and Mori K., "A Multi-scale Pyramid of 3D Fully Convolutional Networks for Abdominal Multi-organ Segmentation," *Lecture Notes in Computer Science (including subseries Lecture Notes in Artificial Intelligence and Lecture Notes in Bioinformatics)*, Vol. 11073 LNCS, Pages 417–425, 2018.
- Hesamian M. H., Jia W., He X. and Kennedy P., "Deep Learning Techniques for Medical Image Segmentation: Achievements and Challenges," *Journal of Digital Imaging*, Vol. 32, Issue 4, Pages 582–596, 2019.

16. Çiçek Ö., Abdulkadir A., Lienkamp S. S., Brox T. and Ronneberger O., “3D U-net: Learning dense volumetric segmentation from sparse annotation,” *Lecture Notes in Computer Science (including subseries Lecture Notes in Artificial Intelligence and Lecture Notes in Bioinformatics)*, Vol. 9901 LNCS, Pages 424–432, 2016.
17. Chen S., Roth H., Dorn S., May M., Cavallaro A., Lell M. M., Kachelrieß M., Oda H., Mori K. and Maier A., “Towards Automatic Abdominal Multi-Organ Segmentation in Dual Energy CT using Cascaded 3D Fully Convolutional Network,” 2017.
18. Isensee F., Jaeger P. F., Kohl S. A. A., Petersen J. and Maier-Hein K. H., “nnU-Net: a self-configuring method for deep learning-based biomedical image segmentation,” *Nature Methods*, Vol. 18, Issue 2, Pages 203–211, 2021.
19. Hatamizadeh A., Tang Y., Nath V., Yang D., Myronenko A., Landman B., Roth H. R. and Xu D., “UNETR: Transformers for 3D Medical Image Segmentation,” in *Proceedings of the IEEE/CVF Winter Conference on Applications of Computer Vision (WACV)*, 2022, Pages 574–584.
20. Cao H., Wang Y., Chen J., Jiang D., Zhang X., Tian Q. and Wang M., “Swin-Unet: Unet-Like Pure Transformer for Medical Image Segmentation,” in *European Conference on Computer Vision*, 2023, Vol. 13803 LNCS, Pages 205–218.
21. Milletari F., Navab N. and Ahmadi S. A., “V-Net: Fully convolutional neural networks for volumetric medical image segmentation,” *Proceedings - 2016 4th International Conference on 3D Vision, 3DV 2016*, Pages 565–571, 2016.
22. Litjens G., Toth R., van de Ven W., Hoeks C., Kerkstra S., van Ginneken B., Vincent G., Guillard G., Birbeck N., Zhang J., Strand R., Malmberg F., Ou Y., Davatzikos C., Kirschner M., Jung F., Yuan J., Qiu W., Gao Q. et al., “Evaluation of prostate segmentation algorithms for MRI: The PROMISE12 challenge,” *Medical Image Analysis*, Vol. 18, Issue 2, Pages 359–373, 2014.
23. Chen J., Lu Y., Yu Q., Luo X., Adeli E., Wang Y., Lu L., Yuille A. L. and Zhou Y., “TransUNet: Transformers Make Strong Encoders for Medical Image Segmentation,” 2021.
24. Ma J., Li F. and Wang B., “U-Mamba: Enhancing Long-range Dependency for Biomedical Image Segmentation,” 2024.
25. Xing Z., Ye T., Yang Y., Liu G. and Zhu L., “SegMamba: Long-range Sequential Modeling Mamba For 3D Medical Image Segmentation,” 2024.
26. Zhao MIT A., Balakrishnan MIT G., Durand MIT F., Guttag MIT J. V and Dalca MIT A. V, “Data Augmentation Using Learned Transformations for One-Shot Medical Image Segmentation,” in *Proceedings of the IEEE/CVF Conference on Computer Vision and Pattern Recognition (CVPR)*, 2019, Pages 8543–8553.
27. Landman B., Xu Z., Igelsias J., Styner M., Langerak T. and Klein A., “MICCAI multi-atlas labeling beyond the cranial vault-workshop and challenge,” 2015.
28. “MONAI - Home,” Available: <https://monai.io/index.html> [Accessed: 20 September 2024]
29. Azad R., Heidary M., Yilmaz K., Hüttemann M., Karimijafarbigloo S., Wu Y., Schmeink A. and Merhof D., “Loss Functions in the Era of Semantic Segmentation: A Survey and Outlook,” 2023.
30. Kline D. M. and Berardi V. L., “Revisiting squared-error and cross-entropy functions for training neural network classifiers,” *Neural Computing and Applications*, Vol. 14, Issue 4, Pages 310–318, 2005.
31. Lin T.-Y., Goyal P., Girshick R., He K. and Dollar P., “Focal Loss for Dense Object Detection,” in *Proceedings of the IEEE International Conference on Computer Vision (ICCV)*, 2017, Pages 2980–2988.
32. Karimi Monsefi A., Karisani P., Zhou M., Choi S., Doble N., Ji H., Parthasarathy S. and Ramnath R., “Masked LoGoNet: Fast and Accurate 3D Image Analysis for Medical Domain,” *Proceedings of the ACM SIGKDD International Conference on Knowledge Discovery and Data Mining*, Pages 1348–1359, 2024.
33. Zheng S., Lu J., Zhao H., Zhu X., Luo Z., Wang Y., Fu Y., Feng J., Xiang T., Torr P. H. S. and Zhang L., “Rethinking semantic segmentation from a sequence-to-sequence perspective with transformers,” in *Proceedings of the IEEE/CVF Conference on Computer Vision and Pattern Recognition*, 2021, Pages 6881–6890.
34. Chen L.-C., Zhu Y., Papandreou G., Schroff F. and Adam H., “Encoder-Decoder with Atrous Separable Convolution for Semantic Image Segmentation,” *arxiv*, 2018.



ULUSLARARASI 3B YAZICI TEKNOLOJİLERİ  
VE DİJİTAL ENDÜSTRİ DERGİSİ

INTERNATIONAL JOURNAL OF 3D PRINTING  
TECHNOLOGIES AND DIGITAL INDUSTRY

ISSN:2602-3350 (Online)

URL: <https://dergipark.org.tr/ij3dptdi>

# BIBLIOMETRIC OF BLOCKCHAIN PUBLICATIONS IN SCIENCE CITATION INDEX EXPANDED FROM 1991 TO 2022

**Yazarlar (Authors):** Yuh-Shan Ho , Samia Aitouche 

**Bu makaleye şu şekilde atıfta bulunabilirsiniz (To cite to this article):** Ho Y. S., Aitouche S., "Bibliometric of Blockchain Publications in Science Citation Index Expanded From 1991 to 2022" *Int. J. of 3D Printing Tech. Dig. Ind.*, 9(1): 92-113, (2025).

DOI: 10.46519/ij3dptdi.1494541

Araştırma Makale/ Research Article

Erişim Linki: (To link to this article): <https://dergipark.org.tr/en/pub/ij3dptdi/archive>

# BIBLIOMETRIC OF BLOCKCHAIN PUBLICATIONS IN SCIENCE CITATION INDEX EXPANDED FROM 1991 TO 2022

Yuh-Shan Ho<sup>a</sup> , Samia Aitouche<sup>b\*</sup> 

<sup>a</sup>CT HO Trend, 3F.-7, No. 1, Fuxing N. Rd., Songshan Dist., Taipei City 105611, TAIWAN

E-mail: dr\_ysho@hotmail.com

<sup>b</sup>Batna 2 University, Technology Faculty, Industrial Engineering Department, ALGERIA

\* Corresponding Author: [s.aitouche@univ-batna2.dz](mailto:s.aitouche@univ-batna2.dz)

(Received: 02.06.24; Revised: 12.03.25; Accepted: 23.03.25)

---

## ABSTRACT

The aim of the paper is to perform a bibliometric study on blockchain which is an emerging technology presenting several advantages reinforcing security, privacy and immutability on a Peer-To-Peer network, inhibiting a central authority like a server. The studied articles are collected from the Clarivate Analytics Web of Science Core Collection database (data updated on 29 June 2023). A total of 11,190 blockchain documents were searched out in the SCI-EXPANDED from 1991 to 2022. The articles are analysed using characteristics of document types. The most used type is articles and reviews, relevant review articles, average numbers of citations per publication by year. The most cited publications are those published in 1991. The most cited Web of Science categories are “information systems computer science” and “electrical and electronic engineering”. The top most productive journals are IEEE journals and the top productive countries are China, USA and India. The top productive institutions are Beijing University of Posts and Telecommunications, Chinese Academy of Sciences, Xidian University. The top ten most frequently cited blockchain articles and the twenty most frequently used author keywords are exhibited to deduce trends of research in blockchain field. The contribution to the literature is reinforced by the given summary about the blockchain technology since 1991 and its developments, its actual shape and its trends toward the future.

**Keywords:** Blockchain, Bibliometrics, Blockchain articles, Bibliometric indicators, Blockchain trends.

---

## 1. INTRODUCTION

Blockchain is a peer-to-peer model that can speed up processes resulting in robust tracking and reducing costs of transactions. It is essential for business professionals to understand the significance of the implications of this far-reaching technology on business activities [1]. The transactions could be financial via cryptocurrency or another content like information. Blockchain technology permits to distribute, encrypt, and secure the records of digital transactions [2]. The blockchain is used in micro-credential to assess the student's knowledge, skill, especially in the pandemic era [3].

It is used in accountability to speak today about decentralized accountability and an immutable audit. The blockchain reinforces the medical traceability of patients and the perishability of

pharmacy products and agri-food. It is very efficient in e-voting and its credibility.

The addition of blocks of transactions to the chain is done by the miners which are nodes of blockchain network in competition to create and validate the block using an algorithm of hashage called consensus protocol. There are several consensus more or less energy consuming, due to the used hardware and algorithm.

A transaction is initiated when one agent sends a cryptocurrency or a digital certificates to another agent. The transaction is controlled by the nodes on the network using a consensus mechanism like “proof Of Work”, solving a complex mathematical problem to validate the new block representing the transaction (Figure 1).

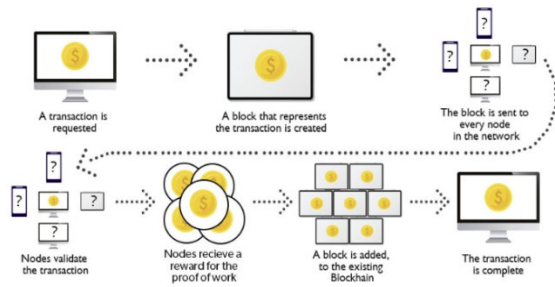


**Figure 1.** How a blockchain works? [75]

The blocks form a chronological chain, where each block in the chain contains a copy of the previous block's hash, ensuring that the data in the blocks cannot be altered. To organize the transactions between stakeholders, the smart contracts are used to self-executing contracts with the terms of the agreement are automated, limiting conflicts.

The blockchain is a decentralized and distributed system, making it more resistant to tampering and hacking, in addition to cryptography ensures that transactions are secure and the consensus mechanism ensures that the ledger is accurate and up-to-date.

The blockchain could enhance sustainability and contribute to the circular economy by optimizing consensus mechanisms.

Deep learning and blockchain technology have now become crucial, as it provides distinct and secure approaches to IoT (Internet of Things) network security [4].

The objective of this article is to perform a bibliometric study of blockchain in general not in a specific field, to help researchers to discover the actual state of the art and the future trends of blockchain.

The article is structured as follows: Section 2 explains methodology followed in the research to collect studied papers, their origin and some criteria applied to their selection. Section 3 presents results and discussion containing several aspects of the study ad comparisons. The article is finished by a conclusion.

## 2. METHODOLOGY

The data reported in this study were retrieved from the online version of the Science Citation Index EXPANDED (SCI-EXPANDED), the Clarivate Analytics Web of Science Core Collection database (data updated on 29 June

2023). In 2022, Journal Citation Reports (JCR) indexed 9,510 journals with citation references across 178 Web of Science categories in SCI-EXPANDED. The 2022 journal's impact factor (*IF2022*) was reported in the Journal Citation Reports (JCR) on 28 June 2023. According to the definition of the journal's impact factor, Chiu and Ho (2021) [5] recommended to search documents published in 2022 from SCI-EXPANDED after *IF2022* was presented.

Quotation marks (“ ”) and Boolean operator “or” were used which ensured the appearance of at least one search keyword in the terms of TOPIC (title, abstract, author keywords, and Keywords Plus). The search was conducted using a targeted keyword, including “blockchain”. To ensure the analysis results are as accurate as possible, uncommon terms such as “blockchains”, “block chain”, and “block chains” were also included. This approach was taken to ensure that the search is comprehensive and covers a wide range of documents related to the field of blockchain research.

A total of 11,190 blockchain documents were searched out in the SCI-EXPANDED from 1991 to 2022. The SCI-EXPANDED was mainly designed for researchers to find published literature, but not for bibliometric studies [6]. Thus, it is necessary to use an appropriate method when using the database for bibliometric studies. After checking, 10,840 documents (97% of 11,190 documents) from the SCI-EXPANDED were found from 1991 to 2022.

It was pointed that since Keywords Plus contains keywords that are selected based on the title of the articles mentioned in the references and footnotes [7], searching through it includes documents that not related directly to the topic [8], which may be suitable as readable sources but not for bibliometric analyzes [9].

The “front page” as a filter, including article title, abstract, and author keywords has been proposed by Ho's research group in 2011 [10,11]. It should be noted that using the “front page” compared to the ‘Topic’ directly in the database has a significant difference in the results [12]. By using “front page” as a filter, 10,248 documents (95% of the 10,840 documents) were defined as blockchain research publications.

The full record in SCI-EXPANDED and the number of citations in each year for each document were downloaded into Excel Microsoft 365, and additional coding was manually performed [13,14]. The functions in the Excel Microsoft 365, for example, Counta, Concatenate, Filter, Match, Vlookup, Proper, Rank, Replace, Freeze Panes, Sort, Sum, and Len were applied [14]. The journal's impact factors (IF2022) were taken from the Journal Citation Reports (JCR) published in 2022.

In the SCI-EXPANDED database, the corresponding author is labelled as reprint author, but in this study, the term corresponding author is used [15]. Single authors in articles with unspecified authorship were both the first as well as corresponding authors [16]. The single institution in articles with unspecified corresponding institutions was both the first as well as corresponding-author institutions [16]. Similarly, in a single-country article, the country is classified as the first as well as the corresponding-author country. In multi-corresponding author articles, all the corresponding authors, institutions, and countries were considered [14]. Articles with corresponding authors in SCI-EXPANDED, that had only address but not affiliation names were checked out and the addresses were changed to be affiliation names [14].

Affiliations in England, Scotland, North Ireland (Northern Ireland), and Wales were reclassified as being from the United Kingdom (UK) [17]. Affiliations in Turkiye were reclassified as being from Turkey. Affiliations from French Guiana were reclassified as being from France [18]. Affiliations in Faroe Islands were reclassified as being from Denmark [19].

### 3. CITATION INDICATORS

Publications were assessed using following citation indicators:

*C*<sub>year</sub>: the number of citations from Web of Science Core Collection in a year (e.g. *C*<sub>2022</sub> describes citation count in 2022) [20].

*TC*<sub>year</sub>: the total number of citations from Web of Science Core Collection received since publication year till the end of the most recent year (2022 in this study, *TC*<sub>2022</sub>) [21].

*CPP*<sub>year</sub>: average number of citations per publication ( $CPP_{2022} = TC_{2022}/TP$ ), *TP*: total number of publications [22].

Countries and institutions indicators Six publication indicators were applied to evaluate publication performance of countries and institutions [23]:

*TP*: total number of articles

*IP*: number of single-country articles (*IPC*) or number of single-institution articles (*IPI*)

*CP*: number of internationally collaborative articles (*CPC*) or number of inter-institutionally collaborative articles (*CPI*)

*FP*: number of first-author articles

*RP*: number of corresponding-author articles

*SP*: number of single-author articles

Six citation indicators (*CPP*<sub>2022</sub>) related to the six publication indicators were also applied to evaluate the publication impact on countries and institutions [24].

## 4. RESULTS AND DISCUSSION

### 4.1. Characteristics of document types

In recent years, Ho's group identify the characteristics of document type based on their average number of citations per publication (*CPP*<sub>year</sub>) and the average number of authors per publication (*APP*) as basic information of document type in a research topic [25]. Using *TC*<sub>2021</sub> and *CPP*<sub>2021</sub> is advantageous owing to their invariability and ensured repeatability as compared to the number of citations from the Web of Science Core Collection directly [26]. A total of 10,248 documents published in the SCI-EXPANDED from 1991 to 2022 were found among 13 document types which are detailed in Table 1. This publication count includes 9,107 articles (89% of 10,248 documents) with an *APP* of 4.2 and *CPP* of 18, which considerably high and related to the novelty of blockchain technology. The document type of reviews with 756 documents had the greatest *CPP*<sub>2022</sub> value of 33 which was found to be 1.8 times of articles. Three of the top ten cited documents were reviews by [27, 28, 29] with a *TC*<sub>2022</sub> of 971, 788, and 767 respectively.

**Table 1.** Citations and authors according to the document type

Document type	<i>TP</i>	%	<i>TP*</i>	<i>AU</i>	<i>APP</i>	<i>TC</i> <sub>2022</sub>	<i>CPP</i> <sub>2022</sub>
Article	9,107	89	9,107	38,612	4.2	161,756	18
Review	756	7.4	756	3,341	4.4	24,768	33
Editorial material	244	2.4	240	688	2.9	3,632	15
Proceedings paper	96	0.94	96	396	4.1	2,529	26
Meeting abstract	58	0.57	58	182	3.1	7	0.12
Book chapter	43	0.42	43	91	2.1	502	12
Letter	25	0.24	25	75	3.0	162	6.5
Correction	23	0.22	23	103	4.5	9	0.39
News item	19	0.19	16	17	1.1	588	31
Retraction	10	0.10	10	31	3.1	0	0
Retracted publication	8	0.078	8	33	4.1	137	17
Book review	6	0.059	6	6	1.0	1	0.17
Data paper	2	0.020	2	10	5.0	12	6.0

*TP*: number of publications; *TP\**: number of publications with author information in the SCI-EXPANDED; *AU*: number of authors; *APP*: average number of authors per publication; *TC*<sub>2022</sub>: the total number of citations from Web of Science Core Collection since publication year to the end of 2022; *CPP*<sub>2022</sub>: average number of citations per publication (*TC*<sub>2022</sub>/*TP*).

**4.2. Relevant review articles**

In [27], IoT (Internet of Things) are more vulnerable to attacks than other endpoint devices. Blockchain also provides a trustworthy

decentralized management, governance, and tracking at every point in the supply chain and lifecycle of an IoT device (Figure 2).

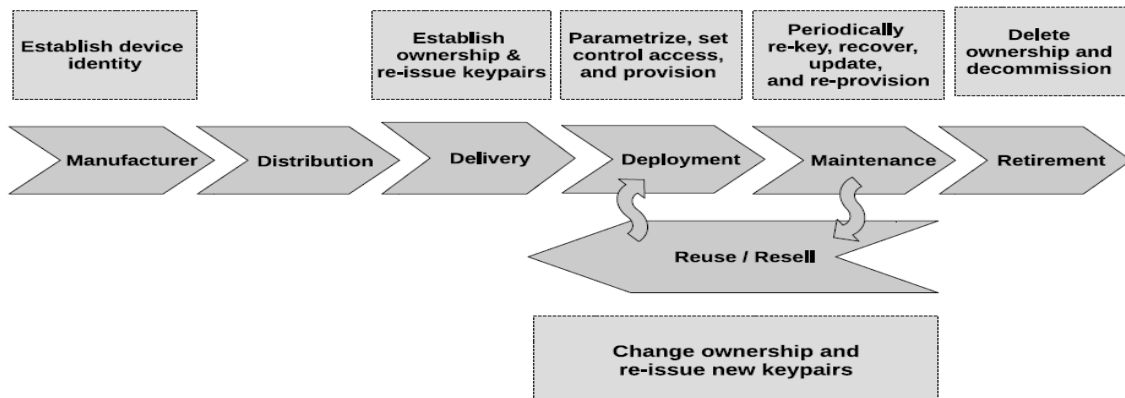


**Figure 2.** IoT device lifecycle security management [27]

According to [28], Figure 3 represents the challenges of blockchain as the lack of control in bitcoin address creation which is solved by certified users addresses from trusted authorities. The private key protection is solved by authentication by sharing private key between wallet and another device. Figure 1 gives a holistic analysis of the literature concerning challenges and their found solutions.

Authors of [29] show that most projects of blockchain in energy systems are in an early development phase, and research is still ongoing on key improvement areas that would allow desired scalability, decentralisation and technologies can be disruptive for energy

companies and face a large variety of challenges to achieve market penetration, including legal, regulatory and competition barriers (Figure 4). Distributed ledger technologies and smart contracts can allow a generating unit to directly trade with a consumer or an energy retail supplier via autonomous trading agents cutting out the middle-man. The agent would search for the best deal in the marketplace that satisfies a consumer’s forecast demand for a given period. The agreement would be safely recorded in the blockchain and automatically executed at the specified time of delivery. Payments would occur automatically at time of delivery as specified in agreed contract.

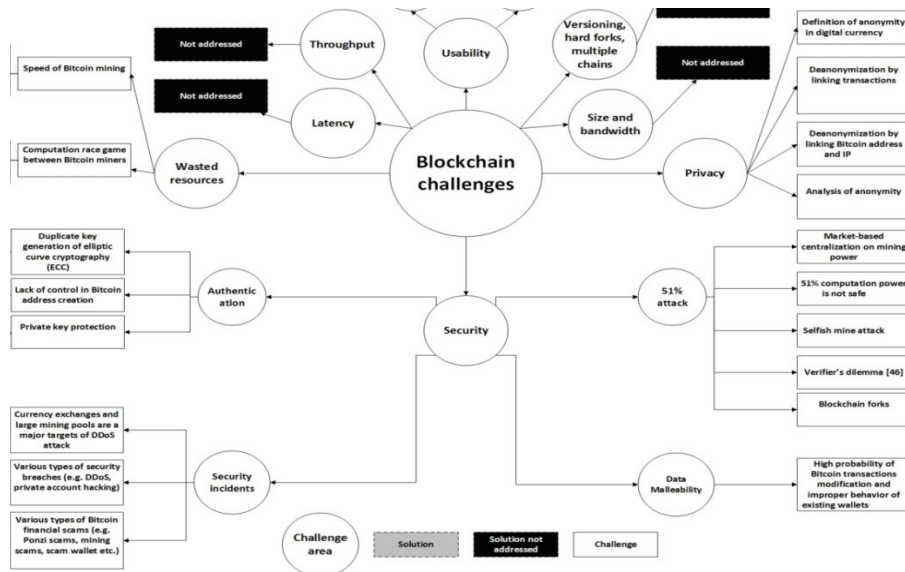


Figure 3. Summary of the identified challenges and solutions of Blockchain Adapted from [28]

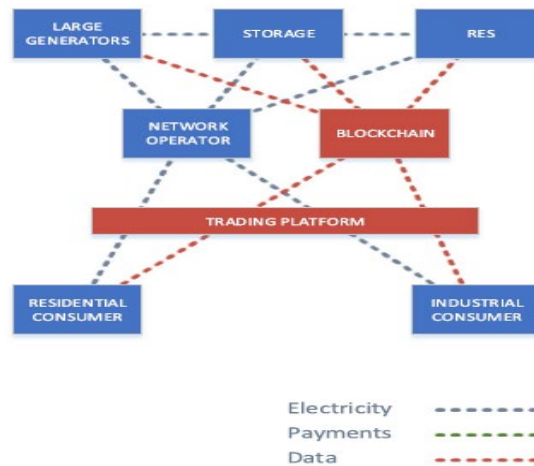


Figure 4. Transformation of market with blockchains according to PWC [29]

The supply chain can include multiple players such as factory, vendor, supplier, distributor, shipper, installer, owner, repairer, reinstaller, etc. As shown in Figure 2, keypairs can be changed and re-issued at multiple points during the lifecycle of an IoT device. Issuance of keypairs can be done initially by the manufacturer, then by the owner, periodically after deployment.

A total of 756 reviews were published in 227 journals mainly in the *IEEE Access* with an *IF2022* of 3.9 (77 reviews; 10% of 756 reviews) and the *Sustainability* with an *IF2022* of 3.9 (59; 7.8%). It was point out that documents could be categorized in two document types in Web of Science Core Collection, for example, 96 proceedings papers, 41 book chapters, seven retracted publication, and one data paper were also classified in document type of articles.

Therefore, cumulative percentages exceed 100% in Table 1 [30].

Contributions of various document types are different. Generally, articles contain introduction, methods, results, discussion, and conclusion, were chosen for further analyses [24].

A total of 9,107 articles were presented in four different languages. The most used language was English with 9,095 articles (99.9% of 9,107 articles) followed distantly by Chinese (7 articles), Japanese (3), and German (2).

### 4.3. Characteristics of publication outputs

Ho (2013) [22] proposed a correlation between annual number of articles (*TP*) and their average number of citations ( $CPP_{year}$ ) by year to understand the development trends and impacts of publications in a research topic. Figure 4

demonstrates the distribution of the annual number of articles ( $TP$ ) and their  $CPP_{2022}$  by year. There were less than 20 annual articles from 1991 to 2015. An extremely increasing trend was appeared since 2017 to reach 3,596 articles in 2022.

In Figure 5, we can see the scientific production increasing since 1991 (2 papers) to achieve 3596 in 2022. It is expected that it will increase in the future. The main average of citations per publication is 242, returns to the year 1991 and two articles about chemicals and polymers [31], [32]. The blockchain they speak about are written «block chain» and it means blocks of polymers and not the blockchain technology as defined in this work. All papers between 1991 and 2008 talk about the block chains of

polymers. The first paper talking about blockchain technology is [33], where a new mutual authentication and privacy scheme for WLAN is proposed to address these security issues. The proposed scheme improves the security mechanisms of IEEE 802.11 and 802.1X by providing a mandatory mutual authentication mechanism between mobile station and access point (AP) based on public key infrastructure (PKI), offering data integrity check and improving data confidentiality with symmetric cipher block chain (CBC) encryption. The effective scientific production in blockchain technology began in 2016 and it is the most cited year with high average of citations (190) after 1991. After that the citations are decreasing until 2022.

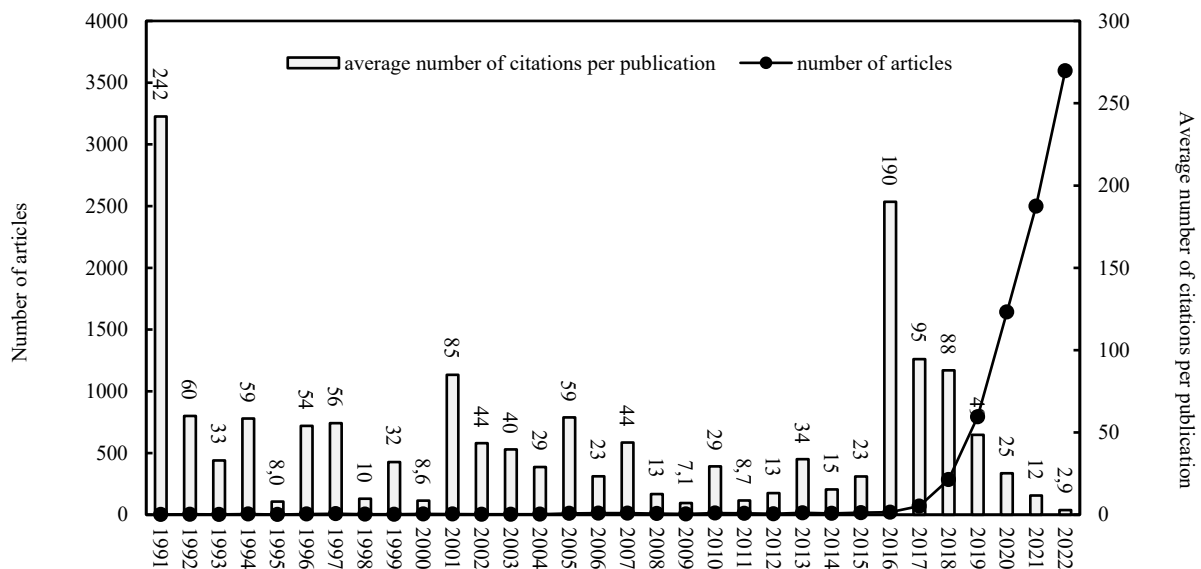


**Figure 5.** Number of blockchain articles and average number of citations per publication by year.

The mean value of  $TC_{2022}$  was 18 with 1,799 as the maximal value for an article by [34]. In 1991, two articles had the greatest  $CPP_{2022}$  of 242 which can be attributed to the article “Ordered structure in mixtures of a block copolymer and homopolymers.

Solubilization of low-molecular-weight homopolymers” [35] by Tanaka, Hasegawa, and Hashimoto from the Kyoto University in Japan, with a  $TC_{2022}$  of 402. In 2016 with 13 articles had second high  $CPP_{2022}$  of 304. The most frequently cited article [34] and top five cited article [36] were published in 2016.

#### 4.4. Web of Science Category and Journal

In 2022, Journal Citation Reports (JCR) indexed 9,510 journals with citation references across

178 Web of Science categories in SCI-EXPANDED. Identify the characteristics of the Web of Science category based on their average number of citations per publication ( $CPP_{year}$ ) and the average number of authors per publication ( $APP$ ) as basic information of the Web of Science category in a research topic were presented in 2021 [37, 24].

Total of 843 journals published articles related to blockchain in 125 Web of Science categories in SCI-EXPANDED. A total of 5,356 articles (59% of 9,107 articles) were published in the top three categories: information systems computer science (3,959 articles; 43% of 9,107 articles), electrical and electronic engineering (3,301; 36%), and telecommunications (3,128; 34%). It

is comprehensible because the blockchain technology uses techniques related to all these categories.

**Table 2.** The top 10 most productive Web of Science categories.

Web of Science category	No. Journals	TP (%)	APP	CPP <sub>2022</sub>
Information systems computer science	242	3959 (43)	4.3	17
Electrical and electronic engineering	275	3301 (36)	4.5	18
Telecommunications	88	3128 (34)	4.4	18
Theory and methods computer science	111	834 (9.2)	4.2	17
Software engineering computer science	108	737 (8.1)	4.1	16
Hardware and architecture computer science	54	720 (7.9)	4.4	17
Interdisciplinary applications computer science	110	551 (6.1)	4.2	27
Industrial engineering	50	436 (4.8)	4.3	41
Applied physics	159	424 (4.7)	4.4	8
Environmental sciences	274	401 (4.4)	3.9	14

TP: total number of articles; %: percentage in all articles; APP: average number of authors per paper; CPP<sub>2022</sub> average number of citations per paper (TC<sub>2022</sub>/TP).

Comparing the top ten categories in Table 2, articles published in the category of industrial engineering had the greatest CPP<sub>2022</sub> of 41. Articles published in category of electrical and electronic engineering had the highest APP of 4.5. Recently, Ho proposed the characteristics of the journals based on their average number of citations per publication (CPP<sub>year</sub>) and the average number of authors per publication (APP) as basic information of the journals in a research topic [38].

Table 3 shows the top 10 most productive journals with journal’s impact factors, CPP<sub>2022</sub>, and APP. The *IEEE Access* (IF<sub>2022</sub> = 3.9) published the most 952 articles which represent 4.3% of 9,107 articles. The *Security and Communication Networks* (IF<sub>2021</sub> = 1,968) and the *Wireless Communications & Mobile Computing* (IF<sub>2021</sub> = 2.146) were not classified in JCR in 2022. Comparing the top 10 productive journals in Table 3, articles published in the *IEEE Transactions on Industrial Informatics* (IF<sub>2022</sub> = 5.0) had the greatest CPP<sub>2022</sub> of 45 while articles in the *Wireless Communications & Mobile Computing* had only 3.2. The APP ranged from 5.1 in the *IEEE Internet of Things Journal* to 3.8 in the *Sustainability*. The journal

with the greatest IF<sub>2022</sub> of 100.3 was the *Nature Reviews Immunology* ranked the top in 161 journals classified in the Web of Science category of immunology with one article followed by the *Nature* (IF<sub>2022</sub> = 64.8) ranked the top in 73 journals classified in the category of multidisciplinary sciences with two articles, and the *Nature Energy* (IF<sub>2022</sub> = 56.7) ranked the top in 115 journals classified in the category of energy and fuels with one article. The journals *Sustainability* and *Nature energy* are present in the list of top ten most productive journals because of the problem of consumption of energy by the mining process of the blockchain and the effect on environment.

**Table 3.** The top 10 most productive journals.

Journal	TP (%)	IF <sub>2022</sub>	APP	CPP <sub>2022</sub>
IEEE Access	952 (10)	3.9	4.3	22
IEEE Internet of Things Journal	367 (4.0)	10.6	5.1	29
Sensors	331 (3.6)	3.9	4.6	12
Sustainability	265 (2.9)	3.9	3.8	11
Security and Communication Networks	229 (2.5)	*1.968	4.6	4.6
Applied Sciences-Basel	204 (2.2)	2.7	4.3	6.9
Electronics	177 (1.9)	2.9	4.2	8.2
Wireless Communications & Mobile Computing	172 (1.9)	*2.146	4.1	3.2
IEEE Transactions on Industrial Informatics	158 (1.7)	12.3	5.0	45
Future Generation Computer Systems-The International Journal of Esience	136 (1.5)	7.5	4.5	44

TP: total number of articles; %: percentage of articles; IF<sub>2022</sub>: journal’s impact factor in 2022; \*: journal’s impact factor in 2021 (IF<sub>2021</sub>); APP: average number of authors per article; CPP<sub>2022</sub>: average number of citations per paper (TC<sub>2022</sub>/TP).

**4.5. Publication performances: countries and institutions**

There were 12 articles (0.13% of 9,107 articles) without affiliations in SCI-EXPANDED. A total of 9,095 articles were published by authors affiliated from 113 countries including 5,444 single-country articles (60% of 9,095 articles) published by authors from 79 countries with a CPP<sub>2022</sub> of 15 and 3,651 internationally collaborative articles (40%) published by authors from 110 countries with a CPP<sub>2022</sub> of 22. The results demonstrated that internationally collaborative raised citations in the research of blockchain. It is widely recognized that two

authors: first and the corresponding authors are considered as the most contributed authors in a research article [39]. At the institutional level, the determined institution of the corresponding author might be a home base of the study or origin of the paper [20]. Six publication indicators [23] and the six related citation indicators ( $CPP_{2022}$ ) [24] were applied to compare the top 20 productive countries (Table 4). China dominated in all the six publication

indicators with a  $TP$  of 4,079 articles (45% of 9,095 articles), an  $IP_C$  of 2,422 articles (44% of 5,444 single-country articles), a  $CP_C$  of 1,657 articles (45% of 3,651 internationally collaborative articles), an  $FP$  of 3,739 articles (41% of 9,095 first-author articles), an  $RP$  of 3,632 articles (40% of 9,083 corresponding-author articles), and an  $SP$  of 165 articles (35% of 466 single-author articles).

**Table 4.** Top 10 productive countries.

Country	TP	TP		IP <sub>C</sub>		CP <sub>C</sub>		FP		RP		SP	
		R	CPP <sub>2022</sub>	R	CPP <sub>2022</sub>	R	CPP <sub>2022</sub>	R	CPP <sub>2022</sub>	R	CPP <sub>2022</sub>	R (%)	CPP <sub>2022</sub>
China	4,079	1 (45)	17	1 (44)	11	1 (45)	26	1 (41)	16	1 (40)	15	1 (35)	4.7
USA	1,352	2 (15)	29	4 (6.5)	36	2 (27)	27	3 (5.9)	32	4 (6.9)	31	2 (13)	21
India	1,000	3 (11)	15	2 (7.4)	7.8	3 (16)	19	2 (9.0)	12	2 (7.6)	12	6 (3.6)	12
South Korea	734	4 (8.0)	16	3 (7.4)	14	8 (9.1)	19	4 (5.5)	16	3 (7.0)	16	3 (5.8)	11
UK	681	5 (7.5)	23	9 (2.1)	24	4 (16)	23	6 (2.5)	26	5 (3.3)	23	9 (2.6)	7.2
Australia	575	6 (6.3)	24	7 (2.3)	21	6 (12)	25	5 (2.5)	27	6 (3.2)	26	7 (3.4)	14
Saudi Arabia	573	7 (6.3)	15	14 (1.2)	4.2	5 (14)	16	13 (1.7)	9.4	10 (2.4)	12	4 (5.2)	3.8
Canada	472	8 (5.2)	26	11 (1.5)	18	7 (11)	28	11 (1.8)	18	11 (2.2)	26	16 (0.86)	12
Taiwan	375	9 (4.1)	19	10 (2.0)	11	10 (7.3)	22	12 (1.7)	11	7 (2.7)	15	10 (2.4)	17
Japan	346	10 (3.8)	23	5 (3.2)	20	11 (4.7)	27	9 (2.4)	22	8 (2.6)	20	5 (4.5)	10

$TP$ : number of total articles;  $TP R (%)$ : total number of articles and the percentage of total articles;  $IP_C R (%)$ : rank and percentage of single-country articles in all single-country articles;  $CP_C R (%)$ : rank and percentage of internationally collaborative articles in all internationally collaborative articles;  $FP R (%)$ : rank and the percentage of first-author articles in all first-author articles;  $RP R (%)$ : rank and the percentage of corresponding-author articles in all corresponding-author articles;  $SP R (%)$ : rank and the percentage of first-author articles in all first-author articles;  $CPP_{2022}$ : average number of citations per publication ( $TC_{2022}/TP$ ); N/A: not available.

Development trends in the publication of the top seven productive countries in the last decade are presented in Figure 6. The China ranked at the top in the last 10 years with a sharply increased since 2018 to reach 1,723 articles in 2022. India and Saudi Arabia also had sharply increased in recent years to reach 531 articles (ranked 2nd) and 290 articles (ranked 4th) in 2022 respectively. However, China had lower citations with a  $TP$ - $CPP_{2022}$  of 17, an  $IP_C$ - $CPP_{2022}$  of 11, an  $FP$ - $CPP_{2022}$  of 16, an  $RP$ - $CPP_{2022}$  of 15, and an  $SP$ - $CPP_{2022}$  of 4.7.

Similarly, India Saudi Arabia also had lower  $CPP_{2022}$  for the six types of publications.

The UK was always exceeding production of China and all countries, but in 2022, China had 1723 articles, almost half of its  $TP$ . According to (Scimago, 2023) [40] ranking, the most productive and cited countries in all domains are USA, China then the UK. We see that Saudi Arabia is another country in perpetual scientific revolution. The blockchain domain is more supported by these countries, and this is the trend of all novelties in the world.

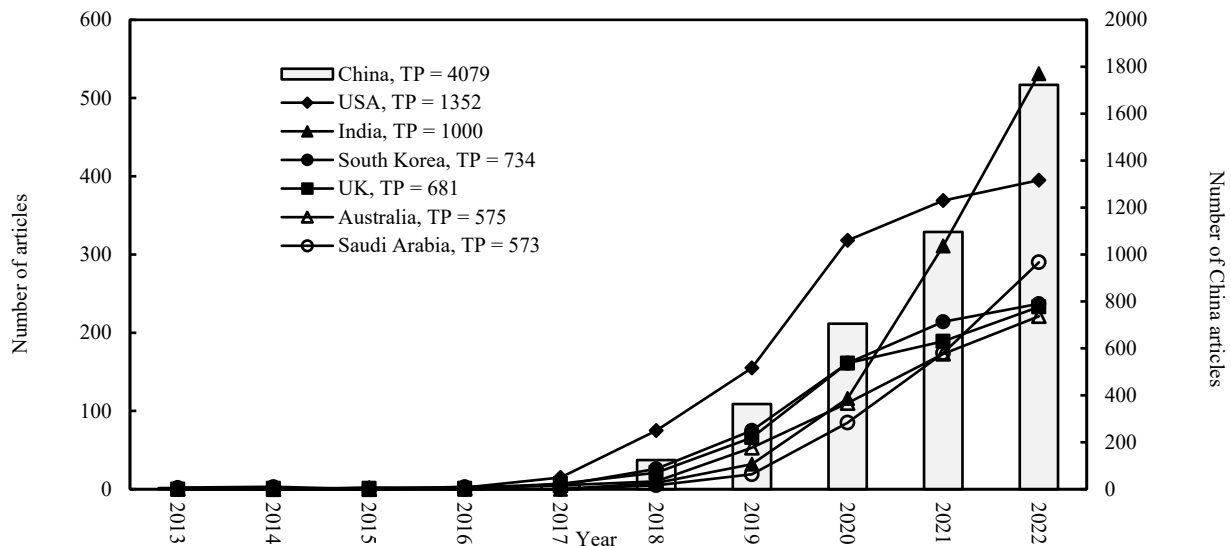


Figure 6. Development trends of the top seven productive countries.

Concerning institutions, 2,831 articles (31% of 9,095 articles) originated from single institutions with a  $CPP_{2022}$  of 15 while 6,264 articles (69%) were inter-institutional collaborations with a  $CPP_{2022}$  of 19.

The results show that international collaborations had higher citations than nationally collaborations. The top 10 productive institutions and their characteristics are presented in Table 5. Seven of the 10 institutions were in China and one in each of Saudi Arabia, Singapore, and Taiwan respectively. The Beijing University of Posts and Telecommunications (BUPT) in China dominated in five of the five publication indicators with a  $TP$  of 218 articles (2.4% of 9,095 articles), an  $IP_1$  of 48 articles (1.7% of 2,831 single-institution articles), an  $FP$  of 160 articles (1.8% of 9,095 first-author articles), and an  $RP$  of 159 articles (1.8% of 9,083 corresponding-author articles).

BUPT is a comprehensive university with information and telecommunication technology as its main feature, engineering and science as its main focus and a combination of engineering, management, humanities and sciences as its main pursuit, which becomes an important base for fostering high-tech talents. BUPT has 11 schools, three research institutes. The three research institutes are Institute of Network Technology, Institute of Optical Communication and Photoelectron and Institute of Sensing Technology and Business [41]. They helped in promoting research. The university is chosen by 99% of Chinese students, it receives

the most competent students, it explains the richness of its research.

The Chinese Academy of Sciences (CAS) in China ranked the top with a  $CP_1$  of 198 articles (3.2% of 6,264 inter-institutionally collaborative articles). Compared to the top 10 productive institutions in Table 5, the Nanyang Technological University (NTU) in Singapore with a  $TP$  of 94 articles, a  $CP_1$  of 91 articles, a  $FP$  of 35 articles, and an  $RP$  of 26 articles had the greatest of  $TP-CPP_{2022}$  of 42,  $CP_1-CPP_{2022}$  of 44,  $FP-CPP_{2022}$  of 69, and  $RP-CPP_{2022}$  of 53 respectively. The Hong Kong Polytechnic University (Poly U) with an  $IP_1$  of eight articles had the greatest of  $IP_1-CPP_{2022}$  of 49. Furthermore, the Asia University with an  $IP_1$  of three articles (ranked 176<sup>th</sup>) and a  $FP$  of nine articles (ranked 167<sup>th</sup>) had much lower  $IP_1-CPP_{2022}$  of 0 and  $FP-CPP_{2022}$  of 1.9 respectively. Furthermore, Neeraj Kumar, affiliated with Thapar Institute of Engineering and Technology in India, utilized multiple affiliations for all articles, primarily with Thapar Institute of Engineering and Technology (TIET), Asia University in Taiwan, and King Abdul Aziz University in Saudi Arabia, to publish a substantial number of articles (56 out of 92) in Asia University. Kumar's role as an "academic mercenary," of Asia University by turning it into a gift institution.

**Table 5.** Top 10 productive institutions.

Institution	TP	TP		IP <sub>1</sub>		CP <sub>1</sub>		FP		RP	
		R (%)	CPP <sub>2022</sub>	R (%)	CPP <sub>2022</sub>	R (%)	CPP <sub>2022</sub>	R (%)	CPP <sub>2022</sub>	R (%)	CPP <sub>2022</sub>
BUPT, China	218	1 (2.4)	30	1 (1.7)	13	2 (2.7)	35	1 (1.8)	29	1 (1.8)	24
CAS, China	202	2 (2.2)	22	117 (0.14)	2.0	1 (3.2)	23	4 (0.88)	23	2 (1.2)	20
Xidian U, China	167	3 (1.8)	21	7 (0.6)	20	4 (2.4)	21	3 (1.1)	19	3 (1.1)	23
KSU, Saudi Arabia	162	4 (1.8)	24	48 (0.28)	10	3 (2.5)	25	77 (0.18)	22	7 (0.73)	25
UESTC, China	153	5 (1.7)	35	3 (0.85)	14	5 (2.1)	39	2 (1.1)	34	3 (1.1)	27
BIT, China	113	6 (1.2)	27	7 (0.6)	8.8	7 (1.5)	31	4 (0.88)	33	5 (0.9)	33
Poly U, China	107	7 (1.2)	33	48 (0.28)	49	6 (1.6)	32	21 (0.42)	53	27 (0.36)	39
WHU, China	99	8 (1.1)	18	31 (0.35)	8.9	9 (1.4)	19	7 (0.66)	20	6 (0.74)	17
NTU, Singapore	97	9 (1.1)	42	69 (0.21)	10	8 (1.5)	44	26 (0.38)	69	46 (0.29)	53
Asia U, Taiwan	92	10 (1)	21	176 (0.11)	0	9 (1.4)	22	167 (0.1)	1.9	38 (0.32)	17

TP: total number of articles; TP R (%): total number of articles and percentage of total articles; IP<sub>1</sub> R (%): rank and percentage of single-institute articles in all single-institute articles; CP<sub>1</sub> R (%): rank and percentage of inter-institutionally collaborative articles in all inter-institutionally collaborative articles; FP R (%): rank and percentage of first-author articles in all first-author articles; RP R (%): rank and percentage of corresponding-author articles in all corresponding-author articles; CPP<sub>2022</sub>: average number of citations per publication (TC<sub>2022</sub>/TP); N/A: not available.

**Institutions**

BUPT: Beijing University of Posts and Telecommunications, CAS: Chinese Academy of Sciences, Xidian U: Xidian University, KSU: King Saud University, UESTC: University of Electronic Science and Technology of China, BIT: Beijing Institute of Technology, Poly U: Hong Kong Polytechnic University, WHU: Wuhan University, NTU: Nanyang Technological University, Asia U: Asia University.

Currently, Thapar Institute of Engineering and Technology in India is ranked 127<sup>th</sup> in the world and 20<sup>th</sup> in engineering [42], in 2023, and has 6 centers of excellence.

Centre for Business Analytics and Excellence focuses on the development of analytical thinking with large, ambiguous and complex data from diversified sources.

Centre for Learning Resource Development is being established with the mission of enriching management education.

Centre for Indian Management Critically evaluating and concretizing the Indian management thought and practice; developing conceptual frameworks, models and tools, thus helping practitioners to operationalize it. The Centre for Governance undertakes action-oriented research which would be implemented by AF in collaboration with State Governments.

The centre for Academic and Corporate Leadership aimed to augment a collaborative academia-business interface.

Centre for Strategy, Sustainability & Society is envisioned to emerge as a catalyst for encouraging business strategy driven sustainability initiatives.

King Abdulaziz university is implementing a precise plan to improve the number and quality of scientific papers and is also keen to increase the rate of publication and citation among faculty

members to achieve its goal of being among the top 100 universities to achieve the Kingdom’s vision 2030. It also has an infrastructure of Specialized scientific and research entities represented by specialized entities, including supporting deanships, specialized research centers and laboratories, and research excellence chairs. The University is also interested in protecting, recording, marketing, and transforming promising ideas and inventions into commercial or industrial products [43].

**4.6. Citation histories of the ten most frequently cited articles**

Total citations are updated from time to time on the Web of Science Core Collection. To improve bibliometric study, the total number of citations from the Web of Science Core Collection since publication year to the end of the most recent year of 2021 (TC<sub>2022</sub>) was applied to improve the bias using data from the database directly [21]. A total of 6,561 articles (72% of 9,107 articles), 8,857 articles (98% of 9,052 articles with abstract in SCI-EXPANDED), and 6,747 articles (87% of 7,757 articles with author keywords in SCI-EXPANDED) contain search keywords in their title, abstract, and author keywords respectively. Seven, eight, and ten of the top ten most frequently cited articles contain search keywords in their title, abstract, and author keywords respectively.

Table 6 shows the top 10 most frequently cited articles with two citation indicators [20]. The USA published four of the top ten articles, followed by China (3 articles), Germany (2),

Norway (2) and one for each of Spain, Canada and United Arab Emirates respectively. Three institutions including the Guangdong University of Technology in China, the Simula Research Laboratory in Norway, and the University of Oslo in Norway had two of the ten most frequently cited articles. Two of the top 10 articles published in the *IEEE Transactions on Industrial Informatics* and *Future Generation Computer Systems-the International Journal of Esience*. Citations of a highly cited article is not always high [44]. It is recommended to understand citation history of a highly cited article. The citation histories of the top ten articles contain search keywords in their title or author keywords are shown in Figure 7.

The fundamental pattern observed was a steady rise in citations over a period of approximately three years, followed by a subsequent decline. Article entitled “Blockchains and smart contracts for the Internet of Things” [34] had the greatest impactful in blockchain research. However, a letter published article entitled “Blockchain technology and its relationships to sustainable supply chain management” [45] was the most impactful in the most recent year of 2022 with a  $C_{2022}$  of 379.

All of the top ten most cited articles has three phases of citations; a weak beginning of citations, crucial phase of citations and then a weak end of citations (Figure 7). The shape of the citation history curves is similar for almost of the articles.

**Table 6.** Top 10 most frequently cited blockchain articles

Rank ( $TC_{2022}$ )	Rank ( $C_{2022}$ )	Title	Country	Reference
1 (1,799)	3 (284)	Blockchains and smart contracts for the Internet of Things	USA	Christidis and Devetsikiotis (2016) [34]
2 (1,185)	2 (331)	Industry 4.0: State of the art and future trends	USA	Xu et al. (2018) [46]
3 (1,139)	4 (281)	Blockchain challenges and opportunities: A survey	China	Zheng et al. (2018) [47]
4 (959)	1 (379)	Blockchain technology and its relationships to sustainable supply chain management	USA	Saberi et al. (2019) [45]
5 (734)	31 (110)	Bitcoin and beyond: A technical survey on decentralized digital currencies	Germany	Tschorsch and Scheuermann (2016) [36]
6 (713)	8 (168)	Designing microgrid energy markets. A case study: The Brooklyn Microgrid	Germany, USA	Mengelkamp et al. (2018) [48]
7 (652)	9 (166)	On blockchain and its integration with IoT. Challenges and opportunities	Spain	Reyna et al. (2018) [49]
8 (611)	20 (127)	Security and privacy in decentralized energy trading through multi-signatures, blockchain and anonymous messaging streams	U Arab Emirates	Aitzhan and Svetinovic (2018) [50]
9 (604)	13 (149)	Consortium blockchain for secure energy trading in industrial Internet of Things	China, Norway	Li et al. (2018) [51]
10 (590)	19 (128)	Enabling localized peer-to-peer electricity trading among plug-in hybrid electric vehicles using consortium blockchains	China, Norway, Canada	Kang et al. (2017) [52]

$TC_{2022}$ : the total number of citations from Web of Science Core Collection since publication year to the end of 2022;  $C_{2022}$ : number of citations of an article in 2022 only.

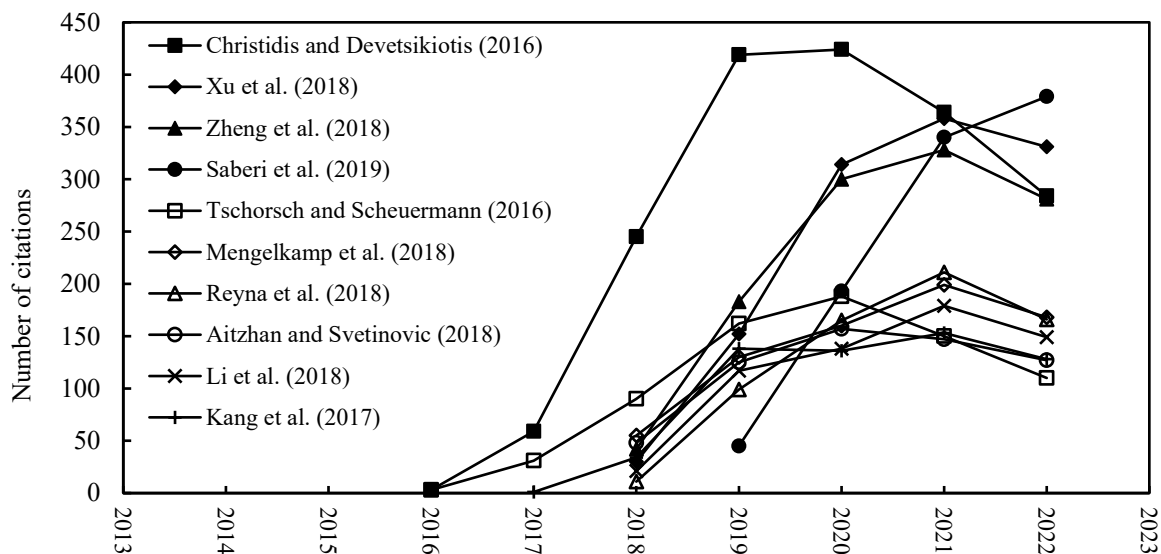


**Figure 7.** The citation histories of the top ten most frequently cited articles.

**Table 7.** Findings and contributions of Top 10 most frequently cited blockchain articles

Title	Findings and contributions
Blockchains and smart contracts for the Internet of Things [34]	blockchain-IoT combination facilitates the sharing of services and resources leading to the creation of a marketplace of services between devices and allows to automate in a cryptographically verifiable manner several existing, time-consuming workflows.
Industry 4.0: State of the art and future trends [46]	Blockchain is an industry 4.0 technology, World Economic Forum predicts that by 2027, 10% of global GDP will be stored on blockchain technology. Some companies have started integrating blockchain concept into manufacturing practices.
Blockchain challenges and opportunities: A survey [47]	The article contains a comparison between consensus mechanisms which represent a vital part concerning the energy consumption and its minimization. It compares PoW, PoS, PBFT, DPOS, Ripple and Tendermint. They found that PoS and DPoS are the less consuming energy.
Blockchain technology and its relationships to sustainable supply chain management [45]	Four blockchain technology adoption barriers categories are introduced: interorganisational barriers (lack of customers' awareness, lack of collaboration, challenge of sustainability practices and cultural differences), intraorganisational barriers (financial constraints, lack of managers' support), technical barriers (security challenge, blockchain not mature, immutability challenge) and external barriers (lack of governmental policy, market competition, lack of stakeholders involvement).
Bitcoin and beyond: A technical survey on decentralized digital currencies [36]	A comparison between bank model and bitcoin model: The bank Model is centralized, survives by interests of loans, value of money depends on rate exchange, and the transfer is mediated and not free, long delay of transaction with high fees).The Bitcoin Model is decentralized, survives by mining operations, value of money depends on demand and supply, and the transfer is direct and not reversible, short delay of transaction with low fees).
Designing microgrid energy markets. A case study: The Brooklyn Microgrid [48]	The article shows that private blockchains are suitable information systems that can facilitate localized energy markets. The BMG is the first project that actually facilitated a blockchain-based electricity transaction. The projects' findings need to be further investigated to evaluate the economic and socio-economic impact of microgrid energy markets on their participants and the entire energy supply system.
On blockchain and its integration with IoT. Challenges and opportunities [49]	Consensus can include IoT as part of the mining processes and distributing even more blockchains. Beyond the scalability and storage capacity which affect both technologies, research should ensure the security and privacy of critical technologies that the IoT and blockchain can become. One of the main concerns about blockchain, and especially cryptocurrencies, resides in its volatility which has also been exploited by people to take unfair advantage of this situation. The integration of the IoT and blockchain will increase the use of blockchain, to establish cryptocurrencies on the same level as current money.
Security and privacy in decentralized energy trading through multi-signatures, blockchain and anonymous messaging streams [50]	Authors implemented a proof-of-concept for decentralized energy trading system using blockchain technology, multi-signatures, and anonymous encrypted messaging streams, enabling peers to anonymously negotiate energy prices and securely perform trading transactions. On the case studies, they found that the appropriate combination of blockchain technology, multi-signatures and anonymous encrypted message propagation streams presents a feasible and reliable direction towards decentralized energy trading with higher privacy and security compared to the traditional centralized trading solutions.
Consortium blockchain for secure energy trading in industrial Internet of Things [51]	In this paper, a unified energy blockchain based on consortium blockchain for secure energy trading in various typical scenarios of IIoT (Industrial IOT), such as microgrids, energy harvesting networks, and vehicle-to-grids. Authors designed a credit-based payment scheme to overcome the transaction limitation caused by transaction confirmation delays, which supports fast and frequent energy trading by credit-based payment among energy nodes. They propose an optimal pricing strategy using Stackelberg game for energy-coin loans to maximize economic benefits of credit banks.
Enabling localized peer-to-peer electricity trading among plug-in hybrid electric vehicles using consortium blockchains [52]	A localized P2P Electricity Trading system with Consortium blockchain (PETCON) method is proposed to illustrate detailed operations of localized P2P electricity trading. Moreover, the electricity pricing and the amount of traded electricity are solved by an iterative double auction mechanism to maximize social welfare in this electricity trading. Security analysis shows that the proposed PETCON improves transaction security and privacy protection. Numerical results based on a real map of Texas indicate that the double auction mechanism can achieve social welfare maximization while protecting privacy of the PHEVs.

Table 7 summarizes the content of the top ten most cited articles. Most of them are reviews of the different aspects of blockchain.

#### 4.7. Research foci

The study conducted by [53] utilized the distribution of words in article titles, abstracts, author keywords, and *Keywords Plus* as a word bank to identify the research's main focuses and their development trends. However, when it comes to new research topics or fields, analysing different periods may not be appropriate. The articles were arranged in ascending order based on their

publication years and were subsequently divided into three distinct "periods". Each period contains one-third of the total articles. In the first period, spanning from 1991 to 2020, amounting to 3,011 articles (33% of the overall 9,107 articles), were accounted for. This initial period represented a smaller proportion of articles each year, suggesting the emergence of a new research topic or field. It took 20 years to publish

**Table 8.** The 20 most frequently used author keywords

Author keywords	TP	1991-2022 Rank (%)	1991-2020 Rank (%)	2021 Rank (%)	2022 Rank (%)
Blockchain	5930	1 (76)	1 (76)	1 (86)	1 (70)
Security	1,076	1 (14)	1 (9.1)	1 (16)	1 (16)
Internet of things	824	2 (11)	1 (9.1)	2 (11)	2 (12)
Smart contract	777	3 (10)	3 (8.8)	3 (10)	3 (11)
Smart contracts	745	4 (10)	4 (8.2)	4 (10)	4 (11)
Privacy	617	5 (8.0)	6 (6.2)	5 (9.3)	5 (8.5)
Bitcoin	425	6 (5.5)	5 (6.7)	7 (5.2)	8 (4.7)
Cloud computing	352	7 (4.5)	8 (4.3)	12 (4.6)	8 (4.7)
IoT	352	7 (4.5)	7 (4.8)	9 (4.9)	11 (4.1)
Blockchain technology	335	9 (4.3)	11 (3.5)	12 (4.6)	7 (4.8)
Edge computing	335	9 (4.3)	10 (3.6)	6 (5.8)	12 (3.9)
Ethereum	331	11 (4.3)	9 (4.3)	7 (5.2)	14 (3.6)
Authentication	329	12 (4.2)	15 (2.9)	9 (4.9)	6 (4.9)
Peer-to-peer computing	280	13 (3.6)	14 (3.0)	14 (4.1)	13 (3.8)
Servers	278	14 (3.6)	23 (1.8)	11 (4.9)	10 (4.2)
Internet of Things (IoT)	276	15 (3.6)	12 (3.4)	15 (3.8)	15 (3.5)
Access control	255	16 (3.3)	16 (2.8)	16 (3.8)	16 (3.3)
Machine learning	214	17 (2.8)	18 (2.3)	20 (3.1)	17 (3.0)
Distributed ledger	212	18 (2.7)	19 (2.2)	18 (3.2)	18 (2.8)
Cryptography	205	19 (2.6)	17 (2.6)	17 (3.4)	29 (2.2)
Scalability	191	20 (2.5)	34 (1.5)	19 (3.1)	19 (2.8)

TP: number of articles contain the keywords; %: percentage in each period.

one-third of the total articles. Moving on to the second period, which encompassed the year 2021, totalling 2,500 articles (27% of the 9,107 total articles). During this period, researchers displayed increased interest, leading to a higher volume of published studies. It took only one year to publish one-third of the total articles. Finally, period three covered 2022, with 3,596 articles (39% of the 9,107 total articles). Again, it only took one year to publish one-third of the total articles. The analysis involved examining the distribution of words in the article titles and abstracts, as well as author keywords, across these three article segments. The analysis of words in article titles and abstracts provides insights limited to individual words. In Table 8, the 20 most frequently used author keywords (excluding search terms) were highlighted.

The results of keyword analyses provide information about the main and possible

research foci as each word cluster comprised several supporting words.

The frequency of the keyword «blockchain» (5930) is added to the frequency of «blockchain technology» (335) to obtain 6265, and because they are synonyms and the most frequent; it is obvious by the nature of the bibliometrics research looking for blockchain articles.

The security is the second most frequent keyword (1,076) to understand that the appeal to the blockchain technology is for its encouraging security aspect. The keywords privacy (617), authentication (329), access control (255) and cryptography (205) belong to the security family. Figure 8 illustrates that the security of the blockchain should be insured at all the levels or layers. The third most frequent keyword is «Internet of Things» (824), added to the keyword IOT (352) and added to Internet of Things (IoT) (276) to obtain 1492 appearances of the keywords having the same meaning. The next trend of blockchain is the acceleration of

integration of blockchain and IOT, because IOT are subject of attacks and the blockchain may reinforce their security.

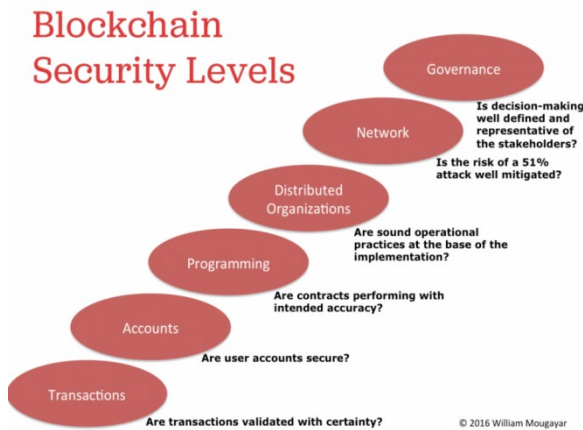


**Figure 8.** Blockchain security levels [54]

The fourth more used keyword is smart contract (777) added to smart contracts (745) to have 1522. The smart contract is an automated contract reflecting the real contract or the traditional contract. It works on blockchain without reminders or negotiations. All is done in advance when designing the blockchain. The fifth most used cryptocurrency or digital money is Bitcoin (425) and followed by Ethereum (331).

The first one appeared in 2008 and was announced by a group under the pseudonym Satoshi Nakamoto (unknown until now) by publishing their white paper « Bitcoin: A Peer-to-Peer Electronic Cash System » [55]. In 2012, the bitcoin achieves 1 billion dollars. In 2013, [56] launched the Ethereum. While both the Bitcoin and Ethereum networks are powered by the principle of distributed ledgers and cryptography, the two differ technically in many ways. For example, transactions on the Ethereum network may contain executable code, while data affixed to Bitcoin network transactions is only used to record transaction information. Other differences include block time (an ETH transaction is confirmed in seconds, compared with minutes for BTC), and their consensus algorithms are different: Bitcoin uses SHA-256, while Ethereum uses LMDGhost [57]. The particularity is that each enterprise can create its own cryptocurrency convertible to other cryptocurrencies and traditional currencies. That is why, there are thousands of cryptocurrencies.

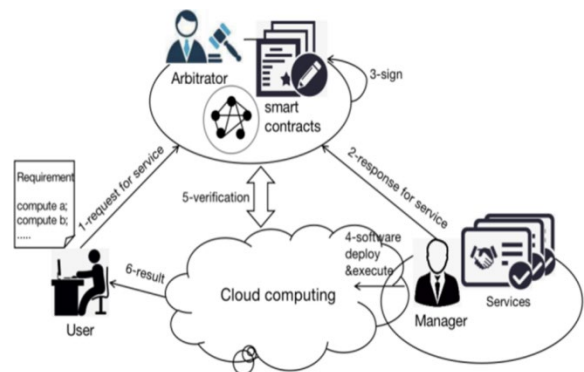
The sixth trend is the computing infrastructure supporting the blockchain represented by the keywords: cloud computing (352), edge computing (335) and peer-to-peer computing (280) to have in final (967) appearances.

The cloud computing is commonly described as the usage of computing resources provided as services over network [58].

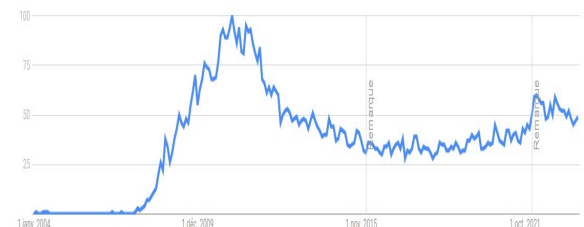
(Zhou et al. 2017) [59] proposed a Cleanroom Security Service Protocol (CSSP), which is actually a bilateral agreement based on a consortium blockchain framework, shown in Figure 9. CSSP was mainly designed for the SaaS (Software as a Service) computing environment [60]. The usage of blockchain with cloud computing is to be more trustful.

Figure 10 shows the asked researches on Google about cloud computing since 2004. It is increasing these last years [61].

The increasing usage of the Internet of Things over the time has caused problems to the centralized resources on Cloud Computing like low throughput, high latency, bandwidth bottlenecks, data privacy, centralized vulnerabilities, and additional costs.



**Figure 9.** Main process in CSSP [60].



**Figure 10.** The trends of research on Google about Cloud computing [61].

To attenuate these problems, the Edge Computing is appeared, simply to delegate the

hard computations to the peripherals and terminals to gain some decentralization [62]. Figure 11 illustrates the increasing trends of researches on Edge Computing over the time [61].

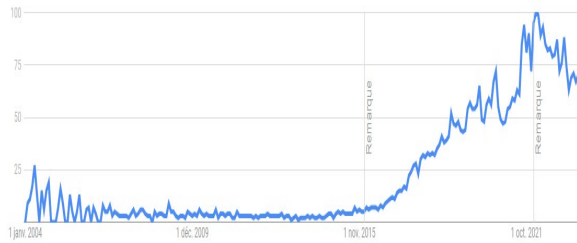


**Figure 11.** The trends of research on Google about Cloud computing [61].

The seventh trend is Peer-To-Peer (P2P) computing (280) added to distributed ledger (212) to have 492. P2P is a computing network without a central server, it is the more adequate to the decentralized architecture of blockchain technology. Figure 12 [63] is the architecture of the P2P network.

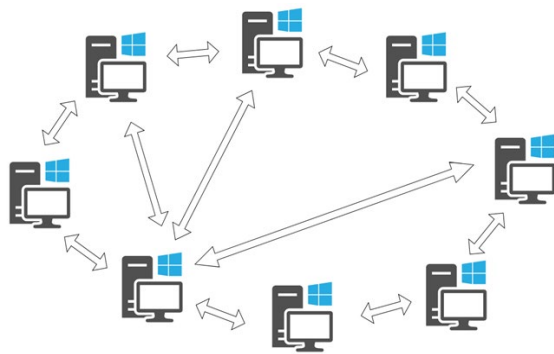


**Figure 12.** A simulation of a peer-to-peer network [63]

Figure 13 [61] illustrates the stabilisation of researches on Google over 12 years, there is probably an increasing use of it with the increasing of use of blockchain in the future.

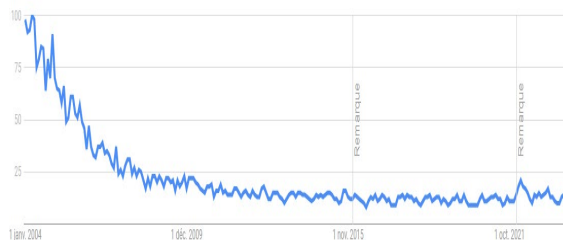


**Figure 13.** The trends of research on Google about P2P Network [61].

#### 4.8. The studied Consensuses

A consensus algorithm is a compliance of each actor in the blockchain network in order to agree on the creation and sequence of each block, it is a tedious verification process ensuring that the blockchain transaction history is correct and tamperproof. All players or nodes of the network must agree to validate an entry in the blockchain register, this is called a consensus algorithm [64].

Table 9 shows the most 12 used consensuses in the studied articles expressed in author keywords. The first keyword is consensus equivalent to algorithm, protocol or mechanism with 480 appearance. It does not specify the used consensus.

We will describe the top 4 used consuses. The most specified used consensus is «Byzantine fault tolerance» (BFT) with a frequency of 111. BFT proposes series of fault-tolerant consensus algorithms that enable the system to reach consensus even in the presence of a certain number of malicious nodes of the blockchain network [65]. While Proof of Work (PoW) with 101 appearances, was the first used in consensus in blockchain, it requires the consent of all nodes in the network without exception for the addition of a block, which makes the process long (10 minutes), energy consuming and above all the most secure. PoW has been improved by several versions to mitigate its disadvantages.

The third consensus is Proof of Knowledge (PoK) (68), a better version of PoK is Zero-knowledge Proof (ZKP) [66]. In this method, one party (Prover) can prove that a specific statement is true to the other party (verifier) without disclosing any additional information. Zero Knowledge Encryption makes sure that no one, except you (not even the service provider or blockchain app development agency) can access your secured data.

The fifth most used consensus is Proof of Stake (PoS) (46). Due to the limitations of PoW as energy inefficiency, delay, and vulnerable to security threats, PoS has been developed enabling to achieve the consensus via proving the stake ownership. This mechanism is expected to become a cutting-edge technology for future blockchain networks [67].

**Table 9.** The most frequently used consensuses

Author keywords	TP
Consensus or Algorithm or Protocol or Mechanism	480
Byzantine fault tolerance	111
Proof of Work	101
proof of Knowledge	68
Proof of Stake	46
Proof of Authority	26
Proof of Delivery	3
Proof of Location	3
Proof of Learning	3
Proof of Contribution	2
Algorand	2

#### 4.9. Sustainable and green blockchain

Blockchains are often stigmatized for their burden on the environment. While it is true that Bitcoin itself and similar proof-of-work (PoW) chains have a considerable ecological impact, proof-of-stake (PoS) chains are vastly more energy efficient. For example, the Ethereum network recently upgraded to PoS, which saw Ethereum's energy usage drop by 99.9% [68].

**Table 10.** The most used consensuses

Author keywords	TP
Smart aspects	519
Energy aspects	180
Sustainability	156
Electric aspects	146
Ecosystem	72
Green aspects	55
Circular economy	54
Carbon aspects	25
Environment aspects	22
Climate	12

There are multiplied efforts to make blockchain sustainable technology, table 10 shows the used keywords to encourage this environmental challenge. The keywords were summed manually by similar aspects, using our experience in the domain. Smart aspects (519) represents most keywords, like smart blockchain, smart home, smart grid, smart device, smart logistics, smart society...etc. All these smart aspects try to make all our society or environment smarter by giving them hard or soft tools to reason and make decisions autonomously to avoid harm the environment.

Smart blockchain is a new generation of blockchain network that allows one or more than a smart contract. The decentralized system of smart contracts collects the data accurately and flawlessly. The decentralized nature of smart blockchain ensures that there is no single point of control or failure, making it resistant to tampering, hacking, and other malicious activities. Simultaneously this decentralization method helps store and register the data in new blocks. The complete process of a transaction is automatic, without any human interaction [69]. Energy aspects appear with great frequency (180), they include energy as a service, energy cost, energy blockchain, energy efficiency, energy financing, energy optimisation, energy saving, energy storage, energy trading etc. The blockchain is a big consumer of energy because of its mining process, the focus is more and more on reduce this consumption by the blockchain by proposing green consensuses like Proof of Stake.

The third most frequent aspect is sustainability (156), it means we have to use resources especially natural ones operational and not waste them to safeguard the health of the terrestrial globe now and to think to the sustainability of these resources for the next generations. This behaviour should take in consideration culture or society, economic efficiency and the environment. The sustainable blockchain is consuming less energy and tries to develop a reusable mining chip which is a hard waste not recyclable.

The electric aspects (146) encourage the consumption of electricity of pollutants as fuel and organic power.

An ecosystem (72) is a geographic area where plants, animals, and other organisms, as well as weather and landscapes, work together to form life [70]. It is integrated in the studied articles because of the nuisance of blockchain to this ecosystem to have to be respected by all the technologies.

Green aspects (55) are focused on greening all the processes in industries to be respectful to the environment and biodegradation of products in the nature.

Circular economy (54) ai all what is related to profitably recycling products.

Carbon aspects (25) have to measure the footprint of all technologies and processes and reduce it to lead it to the allowed worldwide standards.

Environment aspects (22) and the climate aspects (12) are encouraging to be environment-friendly intra-entreprise or extra-entreprise and at all the stages of life cycle of the product or process.

#### 4.10. Medical blockchain

The medical aspects were strongly present in the collection of studied articles, we found 418 keywords related to medical aspects among 15386 keywords. It is suitable to draw attention that the medical area benefits to all offered technologies as blockchain. Before treating keywords, we will look on titles of articles, we found that the word health appears 497 times, medical appears 230 times, hospital appears 15 times and patient appears 60 times. These numbers give an idea about the emergence of blockchain in medical or healthcare in general.

Table 11 illustrates the most used author keywords. The electronic health record and data appears 200 times to demonstrate the importance of the data of patient and their privacy and confidentiality. The blockchain represents a good technology to guarantee the secure access. The question is «Who can access to these records»? the medical staff or the patient? The rules differ from a medical system to another. Medical services (105), e-health aspects (105) and healthcare aspects (89) are related to the electronic healthcare systems encouraging the telemedicine and offer a remote support of patients who are spared from moving to the hospital. Internet of medical things (72) are the sensors used on the body of a patient to measure certain characteristics like temperature, pressure, glycemia,...etc, to inform servers or medical staff to intervene or to autoregulate these measures injecting the appropriate drugs in the body by devices on the body of the patient. Pandemic aspects (71) are also treated because of the harmful after-effects of Covid-19 last years and its enhancement of the use of eHealth systems securely with the blockchain technology.

**Table 11.** The most used health keywords

Author keywords	TP
Electronic health record aspects or data	200
Medical services	142
e-Health aspects	105
Healthcare aspects	89
Internet of medical things	72
Epidemic or pandemic or disease	71
Medical blockchain	55
Biological aspects	50
Medical image	48
Hospital aspects	37
Forensic aspects	35
Pharmaceuticals and medical devices	29
Medical security and insurance	28
Patient centric	20
Medical logistic	12
Emergency aspects	10
Green healthcare	6

Medical blockchain (55) pours directly in the importance of the blockchain technology in healthcare. The most cited article is [71]. The authors proposed a Healthcare Data Gateway (HGD) architecture based on blockchain to enable patient to own, control and share his or her own data easily and securely without violating privacy, which provides a new potential way to improve the intelligence of healthcare systems while keeping patient data private.

The remaining keywords are treating the limitroph aspects around the success of the blockchain technology in healthcare in general. There are several barriers to the use of blockchain like forensic aspects and the governance in multipartite of the blockchain.

#### 4.11. Blockchain and cybersecurity

The blockchain is also used in to sensible sectors like banks, it can be applied in audit operations practically for unanticipated events which can emerge in cyberspace to mitigate inherent risk to residual levels. However, there is ample room to adapt this technology for cybersecurity management and audit practices from the point of view of the labour force, regulations and environmental issues [76].

Staff of companies using blockchain should be trained to intrusion detection and prevention policy for cybercrime [77].

## 5. CONCLUSION

This work is a bibliometric study of the emerging blockchain technology between 1992 and 2022. This choice is not arbitrary, it is due to the lack of such studies in the existing literature, in one hand, and, in the other hand, the importance of this technology for the huge gaining in transparency, security, privacy and immutability. This latter is the most important characteristic, because the blocks of information are added after validation by a consensus and could not be modified or removed. These characteristics are harmful to certain organisations which are not to this transparency in their business. 9107 articles were collected from the online version of the Science Citation Index Expanded (SCI-EXPANDED), the Clarivate Analytics Web of Science Core Collection database (data updated on 29 June 2023), using a combination of query keywords and Boolean operators containing variants of blockchain. This number is obtained after filtering the search removing no significant results. Several analyses are performed using bibliometrics indicators of productivity and citations or impact of production. Some manipulations were necessary to identify and adjust the affiliations of authors, to avoid scientific inflations.

The most used types of documents are articles because they contain basic and experiment studies and original ideas then and reviews because the importance of this type in paving the way for the novice researchers. The content of most three relevant reviews is resumed.

The scientific production and the citations are increasing over years, giving more attention and usability of the blockchain.

The productive Web of Science productive categories are: (1) information systems computer science, (2) electrical and electronic engineering, (3) telecommunications and (4) theory and methods computer science. The nature of the blockchain does so it is taken in account by information and communication fields.

The productive journals in blockchain are: (1) *IEEE Access*, (2) *IEEE Internet of Things Journal*, (3) *Sensors* and (4) *Sustainability*. It is

comprehensible when the Internet of Things are more and more combined to the blockchain to make basical information more reliable coming from connected devices. The sustainability is strongly introduced because of the energy consuming of blockchain and the researchers look for green consensuses of mining to minimize this consumption.

The countries having the higher production are China, USA, India, South Korea and the UK, via their institutions representing of centers of excellence in the domain.

The Chinese institutions are the pioneers in the domain of blockchain (BUPT university, Chinese Academy of Sciences), then comes the Indian Thapar Institute of Engineering and Technology and the Saoudian King Abdulaziz university.

Resumed contents of the top 10 cited articles are presented to enrich the bibliometric study by a breach of contents adding value and comprehension. The citations approximatively follow three different periods, a weak beginning period, a strong period and then a final weak period.

According to the author keywords, The trends are about (1) the security of the blockchain face the malicious intrusions especially in health records of patients and the diversion of cryptocurrencies' transactions, (2) the Internet of Things as physical connected devices measuring situations and in certain cases regulating the flaws if they are smart ones, (3) the use of smart contracts especially in the non monetary applications as blockchain education to save credentials and certificates, (4) the most used cryptocurrency is still the bitcoin.

As important component of blockchain, special attention is given to consensuses used for the process of mining or validating a block of transactions before adding it to a blockchain, the most used is Byzantine fault tolerance resisting in malicious situations, Proof Of Work consuming time and energy, proof of Knowledge minimizing the number of provers and Proof Of Stake minimizing time and energy.

Another aspect is studied, how much the blockchain is aligning with the green philosophy ?. Because of its great consumption of

energy, blockchain is integrated in the use renewable energies and circular economy trying to find a substitution to its non-recyclable ship used in mining.

As an example of fields using the blockchain is the medical one, using body sensors helping in tele-diagnosis and auto regulation by injecting substances in the body.

This study is useful to scientific community in need to know statistical indexes concerning blockchain technology since its birth, its possibilities of use in the majority of domains and certain barriers to its use like its high cost, absence of skilled staff to manage it, absence of law regulating its use and the governance of the blockchain in interoperable context between partners of blockchain.

Among the limitations of the study, self-citations are not distinguished from the remaining citations which could braise even by a small percentage the real impact of an article. The research query is performed on all fields of the articles (titles, abstracts and the body of the article), which affects somewhat the relevancy of some articles related to a blockchain notion existing in chemical field concerning the structure of polymers.

Future research would be (1) on consensuses less consuming energy, using the renewable energies, in a philosophy of greening the blockchain, (2) disclosing the usability of blockchain in all domains, (3) design of a battery of laws to help governments to adopt this technology with the slightest risk, (4) guaranteeing the privacy and determining the new roles and responsibilities of the users of blockchain.

## REFERENCES

1. Menon, M. and Mady A., "Blockchain: An exploratory review of applications in marketing, Glocal Policy and Strategies for Blockchain: Building Ecosystems and Sustainability, Pages 100-125, 2023.
2. Sayed, B., Oral, H.V., "A review on blockchain operations in construction management", *Journal of Sustainable Construction Materials and Technologies*, Vol. 8, Issue 2, Pages 146 - 152, 2023.

3. Alsobhi, H.A., Alakhtar, R.A., Ubaid, A., Hussain, O.K. and Hussain, F.K., "Blockchain-based micro-credentialing system in higher education institutions: Systematic literature review", *Knowledge-Based Systems*, Vol. 265, Issue 110238, 2023.
4. Falayi, A., Wang, Q., Liao, W. and Yu, W. "Survey of Distributed and Decentralized IoT Securities: Approaches Using Deep Learning and Blockchain Technology", *Future Internet*, Vol. 15 Issue 5, 2023.
5. Chiu, W.T. and Ho, Y.S., "Bibliometrics of Latin American research on COVID-19 in the first year of the pandemic: The main trends", *Revista de Biología Tropical*, Vol. 69, Issue 4, Pages 1306-1321, 2021.
6. Ho, Y.S. Comment on: "A Bibliometric Analysis and Visualization of Medical Big Data Research", *Sustainability*, Vol. 10, Issue 12, 2018.
7. Garfield, E., "Keywords Plus: ISI's breakthrough retrieval method. Part 1. Expanding your searching power on Current Contents on Diskette", *Current Contents*, Vol. 32, Pages 5-9, 1990.
8. Fu, H.Z. and Ho, Y.S., "Top cited articles in thermodynamic research", *Journal of Engineering Thermophysics*", Vol. 24, Issue 1, Pages 68-85, 2015.
9. Ho, Y.S., Comments on "Mapping the scientific research on non-point source pollution: A bibliometric analysis" by Yang et al. (2017). *Environmental Science and Pollution Research*, Vol. 25, Issue 30, Pages 30737-30738, 2018.
10. Wang, M.H. and Ho, Y.S., "Research articles and publication trends in environmental sciences from 1998 to 2009", *Archives of Environmental Science*, Vol. 5, Pages 1-10, 2011.
11. Fu, H.Z., Wang, M.H. and Ho, Y.S., "The most frequently cited adsorption research articles in the Science Citation Index (Expanded)", *Journal of Colloid and Interface Science*, Vol. 379, Issue 1, Pages 148-156, 2012.
12. Ho, Y.S., "Rebuttal to: Su et al. "The neurotoxicity of nanoparticles: A bibliometric analysis", *Toxicology and Industrial Health*, Vol. 35, Issue 6, Pages 399-402, 2019.
13. Li, Z. and Ho, Y.S., "Use of citation per publication as an indicator to evaluate contingent valuation research", *Scientometrics*, Vol. 75, Issue 1, Pages 97-110, 2008.

14. Al-Moraissi, E.A., Christidis, N. and Ho, Y.S., "Publication performance and trends in temporomandibular disorders research: A bibliometric analysis", *Journal of Stomatology Oral and Maxillofacial Surgery*, Vol. 124, Issue 1, 2023.
15. Chiu, W.T. and Ho, Y.S., "Bibliometric analysis of tsunami research", *Scientometrics*, Vol. 73, Issue 1, Pages 3-17, 2007.
16. Ho, Y.S., "Classic articles on social work field in Social Science Citation Index: A bibliometric analysis", *Scientometrics*, Vol 98, Issue 1, Pages 137-155, 2014.
17. Chiu, W.T. and Ho, Y.S., "Bibliometric analysis of homeopathy research during the period of 1991 to 2003", *Scientometrics*, Vol. 63, Issue 1, Pages 3-23, 2005.
18. Monge-Nájera, J. and Ho, Y.S., "Bibliometry of Panama publications in the Science Citation Index Expanded: Publication type, language, fields, authors and institutions. *Revista de Biología Tropical*", Vol. 63, Issue 4, Pages 1255-1266, 2015.
19. Ranasinghe, P., Monge-Nájera, J., Liyanage, C.K. and Ho, Y.S., "Half a century of Sri Lanka research: Subjects, researchers, institutions, journals and impact (1973-2019)", *Revista de Biología Tropical*, Vol. 70, Issue 1, Pages 40-52, 2022.
20. Ho, Y.S., "Top-cited articles in chemical engineering in Science Citation Index Expanded: A bibliometric analysis", *Chinese Journal of Chemical Engineering*, Vol. 20, Issue 3, Pages 478-488, 2012.
21. Wang, M.H., Fu, H.Z. and Ho, Y.S., Comparison of universities' scientific performance using bibliometric indicators. *Malaysian Journal of Library & Information Science*, Vol. 16, Issue 2, Pages 1-19, 2011.
22. Ho, Y.S., "The top-cited research works in the Science Citation Index Expanded", *Scientometrics*, Vol. 94, Issue 3, Pages 1297-1312, 2013.
23. Hsu, Y.H.E. and Ho, Y.S., "Highly cited articles in health care sciences and services field in Science Citation Index Expanded: A bibliometric analysis for 1958-2012", *Methods of Information in Medicine*, Vol. 53, Issue 6, 446-458, 2014.
24. Ho, Y.S. and Mukul, S.A., "Publication performance and trends in mangrove forests: A bibliometric analysis", *Sustainability*, Vol. 13, Issue 22, Article Number: 12532, 2021.
25. Monge-Nájera, J. and Ho, Y.S., El Salvador publications in the Science Citation Index Expanded: subjects, authorship, collaboration and citation patterns. *Revista de Biología Tropical*, Vol. 65, Issue 4, Pages 1428-1436, 2017.
26. Ho, Y.S. and Hartley, J., "Classic articles in Psychology in the Science Citation Index Expanded: A bibliometric analysis", *British Journal of Psychology*, Vol. 107, Issue 4, Pages 768-780, 2016.
27. Khan, M.A. and Salah, K., "IoT security: Review, blockchain solutions, and open challenges", *Future Generation Computer Systems-the International Journal of eScience*, Vol. 82, Pages 395-411, 2018.
28. Yli-Huumo, J., Ko, D., Choi, S., Park, S. and Smolander, K., "Where is current research on blockchain technology? A systematic review", *PLoS ONE*, Vol. 11, Issue 10, 2016.
29. Andoni, M., Robu, V., Flynn, D., Abram, S., Geach, D., Jenkins, D., McCallum, P. and Peacock, A., "Blockchain technology in the energy sector: A systematic review of challenges and opportunities", *Renewable and Sustainable Energy Reviews*, Vol. 100, Pages 143-174, 2019.
30. Koizumi, S., Hasegawa, H., & Hashimoto, T. Ordered structures of block copolymer/homopolymer mixtures. 5. Interplay of macro-and microphase transitions. *Macromolecules*, Vol. 27, Issue 22, Pages 6532-6540, 1994.
31. Hashimoto, T., Kimishima, K., & Hasegawa, H., "Self-assembly and patterns in binary mixtures of SI block copolymer and PPO", *Macromolecules*, Vol. 24, Issue 20, Pages 5704-5712, 1991.
32. Jiang, Y., Lin, C., Yin, H., & Chen, Z., "A mutual authentication and privacy mechanism for WLAN security", *Wireless Communications and Mobile Computing*, Vol. 8, Issue 1, Pages 101-112, 2006.
33. Christidis, K. and Devetsikiotis, M., "Blockchains and smart contracts for the Internet of Things", *IEEE Access*, Vol. 4, Pages 2292-2303, 2016.
34. Tanaka, H., Hasegawa, H. and Hashimoto, T., "Ordered structure in mixtures of a block copolymer and homopolymers. 1. Solubilization of low-molecular-weight homopolymers", *Macromolecules*, Vol. 24, Issue 1, Pages 240-251, 1991.
35. Tschorsch, F. and Scheuermann, B., "Bitcoin and beyond: A technical survey on decentralized digital currencies", *IEEE Communications Surveys and Tutorials*, 18, Issue 3, Pages 2084-2123, 2016.

36. Giannoudis, P.V., Chloros, G.D. and Ho, Y.S. "A historical review and bibliometric analysis of research on fracture nonunion in the last three decades", *International Orthopaedics*, Vol. 45, Pages 1663-1676, 2021.
37. Ho, Y.S., "A bibliometric analysis of highly cited publications in Web of Science category of emergency medicine", *Signa Vitae*, Vol. 17, Issue 1, Pages 11-19, 2021.
38. Riesenber, D. and Lundberg, G.D., "The order of authorship: Who's on first", *JAMA-Journal of the American Medical Association*, Vol. 264, Issue 14, 1857, 1990.
39. SJR, "International Science Ranking", <https://www.scimagojr.com/>, July 22, 2023.
40. Beijing University of Posts and Telecommunications, "Apply Online | Study in China", <https://bupt.admissions.cn/>, July 22, 2023.
41. Thapar Institute of Engineering & Technology, "Top Engineering College in Punjab", <https://www.thapar.edu/>, July 23, 2023.
42. King Abdulaziz University, "Jeddah | Saudi Arabia Kingdom", <https://www.kau.edu.sa/>, July 22, 2023.
43. Ho, Y.S., "A bibliometric analysis of highly cited articles in materials science", *Current Science*, Vol. 107, Issue 9, Pages 1565-1572, 2014.
44. Saberi, S., Kouhizadeh, M., Sarkis, J. and Shen, L.J., "Blockchain technology and its relationships to sustainable supply chain management", *International Journal of Production Research*, Vol. 57, Issue 7, Pages 2117-2135, 2019.
45. Xu, L.D., Xu, E.L. and Li, L., "Industry 4.0: State of the art and future trends", *International Journal of Production Research*, Vol. 56, Issue 8, Pages 2941-2962, 2018.
46. Zheng, Z.B., Xie, S.A., Dai, H.N., Chen, X.P. and Wang, H.M., "Blockchain challenges and opportunities: A survey", *International Journal of Web and Grid Services*, Vol. 14, Issue 4, Pages 352-375, 2018.
47. Mengelkamp, E., Ganttner, J., Rock, K., Kessler, S., Orsini, L. and Weinhardt, C., "Designing microgrid energy markets. A case study: The Brooklyn Microgrid", *Applied Energy*, Vol. 210, Pages 870-880, 2018.
48. Reyna, A., Martín, C., Chen, J., Soler, E. and Díaz, M., "On blockchain and its integration with IoT. Challenges and opportunities", *Future Generation Computer Systems-the International Journal of eScience*, Vol. 88, Pages 173-190, 2018.
49. Aitzhan, N.Z. and Svetinovic, D., "Security and privacy in decentralized energy trading through multi-signatures, blockchain and anonymous messaging streams", *IEEE Transactions on Dependable and Secure Computing*, Vol. 15, Issue 5, Pages 840-852, 2018.
50. Li, Z.T., Kang, J.W., Yu, R., Ye, D.D., Deng, Q.Y. and Zhang, Y., "Consortium blockchain for secure energy trading in industrial Internet of Things", *IEEE Transactions on Industrial Informatics*, Vol. 14, Issue 8, Pages 3690-3700, 2018.
51. Kang, J.W., Yu, R., Huang, X.M., Maharjan, S., Zhang, Y. and Hossain, E., "Enabling localized peer-to-peer electricity trading among plug-in hybrid electric vehicles using consortium blockchains", *IEEE Transactions on Industrial Informatics*, Vol. 13, Issue 6, Pages 3154-3164, 2017.
52. Wang, C.C. and Ho, Y.S., "Research trend of metal-organic frameworks: A bibliometric analysis", *Scientometrics*, Vol. 109, Issue 1, Pages 481-513, 2016.
53. Quora, "Is blockchain completely secure", <https://www.quora.com/Is-blockchain-completely-secure>, October 8, 2023.
54. Nakamoto, S., "Bitcoin: A peer-to-peer electronic cash system", *Decentralized business review*, 2008.
55. Buterin v., *Ethereum Whitepaper*, 2013.
56. Investopedia, "Bitcoin vs. Ethereum: What's the Difference?", <https://www.investopedia.com/terms/b/bitcoin-vs-ethereum.asp>, October 3, 2023.
57. Ruparelia, N. B., "Cloud computing", *Mit Press*, 2023.
58. Zhou L, Cui T, Wang G et al, "Cssp: the consortium Blockchain model for improving the trustworthiness of network software services", In *proceedings of 2017 IEEE international symposium on parallel and distributed processing with applications and 2017 IEEE international conference on ubiquitous computing and Communications (ISPA/IUCC)*. IEEE 2017: Pages 101-107, 2017.

59. Li, W., Wu, J., Cao, J., Chen, N., Zhang, Q., & Buyya, R. Blockchain-based trust management in cloud computing systems: a taxonomy, review and future directions. *Journal of Cloud Computing*, Vol. 10, Issue 1, Pages 1-34, 2021.
60. Google, "Google Trends", <https://trends.google.com/>, October 3, 2023.
61. Hua, H., Li, Y., Wang, T., Dong, N., Li, W., & Cao, J., "Edge computing with artificial intelligence: machine learning perspective", *ACM Computing Surveys*, Vol. 55, Issue 9, Pages 1-35, 2021.
62. Digital Citizen, "What are P2P (peer-to-peer) networks and what are they used for?", <https://www.digitalcitizen.life/what-are-p2p-peer-peer-networks-and-what-are-they-used/>, October 8, 2023.
63. Coin Academy, "Homepage", <https://coinacademy.fr/>, October 8, 2023.
64. Zhan, Z., & Huang, R. (2023). Improvement of Hierarchical Byzantine Fault Tolerance Algorithm in RAFT Consensus Algorithm Election. *Applied Sciences*, Vol. 13, Issue 16, 9125.
65. Micali, S., Rabin, M., Kilian, J., "Zero-knowledge sets", 44th Annual IEEE Symposium on Foundations of Computer Science, Pages 80-91, IEEE, 2003.
66. Nguyen, C. T., Hoang, D. T., Nguyen, D. N., Niyato, D., Nguyen, H. T., & Dutkiewicz, E. (2019). Proof-of-stake consensus mechanisms for future blockchain networks: fundamentals, applications and opportunities. *IEEE access*, Vol. 7, Pages 85727-85745.
67. CoinDesk, "Sustainable Blockchains: The Future of Eco-Friendly Business Practices", <https://www.coindesk.com/>, October 18, 2023
68. Tiwari, M. G. D., & Kumar, K. A., "Decentralization System Using Smart Blockchain with Secure Hash" *SN Computer Science*, Vol. 4, Issue 5, Pages 620, 2023.
69. National Geographic, "Ecosystem", <https://www.nationalgeographic.org/encyclopedia/ecosystem/>, October 18, 2023.
70. Yue, X., Wang, H., Jin, D., Li, M., & Jiang, W., "Healthcare data gateways: found healthcare intelligence on blockchain with novel privacy risk control", *Journal of medical systems*, Vol. 40, Pages 1-8, 2016.
71. Buterin, V. (2016). *Ethereum: platform review. Opportunities and Challenges for Private and Consortium Blockchains*, 45.
72. Qu'est-ce qu'un algorithme de consensus sur la blockchain? (coinacademy.fr), visited the October 14th, 2023
73. What is cryptocurrency and how does it work? (kaspersky.com), visited at October 16th, 2023
74. William Mougayar, 2016, *Blockchain Security is Multi-Layered, Here are the 6 Most Important Levels*.
75. Marny Lopez, *Blockchains, how do they work and how do i implement one? | LinkedIn*, cenfotec university, Costa Rica, visited the 06/11/2024
76. Nasr-El-dein Gad, W., Sayed Moawad, T.M., "Testing The Impact of Blockchain Technology on The Internal Control Quality in Non-Financial Companies Listed on The Egyptian Stock Exchange", *Egyptian Journal of Business Studies*, Vol. 48, No. 4, Pages 625-650, 2024.
77. Wylde, V., Rawindaran, N., Lawrence, J., Balasubramanian, R., Prakash, E., Jayal, A., Platts, J., "Cybersecurity, data privacy and blockchain: A review", *SN Computer Science*, Vol. 3, No. 2, Pages 127, 2022.



ULUSLARARASI 3B YAZICI TEKNOLOJİLERİ  
VE DİJİTAL ENDÜSTRİ DERGİSİ

INTERNATIONAL JOURNAL OF 3D PRINTING  
TECHNOLOGIES AND DIGITAL INDUSTRY

ISSN:2602-3350 (Online)

URL: <https://dergipark.org.tr/ij3dptdi>

# FINITE ELEMENT ANALYSIS AND PRODUCTION OF A BALANCE ROBOT DESIGNED TO BE USED IN THE FIELD OF ADVERTISING

**Yazarlar (Authors):** Yusuf Coşkun<sup>ID</sup>\*, Diyar Can Aydın<sup>ID</sup>, Halil Aktöz<sup>ID</sup>, Lale Özyılmaz<sup>ID</sup>

**Bu makaleye şu şekilde atıfta bulunabilirsiniz (To cite to this article):** Coşkun Y., Aydın D. C., Aktöz H., Özyılmaz L., "Finite Element Analysis and Production of a Balance Robot Designed to be Used in the Field of Advertising" *Int. J. of 3D Printing Tech. Dig. Ind.*, 9(1): 114-121, (2025).

DOI: 10.46519/ij3dptdi.1575667

Araştırma Makale/ Research Article

Erişim Linki: (To link to this article): <https://dergipark.org.tr/en/pub/ij3dptdi/archive>

# FINITE ELEMENT ANALYSIS AND PRODUCTION OF A BALANCE ROBOT DESIGNED TO BE USED IN THE FIELD OF ADVERTISING

Yusuf Coşkun<sup>a</sup><sup>\*</sup>, Diyar Can Aydın<sup>a</sup>, Halil Aktoz<sup>a</sup>, Lale Özyılmaz<sup>a</sup>

<sup>a</sup>Istanbul Health and Technology University, Faculty of Engineering and Natural Sciences, Department of Mechatronic Engineering, TURKEY

\* Corresponding Author: [yusuf.coskun@istun.edu.tr](mailto:yusuf.coskun@istun.edu.tr)

(Received: 29.10.24; Revised: 03.02.25; Accepted: 04.04.25)

---

## ABSTRACT

This study presents the finite element analysis and prototype development of a self-balancing robot designed for applications in the advertising sector. The structural behavior and dynamic properties of the robot were analyzed using static, modal, and rigid body simulations in ANSYS software. Static analysis confirmed the mechanical durability of the robot by evaluating the forces acting on the motors and body, while modal analysis identified potential resonance conditions. Notably, in the third vibration mode, a deformation of 330.24 mm at 52.169 Hz was observed, indicating a critical resonance issue. To enhance structural efficiency, topology optimization was applied to the outer casing, resulting in a 14% reduction in mass (from 0.45392 kg to 0.39069 kg) while maintaining structural integrity. During the experimental phase, the prototype successfully demonstrated autonomous movement using integrated distance sensors. However, initial tests revealed a wobbling motion due to insufficient motor power, which will be addressed in future iterations by incorporating higher-torque motors. The proposed robot has the potential to serve as an interactive advertising tool, capable of attracting attention through dynamic motion and engaging promotional content display. Future work will focus on enhancing stability and refining control algorithms to improve performance in real-world advertising environments.

**Keywords:** Self-Balancing Robot, Finite Element Analysis, Topology Optimization, Advertising.

---

## 1. INTRODUCTION

Balance robots stand out as a significant advancement in the field of robotics. These robots have the ability to balance on two wheels and typically maintain stability and movement using PID control algorithms. These algorithms regulate the speed and direction of the motors to ensure the robot remains in equilibrium [1].

Self-balancing robots, a subset of mobile robots, are designed to maintain dynamic balance using control theory principles, often modeled as an inverted pendulum. Their ability to remain upright while navigating various terrains makes them ideal for applications requiring both balance and mobility, such as personal transporters and service robots. Among the different configurations, two-wheeled models are the most common, utilizing horizontally positioned wheels and control

algorithms like PID controllers to ensure stability [2,3].

Spherical self-balancing robots, which operate on a single sphere, provide exceptional maneuverability and dynamic balance adjustments. These robots are classified not only by their physical structure but also by their control strategies, incorporating advanced techniques such as fuzzy logic and reinforcement learning [4]. Beyond mobility and service applications, their autonomous navigation and balancing capabilities open new possibilities in the advertising industry, enabling dynamic and interactive promotional strategies. [5].

Robotic applications in advertising are expanding, particularly with the integration of service robots into marketing strategies. A notable example is the deployment of multiple

robots for distributed questionnaire services at tourist sites and exhibitions, enhancing visitor engagement while simultaneously collecting valuable consumer data to optimize marketing strategies [6].

Moreover, the development of marketing systems that integrate robots with smartphones has been explored, highlighting the synergy between mobile technology and robotics in creating interactive advertising experiences. These systems enable real-time customer engagement and feedback, further enhancing the effectiveness of marketing campaigns [7]. This technological integration allows for a more personalized advertising approach, tailored to individual consumer preferences and behaviors.

In the hospitality sector, consumer acceptance of service robots is influenced by factors such as innovativeness and personal norms, underscoring the importance of marketing strategies that address psychological and social dynamics. Likewise, the adoption of service robots in advertising aligns with broader robotics trends, particularly the rise of collaborative robots ("cobots"), which enhance efficiency by working alongside humans in marketing operations [8,9].

Recent studies indicate that social robots in public spaces, such as shopping malls, function as effective advertising tools by engaging users and distributing promotional materials. Research suggests that adapting their communication styles enhances their effectiveness, making them more engaging and impactful than traditional advertising methods [10,11]. Self-balancing robots are expanding beyond conventional roles, evolving from interactive kiosks into dynamic promotional tools in marketing and retail. Their ability to enhance customer engagement, personalize experiences, and simulate human-like interactions makes them increasingly valuable in advertising applications [12].

Additionally, their autonomous navigation enables direct product delivery, optimizing the shopping experience and efficiency [13]. The marketing potential of self-balancing robots goes beyond mobility, offering creative branding opportunities. They can be customized with brand colors and logos, transforming into mobile advertisements that attract consumer

attention [14]. Their interactive capabilities, such as voice and visual engagement, enhance brand recall and create memorable experiences. Utilizing these robots in promotional events and experiential marketing campaigns can significantly boost consumer engagement and drive sales [15].

Self-balancing robots, traditionally used for mobility and personal transportation, are now emerging as dynamic tools in advertising. Their ability to navigate autonomously, engage users interactively, and serve as mobile promotional platforms offers a significant advantage over static advertising methods. By integrating robotics with marketing strategies, these robots enhance consumer engagement, brand visibility, and personalized advertising experiences. This study highlights the potential of self-balancing robots to transform conventional advertising approaches, making them a valuable asset in modern marketing.

## 2. MATERIAL AND METHODS

This study presents the design and fabrication of a two-wheeled self-balancing robot optimized for advertising applications. Stability and durability were ensured through a 3D model, followed by static, modal, and rigid body dynamics analyses in ANSYS. Static analysis assessed mechanical strength, modal analysis identified natural frequencies to prevent vibrations, and rigid body dynamics simulated real-world motion for smooth indoor operation. Topology optimization reduced the robot's mass by 14%, enhancing mobility while preserving structural strength. Polylactic Acid (PLA) was chosen for its lightweight, cost-effectiveness, and aesthetic appeal, as well as its biodegradable nature, supporting sustainable marketing solutions. Designed as an interactive advertising platform, the robot features dynamic mobility and customizable content display. Manufacturing utilized FDM 3D printing for high-quality, rapid production. Optimized printing parameters included a 0.4 mm nozzle diameter, 0.2 mm layer height, and 30% infill density. A print speed of up to 600 mm/sec significantly reduced production time, while an extrusion temperature of 200°C and a print bed temperature of 60°C ensured dimensional stability and minimized errors.

**2.1. Design**

The mechanical design of the robot was modeled using Autodesk Inventor software. The main body was carefully designed with a balanced structure, ensuring that the center of gravity remains between the wheels to enhance stability and maneuverability during movement. To ensure robustness, studs and mounting elements were meticulously selected to keep all components securely in place.

PLA was specifically selected for this application as it offers sufficient mechanical strength while remaining lightweight, thereby reducing the load on the motors and improving energy efficiency. Additionally, its smooth surface finish enhances the aesthetic appeal, making it particularly suitable for advertising applications. Since the robot is intended for indoor use, PLA’s moderate thermal resistance and biodegradability further support its suitability for this project. The image of the designed model is presented in Figure 1 with enhanced resolution for improved clarity.

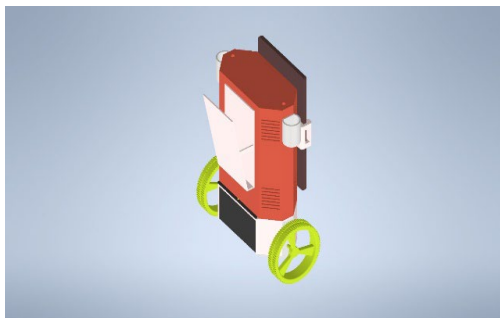


**Figure 1.** Designed model of the self-balancing robot

**2.2. Static Analysis**

The forces applied to the motors and the body in the motion joint of the robot and the forces that may occur during the movement are discussed in detail within the scope of static analysis. Stress, strain and deformation results were carefully calculated in line with the effects of these forces. This study is a basic reference for ensuring the mechanical durability of the snake robot and optimizing the design. In line with the calculations performed using PLA material during the analysis process, the physical prototype will also be built using PLA material during the production phase of the design. Table 1 presents the main properties of PLA material.

**Table 1.** The properties of PLA [16].

Properties	Units	Values
Density	$g/cm^3$	1.24
Tensile Strength	$MPa$	45-65
Elongation at Break	%	5-10
Young’s Modulus	$GPa$	2.7-16
Coefficient of Thermal Expansion	$\mu m/m \cdot K$	68-72

The boundary conditions applied to the robot model are given in Figure 2.

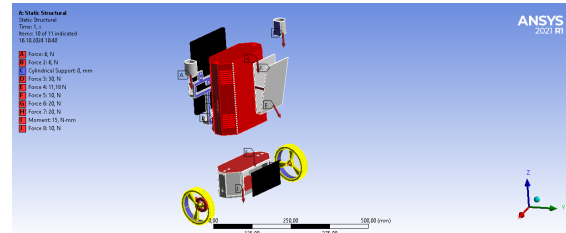


**Figure 2.** Boundary conditions defining constraints and external forces on the robot model

After applying these boundary conditions, total deformation, strain and stress results were obtained. These results are presented in Figures 3, 4 and 5, respectively.

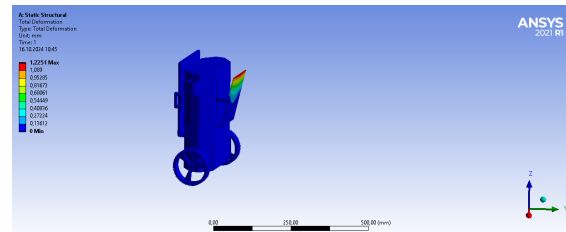


**Figure 3.** Total deformation results of the robot model

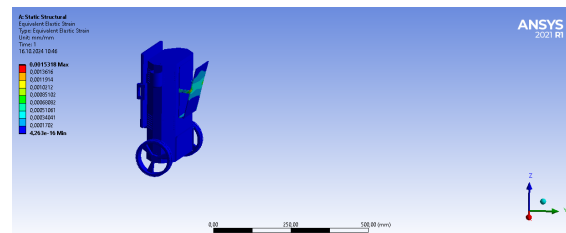


**Figure 4.** Strain distribution in the robot model

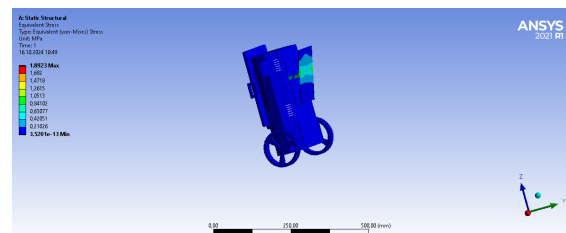


**Figure 5.** Stress distribution in the robot model

The total deformation, stress and strain values obtained as the output of the analysis results are presented in Table 2.

**Table 2.** Results of static analysis

Results	Units	Values
Total Deformation	mm	1.2251
Elastic Strain	Mm	0.0015
Stress	MPa	1.8923

**2.3. Modal Analysis**

A modal analysis was performed to evaluate the dynamic vibration characteristics and structural integrity of the robot. This analysis aims to examine the possible vibration effects on the structure by determining the natural vibration modes and frequencies of each component. The forces due to the motors and other forces that may occur during motion were evaluated. In this way, an important guide is provided to secure and optimize the mechanical stability of the robot. The analysis results obtained provide a better understanding of the flexibility and dynamic behavior of the robot and provide a basic reference for improvements to be made in the design process. The total deformation result for the first mode value are presented in Figure 6.

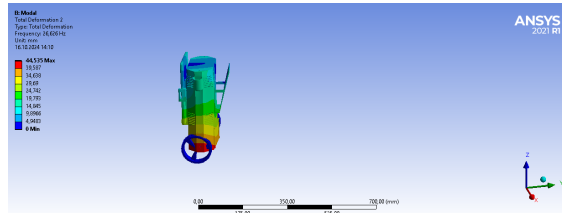


**Figure 6.** First mode shape and corresponding natural frequency of the robot model

As a result, a total of 6 mode values were obtained. Each mode has different frequency values and different deformation values depending on these frequencies. The results are presented in Table 3.

**Table 3.** Modal analysis results with natural frequencies and deformations.

Mode	Frequency(Hz)	Deformation(mm)
1	0,03	23,701
2	26,626	44,535
3	52,169	330,24
4	98,793	514,93
5	101,39	145,98
6	118,09	271,92

**2.4. Rigid Analysis**

A rigid analysis was performed to predict the motion of the robot. This analysis was performed to simulate the joint motion of the robot under certain moment values, to understand how the robot will react under real-world conditions and to determine the necessary measures to stabilize the motion. Furthermore, this analysis, performed before prototype production, helps to identify potential errors and opportunities for performance improvement that may arise during the design process. The result of a 600 mm movement on a flat surface is shown in Figure 7.

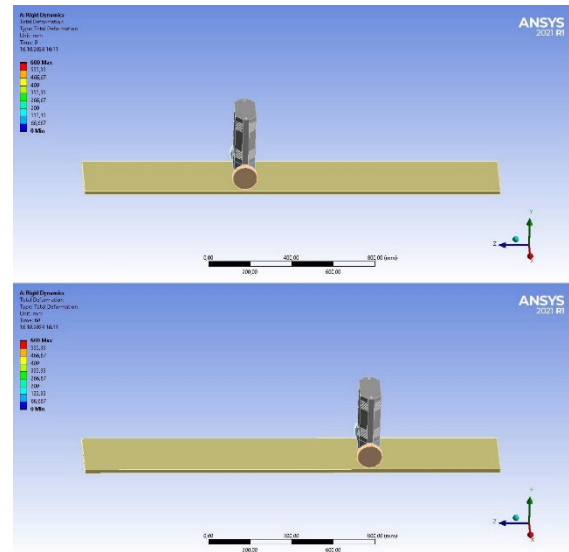


**Figure 7.** Rigid body analysis simulation of the robot model

**2.5. Topology Optimization**

Topology optimization (TO) is a computational design technique that seeks to optimize the material layout within a given design space, subject to specified loads and boundary conditions. This method allows for significant flexibility in structural design, enabling both topological and geometrical changes to achieve high-performance structures [17]. The foundational concept of TO was introduced by Bendsøe and Kikuchi in 1988, and since then, it has evolved into a robust field of study with numerous applications across various engineering disciplines [18,19].

In the outer mold of the robot, topology optimization was performed for mass and volume reduction. In the optimization process, PLA (Polylactic Acid) was selected as the material used and these material properties were assigned to the part to be optimized. In this

study, the initial part mass of 0.45392 kg was reduced to 0.39069 kg at the end of the optimization process. This optimization, which was achieved after 27 iterations in total, resulted in a mass reduction of approximately 14%.

Topology optimization is based on the principle of using only the necessary material and reducing unnecessary masses by improving the part geometry. In this process, the mechanical properties and strength of the part are preserved, increasing productivity, especially in the production process, and improving the overall performance of the robot. The results obtained show that a lighter and more optimized structure can also contribute to a reduction in production costs and energy savings. The appearance of the part before the topology optimisation is presented in Figure 8 and the final version after the optimisation process is presented in Figure 9. These two figures provide an opportunity to visually compare the mass reduction and structural improvements in the part as a result of the optimisation process.



Figure 8. Robot model before topology optimization

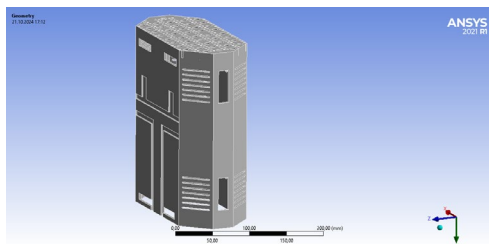


Figure 9. Robot model after topology optimization

The total deformation, stress and strain values obtained as a result of the optimisation are compared in a table for the pre- and post-optimisation cases. This table was created in order to analyse in detail the mechanical effects of structural changes on the part. The differences between the deformation, stress and strain values show the contribution of the optimisation to the performance and the improvements in part strength. These results are given in Table 4.

Table 4 (A: Elastic Strain (mm), B: Stress (MPa), C: Total Deformation (mm), D: Weight (Kg) shows the comparison table of the model before and after optimization.

**Table 4. Comparison Table**

Target Variable	A	B	C	D
Before Optimization	0,0007	1,064	0,007	0.45
After Optimization	0,0014	2,299	0,021	0,39

The total deformation image of the model obtained as a result of topology optimisation is presented in Figure 10, stress distribution image in Figure 11 and strain distribution image in Figure 12. These images clearly show the effects of the optimisation process on the mechanical performance of the model and provide the opportunity to visually analyse how critical parameters such as deformation, stress and strain are distributed on the part.

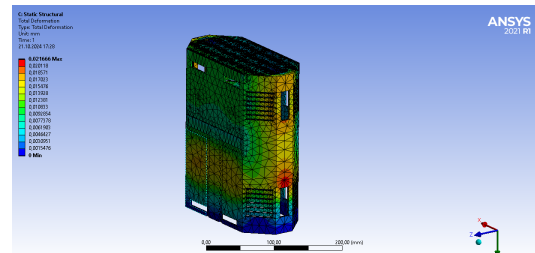


Figure 10. Total deformation results after topology optimization



Figure 11. Stress distribution after topology optimization

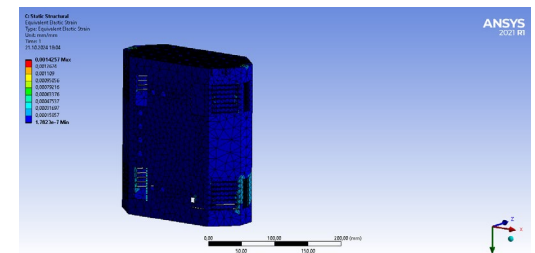


Figure 12. Strain distribution after topology optimization

### 3. EXPERIMENTAL FINDINGS

#### 3.1. Mechanical Design

Various robotic configurations, such as four-wheeled and spherical robots, are widely used in different applications. However, a two-wheeled self-balancing design was chosen for its compact structure, high maneuverability, and dynamic interaction potential. While four-wheeled robots offer stability but require larger turning radii, spherical robots allow omnidirectional movement but face stability and control challenges. In contrast, the two-wheeled configuration enables agile and engaging movement, making it ideal for promotional settings.

The prototype was fabricated using 3D-printed PLA material and designed for advertising applications. It includes pen holders on the sides, a brochure pocket at the back, and a front-mounted screen for promotional displays. A sensor slot allows obstacle detection during autonomous movement, while rubber strips on the wheels enhance traction. These features collectively enhance the robot's effectiveness as an interactive and attention-grabbing promotional tool. The front view of the prototype is shown in Figure 13 and the rear view is shown in Figure 14.



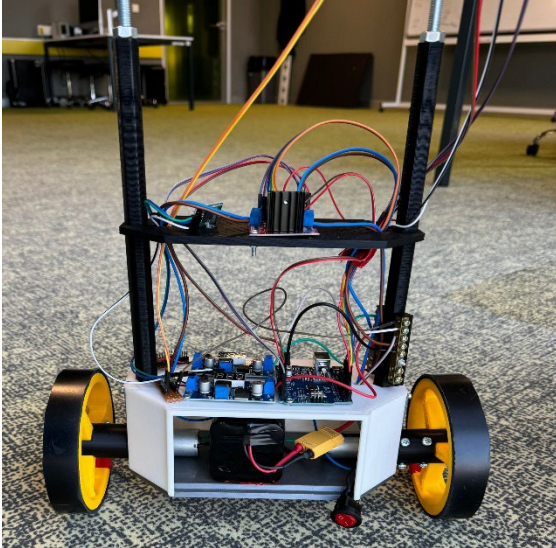
Figure 13. Front view of the manufactured prototype



Figure 14. Rear view of the manufactured prototype

#### 3.2. Electronic Design

Two motors, a Bluetooth module, a motor driver board, distance sensors, an Arduino and MPU67 integration were used in the electronics of the prototype. The motors are used to provide the mobility of the robot and the two motors control the movement direction and speed of the robot. The Bluetooth module is used to provide wireless communication between the robot and external devices so that the user can remotely control the robot or perform data transfer. The motor driver board regulates the current and voltage required for the control of the motors, ensuring the correct operation of the motors. Distance sensors are used to prevent collisions during autonomous movement by detecting obstacles around the robot, and the sensors provide data to guide the robot's movement. The Arduino acts as the robot's control unit, integrating all components and controlling the movement of the motors by processing data from the sensors. The MPU67 is used to track the robot's position and movement, and this integration supports the robot's balance and guidance systems, increasing its autonomous movement capabilities. These components are integrated to enhance the robot's autonomous movement capabilities and to enable it to detect environmental obstacles and steer effectively. The electronic connections of the robot are given in Figure 15.



**Figure 15.** Electronic assembly

#### 4. RESULTS

This study presents the finite element analysis and prototype fabrication of a two-wheeled self-balancing robot for advertising applications. Structural evaluations using static, modal, and rigid body analyses confirmed mechanical integrity, though modal analysis identified a resonance deformation of 330.24 mm at 52.169 Hz, highlighting the need for improved stability. Topology optimization reduced mass by 14% without compromising strength, enhancing material efficiency.

Experimental tests revealed significant yawing motion due to insufficient motor torque and suboptimal PID control parameters. Future improvements will focus on optimizing PID gains, integrating higher-torque motors, and exploring adaptive control strategies for enhanced stability. While the prototype demonstrated autonomous functionality, further studies are needed to assess performance in real-world environments, such as outdoor or crowded spaces, and to improve sensor integration for better maneuverability.

Unlike conventional self-balancing robots designed for mobility or industrial use, this study introduces a novel application in advertising. The robot features a digital display, brochure compartments, and interactive elements, making it a dynamic promotional tool. Additionally, topology optimization has improved energy efficiency. Future advancements, including AI-driven balance algorithms and adaptive control, will further enhance functionality and commercial viability,

contributing to both engineering analysis and practical applications.

#### ACKNOWLEDGES

This project was supported by the application numbered 1919B012335179 within the scope of TÜBİTAK 2209-A University Students Research Projects Support Programme 2023 second term.

#### REFERENCES

1. Mudeng, V., Hassanah, B., Priyanto, Y. T. K., & Saputra, O., "Design and simulation of two-wheeled balancing mobile robot with pid controller", *International Journal of Sustainable Transportation Technology*, Vol. 3 Issue 1, Pages 12-19, 2020.
2. Sujiwa, A. and Suhadata ., "Design and construction of a self balancing robot using long range control based on nrf24l01", *BEST : Journal of Applied Electrical, Science, & Technology*, Vol. 5, Issu 2, Pages 34-37, 2023
3. Nguyen, P., Nguyen, V., Cu, M., Nguyen, M., Trinh, M., Hoang, D., ... & Hoang, D., "Pid controller for balancing one-wheeled self-balancing robot", *Robotica & Management*, Vol. 27 Issue 1, Pages 23-27, 2022
4. Ruan, X., Dynamic modeling and nonlinear control of spherical-wheeled robot. *DEStech Transactions on Computer Science and Engineering*, (CCNT), 2018.
5. Yan, J. and Yang, H., "Hierarchical reinforcement learning based self-balancing algorithm for two-wheeled robots", *The Open Electrical & Electronic Engineering Journal*, Vol. 10 Issue 1, Pages 69-79, 2016.
6. Narita, M., Aoki, D., Miyauchi, M., Nakagawa, S., Tsuchiya, Y., & Matsuhira, N. Demonstration experiments of a distributed questionnaire service using multiple robots with the aim of marketing at a tourist site. *International Journal of Smart Computing and Artificial Intelligence*, Vol. 2 Issue 1, Pages 1-21, 2018.
7. Nakagawa, D., Akutsu, H., Furuta, N., Yasuda, K., Takahashi, K., Watase, M., ... & Narita, M. Marketing system utilizing a robot and smartphone. *2015 IEEE/SICE International Symposium on System Integration (SII)*, Pages 662-66, 2015..
8. Han, H., Kim, S. I., Lee, J., & Jung, I. Understanding the drivers of consumers' acceptance and use of service robots in the hotel industry. *International Journal of Contemporary Hospitality Management*, Vol. 37, Issue 2, Pages 541-559, 2024.

9. Knudsen, M. S. and Kaivo-oja, J. Collaborative robots: frontiers of current literature. *Journal of Intelligent Systems: Theory and Applications*, Pages 13-20, 2020.
10. Sakaguchi, T., Okafuji, Y., Matsumura, K., Baba, J., & Nakanishi, J. An estimation framework for passerby engagement interacting with social robots, 2022.
11. Okafuji, Y., Ozaki, Y., Baba, J., Nakanishi, J., Ogawa, K., Yoshikawa, Y., ... & Ishiguro, H. Behavioral assessment of a humanoid robot when attracting pedestrians in a mall. *International Journal of Social Robotics*, Vol. 14, Issue 7, Pages 1731-1747, 2022.
12. Pertiwi, K., Agustian, A., Silitonga, J., Sinaga, H., Siahaan, F., Silverius S, H., ... & Joni, J. Perbandingan metode kontrol p, pd, pi, dan pid pada robot self-balancing beroda dua. *Briliant: Jurnal Riset Dan Konseptual*, Vol. 9, Issue 1, Pages 214, 2024.
13. González-Jiménez, H. Taking the fiction out of science fiction: (self-aware) robots and what they mean for society, retailers, and marketers. *Futures*, Vol. 98, Pages 49-56, 2018.
14. Qu, B. Development space and prospects of self-balancing car. *Highlights in Science, Engineering and Technology*, Vol. 46, Pages 42-48, 2023.
15. Zhang, Y., Song, Y., Lu, F., Zhang, D., Yang, L., Cui, T., & Zhang, K. Design and experiment of greenhouse self-balancing mobile robot based on PR joint sensor. *Agriculture*, Vol. 13, Issue 10, Pages 2040, 2023.
16. Letcher, T., & Waytashek, M., "Material property testing of 3D-printed specimen in PLA on an entry-level 3D printer", In *ASME International Mechanical Engineering Congress and Exposition*, Vol. 46438, Pages V02AT02A014, November 2014. American Society of Mechanical Engineers.
17. Koçak, M. T., & Bayraklılar, M. S. Mechanical shaft optimization: A study on static structural analysis and topological optimization in ANSYS. *International Journal of 3D Printing Technologies and Digital Industry*, Vol. 7, Issue 3, Pages 541-549, 2023.
18. Nishiwaki, S. and Terada, K. (2017). Advanced topology optimization. *International Journal for Numerical Methods in Engineering*, Vol. 113, Issue 8, Pages 1145-1147.
19. Chuang, C., Chen, S., Yang, R., & Vogiatzis, P. (2017). Topology optimization with additive manufacturing consideration for vehicle load path development. *International Journal for Numerical Methods in Engineering*, Vol. 113, Issue 8, Pages 1434-1445.



ULUSLARARASI 3B YAZICI TEKNOLOJİLERİ  
VE DİJİTAL ENDÜSTRİ DERGİSİ

INTERNATIONAL JOURNAL OF 3D PRINTING  
TECHNOLOGIES AND DIGITAL INDUSTRY

ISSN:2602-3350 (Online)

URL: <https://dergipark.org.tr/ij3dptdi>

# INVESTIGATION TO THE V-I CHARACTERISTICS OF ROGOWSKI COILS WITH MAGNETIC FILAMENTS BY REGRESSION ANALYSIS

**Yazarlar (Authors):** Gizem Merve Aydın<sup>ID</sup>, Gülsüm Yıldırım<sup>ID</sup>, Emin Yıldırım<sup>ID\*</sup>

**Bu makaleye şu şekilde atıfta bulunabilirsiniz (To cite to this article):** Aydın G. M., Yıldırım G., Yıldırım E., "Investigation to the V-I Characteristics of Rogowski Coils with Magnetic Filaments by Regression Analysis" *Int. J. of 3D Printing Tech. Dig. Ind.*, 9(1): 122-128, (2025).

DOI: 10.46519/ij3dptdi.1654785

Araştırma Makale/ Research Article

Erişim Linki: (To link to this article): <https://dergipark.org.tr/en/pub/ij3dptdi/archive>

# INVESTIGATION TO THE V-I CHARACTERISTICS OF ROGOWSKI COILS WITH MAGNETIC FILAMENTS BY REGRESSION ANALYSIS

Gizem Merve Aydın<sup>a</sup>, Gülsüm Yıldırım<sup>b</sup>, Emin Yıldırım<sup>c\*</sup>

<sup>a</sup>Sakarya Electricity Distribution Inc., TÜRKİYE

<sup>b</sup>Duzce University, Duzce Vocational School, Electricity Program, TÜRKİYE

<sup>c</sup>Duzce University, Faculty of Engineering, Electrical-Electronics Engineering Department, TÜRKİYE

\* Corresponding Author: [emin yıldırım@duzce.edu.tr](mailto:emin yıldırım@duzce.edu.tr)

(Received: 10.03.25; Revised: 08.04.25; Accepted: 11.04.25)

## ABSTRACT

The efficiency and magnetic saturation performances of the 3D printed magnetic composite cores are currently a bit far from competing with silicon steel in traditional motor topologies and transformer applications. However, the flexibility provided in 3D design and the rapid advancement in the production technologies are rapidly reducing the gap between these performances. Linear V-I characteristics can be obtained in the 3D printing magnetic cores using the filaments produced by mixing magnetic powders such as Iron, Nickel, Cobalt with polymer in different ratios. This makes them suitable for the Rogowski Coil (RC) applications. RCs are required to have linear V-I characteristics in order to measure low and high currents with the same sensitivity in the defined current measurement range. In this paper, nickel-filled filaments produced by mixing nickel and polymer in different ratios were used for the production of flexible RC cores. The V-I characteristics of RCs produced using 40% and 60% nickel-filled filaments and air-core RC have been modeled using the linear regression analysis. The success of the mathematical models has also been tested with four different error analyses. The proven mathematical models of the RCs will provide new inspiration to the researchers for magnetic applications. Optimal RC designs can be investigated using the mathematical models in the Finite Element Analysis (FEA) package programs.

**Keywords:** Nickel-Filled Filament, Flexible Magnetic Core, Rogowski Coil.

## 1. INTRODUCTION

In many electric motors and transformers used today, since magnetic fluxes move in two axes, oriented or non-oriented silicon steels are used as core material. In addition, soft magnetic composite (SMC) cores are also used in complex geometry or innovative electrical machine designs due to their 3D magnetic flux paths [1-3]. The eddy current losses of the SMC cores are lower than the cores formed by packing silicon steels due to particulate structure of SMCs. The stator or rotor core of any motor can be obtained after the silicon steels is cut with a mold or laser, aligned appropriately, pressed, riveted, welded, etc. On the other hand, an SMC core produced by additive manufacturing can be produced in a single process. On the other hand, an SMC core produced by additive manufacturing can be produced in a single process. In addition, the use

of SMC provides designers with flexibility for the development of new core models. Iron-cobalt (FeCo), iron-nickel (FeNi) and iron-silicon (FeSi) alloys are generally used in SMCs produced by additive manufacturing [4]. The costs and production methods of electromagnetic materials produced by additive manufacturing used in the electrical machines are explained comparatively in [5].

The magnetic saturation points of 3D printed SMC cores are lower than silicon steels. Experimental results of two 10W axial flux PM machines produced from grain-oriented (GO) steel and 3D printed SMC cores are compared in [6]. Accordingly, the SMC core model produced less torque at the same electrical loading, and also hysteresis losses should be taken into account. According to the experimental results presented in [7], the

efficiency of the laser additively manufactured core induction motor is 2/3 of the efficiency of the reference conventional induction motor. The thermal dissipation performance of SMC is also lower than that of the laminated electrical steels [8]. These results show that 3D printed SMCs are not yet ready for use in the conventional motor and transformer applications, but rapid progress is being made.

The transformer cores were printed with Rustable Magnetic Iron filament consisting of a polymer matrix and a particulate phase of 40 wt% iron in [9]. Transformer cores were produced with 3D printing in different patterns and filling ratios and all of them have a linear V-I characteristic. According to these results, the magnetic filaments are useful for the RC applications where linear magnetic characteristics are required.

RCs are long-known current measuring devices that do not use high permeability magnetic cores, unlike current transformers. Their areas of use have become widespread with advanced signal processing techniques in recent years [10]. The secondary windings are wound on a hollow silicone rubber case in traditional RCs [11]. Since conventional RCs do not have saturation problems, they can measure both nominal current and currents well above nominal current with the same accuracy. Unlike current transformers, they have a linear V-I characteristic with their air-core structure [12]. They are low cost. They can operate in wide bands from a few Hz to a few MHz. Therefore, they are frequently used in the measurement of high currents and transient pulses [13-16].

Like traditional RCs, Printed Circuit Board (PCB) RCs are also air-core. PCB RCs are used not only for high currents [17] but also for monitoring switching states [18]. The secondary output signals are small in the measurement of small currents, since the magnetic permeability in air-core RCs is very low. In order to process low amplitude signals, their amplitudes need to be increased [19]. For this, the RC output signal can be connected to an active integrator circuit [20]. The integrator circuit can be an inverting or non-inverting integrator [21]. Apart for these, the hybrid integrator can be also used to reduce the measurement noises [22]. However, since error signals can also be amplified at the outputs of

the amplifiers, it is important for measurement accuracy that the main signal is high. In order to eliminate this drawback, the use of three different superparamagnetic magnetite cores has been proposed in [23]. The use of magnetic powders and production technologies affect production costs to a certain extent. However, progress in the additive manufacturing technology is exciting and costs are expected to decrease as application areas become more widespread. Three different rigid RCs have been obtained by placing 50-100 nm  $\text{Fe}_3\text{O}_4$  commercial magnetite powder, 5  $\mu\text{m}$   $\text{Fe}_3\text{O}_4$  commercial magnetite powder and synthetic magnetite ( $\text{Fe}_3\text{O}_4$ ) in the inner cavity of the RC case produced from polymer with a 3D printer. The researchers concluded that synthetic magnetite Nano powder is the best solution because it maintains its linearity up to high current values. However, the lack of flexibility of the RCs tested in this paper was ignored. A flexible RC has been developed by developing a composite magnetic core with manganese-zinc ferrite + permalloy + silicone rubber in [24]. However, no information was presented about the V-I characteristics of the flexible core RC.

In this paper, the V-I characteristics of flexible core RCs produced by directly use of nickel-filled filaments have been investigated. Taking into account measurement errors, the regression analysis has been performed for each produced RCs, and the mathematical models of the RCs have been derived. The error analyses and comparative results of the mathematical models based on linear regression have been shared.

## 2. PRODUCTION OF THE MAGNETIC CORE RCs

A combination of Polylactic Acid (PLA) or polymer derivatives with ferromagnetic powders can be used to produce flexible magnetic cores. For example, the filaments produced using PLA+Iron are often encountered in applications such as magnetic and biomedical devices [25]. In this paper, magnetic core RCs with flexibility like traditional RCs have been used. The magnetic properties of the filaments produced by adding iron, nickel or cobalt to the polymer can be increased. According to [26], the average particle size of the magnetic nanoparticles affects the magnetic properties of the filaments. In this paper, the magnetic filaments obtained

using polymer with different alloy ratios and nickel filler with particle sizes up to 44  $\mu\text{m}$  have been used to obtain the flexible magnetic cores. A single screw extrusion machine with a 2 mm nozzle has been used to produce nickel alloy filaments. Extra care should be taken to ensure homogeneous production in the extrusion process of filaments with metal particles. Thus, a uniform magnetic flux density can be achieved in the magnetic filament. In addition, the use of metal particles with high thermal conductivity may cause uneven cooling of the filament coming out of the nozzle [27]. So, a homogeneous filament production is important for thermal and magnetic performance.

For this reason, the filament production temperature has been kept in the range of 210-220  $^{\circ}\text{C}$ . Magnetic filaments with a diameter of 1.75 mm have been obtained with constant tension at the nozzle exit. Before the production, a drying process was carried out at 80  $^{\circ}\text{C}$  for 6 hours to remove moisture from both the nickel fillings and the polymer material. A part of the produced nickel alloy filament is seen in Figure 1a. These filaments have been placed inside 1.2 mm thick plastic sheath of the RC without any further processing. Then, a secondary winding of 825 turns has been formed on the flexible magnetic RC core using 0.4 mm diameter H type enameled copper wire (Figure 1b). After the aluminum shielding has been applied on the windings, an insulating strip has been drawn for physical protection. The final RCs obtained are shown in Figure 1c. The outer diameter of the developed RCs is 140 mm and the inner diameter is around 114 mm.

Using the magnetic filaments produced with 40% and 60% nickel filling, two flexible core RCs and one air-core RC with the same physical properties have been produced. Thus, the effect of nickel filler ratio on the secondary voltage produced by flexible core RCs and error analysis could be comparatively investigated.

### 3. TEST METHODS OF THE MATHEMATICAL MODELS

Regression analysis is used to present a meaningful mathematical model between the inputs and the output of a system. When a system can be expressed mathematically, the resulting equation is also an estimation equation for intermediate and extreme values that cannot be measured experimentally. The analysis

begins by examining the positioning of the numerical data on the analytical plane. This positioning gives an idea of the type of curve to be fitted. Linear regression, polynomial regression, exponential regression, etc. can be preferred depending on the distribution of experimental data. The V-I change of the experimental data of the RCs is expected to be linear [28-30]. Linear data distributions can also be defined with Sum of Sines, Fourier, and Gaussian. However, the mathematical equation to be obtained will be complex, and the equation performance will decrease since it will contain high-order components. Therefore, linear regression has been preferred in this paper. Linear regression analysis is shown in Eq. (1). Here,  $a$  represents the fixed effect of linear regression,  $b$  represents the effect depending on the variable, and they are calculated by Eq. (2) and Eq. (3), respectively.

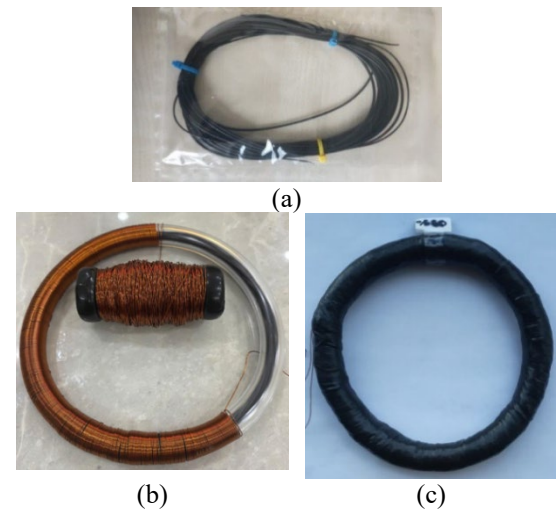


**Figure 1.** The manufacturing processes of the flexible magnetic core RC: (a) Nickel alloy filament manufacturing, (b) Secondary winding of RC, (c) Final view of RC (%60 nickel filling)

$$y_t = a + bx_t \quad (1)$$

$$b = \frac{\sum_{t=1}^n (x_t - \bar{x})(y_t - \bar{y})}{\sum_{t=1}^n (x_t - \bar{x})^2} \quad (2)$$

$$a = \bar{y} - b\bar{x} \quad (3)$$

Error tests such as  $R^2$  (Coefficient of Determination), Adj.  $R^2$  (Adjusted Coefficient of Determination), RMSE (Root Mean Square Error) and MAPE (Mean Absolute Percentage Error Value) are used to test the accuracy of the regression analysis.

### 3.1. R<sup>2</sup> Test

The R<sup>2</sup> test measures the difference between the available data and the average of the data produced from the mathematical model. The coefficient of determination is a value between zero and one and essentially measures the proximity to one. The closer the result is to 1, the higher the success of the study is considered. Equality (4) defines the R<sup>2</sup> test. Here,  $n$  represents the number of samples,  $y_i$  represents the measurement data, and  $\bar{y}_i$  represents the mathematical model outputs.

$$R^2 = 1 - \frac{\sum_{i=1}^n (y_i - \bar{y}_i)^2}{\sum_{i=1}^n y_i^2 - \frac{(\sum_{i=1}^n y_i)^2}{n}} \quad (4)$$

### 3.2. Adj. R<sup>2</sup> Test

The increase in the number of data to be tested causes a natural increase in the R<sup>2</sup> value. As the number of data in the system increases, even if the difference between the measurement data and the mathematical model outputs increases, there is no significant decrease in R<sup>2</sup>. In most cases, each variable added to the system will cause the value of R<sup>2</sup> to increase and approach to one. For this reason, in order to test the accuracy of the analyses with a large amount of data, the Adj. R<sup>2</sup> test, which supports the accuracy of the test, is also applied together with R<sup>2</sup> (5). Here,  $k$  represents the number of predictors.

$$Adj. R^2 = 1 - \frac{\sum_{i=1}^n (y_i - \bar{y}_i)^2}{\sum_{i=1}^n y_i^2 - \frac{(\sum_{i=1}^n y_i)^2}{n}} \frac{n-1}{n-k-1} \quad (5)$$

### 3.3. RMSE

RMSE is one of the error tests that measure the similarity between the measurement data and the mathematical model outputs in a system that is desired to be verified. When applying the RMSE error test, the standard deviation between the data is taken into account. RMSE focuses on the distribution in error values (6). The approach of the RMSE value to zero indicates the closeness between the measurement results and the mathematical model outputs. The closer the result is to zero, the more successful the test result is.

$$RMSE = \sqrt{\frac{\sum_{i=1}^n (y_i - \bar{y}_i)^2}{n}} \quad (6)$$

### 3.4. MAPE

MAPE is a test that calculates the percentage error in proportion. When applying the test, if there is a "zero" value among the measurement data, this data is not taken into account, as it will make the calculation undefined. If the MAPE error test result is below 10%, it indicates that the accuracy of the study is high. The smaller the MAPE error value, the higher the accuracy of the study. The MAPE calculation equation is given in Eq. (7).

$$MAPE = \left( \frac{100}{n} \sum_{i=1}^n \left| \frac{y_i - \bar{y}_i}{y_i} \right| \right) \quad (7)$$

## 4. EXPERIMENTAL FINDINGS AND REGRESSION ANALYSIS OF THE RCs

Epstein frame or single sheet test method is used to determine B-H curves of magnetic materials such as laminated steel [31]. However, these methods are not suitable for magnetic cores that can carry 3D flux. In this paper, toroid method [32] is considered to determine magnetic properties of flexible core RCs. The test setup created is shown in Figure 2. The current passing through the primary, a regulated AC power supply and a 50/1 ratio transformer have been used to change the primary current in the range of 5-400 A. The tests have been repeated separately for each RC developed.

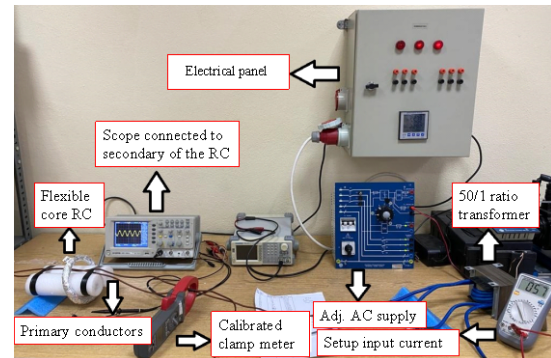
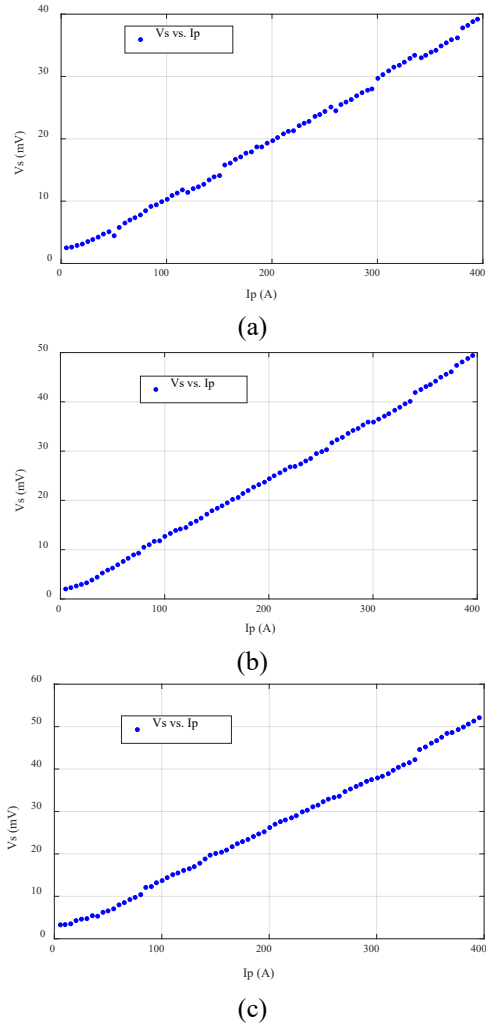


Figure 2. Test bench of the developed RCs [33].

According to the test results, the secondary voltages of air-core, 40% nickel-filled and 60% nickel-filled flexible magnetic core RCs increase linearly depending on the primary current, as seen in Figure 3. However, due to possible measurement errors due to the wide measurement ranges inherent in experimental studies, the graphs do not form a complete line. For this reason, linear regression has been used to find the mathematical model to be created with the measurement results. According to the regression analyses, the mathematical models

obtained for the primary current versus secondary voltage ( $V_S$ - $I_p$ ) characteristics of the flexible core RCs produced using conventional air-core RC, 40% and 60% nickel-filled filaments are given in equations (8) to (10), respectively.



**Figure 3.** Secondary voltages of the developed RCs measured in the range of 5-400A: (a) Air-core, (b) 40% nickel-filled, (c) 60% nickel-filled.

$$V_{air-core} = 0,6863 + 0,09542 * I \tag{8}$$

$$V_{%40\_Ni} = 0,2752 + 0,121 * I \tag{9}$$

$$V_{%60\_Ni} = 0,7674 + 0,1268 * I \tag{10}$$

The closeness of the mathematical models expressing the characteristics of the developed RCs ( $V_S$ - $I_p$ ) to the experimental results is shown in Figure 4. At high primary currents, the difference between the results of the mathematical model produced and the experimental results seems relatively greater. On the other hand, at low primary currents, the

mathematical model and the measurement results are quite close. For the success of the mathematical models, the test methods examined in Section 2 were used and the results are presented in Table 1. A comparison of experimental results with air core, 40% nickel-filled and 60% nickel-filled RCs is given in Table 1. In the table,  $R^2$  converges to one for all RCs. This shows that the experimental results and the mathematical model results are quite close to each other. The closeness of the  $R^2$  value to one indicates that the mathematical model has high performance.

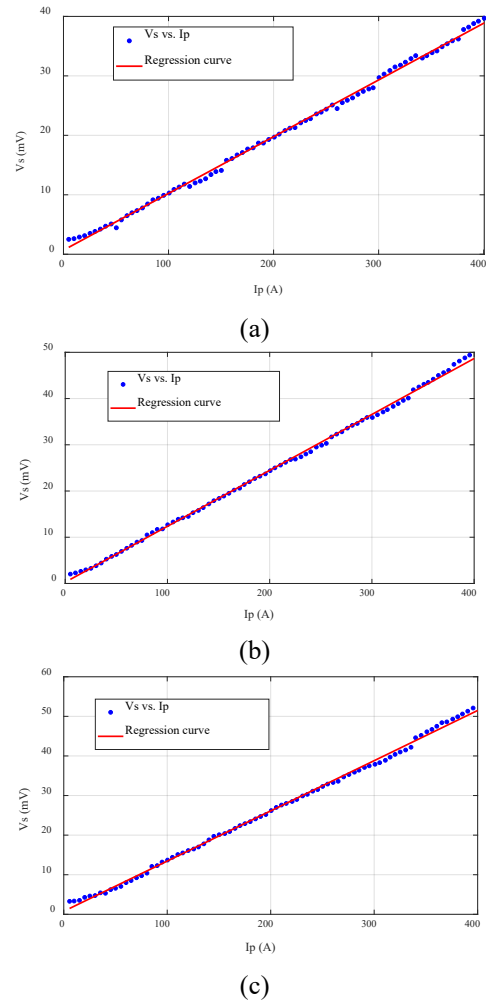


**Figure 4.** Experimental results and generated mathematical models: (a) Air-core, (b) 40% nickel-filled, (c) 60% nickel-filled.

**Table 1.** Comparison of the error tests

	Air-core RC	%40 Nickel-filled RC	%60 Nickel-filled RC
<b>R<sup>2</sup></b>	0.997916	0.998656	0.997929
<b>Adj. R<sup>2</sup></b>	0.997862	0.998621	0.997875
<b>RMSE</b>	0.504114	0.5130061	0.667632
<b>MAPE(%)</b>	3.913323	2.840462	3.97555

## 5. CONCLUSIONS

The V-I characteristics of the air-core RC and the flexible core RCs developed using nickel-filled filaments have been subjected to the regression analysis in this paper. Four different tests have been applied to the mathematical models of the RCs obtained by linear regression analysis, and high accuracy has been observed in all of them. Thus, for intermediate and extreme values that could not be realized experimentally, the secondary voltages of the examined RCs can be calculated using the mathematical models obtained by linear regression analysis. With a realistic mathematical model, it is possible to investigate new RC designs and optimal PLA+magnetic powder composite in the future studies. Using the mathematical models in numerical analyses such as FEA enables novel research topics such as magnetic performance and shielding design of the flexible RCs to be developed.

The slope of the mathematical model of the 40% nickel-filled flexible magnetic core RC is 26.80% higher than the slope of the linear model of the air-core RC. This ratio increased to 32.89% in the RC produced with 60% nickel-filled filament. It is seen that as the nickel filling ratio of the produced filaments increases, they contribute positively to the V-I characteristics without compromising the linearity properties in the flexible magnetic core RCs they are used in.

## REFERENCES

1. Wang, B., Xu, Y., Xu, L., and Xin, F., "A novel PMSM with 3-dimensional magnetic circuit using SMC core", In 2017 IEEE Transportation Electrification Conference and Expo, Asia-Pacific (ITEC Asia-Pacific), Pages 1-5, 2017.
2. Boomiraja, B., and Kanagaraj, R., "A novel hybrid flux machine with transverse flux stator and longitudinal flux rotor: Design and comparative analysis", *Electrical Engineering*, Vol. 102, Issue 3, Pages 1413-1422, 2020.
3. Yıldırım, E., and Önbilgin, G., "Comparative study of new axial field permanent magnet hybrid excitation machines", *IET Electric Power Applications*, Vol. 11, Issue 7, Pages 1347-1355, 2017.
4. Pham, T., Kwon, P., and Foster, S., "Additive manufacturing and topology optimization of magnetic materials for electrical machines—A review", *Energies*, Vol. 14, Issue 2, 283, 2021.
5. Tiismus, H., Kallaste, A., Vaimann, T., and Rassõlkin, A., "State of the art of additively manufactured electromagnetic materials for topology optimized electrical machines", *Additive Manufacturing*, Vol. 55, 102778, 2022.
6. Karabulut, Y., Meşe, E., Ayaz, M., and Aktaş, S., "Comparison study on SMC and grain-oriented laminated steel core for small-size axial flux permanent-magnet synchronous machines", *Materials Research Express*, Vol. 11 Issue 10, 106102, 2024.
7. Tiismus, H., Kallaste, A., Naseer, M. U., Vaimann, T., and Rassõlkin, A., "Design and performance of laser additively manufactured core induction motor", *IEEE Access*, Vol. 10, Pages 50137-50152, 2022.
8. Kim, C. W., Jang, G. H., Kim, J. M., Ahn, J. H., Baek, C. H., and Choi, J. Y., "Comparison of axial flux permanent magnet synchronous machines with electrical steel core and soft magnetic composite core", *IEEE Transactions on Magnetics*, Vol. 53, Issue 11, Pages 1-4, 2017.
9. Bollig, L. M., Hilpisch, P. J., Mowry, G. S., and Nelson-Cheeseman, B. B., "3D printed magnetic polymer composite transformers", *Journal of Magnetism and Magnetic Materials*, Vol. 442, Pages 97-101, 2017.
10. Nanyan, A. N., Isa, M., Hamid, H. A., Rohani, M. N. K. H., and Ismail, B., "The rogowski coil sensor in high current application: A review", In *IOP Conference Series: Materials Science and Engineering*, Vol. 318, Issue 1, 012054, 2018.
11. Shafiq, M., Stewart, B. G., Hussain, G. A., Hassan, W., Choudhary, M., & Palo, I., "Design and applications of Rogowski coil sensors for power system measurements: A review", *Measurement*, Vol. 203, 112014, 2022.
12. Kojovic, L. A., and Beresh, R. "Practical aspects of Rogowski coil applications to relaying". *IEEE PSRC special report*, Pages 12-14, 2010.
13. Metwally, I. A., "Self-integrating Rogowski coil for high-impulse current measurement", *IEEE Transactions on Instrumentation and Measurement*, Vol. 59 Issue 2, Pages 353-360, 2009.
14. Ward, D. A., and Exon, J. L. T., "Using Rogowski coils for transient current measurements", *Engineering science and education journal*, Vol. 2, Issue 3, Pages 105-113, 1993.
15. Ramboz, J. D., Destefan, D. E., and Stant, R. S., "The verification of Rogowski coil linearity from

200 A to greater than 100 kA using ratio methods”. 19th IEEE Instrumentation and Measurement Technology Conference, Vol. 1, Pages 687-692, 2002.

16. Gu, P. Y., Chen, Q., Li, H. B., Hu, C., Gong, H., and Jiao, Y., “PCB Rogowski coils for 300 kA current measurement on a multi-split conductor”, IEEE Sensors Journal, Vol. 19, Issue 16, Pages 6786-6794, 2019.

17. Gu, P. Y., Chen, Q., Li, H. B., Hu, C., Gong, H., and Jiao, Y., “PCB Rogowski coils for 300 kA current measurement on a multi-split conductor”, IEEE Sensors Journal, Vol. 19, Issue 16, Pages 6786-6794, 2019.

18. Kang, J., Zhu, A., Chen, Y., Luo, H., Yao, L., and Xin, Z., “An online gate oxide degradation monitoring method for SiC MOSFETs with contactless PCB Rogowski coil approach”, IEEE Transactions on Power Electronics, Vol. 38, Issue 8, Pages 9673-9684, 2023.

19. Kabakulak, M., & Arslan, S., “An Electromagnetic Energy Harvester for Wireless Sensors from Power Lines: Modeling and Experiment Verification”, Gazi University Journal of Science, Vol. 34, Issue 3, Pages 786-806, 2021.

20. Zhou, Z., Xin, Z., Liu, Q., & Li, C., “A differential compensated air coil current sensor for switching current measurement of power devices”, IEEE Transactions on Industrial Electronics, Vol. 70, Issue 5, Pages 5356-5364, 2022.

21. Shi, Y., Xin, Z., Loh, P. C., & Blaabjerg, F., “A review of traditional helical to recent miniaturized printed circuit board Rogowski coils for power-electronic applications”, IEEE Transactions on Power Electronics, Vol. 35, Issue 11, Pages 12207-12222, 2020.

22. Tan, Q., Zhang, W., Tan, X., Yang, L., Ren, Y., & Hu, Y., “Design of open-ended structure wideband PCB Rogowski coil based on new winding method”, Electronics, Vol. 11, Issue 3, 381, 2022.

23. Marracci, M., Tellini, B., and Bertolucci, E., “Study and characterization of a Rogowski coil with superparamagnetic magnetite core”, IEEE International Instrumentation and Measurement Technology Conference (I2MTC), Pages 1-6, 2017.

24. Wei, C., Lin, C., Boyang, M., Yuntao, G., and Shi, Y., “Development of magnetic core framework for flexible Rogowski coil current transducer”, In

IECON 2020 The 46th Annual Conference of the IEEE Industrial Electronics Society, Pages 3493-3497, 2020.

25. K. Doungkeaw ve J. Tungtrongpaioj, “Printability and Mechanical Properties of PLA/Iron Composites for FDM 3D Printing”, Key Eng. Mater., Vol. 978, Pages 47-51, 2024.

26. Sarac M.F., “In-Situ Synthesis of 3D-Printed Magnetic Nanoparticles Embedded Photopolymers” Int. J. of 3D Printing Tech. Dig. Ind., Vol. 5, Issue 2, Pages 164-170, 2021.

27. Güneç B., Durak E., “Eklemeli İmalat ile Demir Katkılı Filaman Üretimi İçin Ekstrüzyon Cihazının Tasarımı, İmalatı Ve Cihazın Termal Analizi” Int. J. of 3D Printing Tech. Dig. Ind., Vol. 8, Issue 3, Pages 459-467, 2024.

28. Chidimma, Abigail O., Chidi O. I., and Victor O., "An Optimized Approach for Improving Current Sensing In Digital Wattmeters Using Rogowski Coils." American Journal of Engineering Research, Vol. 6, Issue 4, Pages 207-222, 2017.

29. Lee, J. H., Lim, H. R., Shin, H. K., Cho, S. C., & Kim, J. O., “Simulation and development of Rogowski coil for lightning current measurement”, Journal of Electrical Engineering & Technology, Vol. 14, Pages 1831-1839, 2019.

30. Draxler, K., & Styblikova, R., “Magnetic shielding of Rogowski coils”, IEEE Transactions on Instrumentation and Measurement, Vol. 67, Issue 5, Pages 1207-1213, 2018.

31. Zengin, K., “Epstein Çerçevesi Kullanarak Manyetik Malzeme B-H Eğrisi Ve Kayıplarının Belirlenmesi”, Yüksek Lisans Tezi, [Determining Magnetic Material B-H Curve And Losses With Epstein Frame] [Thesis in Turkish], Kocaeli Üniversitesi, Kocaeli, 2016.

32. Ayvaz, M., “Eklemeli Üretim İle 400 Hz Asenkron Motor Tasarımı”, Yüksek Lisans Tezi, [Applications of Additive Magnetic Materials in 400 Hz Induction Motor Design] [Thesis in Turkish], Marmara Üniversitesi, İstanbul, 2024.

33. Aydın, G. M., “Nikel Alaşımli Esnek Filament Nüveli Rogowski Bobinin Tasarımı Ve Geliştirilmesi”, Yüksek Lisans Tezi, [Design and Development Of Rogowski Coil with Nickel Alloy Flexible Filament Core] [Thesis in Turkish], Düzce Üniversitesi, Düzce, 2023.



ULUSLARARASI 3B YAZICI TEKNOLOJİLERİ  
VE DİJİTAL ENDÜSTRİ DERGİSİ

INTERNATIONAL JOURNAL OF 3D PRINTING  
TECHNOLOGIES AND DIGITAL INDUSTRY

ISSN:2602-3350 (Online)

URL: <https://dergipark.org.tr/ij3dptdi>

# ROBOTİK KOL ENTEGRELİ MOBİL ARAMA VE KURTARMA ROBOTUNUN TASARIMI VE UYGULAMASI

DESIGN AND IMPLEMENTATION OF MOBILE SEARCH  
AND RESCUE ROBOT INTEGRATED WITH A ROBOTIC  
ARM

**Yazarlar (Authors):** Cemal Beik , Merdan Özkahraman 

**Bu makaleye şu şekilde atıfta bulunabilirsiniz (To cite to this article):** Beik C., Özkahraman M., "Robotik Kol Entegreli Mobil Arama ve Kurtarma Robotunun Tasarımı ve Uygulaması" *Int. J. of 3D Printing Tech. Dig. Ind.*, 9(1): 129-141, (2025).

DOI: 10.46519/ij3dptdi.1595180

Araştırma Makale/ Research Article

Erişim Linki: (To link to this article): <https://dergipark.org.tr/en/pub/ij3dptdi/archive>

# ROBOTİK KOL ENTEGRELİ MOBİL ARAMA VE KURTARMA ROBOTUNUN TASARIMI VE UYGULAMASI

Cemal Beik<sup>a</sup>  Merdan Özkahraman<sup>a</sup> 

<sup>a</sup>Isparta Uygulamalı Bilimler Üniversitesi, Teknoloji Fakültesi, Mekatronik Mühendisliği Bölümü,  
TÜRKİYE

\* Sorumlu Yazar: [cemalbeik@gmail.com](mailto:cemalbeik@gmail.com)

(Geliş/Received: 02.12.24; Düzeltme/Revised: 27.01.25; Kabul/Accepted: 27.02.25)

## ÖZ

Son yıllarda yaşanan doğal afetler, arama ve kurtarma operasyonlarının hızını ve etkinliğini artıracak teknolojik çözümlere duyulan ihtiyacı ortaya koymuştur. Bu çalışmada, doğal afetler sırasında kullanılmak üzere robotik kol entegreli mobil bir arama ve kurtarma robotu tasarımı ve gerçekleştirilmesi ele alınmaktadır. Robot, dar alanlarda manevra yapabilme ve enkaz altındaki hayatta kalanlara temel ihtiyaç malzemelerini ulaştırabilme kapasitesine sahiptir. Robotun termal kameralar, ses sensörleri gibi ileri teknolojilerle donatılması ve insan kurtarma ekipleri ile etkili bir şekilde iletişim kurabilmesi, kurtarma operasyonlarının verimliliğini artırmaktadır. Robotun kabiliyetleri, zamanın kritik olduğu acil durumlarda hızlı müdahale imkânı sunarak hayatta kalanların bulunmasını ve kurtarılmasını hızlandırmaktadır. Ayrıca, robotun riskli bölgelere insanların girmesine gerek kalmadan müdahale edebilme yeteneği, kurtarma ekiplerinin güvenliğini artırmaktadır. Robotun tasarımı ve gerçekleştirilmesi sürecinde kullanılan ileri teknolojiler ve mühendislik çözümleri, bu tür robotların gelecekteki arama ve kurtarma operasyonlarında yaygın olarak kullanılmasını sağlayabilir. Bu çalışma, ülkenin afetlerle başa çıkma yeteneğini artırmak için teknolojik yenilik ve istihdam fırsatları sunmaktadır.

**Anahtar Kelimeler:** Mobil Robot, Robotik, Robotik Kol, Arama ve Kurtarma Teknolojileri.

## DESIGN AND IMPLEMENTATION OF MOBILE SEARCH AND RESCUE ROBOT INTEGRATED WITH A ROBOTIC ARM

### ABSTRACT

Recent natural disasters have highlighted the need for technological solutions that enhance the speed and efficiency of search and rescue operations. This study focuses on the design and implementation of a mobile search and rescue robot integrated with a robotic arm, intended for use during natural disasters. The robot is capable of maneuvering in confined spaces and delivering essential supplies to survivors trapped under debris. Equipped with advanced technologies such as thermal cameras and sound sensors, the robot can effectively communicate with human rescue teams, thereby improving the efficiency of rescue operations. The robot's capabilities allow for rapid response in critical emergency situations, expediting the location and rescue of survivors. Furthermore, the robot's ability to operate in hazardous areas without requiring human entry enhances the safety of rescue teams. The advanced technologies and engineering solutions employed in the design and implementation of this robot could facilitate its widespread use in future search and rescue operations. This study offers technological innovation and employment opportunities to enhance the country's disaster response capabilities.

**Keywords:** Mobile Robot, Robotics, Robotic Arm, Search and Rescue Technologies.

## 1. GİRİŞ

Afetlerde artan ölümlerin başlıca nedenleri arasında zamanında ilk yardımın yapılamaması, duruma hemen müdahale edilememesi veya afet mağdurunun yerinin tespit edilememesi bulunmaktadır. Ne yazık ki, afet mağdurunun hayatta kalma şansı dakikalarla ölçülmektedir. Türkiye, Kuzey Anadolu Fay Hattı olarak bilinen dünyanın en aktif fay hatlarından birinin üzerinde yer almaktadır. Ayrıca, Türkiye sismik aktivite bakımından dünyada üçüncü sıradadır. Her gün yaklaşık 2.0 büyüklüğünde 10 deprem kaydedilmektedir. Kuzey Anadolu Fay Hattı, 1939'dan bu yana 7 büyük deprem üretmiştir. Uzmanlara göre, İstanbul'da önümüzdeki 20-25 yıl içinde 7.0 büyüklüğünde yıkıcı bir deprem beklenmektedir [1-3]. Nitelsiz yapıların fazlalığı ve arama-kurtarma çalışmalarındaki yetersizlikler, afetten etkilenen insan sayısını artırmaktadır. Geçmiş yıllarda, arama-kurtarma operasyonları insan ve hayvan gücüyle gerçekleştirildiğinden dramatik sonuçlar doğurmuştur. Günümüzde bu tür operasyonlarda modern yaklaşımlar, karmaşık makineler ve özel kurtarma ekipmanlarının kullanımını önermektedir. Ancak, bu tür gelişmiş cihazlar bile mağdurların yerini tespit edemeyebilir; bu durum kurtarma çalışmalarının yavaşlamasına ve dramatik sonuçlara yol açabilir. Bunun başlıca nedenleri arasında, mağdurun enkaz altındaki yerinin tespit edilmesindeki zorluklar, inşaat ekipmanlarının yavaş hareket kapasitesi, kurtarma ekipmanlarının sınırları ve eğitimli personel ihtiyacı bulunmaktadır [4,6].

Son yıllarda, farklı boyutlarda ve kapasitelerde arama kurtarma amaçlı mobil robotlar tasarlanmış ve uygulanmıştır. Bu sayede afetzedelerin tespit edilmeleri ve arama kurtarma personeli için potansiyel tehlikelerin belirlenmesi mümkün olmuştur [7]. Arama ve kurtarma için kullanılan mobil robotların genel amacı, acil durumlar ve afetler gibi riskli veya tehlikeli koşullarda insan hayatını kurtarmak ve yardımcı olmaktır. Bu robotlar genellikle yangınlar, depremler, patlamalar veya doğal afetler gibi durumlarla ilişkilendirilen yıkıcı olaylara müdahale etmek için kullanılmaktadır [10]. Bu çalışma, acil durum koşullarında daha etkin arama-kurtarma operasyonları gerçekleştirmek amacıyla "Kurtarma operasyonlarında kullanılmak üzere robotik kol entegreli mobil arama robotu geliştirilmesi" konseptine odaklanmıştır. Geliştirilen model,

güncel teknolojik gerekliliklerden faydalanarak hareket kabiliyetini ve esnekliği en üst düzeye çıkarmayı hedeflemektedir. Robot tasarımında kullanılan robotik kol, dar ve zorlu alanlarda manevra yapabilme yeteneğine sahip olup, kurtarma operasyonlarını daha etkili hale getirmesi amaçlanmıştır. Ayrıca, mobil robotun haberleşme sistemi, enkaz altında mahsur kalan kişileri tespit etme ve yerlerini doğru bir şekilde belirleme konusunda fayda sağlaması beklenmektedir. Bu sayede, gelecekteki acil durum senaryolarında daha hızlı ve güvenilir müdahalelerin gerçekleştirilmesine katkıda bulunulması hedeflenmektedir.

## 2. LİTERATÜR İNCELEMESİ

Afet durumlarında, mobil robotlar insan kurtarma ekiplerine kritik destek sağlayarak, bu tür zorlu görevlerde önemli araçlar olarak öne çıkmaktadır. Literatürde, mobil robotların bağımsız bir şekilde çalışarak kurtarma ekiplerine işlevsel ve hayati bilgiler sağladığı vurgulanmaktadır. Ancak, bu verilerin doğruluğunu değerlendirmek ve operasyonel sonuçları güvence altına almak için insan gözetiminin gerekliliği sıklıkla ifade edilmiştir. Özellikle küçük boyutlu ve yüksek hareket kabiliyetine sahip mobil robotların, literatürde kurtarma operasyonları için sağladığı avantajlara dikkat çekilmektedir. Bu robotların, ekipmanların ve arama köpeklerinin erişemediği dar alanlara ve enkaz yığınlarındaki yaşam üçgenlerine ulaşabilme yeteneği, kurtarma süreçlerinde önemli bir fark yaratmaktadır. Ayrıca, çökmüş binaların dengesiz ve dinamik yapılar sergilediği, artçı sarsıntılarla tetiklenebilecek ek çöktürmelerin kurtarma ekipleri için ciddi bir tehlike oluşturduğu vurgulanmaktadır. Mobil robotlar, bu tür tehlikeli bölgelerde güvenli bir mesafeden veri toplanmasını sağlayarak, ekip üyelerinin güvenliğini artırmaktadır.

Bu çalışmada, özellikle deprem operasyonları için tasarlanan mobil kurtarma robotlarının geliştirilmesi üzerine odaklanılmıştır. Literatür, afet sonrası insanlara yardım etme amacıyla geliştirilen kurtarma robotlarının mekanik tasarımında, hareket kabiliyeti ve güvenlik unsurlarının kritik öneme sahip olduğunu göstermektedir. Bu doğrultuda, acil durum müdahale ekiplerinin hayat kurtarma misyonlarını desteklemek üzere robotik çözümlerin tasarlanması ve uygulanması

gerektiği literatür kapsamında sıkça dile getirilmektedir.

### 2.1. Arama ve Kurtarma Mobil Robotunun Temel Hedefleri

**İnsan Hayatını Kurtarmak:** Arama ve kurtarma robotları, acil durum bölgelerine hızlı bir şekilde ulaşabilir ve mahsur kalmış veya tehlikede olan insanları tespit edebilir. Bu robotlar, insanları kurtarmak için gereken hızlı ve etkili müdahaleyi sağlayabilir [12].

**Bilgi Toplamak:** Robotlar, afet bölgelerindeki durumu izlemek, hasar tespiti yapmak ve verileri toplamak için kullanılabilir. Bu veriler, kurtarma ekiplerine yardımcı olmak ve afet sonrası çalışmaları planlamak için kullanılabilir [11].

**Çevre Tespiti ve Analizi:** Arama ve kurtarma robotları, tehlikeli kimyasalların sızıntılarını veya zararlı gazları tespit etmek için kullanılabilir. Ayrıca, hasarlı yapıların stabilitesini değerlendirebilir ve kurtarma ekiplerine güvenli bölgeler hakkında bilgi sağlayabilir [14, 15].

**İletişim Sağlamak:** Afet bölgelerinde iletişim altyapısının hasar görmesi durumunda, arama ve kurtarma robotları iletişim kanallarını kurabilir veya sağlamlaştırabilir. Bu sayede, mahsur kalmış insanlarla iletişim kurulabilir ve acil yardım talepleri yönlendirilebilir [16,18].

**Lojistik ve Malzeme Taşıma:** Arama ve kurtarma robotları, enkaz altında mahsur kalanlara acil tıbbi malzemeler, su, yiyecek ve diğer önemli kaynakları taşıyarak kurtarma ekiplerinin işini kolaylaştırabilir [19, 20].

### 2.2. Mevcut Arama Kurtarma Robotları

Günümüzde standart bir arama ve kurtarma ekibi yaklaşık on kişiden oluşmaktadır. Her ekipte köpekler, bir sağlık görevlisi, bir mühendis ve çeşitli uzmanlar bulunmakta olup, mağdurları bulmak ve kurtarmak için özel ekipmanlar kullanılmaktadır. Mevcut ekipmanlar arasında kameralar ve çeşitli dinleme cihazları yer almaktadır. Genellikle video kameralar, mağdurların izlerini aramak için cihazların üzerine monte edilen ve boşluklara ve deliklere yerleştirilebilen arama kameraları olarak kullanılmaktadır. Diğer tarafta boş bir alanın varlığı şüphesi varsa, genellikle engelleyici duvarlara delik açılır.

Hareket eden veya kurtarıcılara tepki vermeye çalışan bir kişiyi dinlemek için oldukça hassas mikrofonlar ve dinleme cihazları da kullanılır. Bir binayı aramak için yapılan toplam arama faaliyetleri saatler sürebilir. Eğer bir kişi bulunursa, tüm kurtarma operasyonları daha da uzun sürebilir. Kurtarma operasyonlarındaki ilk ve en önemli görevler, durumu değerlendirmek, mağdurların koordinatlarını belirlemek ve onlarla ilk teması kurmaktır. Bunu yapmak, insan kurtarıcılar için hem çok zor hem de çok risklidir. Çökmüş yapılar dirençsizdir, delikler ve boşluklar insan geçişi için çok dar olabilir, enkazda yön bulmak zordur ve yangın ile duman görüşü engelleyebilir. Kurtarma ekiplerinin görevlerini yerine getirdiği tehlikeli ortamlardan dolayı, ikincil afetlerden yaralanmalar yaşayabilirler. Bu nedenle, afetin tehlikeli ortamında insan hayatını kurtaran kurtarma makineleri veya robotlarının geliştirilmesi ve itfaiye istasyonları, polis karakolları, tren istasyonları ve belediye binaları gibi yerlere temin edilmesi gerekmektedir [22, 23].

Özellikle kurtarma robot türleri, RoboCup Kurtarma yarışmalarında görülmektedir. Yaklaşık yarısı tekerlekli araçlar, diğer yarısı ise paletli araçlar olmuştur [28, 29]. Bir dizi sensör kullanılmıştır, örneğin sonar, video kameralar, mesafe ölçerler, tamponlar ve mikrofonlar. Boyutlar 100 mm kareden 500 mm kareye kadar değişmektedir. Bu robotların çoğu kablosuz bağlantılar üzerinden uzaktan kumanda edilmektedir, yani çok az otonomileri vardır. Tanım gereği, bir afet durumundaki koşullar tam olarak tahmin edilemez veya kontrol edilemez. Kurtarma robotlarının tasarımında çeşitli modeller ve uygulamalar test edilmiştir. Bu robotların performansını ve etkinliğini artırmak için araştırmacılar doğadan ilham almışlardır. Kurtarma robotları kategorize edildiğinde, robotların hareket sistemi genellikle ya paletli araçlar ya da yılan tipi robotlar olarak görülmektedir. Şekillerini değiştirebilirlerse, dar alanlarda tırmanma ve manevra yapmalarına yardımcı olacağı da önerilmiştir. Tekerlekli bir robotun kurtarma operasyonlarında kolayca kullanılamamasının nedeni, bir tekerleğin çapından daha büyük bir engelin üzerinden geçememesi nedeniyle engelleri aşma kabiliyetinin daha az olmasıdır. Yılan tipi robotun mekanik tasarım avantajı, genişlik ve yükseklik açısından küçük olabilmesi, bu da robotun paletli bir araca

kıyasla enkazın içine daha kolay nüfuz etmesini sağlamaktadır. Ancak; yılan tipi robotlar daha zor kontrol edilir ve yük taşıma kapasitesi paletli bir robota göre daha düşüktür [25, 26].

### 2.2.1. Tekerlekli robotlar

Robotların, normal ofis ortamlarında ihtiyaç duyulan özelliklerin ötesine geçebilen, sağlam bir yapıya ve yeterli hareket kabiliyetine sahip olacak şekilde tasarlanması gerekmektedir. Ayrıca, bu robotların alandaki çözülmemiş bilimsel soruların incelenmesine olanak tanıyacak bir esnekliğe sahip olmaları önemlidir. Japonya'nın Fukuoka şehrinde düzenlenen 2002 RoboCup Kurtarma yarışmasına katılan prototip robotlarla elde edilen deneyimler temel alınarak yeni bir robot türü geliştirilmiştir. Bu robot, mekanik sistemlerden sensörlere ve aktüatörlere kadar tamamen iç tasarım odaklı olarak oluşturulmuştur. Böyle bir tasarım, kurtarma operasyonlarına özgü görevlerin optimize edilmesine olanak sağlamıştır. Geliştirilen robotlar, CubeSystem temelinde yapılandırılmış olup, ultrasonik sonar, aktif kızılötesi sensörler, USB kameralar, motor kontrol birimleri, hareket kontrol mekanizmaları ve odometri gibi zengin bir donanım ve yazılım modülleri setine sahiptir [27]. Robotların yarı otonom bir yapıya sahip olduğu ve teleoperasyona izin vermekle birlikte oldukça bağımsız işlevsellik sunduğu belirlenmiştir. Geliştirilen bu sistem, insan tarafından okunabilir haritalar oluşturabilme özelliğiyle dikkat çekmiştir. Bu haritalar, doğrudan kurtarma ekiplerine iletilerek mağdurların hızlı bir şekilde tespit edilmesine katkıda bulunmuştur. Robot, bu özelliğiyle kurtarma operasyonları için benzersiz bir çözüm sunmaktadır. Bu kapsamda, AMBOT firmasının geliştirdiği IP tekerlekli robot sistemi, özellikle hareket kabiliyeti ve esnekliğiyle dikkat çekmektedir (Şekil 1). AMBOT'un geliştirdiği bu sistem, robotların dar alanlarda manevra yapmasını ve karmaşık yüzeylerde etkin bir şekilde hareket etmesini mümkün kılarak, kurtarma operasyonlarında kullanılacak etkili bir çözüm sunmaktadır [28].

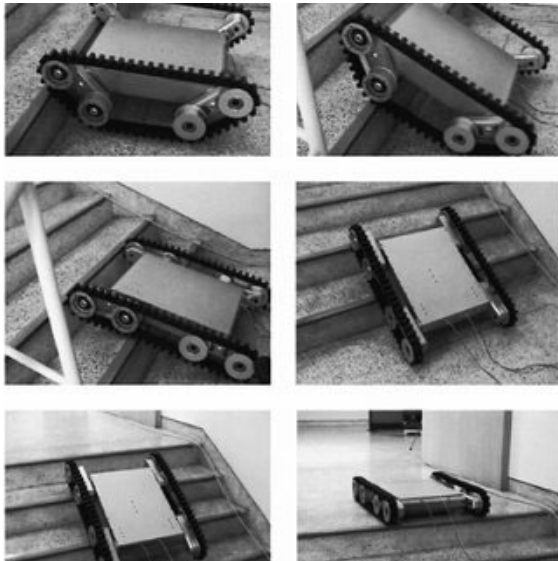


Şekil 1. Tekerlekli mobil robot [28].

### 2.2.2. Paletli Robotlar

Paletli robotların, tekerlekli robotlar ile böcek veya ayak tipi robotlara kıyasla daha üstün arazi performansı sunduğu bilinmektedir. Düzensiz arazilerdeki hareket kabiliyetini artırmak amacıyla çeşitli paletli robot tasarımları geliştirilmiştir. Genel bir mühendislik bakış açısıyla, bir robotun sahip olduğu mekanik parçaların ve serbestlik derecelerinin azalması, mekanik arızaların meydana gelme olasılığını da azaltmaktadır. Bu nedenle, mekanik tasarımların mümkün olduğunca basit ve işlevsel bir yapıda olması hedeflenmektedir [29]. Robot, önde, ortada ve arkada olmak üzere üç ana gövdeden oluşmakta ve bu gövdeler, merkez gövdenin pitch ve yaw eksenleri etrafında simetrik olarak hareket eden özel bir iki boyutlu eklem mekanizması ile bağlanmaktadır. Bu mekanizma, robotun esnekliğini artırırken, aynı zamanda mekanik karmaşıklığı sınırlamaktadır. Robotun palet sistemi, altı segmentin tamamını tek bir elektrik motoru ile hareket ettirecek şekilde tasarlanmıştır. Böylelikle, toplamda yalnızca üç serbestlik derecesi kullanılarak hem hareket kabiliyeti sağlanmış hem de sistemin güvenilirliği artırılmıştır. Bu tasarım, basit ama etkili bir yapı sunarak, çeşitli felaket sahnelerinde kurtarma operasyonları için uygun bir çözüm haline gelmiştir. Ayrıca, robotun ön kısmına yerleştirilen CCD kamera ve mikrofon, enkaz altında kalan kurbanların tespit edilmesine olanak tanımaktadır. Bu özellikleriyle, robot, kurtarma operasyonlarında hem güvenli hem de verimli bir araç olarak kullanılmaya uygun hale getirilmiştir. Literatürde, bu tür robotların felaket senaryolarında hızlı ve güvenilir veri toplama kabiliyeti sayesinde, kurtarma ekiplerinin iş yükünü azalttığı ve operasyon güvenliğini artırdığı belirtilmektedir [11].

Paletli robotlar genellikle tekerlekli robotlardan, böcek veya ayak tipi robotlardan daha iyi off-road yeteneğine sahiptir. Düzensiz arazide performansı artırmak için birçok paletli araç tasarlanmıştır. Genel bir makine mühendisliği bakış açısından, bir robotun sahip olduğu mekanik parçalar ve serbestlik dereceleri ne kadar az ise, mekanik arızaların olasılıkları o kadar azdır. Yılan benzeri robotların mekanik tasarımını optimize etmek için paletli bir tür eklemli gövdeli hareketli bir araç geliştirildi. Sınırlı sayıda serbestlik derecesi ile tasarlanmış olmasına rağmen, yine de yılan robotlara özgü iyi hareket kabiliyeti özellikleri sunmaktadır. Bu robot, önde, ortada ve arkada olmak üzere üç gövdeden oluşur; bu gövdeler, merkez gövdenin pitch ve yaw ekseninde simetrik olarak ön ve arka gövdelerin duruşunu değiştiren özel 2 boyutlu eklem mekanizmalarıyla birbirine bağlıdır. Ayrıca, tüm 6 palet segmenti tek bir elektrik motoru ile hareket ettirilir, böylece robotun tamamı için sadece 3 serbestlik derecesi toplamda bulunur. Bu robot, en önde bir CCD kamerası ve bir mikrofon içerir ve bir felaket sahnesinin enkazı altında gömülü kurbanları bulmak için uygundur [11]. Jeong ve arkadaşları (2008), değişken tek paletli bir robotun engel aşma sırasında sürüş modu karar mekanizmasını detaylı bir şekilde incelemişlerdir. Bu çalışmada, robotun hareket kabiliyeti, arazi koşullarına adaptasyonu ve engel aşma performansı görselleştirilmiş ve optimize edilmiştir. Şekil 2’de tasarlanmış olan paletli robot kol görselleri yer almaktadır.



Şekil 2. Paletli mobil robot.[38]

### 2.2.3. Yılan Benzeri Robotlar

Yılan benzeri robotların tasarımı, sahip oldukları yüksek serbestlik derecesi ve karmaşık hareket planlaması nedeniyle oldukça zorlu bir süreçtir. Literatürde, bu tür robotların çeşitli yenilikçi türlerinin geliştirilmiş olduğu belirtilmektedir. Ancak, elde edilen başarılı performansa rağmen, bu robotlar için enerji kaynağı hala büyük bir endişe konusudur. Arama ve kurtarma robotlarının saatlerce, hatta günlerce kesintisiz çalışabilmesi gerekmektedir. Robotların sadece enerji ihtiyacını karşılamak için operasyon alanını terk etmesi kabul edilemez bir durumdur. Bu tür bir senaryoda, robotun geri döneceği varsayımında bulunmak da gerçekçi bir yaklaşım olarak görülmektedir [30, 31]. Kentsel arama ve kurtarma, tehlikeli ortamlarda endüstriyel denetimler ve askeri istihbarat gibi çeşitli alanlarda, çökmüş bina enkazı üzerinde hareket edebilen, dar alanlardan geçebilen ve düşman sığınaklarına girerek istihbarat toplayabilen küçük boyutlu mobil robotlara ihtiyaç duyulmaktadır. Bu tür yüksek hareket kabiliyetine sahip robotların başlıca örneklerinden biri yılan robotlarıdır. Yılan robotları, eklemlerinin dalga benzeri hareketlerinden itiş gücü elde eden çok segmentli mekanizmalardır ve bu özellikleriyle tekerlek, bacak veya palet kullanmaksızın hareket edebilirler [32]. Yılan robotlar, karmaşık bir yapıya sahip olmalarına rağmen, ince ve uzun tasarımları sayesinde dar alanlara erişebilir ve küçük çatlaklarda etkili bir şekilde hareket edebilirler. Bu tür robotlar, hareket sırasında gövdelerini bacak gibi kullanabilirken, geçiş yaparken kollar gibi işlev görebilir. Ancak, enerji kaynağı, hız ve elektronik bileşenler için yeterli alan sağlama gibi dezavantajları bulunmaktadır. Batarya kapasitesinin yüksek olması, mekanik bağlamaların çalıştırılması için kritik öneme sahiptir; ancak bu durum, robotun toplam ağırlığında artışa neden olabilir. Genellikle üç veya daha fazla sert segmentten oluşan yılan benzeri robotlar, 2 veya 3 serbestlik derecesine sahip eklemlerle birbirine bağlanmaktadır. Segmentler, güçlendirilmiş tekerlekler, paletler veya bacaklarla itiş sağlarken, eklemler hareket kabiliyeti için güçlendirilmiş olabilir. Örneğin, OmniTread tasarımında (Şekil 3), her biri dört tarafında iki uzunlamasına palet bulunan dört segment yer almaktadır ve bu sayede toplam sekiz palet kullanılmaktadır. Segmentler arasındaki iki serbestlik derecesine sahip

eklemler, pnömatik silindirlere hareket ettirilmektedir.



Şekil 3. OmniTread serpentine robot. [37]

Yılan benzeri robotların farklı bir tasarım yaklaşımı, "Spirochete" adlı burulma hareketi yapan mikroorganizmanın hareketini temel alan bir 3D aktif kordon mekanizmasıdır. Bu tasarım, amfibik robotların su ve karada etkili bir şekilde hareket edebilmesini sağlamaktadır. Böyle bir tasarım, özellikle kıyı alanlarında gerçekleştirilen arama ve kurtarma operasyonları için son derece faydalı olma potansiyeline sahiptir.

Mekanik yılanların tasarımı zordur çünkü çok sayıda serbestlik derecesi ve hareket planlamasındaki karmaşıklıklar vardır. Buna rağmen, yazarlar benzersiz özelliklere sahip birçok yeni tür yılan benzeri robotlar geliştirmiştir. Ancak, mobil robotlarımız tarafından elde edilen iyi performansa rağmen, hala büyük bir endişe konusu bulunmaktadır: enerji kaynağı. Arama ve kurtarma robotları, saatlerce, hatta günlerce kesintisiz çalışmalıdır ve bir robotun sadece şarj etmek veya pilleri değiştirmek için yüzeye dönmesine tahammül edilemez. Gerçekçi olmak gerekirse, robotun geri dönmeyi başaracağını beklemek mümkün değildir.

Kentsel arama ve kurtarma, tehlikeli ortamlarda endüstriyel denetimler ve askeri istihbaratın ortak bir ihtiyacı vardır: çökmüş bir binanın enkazı üzerinde hareket edebilen, dar sürünme alanlarından geçebilen ve istihbarat toplamak için düşman sığınaklarına girebilen küçük boyutlu mobil robotlar. Bu tür yüksek hareket kabiliyetini sağlayabilecek mobil robot türlerinden biri, yılan robotu veya yılan benzeri robottur. Bir "yılan robotu" veya yılan benzeri robot, dalgalanmalardan (sadece eklemlerin dalga benzeri hareketi) itiş gücü elde eden çok segmentli bir mekanizmadır, yani itiş için tekerlekler, bacaklar veya paletler kullanmaz.

Yılan robotlar ileri hareket yeteneklerine sahiptir. Hareket ederken vücutlarını bacak olarak veya geçiş yaparken kol olarak kullanabilirler. Uzun ve ince yapıları sayesinde dar yerlere girebilir ve küçük çatlakların içinde hareket edebilirler. Yılanların karmaşık bir tasarıma sahip olması gerekir çünkü birçok serbestlik derecesine ihtiyaç duyarlar. Bu tür robotların diğer dezavantajları enerji kaynağı, hız ve elektronik bileşenler, sensörler ve devreler için yeterli alanın olmamasıdır. Bataryanın kapasitesi yüksek olması çalışabilme kolaylığı sunarken robotun toplam ağırlığının azalmasına neden olmaktadır. Üç veya daha fazla sert segmentten oluşan yılan benzeri robotlar genellikle 2 veya 3 serbestlik derecesine sahip eklemlerle birbirine bağlanır. Segmentler genellikle güçlendirilmiş tekerlekler, paletler veya bacaklarla ileri doğru itiş sağlar, eklemler ise güçlendirilmiş veya güçlendirilmiş olabilir [32, 33]. Robot News platformunda sunulmuş olan yılan benzeri mobil robot görseli Şekil 4'te sunulmaktadır [34]. Bu robotun tasarımı, hareket kabiliyeti ve dar alanlarda çalışma kapasitesi ile özellikle arama ve kurtarma operasyonlarında etkili bir çözüm sunmaktadır.



Şekil 4. Yılan benzetimli mobil robot [34].

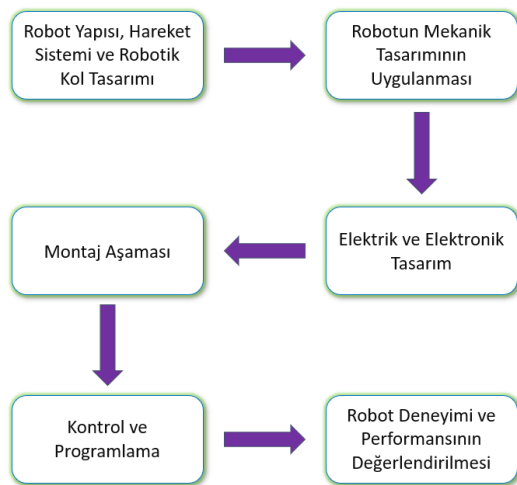
### 2.3. Robotların Sınırlamaları

Mobil robotların tasarımında görev süresi, kablosuz çalışma mesafesi, zorlu arazi koşullarına uyum ve düşme dayanıklılığı gibi temel sınırlamaların dikkate alınması gerekmektedir. Enkaza müdahale eden bir robotun, kurtarma operasyonlarında ek kısıtlamaları karşılaması beklenmektedir. Bu bağlamda, mobil robotların enkaz alanındaki dengesiz nesnelere zarar vermeyecek kadar küçük ve hafif bir yapıya sahip olması gerekmektedir. Bunun yanı sıra, zorlu arazi koşullarında etkin bir şekilde hareket edebilen

mobil bir tabanın tasarlanması, kurtarma robotu geliştirilmesinde karşılaşılan en önemli zorluklardan biridir. Literatürde, Dünya Ticaret Merkezi'nde kullanılan mobil robotların çoğunlukla askeri uygulamalar için tasarlandığı, bu nedenle deprem bölgeleri gibi afet alanlarındaki kurtarma operasyonlarında sınırlı bir etkililik sergilediği belirtilmiştir [11]. Bu robotların gözetim amaçlı kullanımında başarı sağlanmış olsa da, kurtarma operasyonları için gereken özel gereksinimlere uygun olmadıkları ifade edilmektedir. Önceki çalışmalarda, kurtarma alanlarında mobil robotların karşılaştığı sorunlara değinilmiş olmasına rağmen, robot tasarım süreçleri detaylı bir şekilde ele alınmamıştır. Bu durum, kurtarma robotlarının tasarımında yenilikçi yaklaşımların gerekliliğini ve zorlu arazi şartlarına uygun hareket mekanizmalarının geliştirilmesinin önemini ortaya koymaktadır.

### 3. MATERYAL VE METOT

Bu çalışmada geliştirilen robotik kol entegreli mobil arama-kurtarma robotunun tasarım ve uygulama süreci, sistematik bir yaklaşım benimsenerek gerçekleştirilmiştir. Tasarım süreci; mekanik yapı, elektrik-elektronik tasarım, montaj, kontrol ve programlama aşamalarını kapsamaktadır. Şekil 5'de, projenin adım adım gerçekleştirilme süreci ile bu aşamalar arasındaki ilişkiler görselleştirilmiştir. Tüm tasarım aşamaları, robotun işlevselliğini en üst düzeyde sağlayacak şekilde planlanmış ve uygulanmıştır.



Şekil 5. Arama kurtarma robotu üretim süreci ve yöntemlerinin ayrıntılı blok diyagramı.

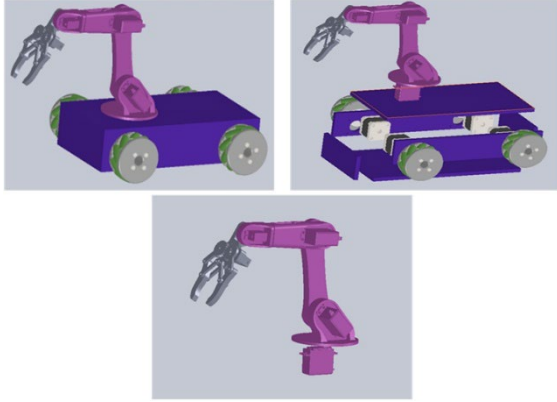
Bu çalışmada geliştirilen robotik kol entegreli mobil arama-kurtarma robotunun tasarımı ve

uygulanması, mevcut teknolojik çözümlerden yararlanılarak gerçekleştirilmiştir. Robotun tasarımında How to Mechatronics web sitesinde yer alan açık kaynak kodlu bir robotik platformun temelleri kullanılmıştır. Bu açık kaynak tasarım, çalışmanın ihtiyaçlarına göre güncellenmiş ve özelleştirilmiştir. Robotun orijinal hali etik kurallar gözetilerek değiştirilmiş olup, robotun işlevselliği artırılmıştır. Bu kapsamda orijinal platformun sahip olduğu mekanik ve elektronik sistemler yeniden gözden geçirilmiş ve arama-kurtarma operasyonları için optimize edilmiştir.

#### 3.1. Mekanik Tasarım

Robotun çeşitli parçalarının üretiminde 3 boyutlu baskı teknolojisi kullanıldı, ardından basılan 3 boyutlu model incelendi, kalitesi ve doğruluğu gözden geçirildi. Basılı modelden alınan geri bildirimlere dayalı olarak orijinal tasarımda iyileştirmeler ve değişiklikler yapıldı. Robotun kolu için dayanıklılığı ve hafifliği nedeniyle ABS plastik tercih edilmiştir. 3 boyutlu baskı ile üretilen bu parçalar, daha sonra birleştirilerek robotun kolu oluşturulmuştur. Tahtadan robot kutusu yapıldı. Tahta kutu ise, robotun elektronik bileşenlerini korumak için seçilmiştir. Tahta, hafif, kolay işlenebilir ve çevre dostu bir malzemedir. Robot kolu ve uç işlevcisi için ise, esneklik ve dayanıklılık gerektiğinden, 3 boyutlu baskı ile üretilen esnek bir filament tercih edilmiştir. Bu sayede robot, hem güçlü hem de hızlı hareket edebilme özelliğine sahip olmuştur. Mobil robot uzunluğu 34 cm, genişliği 28 cm, yüksekliği 52 cm olarak tasarlanmıştır. Prototip ağırlığı 5560 gr olarak bulunmuştur. Pil ömrü olarak 3 saatlik bir çalışma süresi hedeflenmektedir. Bu çalışma süresi robotun kullanım türüne ve hareket sıklığına göre değişmektedir.

Robotun mekanik yapısı, çeşitli afet senaryolarında kullanılabilecek şekilde tasarlanmıştır. Robot, dar alanlarda manevra yapabilmesi ve engebeli arazilerde etkili bir şekilde hareket edebilmesi için Mecanum tekerlek sistemi ile donatılmıştır. Robot kolunun tasarımı, enkaz altındaki objelere ulaşma ve onları manipüle edebilme kapasitesini artırmak için optimize edilmiştir. Kol sistemi, dar alanlarda hassas hareket yeteneği sunmak üzere 6 serbestlik derecesine (6-DOF) sahiptir ve bu sayede karmaşık manipülasyonlar gerçekleştirilebilir.



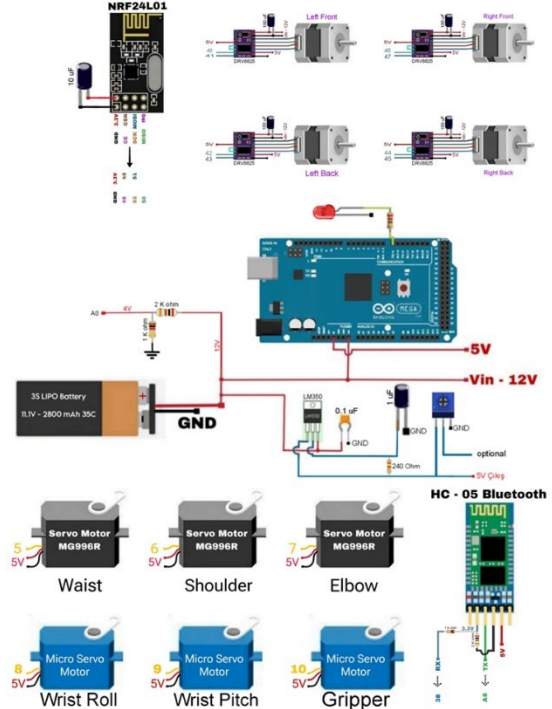
Şekil 6. Mobil robot simülasyonu benzetimi.

Mobil robotun üzerinde konlandırılmış olan robotic kol; Temel (base), omuz, dirsek ve bilek olmak üzere dört döner eklemden oluşur. Temel, kolu z-ekseni etrafında döndürürken, diğer üç ekleme x-ekseni etrafında döner. Y-ekseni etrafında dönüş yoktur, bu da hareketleri sınırlasa da kinematik hesaplamaları kolaylaştırır. Her eklemden, bilek, dirsek ve omuz için ileri ve geri, temel için ise sağa ve sola dönüş sınırlamaları vardır. Kolun tutacağı, döner dişlilerle açılıp kapanır ancak prongları paralel kalır. Bu nedenle tutma hareketi bir ekleme olarak kabul edilmez. Sonuç olarak:

- Robot tutacağı katlanabilir.
- Kolun bileği 180° dönebilir.
- Kolun aparatı 180° hareket edebilir.
- Kolun zemin kısmı 180° dönebilir.
- Zemin eklemi aparatı, 180° ileri ve geri hareket edebilir.

### 3.2. Elektronik Tasarım

Robotun elektronik kısmında Arduino Mega mikrodenetleyicisi kullanılmış ve robotun motorları, sensörleri ve iletişim sistemi bu platform üzerinden kontrol edilmiştir. İletişim, Bluetooth 5.0 modülü kullanılarak uzaktan kumanda edilmiştir. Bu sayede operatör, robotu güvenli bir mesafeden yönetebilme olanağına sahip olmuştur. Arduino MEGA kullanılarak, tekerlekler için 4 adet Step Motor ve 4 DRV8825 sürücü, kol hareketi için 3 adet standart Servo motor ve uç işlevsellik için 3 adet Mini Servo motor tercih edilmiştir. Kablosuz iletişim için NRF24L01 modülü ve anten kullanılmıştır. Güç kaynağı olarak ise Li-Po 12V pil tercih edilmiştir. Bu bileşenlerin tümü, Şekil 7'de mobil robotun elektronik yapısının şematik gösterimiyle detaylandırılmıştır.



Şekil 7. Mobil robot elektronik şematik gösterimi.

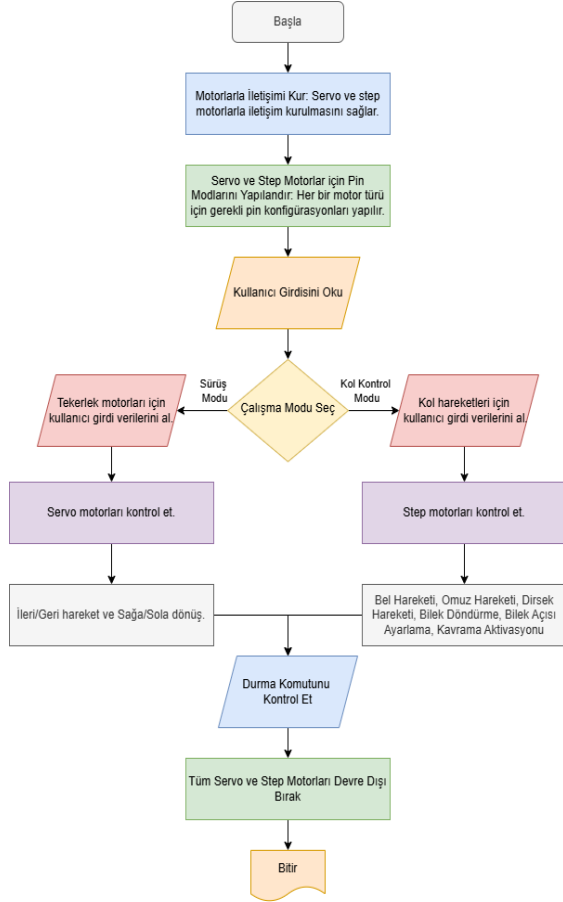
LiPo (Lithium Polymer) piller şarj edilebilir bir batarya türü olup, küçük boyutlarına rağmen yüksek enerji sağlayabilme kapasitesi sayesinde robotik uygulamalarda kullanılabilir. Bu projede, robotu verimli bir şekilde çalıştırmak için 2800mAh kapasiteye ve 11.1V gerilime sahip bir LiPo pil kullanılmıştır. Bu pil ile robotun yaklaşık 3 saat boyunca çalışması hedeflenmektedir.

Mobil robot üzerinde kullanılan HC-05 Bluetooth modülü Bluetooth 5.0 teknolojisini desteklemektedir. Yüksek hız, düşük güç tüketimi ve uzun menzil gibi avantajlara sahip olup, 2.4 GHz frekansında haberleşme sağlamaktadır. Bağlantı stabilitesi testleri, modülün 10 metreye kadar çalışma mesafesinde sorunsuz bir şekilde veri iletimi sağladığını göstermektedir. Çalışma gerilimi 1.7 ile 3.6V arasında olup, Arduino üzerinden 3.3V çıkışıyla beslenmelidir. Ayrıca, modülün senkron hızı 2Mbps, asenkron hızı ise 5Mbps'dir ve üzerinde kimlik doğrulama ve şifreleme yazılımı bulunmaktadır.

### 3.3. Programlama ve Kontrol Sistemi

Robotun kontrol algoritmaları, Arduino IDE platformu kullanılarak kodlanmış ve robotun çeşitli görevleri yerine getirmesi için gerekli yazılım altyapısı oluşturulmuştur. Robotun hareketleri ve kol operasyonları, uzaktan komutlarla yönlendirilmiş olup, sistemin genel

performansı optimize edilmiştir. Şekil 8'de mobil robotun kontrol akış şeması verilmiştir. Şekil 10'da ise robotun mobil uygulamadan kontrolünü sağlayacak arayüz tasarımının görseli görülmektedir.



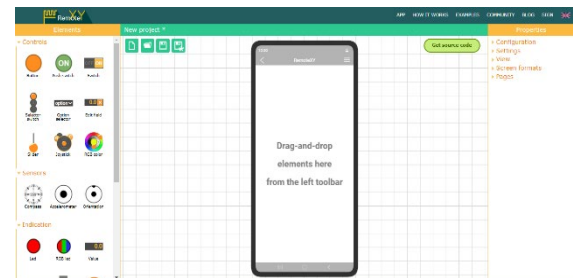
Şekil 8. Mobil robot kontrol akış şeması.

Şekil 8'de verilmiş olan akış şeması, bir mobil robot ve robot kol mekanizmasını kontrol etmek için kullanılan bir sistemin kontrol mantığını göstermektedir. İlk adımda işlem başlar ve sistem, servo ve step motorlarla iletişim kurar. Bu adım, motorların çalışmasını mümkün kılacak iletişim altyapısını oluşturur. Ardından, her motor türü için gerekli pin modları yapılandırılarak motorların çalışması için gereken teknik altyapı sağlanır. Bu süreç, motorların doğru bir şekilde çalışabilmesi için kritik öneme sahiptir. Sistemin bir diğer önemli aşaması, kullanıcı girdisinin alınmasıdır. Kullanıcıdan alınan bilgilerle çalışma modu belirlenir. İki temel çalışma modu sunulmaktadır: sürüş modu ve kol kontrol modu. Sürüş modu, robotun hareketlerinin servo motorlar aracılığıyla kontrol edilmesini sağlar. Bu modda servo motorlar ileri, geri, sağa ve sola hareketleri gerçekleştirir. Diğer taraftan,

kol kontrol modu step motorların kullanımını içerir. Bu mod, robot kolunun farklı hareketlerini sağlar. Temel, omuz, dirsek, bilek ve kavrama gibi hareketlerin her biri, kullanıcı tarafından belirlenen komutlara göre gerçekleştirilir.

Sistem, çalışma sırasında durma komutunu kontrol etmek için sürekli bir izleme mekanizması kullanır. Eğer durma komutu algılanırsa, tüm servo ve step motorlar devre dışı bırakılır. Bu, sistemin güvenli ve kontrollü bir şekilde sonlandırılmasını sağlar. İşlem, durma komutunun ardından sonlandırılarak tamamlanır.

Sayısal veri iletişimde bağlantı hızı (baud rate) ve pin kullanımı, sistemin performansı ve doğru çalışması açısından kritik unsurlar arasında yer alır. HC-05 Bluetooth modülleri, varsayılan olarak 9600 baud hızında çalışır. Bu hız, sistemin veri aktarım hızını belirler ve çoğu standart uygulama için yeterli bir değer sunar. Ancak, kullanıcı AT komutlarını kullanarak bu hızı değiştirebilir. Maksimum hız, Software Serial bağlantılar için 38400 baud ile sınırlıdır. Sistemin tasarımında, kullanıcı dostu özellikleri ve gerekli işlevselliği bir araya getiren Remote XY programı tercih edilmiştir. Remote XY programı, web tabanlı bir platformda basit ve anlaşılır bir arayüz sunar. Bu arayüzde, robotun tekerlek ve kol hareketlerini kontrol etmek için uygun düğmeler ve komutlar eklenmiştir. Kullanıcı, Bluetooth modülünün tipini seçer ve projede kullanılan Arduino modelini belirler. Ardından, Bluetooth modülünün Arduino'ya nasıl bağlanacağına dair bir diyagram ve uygun kodların nasıl indirileceği hakkında bilgi sağlanır. Bağlantı kurulduktan sonra, sistem test edilir ve robot, Remote XY aracılığıyla sorunsuz bir şekilde kontrol edilebilir hale gelmektedir. Şekil 9'da Remote XY uygulama arayüzü verilmiştir.



Şekil 9. Remote XY Uygulama Arayüzü.



Şekil 10. Mobil robot kontrol arayüz görseli.

#### 4. UYGULAMA BULGULARI

Bu çalışmada geliştirilen robotik kol entegreli mobil arama ve kurtarma robotu, tasarım ve uygulama süreçlerinde test edilmiş ve aşağıdaki önemli bulgular elde edilmiştir:

- **Hareket Kabiliyeti:** Robot, mecanum tekerlek sistemi sayesinde dar alanlarda manevra yapabilme ve engebeli arazilerde etkili bir şekilde hareket edebilme yeteneğini göstermiştir. Bu özellik, karmaşık ve dengesiz enkaz ortamlarında hızlı ve güvenli müdahaleler için büyük avantaj sağlamaktadır.

- **Algılama ve Tespit Performansı:** Robot, termal kameralar ve ses sensörleri gibi ileri teknoloji ile donatılabilme potansiyeline olup, enkaz altında mahsur kalan mağdurları yüksek hassasiyetle tespit edebileceği düşünülmektedir. Bu sistemler, arama ve kurtarma ekiplerinin kritik bilgilere zamanında ulaşmasını sağlayacaktır.

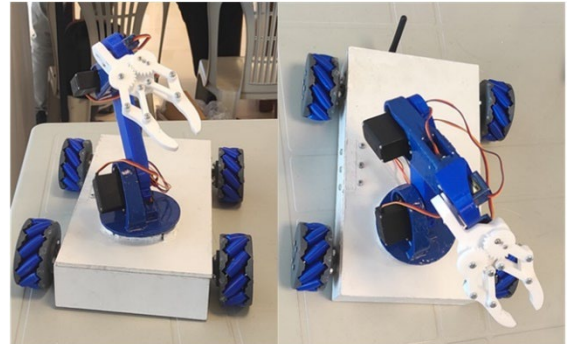
- **Robotik Kolun İşlevselliği:** 6 serbestlik derecesine sahip robotik kol, dar alanlarda hassas manipülasyon görevlerini yerine getirebilmektedir. Şekil 11'de gösterildiği gibi, robot kolun parçaları üç boyutlu yazıcı kullanılarak üretilmiş, bu tasarım hem maliyeti düşürmüştür hem de özelleştirme imkânı sunmuştur. Şekil 12'de ise robotun nihai hali gösterilmekte, bu kolun operasyonel ortamda işlevselliği başarıyla sergilenmektedir.

- **Uzaktan Kontrol ve İletişim:** Bluetooth 5.0 modülü sayesinde, robot operatörler tarafından güvenli bir mesafeden kontrol edilebilmiştir. Bu özellik, kurtarma ekiplerinin güvenliğini artırırken operasyonların koordinasyonunu da kolaylaştırması beklenmektedir.

Bu bulgular, robotun sahada uygulanabilirliğini ve başarısını göstermiş, gelecek arama ve kurtarma operasyonlarında kullanım potansiyelini ortaya koymuştur.



Şekil 11. Mobil robotun üretim görselleri.



Şekil 12. Robotik kol entegreli mobil arama ve kurtarma robotunun nihai hali.

#### 5. SONUÇ

Bu çalışma, doğal afetler ve acil durumlar için robotik kol entegreli mobil bir arama ve kurtarma robotu tasarımını ve uygulamasını kapsamaktadır. Robotun test sonuçları, tasarım hedeflerinin başarıyla gerçekleştirildiğini ortaya koymuştur. Robotun hareket kabiliyeti, algılama sistemleri, manipülasyon becerisi ve uzaktan kontrol yetenekleri, mevcut arama ve kurtarma teknolojilerinin ötesine geçecek nitelikte sonuçlar vermiştir. Bu bağlamda çalışmanın sunduğu katkılar şu şekilde özetlenebilir:

- İnsan Güvenliğine Katkı: Robot, tehlikeli bölgelerde insanların yerine geçerek kurtarma ekiplerinin güvenliğini sağlamıştır. Bu özellik, afet bölgelerinde riskleri önemli ölçüde azaltmıştır.
- Operasyonel Verimlilik: Robotun teknolojik kabiliyetleri, arama ve kurtarma operasyonlarının daha hızlı ve verimli bir şekilde gerçekleştirilmesine olanak tanımış, bu da hayatta kalanların kurtarılma şansını artırmıştır.
- Afet Müdahalesine Yeni Yaklaşımlar: Bu çalışma, robotik teknolojilerin afet yönetimi süreçlerinde ne denli kritik bir rol oynayabileceğini göstermiştir.

Geleceğe yönelik olarak, bu tür arama ve kurtarma robotlarının, otonom karar verme yeteneklerinin geliştirilmesi, yapay zekâ tabanlı tespit algoritmaları ile donatılması ve daha dayanıklı malzemelerle üretilmesi hedeflenmelidir. Ayrıca, bu robotların yalnızca afet yönetiminde değil, endüstriyel kazalar, yangın müdahaleleri ve hatta savaş alanlarında kullanılabilirliği artırılabilir. Gelişmiş batarya teknolojileri, robotların daha uzun süreli operasyonlar gerçekleştirmesine olanak tanıyabilir.

Bu tür robotların yaygınlaşması hem insani hem de ekonomik anlamda olumlu etkiler yaratacaktır. Geliştirilen teknolojilerin, uluslararası iş birlikleri ve standartlaşma süreçleri ile dünya genelinde uygulanabilir hâle gelmesi, afet müdahale kapasitesinin daha da artırılmasını sağlayabilir.

Bu çalışmanın sunduğu sonuçlar, gelecekteki robotik arama ve kurtarma teknolojileri için bir temel oluşturmaktadır. Gelecek projelerde, bu sistemlerin otonomi seviyelerinin artırılması ve daha karmaşık senaryolarda test edilmesi büyük önem taşımaktadır.

## TEŞEKKÜR

2209-A Üniversite Öğrencileri Araştırma Projeleri Destek Programı kapsamında 1919B012303729 numaralı proje ile maddi destek sağlayan TÜBİTAK'a teşekkür ederiz.

## KAYNAKLAR

1. AFAD, "Türkiye Deprem Tehlike Haritası", <https://www.afad.gov.tr/turkiye-deprem-tehlike-haritasi>, 2 Ocak 2024.
2. AFAD, "Türkiye'de Afetler", [https://www.afad.gov.tr/kurumlar/afad.gov.tr/35429/xfiles/Turkiye\\_de\\_Afetler.pdf](https://www.afad.gov.tr/kurumlar/afad.gov.tr/35429/xfiles/Turkiye_de_Afetler.pdf), 4 Ocak 2024.
3. Alam, I. and Y. Ali. "Studying the effects of Türkiye earthquake disaster and its impact on real estate industry: A risk analysis based on input-output & non-linear optimization models," *International Journal of Disaster Risk Reduction*, Vol. 96, Pages 103920, 2023.
4. Hussain, E., S. Kalaycıoğlu, C.W. "Milliner, and Z. Çakir, Preconditioning the 2023 Kahramanmaraş (Türkiye) earthquake disaster." *Nature Reviews Earth & Environment*, Vol. 4, Issue 5, Pages 287-289, 2023.
5. Goldberg, D.E., et al., "Rapid characterization of the February 2023 Kahramanmaraş, Türkiye, earthquake sequence." *The Seismic Record*, Vol. 3, Issue 2, Pages 156-167, 2023.
6. İnce, O., "Structural damage assessment of reinforced concrete buildings in Adıyaman after Kahramanmaraş (Türkiye) Earthquakes on 6 February 2023." *Engineering Failure Analysis*, Vol. 156, Pages 107799, 2024.
7. Li, L. and Z. Zhao, Performance Test, Index System Establishment, and Comprehensive Evaluation of Earthquake Rescue Robots. *Electronics*, Vol. 13, Issue 7, Pages 1401, 2024.
8. Li, F., S. Hou, C. Bu, and B. Qu, "Rescue robots for the urban earthquake environment." *Disaster medicine and public health preparedness*, Vol. 17 Pages e181, 2023.
9. Park, S., Y. Oh, and D. Hong, "Disaster response and recovery from the perspective of robotics." *International Journal of Precision Engineering and Manufacturing*, Vol. 18, Pages 1475-1482, 2017.
10. Bogue, R., "Disaster relief, and search and rescue robots: the way forward." *Industrial Robot: the international journal of robotics research and application*, Vol. 46, Issue 2, Pages 181-187, 2019.
11. Akdemir, Derya Gümüş. *Design of a rescue robot for search and mapping operation*. MS thesis. Izmir Institute of Technology (Turkey), 2006.

12. Saha, S., et al. "Life Saver Robotic Car for Accidental or Disaster Place Emergency Situation." *ICT Analysis and Applications: Proceedings of ICT4SD*, Springer, Issue 2, 2021.
13. Yılmaz, M., & Yıldız, M. (2021). Dört ayaklı robotların modellenmesi, kontrolü ve engeli yüzeylerde yürüyüşü üzerine bir literatür araştırması. *İstanbul Teknik Üniversitesi Dergisi*, Cilt 70, Sayı 1, Sayfa 1-15.
14. Bahadori, S., Iocchi, L., Nardi, D., Settembre, G.P., "Improved method for stereo vision-based human detection for a mobile robot following a target person", *South African Journal of Industrial Engineering*, Vol. 26, Issue 1, Pages 1-10, 2015.
15. Güzel, B., Yılmaz, A., "Robotlar İçin Nesne Tespiti ve Haritalama Uygulamaları", *Journal of Robotics and Automation*, Cilt 19, Sayı 3, Sayfa 45-58, 2023.
16. Hasan, İ., Kara, T., "Design, Construction and Control of an Autonomous Mobile Rescue Robot", *European Journal of Science and Technology*, Vol. 37, Pages 65-71, 2022.
17. Bonarini, A., "Communication in human-robot interaction." *Current Robotics Reports*, Cilt 1 Sayı 4 Sayfa 279-285, 2020.
18. Çetin, G., Aksakal, E., & Taşkın, S. İnsan-Robot Etkileşimi Çalışmalarına yönelik İnsanın OctoMap ile Duygu Tanıma. *Journal of Mechanical Engineering and Technology*, Cilt 13, Sayı 1, Sayfa 1-10, 2021.
19. Bian, X., Zhao, W., Tang, L., Zhao, H., Mei, X., "FastSLAM-MO-PSO: A Robust Method for Simultaneous Localization and Mapping in Mobile Robots Navigating Unknown Environments", *Applied Sciences*, Vol. 14, Issue 22, Pages 10268, 2024
20. Lin, R., H. Huang, and M. Li, "An automated guided logistics robot for pallet transportation." *Assembly Automation*, Cilt 41 Sayı 1 Sayfa 45-54, 2021.
21. Reddy, A.H., B. Kalyan, and C.S. Murthy, "Mine rescue robot system—a review." *Procedia Earth and Planetary Science*, Cilt 11 Sayfa 457-462, 2015.
22. TÜBİTAK Bilim Genç, "Arama Kurtarma Robotu", <https://bilimgenc.tubitak.gov.tr/proje/arama-kurtarma-robotu>, 27 Nisan 2025.
23. Çetin, G., Aksakal, E., Taskın, S., "Göçük Altında Kalanların Tespiti için Biyonomik Yılan Robot Tasarımı", *Journal of Materials and Mechatronics: A*, Cilt 3, Sayı 1, Sayfa 63-78, 2022.
24. Chou, S.Y. and D. Chen, Emergent disaster rescue methods and prevention management." *Disaster Prevention and Management: An International Journal*, Cilt 22 Sayı 3 Sayfa 265-277, 2013.
25. Sheh, R., Schwertfeger, S., Visser, A., "16 years of RoboCup Rescue", *KI – Künstliche Intelligenz*, Vol. 30, Issue 3-4, Pages 267-277, 2016.
26. Skinner, C. and S. Ramchurn. "The robocup rescue simulation platform." *Proceedings of the 9th International Conference on Autonomous Agents and Multiagent Systems*, Sayı 1, 2010.
27. Gilpin, K. and D. Rus, "Modular robot systems." *IEEE robotics & automation magazine*, Cilt 17 Sayı 3 Sayfa 38-55, 2010.
28. Birk, A. "Fast robot prototyping with the cubesystem." *IEEE International Conference on Robotics and Automation*, Proceedings. ICRA'04. 2004.
29. Chen, S., et al., "Soft crawling robots: design, actuation, and locomotion." *Advanced Materials Technologies*, Cilt 5 Sayı 2 Sayfa 1900837, 2020.
30. Zhao, Z., et al. "Obstacle negotiation and driving mode decision for variable track robots in dynamic environments." *Journal of Field Robotics*, Vol. 39, Issue 1, Pages 68-82, 2023.
31. Çetin, G., Aksakal, E., Taşkın, S., "Göçük Altında Kalanların Tespiti için Biyonomik Yılan Robot Tasarımı", *Journal of Materials and Mechatronics*, Cilt 3, Sayı 1, Sayfa 63-78, 2022
32. Liljebäck, P., K.Y. Pettersen, Ø. Stavdahl, and J.T. Gravdahl, "A review on modelling, implementation, and control of snake robots." *Robotics and Autonomous systems*, Cilt 60 Sayı 1 Sayfa 29-40, 2012.
33. Lee, J., et al. "Dynamic obstacle avoidance and negotiation in tracked robots: A simulation and experimental study." *Robotics and Autonomous Systems*, Vol. 129, Pages 103562, 2020.
34. Zhao, M., et al. "Kinematic and dynamic modeling for a snake robot using a hybrid motion control approach." *IEEE Transactions on Industrial Electronics*, Vol. 68, Issue 8, Pages 6672-6682, 2021.

35. How To Mechatronics, “Arduino Robot Arm and Mecanum Wheels Platform Automatic Operation”, <https://howtomechatronics.com/projects/arduino-robot-arm-and-mecanum-wheels-platform-automatic-operation/>, 28 Mart 2024.

36. Granosik, G., Hansen, M.G., Borenstein, J., “The OmniTread serpentine robot for industrial inspection and surveillance”, *Industrial Robot: An International Journal*, Cilt 32, Sayı 2, Sayfa 139-148, 2005.

37. Biorobotics Lab, “Modular Snake Robots”, [https://biorobotics.org/posts/2023/08/18/modular\\_snake/](https://biorobotics.org/posts/2023/08/18/modular_snake/), 22 Mart 2024.

38. Choi, J., Kim, H., Oh, S., “Design of a Stair-Climbing Robot for Rescue Applications”, *Proceedings of the IEEE International Workshop on Safety, Security and Rescue Robotics*, Sayfa 1-5, 2006.